

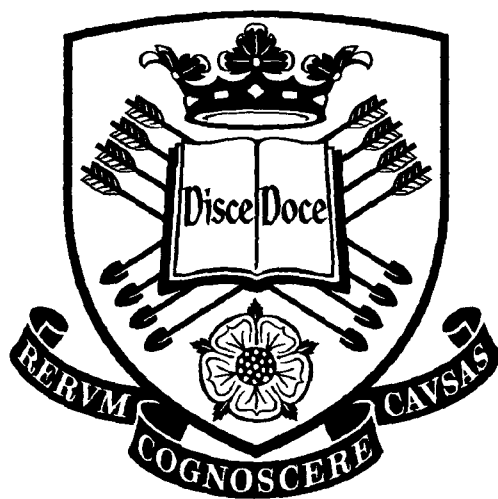
An experimental study of adhesion and conformational transitions in polyelectrolytes

by

Lorena Ruiz-Pérez

A thesis submitted to the University of Sheffield for the degree of
Doctor of Philosophy

May 2006



University of Sheffield
Department of Physics and Astronomy

To Beppe

Declarations

I declare that this thesis is the result of my own work, except where the nature of
others is stated, either explicitly or by the use of references.

No part of this dissertation has been submitted for publication or any other university.



Laura Ruiz-Perez

May 2006

*"But I don't want to go among mad people,"
Alice remarked.*

*"Oh, you can't help that," said the Cat: "we're
all mad here. I'm mad. You're mad."*

"How do you know I'm mad?" said Alice.

*"You must be," said the Cat, "or you wouldn't
have come here."*

Lewis Carroll, Alice's Adventures in Wonderland.

Cheshire cat by John Tenniel in the 1866 publication.

Declarations

I declare that this thesis is the result of my own work except where the work of others is cited, either explicitly or via the list of references.

No part of this dissertation has been submitted for a degree, diploma or other qualification at any other university.

Lorena Ruiz-Pérez

May 2006

Abstract

We revisit the pH-induced conformational structure of poly(methacrylic) acid (PMAA) chains in dilute solution using a combination of fluorescence techniques: non-radiative energy transfer, fluorescence lifetime, and time-resolved anisotropy. These measurements are supplemented with dynamic light scattering and transmission electron microscopy experiments. The fluorescence lifetime results suggest that the PMAA has a more complex structure than previously considered, with graded changes in density in the collapsed state (low pH). Such structure also suggests that the swelling of these dilute chains is of a progressive nature, with the outermost parts responding to the changing pH before the central regions, rather than a simultaneous swelling.

We have used neutron reflectometry to characterize the volume fraction-depth profiles of poly[(diethyl amino)ethyl methacrylate] (PDEAMA) and poly(methacrylic) acid (PMAA) brushes in aqueous solution as a function of pH. The polymers were synthesized by atom transfer radical polymerization in order to create a dense brush layer. In the case of PDEAMA the brushes are collapsed at high pH, and swell at a pH of between 3 and 4. The depth profiles of swollen brushes have an unusual shape, with depletion in brush concentration close to the substrate, which increases away from the substrate. Such a profile is unexpected for weak polyelectrolytes and we propose that entanglements created during the growth of the brush are an important consideration, creating a long-lived metastable equilibrium.

The PMAA brush was exposed to a pH cycle, showing a collapsed and expanded brush at low and high pH values respectively.

In addition, we introduce and test here a new technique as a means to measure interactions between polymer networks and brushes when immersed in aqueous solution. The important feature offered by this technique is that measurements are performed *in situ*. We have performed measurements showing that there is a difference between the behaviour of PMAA gel/blank silicon and PMAA gel/brush systems. These early results show interactions occurring at the interface between gel and brush, which may be due to adhesion.

Acknowledgements

This thesis would not have been possible without the contribution of many people who I want to thank.

First and foremost I should like to acknowledge the contribution to this work made by Professor Ian Soutar who died suddenly on August 14, 2003. Ian was a very helpful collaborator who gave me many ideas about how to proceed with the work presented in Chapter 5. Sadly, he is not here to see how this part of my project turned out.

I want to thank my supervisor Dr Mark Geoghegan for his trust, guidance and support through the period of this Ph.D. His supervision and enthusiasm has been the best a student can get. Thanks go also for the people of the Geoghegan group which just started with me as first Ph.D student but has grown over these years. Thanks go also to Professor Richard Jones and his group (past and present members), in particular Andrew Parnell for making some of the brushes that are presented in this thesis and sharing the endless hours of neutron measurements and Dr Simon Martin for his much needed help with neutrons in the early days of my Ph.D.

In the Chemistry department I would like to thank Professor Tony Ryan for letting me use his labs all the time and for his collaboration. Thanks go to the Ryan's group particularly Dr Collin Crook, Dr Paul Topham and Dr Jonathan Howse for making the brushes used for this thesis and for their advice and help through this period. Thank you Dr Nadia Tzokova for being always so genuinely interested in all my things.

Thanks go to Dr Linda Swanson for her collaboration with the fluorescence section and for letting me use her labs. A big thank goes to: Dr Andrew Pryke for his patience in introducing me to that obscure world of polymer synthesis and his advices in all things related to Chemistry. Thanks also to Dr Ramune Rutkaite for always being there to explain me all the tricks about fluorescence measurements. Thanks to Rod and in general to all the people in F floor. I should also thank Dan, the glass blower for his bright ideas and skills in designing the strangest glass moulds I asked him to make for my samples.

At the Rutherford Appleton Laboratory (ISIS) I would like to thank Drs John Webster and Stephen Holt at SURF and Rob Dalgliesh at CRISP for providing the necessary

assistance to run the neutron experiments. Thanks also to Dr Devinder Sivia from the data analysis group at ISIS for providing the slab-fit software. I would also like to thank Dr Alain Manelle and Dr Fabrice Cousin at the Laboratoire Léon Brillouin, CEA at Saday (France). Beside their scientific assistance they provided us with priceless information about french transport, french bureaucracy...

The Engineering and Physical Sciences Research Sciences (EPSRC) is gratefully acknowledged for their financial support during the time of my Ph.D

I would like to thank the friends I made in Sheffield. They say, I apologize to the reader for not giving here a reference, that when you laugh the whole world laughs with you but when you cry you do it alone. I am deeply grateful for those persons who were with me, in their own different ways, not only in the happy times but also and more significantly in the not-so-happy-times: Anne, Sonia, Zubin, Zee and especially Ana. Thank you. I also want to thank Lindy Ann for looking after me so kindly when I just arrived to Sheffield.

Most of all I want to thank my parents: Juan and Maria Luisa, for they have always taught me that I could do anything I wanted to do: this thesis is the culmination of that. *Por ser mis raices y referencias esté donde esté y haga lo que haga.* Finally I want to thank Beppe for his patience, encouragement, support and love every single day throughout this period, especially during the critical final days of this thesis.

Contents

Symbols and abbreviations	v
Chapter 1. Introduction	1
I Theoretical background	
Chapter 2. Neutral and Charged Polymers	6
2.1 Neutral polymer chains	6
2.1.1 The polymer chain	6
2.1.1.1 Ideal polymer chain: the Freely Jointed Chain (Flexible Chain) and its Gaussian limit	7
2.1.1.2 Ideal polymer chains: the Freely Rotating Chain (Semi-flexible Chain)	8
2.1.1.3 Real polymer chains and the Self Avoiding Walk	10
2.1.1.4 Self-consistent mean Field Theory	11
2.1.2 Polymers in Solution	12
2.1.2.1 Good and bad solvent and the theta condition	12
2.1.2.2 Concentration regimes	13
2.2 Charged polymers: Polyelectrolytes	15
2.2.1 Introduction	15
2.2.2 Interaction between charged objects	16
2.2.3 Poisson Boltzmann and Debye-Hückel Theory	17
2.2.4 Counterion Condensation	18
2.2.5 Persistence length in polyelectrolyte solutions	21
2.2.6 Electrostatic Excluded Volume	22
2.2.7 Dilute polyelectrolyte solutions	23
Chapter 3. Polyelectrolyte Systems: Brushes and Hydrogels	26
3.1 Introduction to charged systems	26

3.2	Polyelectrolyte Brushes	28
3.2.1	Polymer Brushes: General features	28
3.2.2	Synthesis of Polymer Brushes	30
3.2.2.1	Polymer Brushes via Physisorption	30
3.2.2.2	Polymer Brushes via Chemisorption	31
(a)	Polymer Brushes via the 'grafting to' technique	31
(b)	Polymer Brushes via the 'grafting from' technique	32
3.2.3	The physics of neutral Polymer Brushes	33
3.2.3.1	Semi-Dilute conditions and Alexander scaling arguments	33
3.2.3.2	Concentrated conditions and Flory calculations	34
3.2.3.3	Parabolic Brushes and Self-Consistence Theory	35
3.2.3.4	Poor solvent conditions	37
3.2.4	The physics of Polyelectrolyte Brushes	38
3.2.4.1	Strong Polyelectrolyte Brushes	38
(a)	Counterions extended over the brush height: $C \gg h$ (weak-charged limit)	39
(b)	Counterions confined within the brush height: $C \approx h$ (strong-charged limit)	41
3.2.4.2	Weak Polyelectrolyte Brushes	43
3.3	Polyelectrolyte Hydrogels	48
3.3.1	Hydrogels: general features	48
3.3.1.1	Physical gels (reversible)	49
(a)	Microcrystalline regions	50
(b)	Microphase separation	50
3.3.1.2	Chemical gels (irreversible)	51
3.3.2	The physics of neutral gels	51
3.3.3	The physics of ionisable (weak polyelectrolyte) gels	55
3.3.4	Physical properties of hydrogels	61
3.3.4.1	Mechanical properties	61
3.3.4.2	Diffusion properties	62

II Experimental

Chapter 4. Experimental Techniques	66
4.1 Labelled poly(methacrylic) acid	66
4.1.1 Sample preparation	66
4.1.2 Sample characterisation	68
4.1.2.1 Gel-Permeation Chromatography (GPC)	68
4.1.2.2 Ultraviolet (UV) spectra	68

4.1.3	Fluorescence measurements: Instrumentation and Analysis	69
4.1.3.1	Steady State measurements	69
4.1.3.2	Lifetime measurements	71
4.1.3.3	Time Resolved Anisotropy measurements (TRAMS)	73
4.1.4	Dynamic Light Scattering measurements (DLS)	75
4.1.5	Transmission Electron Microscopy measurements (TEM)	76
4.2	Polyelectrolyte Brushes	77
4.2.1	Brush preparation	77
4.2.1.1	Polyacid brushes	77
4.2.1.2	Polybase brushes	79
4.2.2	Neutron Reflectivity measurements: Instrumentation and Analysis	81
4.2.2.1	Instrumentation	81
4.2.2.2	Theoretical background and analysis	85
4.3	Poly(methacrylic) acid hydrogels	92
4.3.1	Hydrogels preparation	92
4.3.2	Contact area measurements: Instrumentation and Analysis	94
	Chapter 5. Poly(methacrylic) acid in Solution	97
5.1	Introduction	97
5.2	Fluorescence measurements	100
5.2.1	Steady State measurements in aqueous solution	100
5.2.1.1	Donor and donor-acceptor labelled PMAA comparison	100
5.2.1.2	Donor-acceptor labeled PMAA and Energy Transfer	101
5.2.2	Fluorescence Lifetime measurements in aqueous solution	103
5.2.2.1	Comparison between donor and donor-acceptor labelled PMAA	103
5.2.2.2	Donor-acceptor labelled PMAA	107
5.2.2.3	Proposed Model: the 'Onion' model	108
5.2.2.4	Acceptor labelled PMAA	111
5.2.3	Time Resolved Anisotropy measurements in aqueous solution	114
5.2.4	Fluorescence Lifetime and TRAMS measurements in methanol	118
5.3	Dynamic Light Scattering	122
5.4	Transmission Electron Microscopy	123
	Chapter 6. Swelling behaviour of polybase and polyacid brushes	127

6.1	Polybase brush: poly(diethylamino) ethyl methacrylate (PDEAMA)	127
6.1.1	Preliminary data analysis using a hyperbolic tangent function	128
6.1.2	Data analysis using the slab-fit programme	130
6.1.2.1	Possible explanation of the "depletion zone"	135
6.2	Polyacid brush: poly(methacrylic) acid (PMAA)	138
6.2.1	Data analysis using the slab-fit programme	138

Chapter 7. Poly(methacrylic) acid network/brush interactions as a function of pH **142**

7.1	Introduction	142
7.2	Preliminary Contact Area measurements	144
7.2.1	Poly(methacrylic) acid network and silicon	145
7.2.2	Poly(methacrylic) acid network and brush	148
7.2.2.1	Comparison with measurements performed on blank silicon	151
7.2.2.2	Comparison with measurements performed with a gel of different crosslink density on a different brush	153
7.3	Future directions	155

Chapter 8. Conclusions **159**

8.1	Single poly(methacrylic) acid chains in solution	159
8.2	Poly(diethylamino) ethyl methacrylate and poly(methacrylic) acid brushes	160
8.3	poly(methacrylic) acid network/brush	160

Appendices

Appendix 1.		
	Polybase brushes: scattering length densities as a function of depth	162
Appendix 2.		
	Calculation of chromophore concentration in poly(methacrylic) acid	163
A2.1	Obtaining absorbance values of naphthalene and anthracene chromophores in double labelled poly(methacrylic) acid sample (NA-PMAA) from UV spectra	163
A2.2	Concentration of naphthalene and anthracene chromophores in double labelled poly(methacrylic) acid sample (NA-PMAA) from UV spectra	164
Appendix 3.		
	Basic concepts related to acids and bases	166
A3.1	Acids and Bases	166
A3.2	pH calculations	168

Symbols and abbreviations

α	linear expansion coefficient (chapter 2)
α	degree of dissociation (chapter 3)
α^b	(virtual) degree of dissociation in the bulk
a	Kuhn length or effective monomer size.
a	average distance between charges along a linear polyelectrolyte chain
A	(9-Anthryl) methylmethacrylate anthracene chromophore
A^-	negatively charged brush segment
HA	uncharged acidic brush segment
AIBN	2,2'-Azobisisobutyronitrile initiator
AMPA	2,2'-azobis(2-methylpropionamide) dihydrochloride initiator
ATRP	atom transfer radical polymerization
β	optical path length for neutrons in a film
β_{gel}	expansion factor for polymer networks
b	monomer size (chapter 2)
b	neutron scattering length (chapter 4)
B	uncharged basic brush segment
HB^+	positively charged brush segment
χ	Flory-Huggins interaction parameter
c	concentration of polymer in solution
c^*	coil overlap concentration threshold
C	height of counterions cloud in strongly charged brushes
d	average distance between two grafting sites in polymer brushes
D	diffusion constant for networks
D_t	diffusion coefficient employed for dynamic light scattering
DEAMA	diethylamino ethyl methacrylate monomer
DLS	dynamic light scattering
ϵ	medium dielectric constant
ϵ_r	medium relative dielectric constant
ϵ_0	bulk dielectric constant (or permeability in free space)
ϵ_{ps}	energy of interaction between a neighbouring polymer and solvent segment
ϵ_{pp}	energy of interaction between two neighbouring polymer segments
ϵ_{ss}	energy of interaction between two neighbouring solvent segments
e	elementary charge
E	Young modulus

$E(y)$	local electrostatic potential in a weakly charged brush
E_f	energy transfer efficiency
ET	energy transfer
φ_1	molar volume of solvent in polymer networks
ϕ_b	polymer volume fraction inside the brush (described as blobs)
$\phi(y)$	brush volume fraction at a distance y from the substrate
ϕ_0	brush volume fraction at the initiator layer $y=0$
Φ	polymer volume fraction in a solution
Φ^*	polymer volume fraction threshold in a solution
f	fraction of charged monomers in a polyelectrolyte
f_c	characteristic charge fraction in a strongly charged brush
F	free energy
F_{el}	elastic free energy
F_{rep}	repulsive free energy
F_T	total free energy
$F_{electrost}(r)$	electrostatic interactions between two charge points separated by a distance r
$F_{DH}(r)$	Debye-Hückel effective electrostatic interactions between two charge points separated by a distance r
F°_{el}	electrostatic elastic energy for polyelectrolytes
F°_{rep}	electrostatic repulsive energy for polyelectrolytes
F°_T	electrostatic total free energy for polyelectrolytes
F_{os}	osmotic free energy in a polymer brush
F_{st}	conformational free energy of stretching in a polymer brush
$F_{T,chain}$	total free energy per N chains in a polymer brush
$F_{T,PE brush}$	total free energy per N chains in a charged polymer brush
ΔF_{mix}	total free energy of mixing in polymer networks
$\Delta F_{elastic}$	total elastic free energy in polymer networks
ΔF_{ion}	total free energy due to ionic species in charged polymer networks
ΔF_{Coul}	total free energy due coulombic interactions in charged polymer networks (term included in ΔF_{ion})
FJC	freely jointed chain model
FRC	freely rotating chain model
G	Elastic shear modulus
$G_A(y)$	statistical weight of finding a segment of type A^- in layer y in a polymer brush
$G_A(y)$	statistical weight of finding a segment of type A in layer y in a polymer brush
$G_{HA}(y)$	statistical weight of finding a segment of type HA^- in layer y in a polymer brush

GPC	gel permeation chromatography
Γ	linear relaxation rate for dynamic light scattering measurements (chapter 4)
Γ	distribution function used in mean field theory (chapter 2)
h	brush height
$h_{osmotic}$	osmotic brush height
$h_{osmotic,w}$	osmotic brush height for weakly charged brushes
h_{Pincus}	Pincus brush height
$h_{q-neutral}$	quasi-neutral brush height
$h_{salted,wc}$	brush height for a weakly charged brush at high salt concentration
η	solvent viscosity
I	ionic strength
$I(t)$	fluorescence intensity decay
I_{420}/I_{340}	ratio between increased anthracene emission (420 nm) and quenched naphthalene emission (340 nm)
κ^{-1}	Debye- Hückel length (screening length)
K	Donnan ratio (chapter 3)
K	wavevector (normal to the interface) for neutron reflectometry (chapter 4)
K_c	critical value for wavevector
K_a	acid dissociation constant
K_b	base dissociation constant
k_B	Boltzmann constant
$k_B T$	thermal energy
λ	wavelength
λ_{ex}	excitation wavelength
λ_{em}	emission wavelength
λ_{GC}	Gouy-Chapman length
l_B	Bjerrum length
l_o	persistence length of the neutral chain or bare persistence length
l_e	electrostatic persistence length
l_{OSF}	electrostatic persistence length given by the Odjik, Skolnick and Fixman theory
l_t	total persistence length
L	contour length of polymer chain
μ	chemical potential
μ_1	chemical potential of solvent inside a polymer network
μ_1^o	chemical potential of solvent outside a polymer network (in the reservoir)

μ^*_1	chemical potential of solvent containing ions outside a polymer network (in the reservoir)
m	order of the diffracted beam in the Bragg equation
M_n	number average molecular weight
M_w	weight average molecular weight
M_c	average molecular weight between two neighbouring crosslinks in a polymer network
MAA	methacrylic acid monomer
MFT	mean field theory
ν	dimensionless excluded volume parameter or Flory exponent for the polymer size
ν_i	stoichiometric coefficients of the i -th ions
n	refractive index
n_i	concentration of the i -th ions
n^*_i	concentration of the i -th ions in the external solution outside a polymer network
$n_{neutral}$	concentration of neutral solute (undissociated ions) in a polymer network
$n^*_{neutral}$	concentration of neutral solute (undissociated ions) in the external solution outside a polymer network
n_2	molar concentration of fixed ionisable charges in a charged network
N^*_1	mole fraction of solvent (containing ions) outside a polymer network
n_s	salt concentration
n_{cl}	concentration of counterions inside a charged brush
N	number of monomer units per polymer chain or the degree of polymerization
N_A	Avogadro's constant
N_b	scattering length density
N_b	number of monomers per blob
N_c^{gel}	average number of 'effective' chains between crosslinks in a polymer network
NR	neutron reflectometry
NRET	non-radiative energy transfer
OB	osmotic brush
OSF	Odjik, Skolnick and Fixman theory
Π	osmotic pressure
$P(R, N)$	gaussian distribution of possible end-to-end distances in random, polymer coils
ρ_i	number of ions in the polymer network
ρ_a	number of dissociated acrylic acid in the charged network

pK_a	negative logarithm of the acid dissociation constant K_a
pK_b	negative logarithm of the base dissociation constant K_b
PB	Poisson-Boltzmann (chapter 2)
PB	Pincus Brush (chapter 3)
PE	polyelectrolyte
PMAA	poly(methacrylic) acid
NA-PMAA	naphthalene-anthracene labelled poly(methacrylic) acid
N-PMAA	naphthalene labelled poly(methacrylic) acid
A-PMAA	anthracene labelled poly(methacrylic) acid
PDEAMA	poly[(diethyl amino) ethyl methacrylate]
PS	polystyrene
PSSNa	poly(styrene sulfonate sodium salt)
PTFE	polytetrafluoroethylene
PVP	poly(4-vinyl pyridine)
q	swelling ratio in a polymer network
q_m	maximum swelling ratio in a polymer network in equilibrium
Q	Momentum transfer in neutron reflectometry
QNB	quasi-neutral brush
ρ	charge density in a polyelectrolyte chain
ρ_{eff}	effective charge density in a polyelectrolyte chain (Manning condensation)
ρ_c^{gel}	gel crosslinking density
$\rho_{PE, brush}$	charge density of a grafted polyelectrolyte chain
r	distance (sometimes in a distance distribution)
$r(t)$	anisotropy decay
r_o	intrinsic anisotropy
$r_{n-1,n}$	reflection coefficient for the reflection of a neutron beam at the interface between media $n-1$ and n
rms	root mean square
R	reflectivity
$R(t)$	anisotropy function
R	end-to-end vector of a polymer chain (chapter 2)
R	reflectivity (chapter 4)
R_o	Forster distance in energy transfer
$\langle R^2 \rangle$	end-to-end distance or mean square displacement
R_F	Flory radius
R_H	hydrodynamic radius
R_g	radius of gyration
R_c^{gel}	average linear distance between adjacent crosslinks in a polymer network (mesh size)
$\langle (R_o^{gel})^2 \rangle$	unperturbed end-to-end distance between adjacent crosslinks in a polymer network

RW	random walk
σ	grafting density in a polymer brush (dimensionless)
σ^*	overlap threshold in grafting density
σ_c	characteristic grafting density in strongly charged brushes
S	entropy
SB	salted brush
SAW	self-avoiding-walk
SCF	self consistent field theory
SFM	scanning force microscopy
θ	fixed angle between monomers in the freely jointed chain model
θ_o	angle of incidence of a neutron beam
θ_r	angle of reflection of a neutron beam
θ_c	critical angle for a neutron beam
τ	lifetime given by multiexponentials fitting to fluorescence decay
$\langle \tau \rangle$	average lifetime
τ_c	correlation time
τ_d	time constant representing the temporal decay in light scattering intensity
T	temperature
TEM	transmission electron microscopy
TRAMS	time resolved anisotropy measurements
ν_1	volume fraction of solvent in a swollen network
ν_2	volume fraction of polymer in a swollen network
ν_{2m}	volume fraction of polymer in a swollen network at equilibrium
$u(r,t)$	displacement vector in a polymer network (used for diffusion properties of polymer networks)
$u_A(y)$	potential of mean force for A segments in a layer y of weakly charged polymer brushes
u_A^b	reference potential of mean force for A segments (potential in the bulk)
U	Donnan potential energy
UV	ultra-violet spectroscopy
\bar{v}	specific volume of polymer in a polymer network
V_o	total volume of a relaxed polymer network
V	total volume of a swollen polymer network
$V_e(r)$	Coulomb interactions between two elementary charges separated by a distance r
ξ	Manning parameter
ξ_c	critical value of the Manning parameter

$\psi(r)$	local electrostatic potential satisfying the Poisson equation of electrostatics
$\psi_{DH}(r)$	Debye- Hückel electrostatic potential
z_i	valence of the i -th ion
∇^2	Laplace operator

Chapter 1

Introduction

Polymer is a generic term used to describe very long molecules consisting of structural and repeating units connected by covalent chemical bonds. The term is derived from the Greek words: *polys* meaning *many*, and *meros* meaning *parts*.¹ The key feature that distinguishes polymers from other molecules is the repetition of many identical, similar, or complementary molecular subunits called monomers in these chains. Polymers have replaced natural materials for many applications and indeed most of the things surrounding us in everyday life are or include polymeric materials.

An important type of polymers are polyelectrolytes: polymers bearing ionizable groups which in polar solvents can dissociate into charged polymer chains leaving ions (counterions) in solution. Very often the polar solvent is water. Because of their fundamental importance in biology and biochemistry, and their hydrosolubility, polyelectrolytes have been the subject of continued interest since the early days of polymer science.²⁻⁵ Well-known examples of such systems are proteins, nucleic acids and synthetic systems such as sulfonated polystyrene or poly(methacrylic) acid.

This thesis is focused on the study of weak polyelectrolytes in solution. Weak polyelectrolytes are polyelectrolyte whose charge fraction is not fixed but is controlled by the pH of the solution. Such responsiveness to pH is responsible for the chains to pass from coiled to expanded structures in poor and good solvent conditions respectively, and do so in a reversible manner. Reversible behaviour is central to many device functions in the way that on/off switches are most useful when they can be used repeatably. Thus, polyelectrolytes can be used as the

building blocks of more complex structures in order to create 'smart' systems, emphasizing switchability and reversibility.

On the macroscopic scale, responsive gels (networks), formed by crosslinked polyelectrolytes, can pass from a collapsed to a swollen state and vice versa upon variations in pH. Such stimuli-responsive features coupled with their elastic properties can be utilized for numerous technological applications such as biomaterials,⁶ drug delivery systems,⁷⁻⁹ surface patterning,^{10,11} and actuators for artificial muscles⁶ among others. At the nanoscale, general interest is found in end-functionalised polymers (attached with one end only to a substrate) as polymer brushes. In such brushes the rest of the polymer is not particularly attracted to (or repelled from) the grafting surface. Thus, it attains a random coil structure in the surrounding area of the surface at low grafting densities. At high grafting densities a brush-like structure is formed. The incentive to investigate such terminally attached polymers arises from their improved route to stabilize particles and surfaces against flocculation, compatibilization between organic and inorganic materials and lubrication.¹² Such applications are greatly enhanced when polyelectrolytes are used for the grafted layers, since they provide 'switchability' with potential uses as actuators in nanotechnologies,^{13,14} including pH-controlled wetting and adhesion.

One way to achieve adhesion between an inorganic substrate and a polymer network is by chemically grafting polymer chains (i.e. polymer brushes) to the substrate. When the brush and network are placed in contact, the grafted chains would entangle with the network to create adhesion. O'Connor and McLeish¹⁵ introduced the term '*Molecular Velcro*' to describe such entanglement. The mesh of the network plays the role of the loops in Velcro whereas the grafted chains of the polymer brush act like the hooks. A schematic diagram of '*Molecular Velcro*' is shown in Fig. 1.1

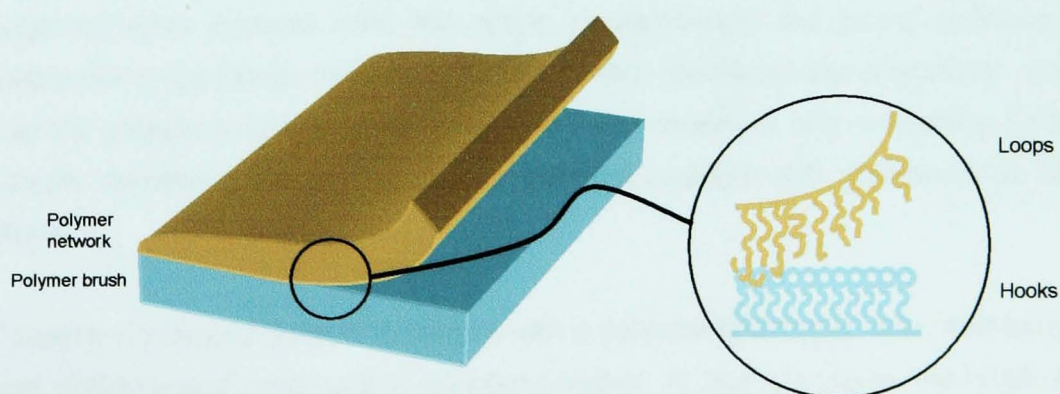


Fig. 1.1 Schematic diagram showing a '*Molecular Velcro*' formed by a polymer network (tanned) placed in contact with a polymer brush (blue). The network would act like the loops in the Velcro while the grafted chains of the brush would play the role of hooks. The adhesion is achieved by entanglement of loops and hooks. The diagram is not to scale.

The '*Molecular Velcro*' shown in Fig.1.1 is an attempt to mimic a real Velcro (Fig. 1.2) at the molecular level

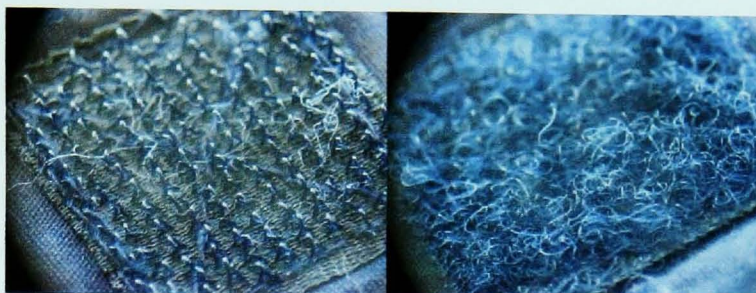


Fig. 1.2 Photograph of real Velcro where it can be seen clearly the hooks (left hand side) and the loops (right hand side). Adapted from <http://en.wikipedia.org/wiki/Velcro>

Molecular Velcro has been studied theoretically¹⁵ and experimentally.¹⁶⁻¹⁸ Geoghegan et al¹⁷ used polystyrene (PS) networks and brushes and via neutron reflectometry measurements they observed that the growth of the interface was logarithmic in time. Polydimethylsiloxane (PDMS) networks and brushes have been used in other experiments.^{16,18}

The ambitious objective of the present work is to apply '*Molecular Velcro*' to a polyelectrolyte system and test its reversibility. Using polyelectrolytes (weak polyelectrolytes) has an advantage over PS and PDMS systems regarding the disentanglement process. As we have said previously, the grafted polymer chains would entangle with the network to create adhesion. To disentangle, the grafted chains must follow exactly the same path that they used to go into the network, which is entropically forbidden. Thus, bond breakage is the only way to eliminate the adhesion, which may destroy and/or vary the system. pH-responsive polyelectrolytes systems offer the option to disentangle the strong interface by simply switching the pH from bad to good solvent conditions and vice versa. In this way the polyelectrolyte swelling (in good solvent condition) and contracting (in bad solvent condition) favors the disentanglement-entanglement processes to take place.

Consider a polyacid network in contact with a polyacid brush (e.g. poly (methacrylic acid) (PMAA)) and immersed in aqueous solution. At high pH values the brush and network will swell. If the pH is decreased the two should collapse together. The brush and network may collapse around each other creating a strong interface: adhesion. As the solvent is driven back to high pH, the two should swell, the

swelling would make the network and polymer chains to disentangle without the need of breaking preformed bonds. Indeed, studies of the interactions between a PMAA brush in contact with a PMAA gel upon changes in pH constitute the last chapter of this thesis.

Three separate research lines related to the goals of the project have been followed. The first one involved a highly detailed study of the pH-induced conformational transition of dilute poly(methacrylic) acid (PMAA) chains in aqueous solution via fluorescence measurements. These results would be useful to compare to the collapse and swelling of PMAA brushes as measured by neutron reflectometry. As it turned out, the polybase poly[(diethyl amino) ethyl methacrylate] (PDEAEMA) became the first candidate for the brush experiments, and these data have been analysed by neutron reflectometry. In addition, a PMAA brush has been analysed via neutron reflectometry. The third part of the work involved measuring the adhesion between a PMAA network and brush.

This thesis is divided into two parts:

In Part I, the necessary theoretical background concerning polyelectrolytes is introduced. This part consists of Chapter 2 and Chapter 3. Chapter 2 introduces the fundamental scaling laws of polymer physics for both neutral and charged polymer chains. In Chapter 3 the theoretical tools necessary to understand the complex behaviour of polyelectrolytes brushes and networks are given.

Part II presents the experimental work. This part includes Chapters 4,5,6,7 and 8. Chapter 4 presents a description of sample preparation as well as the experimental techniques. Neutron reflectometry is explained in detail. Chapter 5 is devoted to the study of the conformational behaviour of single PMAA chains in dilute solutions via fluorescence spectroscopy. Chapter 6 covers neutron reflectometry measurements of PDEAMA and PMAA brushes upon changes in pH. Chapter 7 presents preliminary results obtained from a PMAA network in contact with a PMAA brush as a function of pH. Such preliminary results on the interactions between the two constitute an initial stage from where the ultimate goal of adhesion can be achieved. Future directions to follow for further characterization of the charged network/brush system are also given in this chapter. Chapter 8 presents the conclusions to the work presented here.

The thesis is finally completed with the appendices where short theoretical considerations are covered in order to provide practical information to the reader.

REFERENCES

- (1) www.etymonline.com Online Etymology dictionary.
- (2) Oosawa, F. *Polyelectrolytes*; Marcel Dekker: New York, 1971.
- (3) Tripathy, S.; Kuma, J.; Nalwa, H. S., Eds. *Handbook of Polyelectrolytes and Their Applications*; American Scientific Publishers, 2003; Vol. Vols1-3.
- (4) Wensel, T. G.; Meares, C. F.; Vlachy, V.; Matthew, J. B. *Proc. Natl. Acad. Sci.* **1986**, *83*, 3267.
- (5) Tanford, G. *Physical Chemistry of Macromolecules*; Wiley: New-York, 1961.
- (6) Okano, T. *Biorelated Polymers and Gels*; Academic Press: San Diego, CA, 1998.
- (7) Qiu, Y.; Park, K. *Adv. Drug. Del. Rev* **2001**, *53*, 321-339.
- (8) Kikuchi, A.; Okano, T. *Adv. Drug Del. Rev* **2002**, *54*, 53-77.
- (9) Torres-Lugo, M.; Peppas, N. A. *macromolecules* **1999**, *32*, 6646-6651.
- (10) Sato-Matsuo, E.; Tanaka, T. *Nature* **1992**, *358*, 482-485.
- (11) Hu, Z.; Chen, Y.; Wang, C.; Zheng, Y.; Li, Y. *Nature* **1998**, *393*, 149-152.
- (12) Motonov, M.; Netz, R. R.; Schmidt, M.; Seidel, C.; Stamm, M.; Stephan, T.; usov, D.; Zhang, H. *Adv. Polym. Sci* **2004**, *165*, 79-150.
- (13) Ryan, A. J.; Crook, C. J.; Howse, J. R.; Topham, P.; Jones, R. A. L.; Geoghegan, M.; Parnell, A. J.; Ruiz-Perez, L.; Martin, S. J.; Cadby, A.; A, M.; Webster, J. R. P.; Gleeson, A. J.; Bras, W. *Faraday Discuss.* **2005**, *128*, 55-74.
- (14) Ryan, A. J.; Crook, C. J.; Howse, J. R.; Topham, P.; Geoghegan, M.; Martin, S. J.; Parnell, A. J.; Ruiz-Perez, L.; Jones, R. A. L. *J. Macromol. Sci. B:Phys* **2005**, *44*, 1103-1121.
- (15) O'Connor, K. P.; McLeish, T. C. B. *Macromolecules* **1993**, *26*, 7322-7325.
- (16) Deruelle, M.; Leger, L.; Tirrell, M. *Macromolecules* **1995**, *28*, 7419-7428.
- (17) Geoghegan, M.; Clarke, C. J.; Boue, F.; Menelle, A.; Russ, T.; Bucknall, D. G. *Macromolecules* **1999**, *32*, 5106-5114.
- (18) Vilmin, T.; Tardivat, C.; Léger, L.; Brown, H.; Raphael, E. *Euophys. Lett.* **2004**, *68*, 542-549.

Part I

Theoretical Background

Chapter 2

Neutral and Charged Polymers

To understand the conformational behaviour of charged polymers is one of the main purposes of the work presented here. In order to study complex polyelectrolyte systems such as brushes or gels, we have started with the simpler system: single polyelectrolyte chains in solution. In this chapter we start introducing the fundamental scaling laws that govern the behaviour of isolated neutral polymer chains as well as polymers in solution. It follows with the general physics behind charged polymer chains. In addition, important concepts commonly discussed in work regarding polyelectrolytes in solution, such as counterion condensation and electrostatic persistence length are explained.

2.1 NEUTRAL POLYMER CHAINS

2.1.1 The Polymer chain

As defined previously, a polymer is a molecule with high molecular weight consisting of a number of structural units linked together by covalent bonds. Such structural units are molecules called monomers.

In a linear polymer, the structural units are connected in a chain arrangement and thus need only be bifunctional (i.e., have two bonding sites). When the structural unit is trifunctional (has three bonding sites), a non-linear, or branched polymer results. The number of monomers in the chains determines the molecular weight

(M_w), while the monomers employed in the sequence will determine the type of polymer as well as the adopted structure.

2.1.1.1 Ideal polymer chain: the Freely Jointed Chain (Flexible Chain) and its Gaussian limit.

The simplest model used to describe a polymer chain is the Freely Jointed Chain model (FJC). In this model, the chain consists of N links or bonds defined by bond vectors \mathbf{r}_i . Each bond vector has a fixed length $|\mathbf{r}_i| = a$ corresponding to the Kuhn length and can rotate freely in space. Since each link has different orientation, the path of the polymer in space is a random walk (similar to Brownian motion of particles in a fluid).^{1,2}

The end-to-end vector R gives the characteristic size of a FJC. Since the possibility of direction $+R$ is as probable as a direction $-R$, the average $\langle R \rangle$ is zero thus the end-to-end distances are expressed as $\langle R^2 \rangle$. With the random walk model (RW), the mean square displacement $\langle R^2 \rangle$ is proportional to N as

$$\langle R^2 \rangle = a^2 N = La, \quad (2.1)$$

where the contour length of the chain is given by $L = Na$.

The end-to-end distances are easily calculated for linear chains but not for branched polymers. Consequently, a better approach to estimate the size of polymers is given by the radius of gyration R_g defined as the root-mean-square (rms) distance of the segments from the centre of mass

$$R_g^2 = \frac{1}{6} a^2 N = \frac{1}{6} \langle R^2 \rangle. \quad (2.2)$$

Random polymer coils are often called gaussian chains because the distribution of possible end-to-end distances is a gaussian distribution (in the limit of large N). In such a distribution, the probability that a chain with N links which has one end at the origin and its other end at a position R is given by

$$P(R, N) = \left(\frac{3}{2\pi Na^2} \right)^{\frac{3}{2}} \exp\left(\frac{-3R^2}{2Na^2} \right), \quad (2.3)$$

where $\langle R^2 \rangle = a^2 N$. Eq. (2.3) allows us to express the entropy of the chain as a function of its elongation as

$$S(R) = S(0) - \frac{3k_B R^2}{2Na^2}, \quad (2.4)$$

where k_B is the Boltzmann constant. When the elongation increases (stretched polymers), the conformational entropy is lowered. Eq (2.4) can be rewritten in terms of the free energy

$$F(R) = F(0) + \frac{3k_B T R^2}{2Na^2}. \quad (2.5)$$

This is an important equation since it describes the behaviour of the polymer chain as an entropic spring. When it is stretched there is a restoring force proportional to the extension. The origin of such a force is entropic, in other words, the random walk model enables the polymer chains to maximize their conformational entropy.

The FJC model is schematically shown in Fig. 2.1

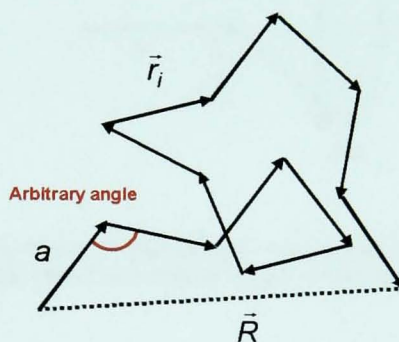


Fig. 2.1 Freely jointed chain (FJC) model, where N bonds of length a are connected to form a flexible chain. The angle between the link vectors is considered an arbitrary angle. The end-to-end vector is R

2.1.1.2 Ideal polymer chains: the Freely Rotating Chain (Semi-flexible Chain)

A more general model for ideal chains is the freely rotating chain (FRC) model. In this model different chain conformations are given by torsional rotations (given by β) of the polymer backbone bonds of length b at fixed angle θ . This model is closer to real synthetic polymers than the FJC model. In the FRC model, the correlations between two neighboring bond vectors do not cancel and are given by $\langle r_i \cdot r_j \rangle = b^2 \cos \theta$. The mean end-to-end distances for this model in the limit of long chains is given by³

$$\langle R^2 \rangle \cong Nb^2 \frac{1 + \cos \theta}{1 - \cos \theta}. \quad (2.6)$$

In the FRC model, the contour length is given by $L = Nb \cos(\theta/2)$. The relation between the Kuhn length a (given in the FJC) and the monomer size b is given by

$$a = b \frac{1 + \cos \theta}{\cos(\theta/2)(1 - \cos \theta)}, \quad (2.7)$$

A typical bond angle value for saturated carbon backbones is $\theta \approx 70^\circ$, which gives the relation of $a \approx 2.5 b$. With typical values of $b \approx 0.15 \text{ nm}$, this yields $a \approx 0.38 \text{ nm}$. In the present work, the exposed models will be with flexible chains characterized by the Kuhn length a . The FRC model is shown in Fig. 2.2

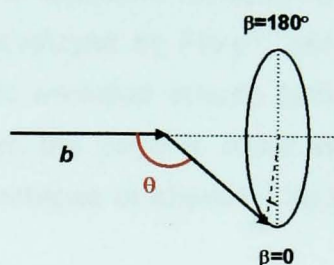


Fig. 2.2 Freely rotating chain (FRC) model, where the chain consists of N bonds of length b (monomer size), with fixed angles θ , but with freely rotating torsional angles β

Another important parameter is the persistence length ℓ_o which essentially describe how far the polymer extends in a given direction before becoming random.⁴ In other words ℓ_o can be defined as the length over which the tangent vectors at different locations on the chain are correlated. For the semi-flexible polymer model (FRC), the correlations between tangent vectors exhibit an exponential decay with distance. Taking into account this exponential decay the mean squared end-to-end radius can be written in terms of its contour length L as⁵

$$\langle R^2 \rangle = 2\ell_o L + 2\ell_o^2 (e^{-L/\ell_o} - 1), \quad (2.8)$$

where contour length L can be defined as the maximum end-to-end distance of a linear polymer chain. From eq.(2.8) two limiting behaviors for R can be obtained such as:

For long chains $L \gg \ell_o$ the chain behaves like a flexible one and $\langle R^2 \rangle \cong 2\ell_o L$.

For short chains $L \ll \ell_0$ the chain behaves like a rigid rod and $\langle R^2 \rangle \approx L$.

Comparison of the scaling of FRC with the FJC (where $\ell_0=0$) in eq (2.1) shows that flexible chains can be described by a semi-flexible FJC model when $a \approx \ell_0$ and $N \approx L/\ell_0$. For stiff chains ℓ_0 tends to L .

2.1.1.3 Real polymer chain and the Self Avoiding Walk

In the FJC and FRC models, the polymer chain is allowed to intersect itself (each link is a volume-less vector). In real polymer molecules, the monomer units occupy a given volume and the chain cannot cross itself. We thus have a Self-Avoiding Walk (SAW)

The mathematics of a SAW are more complex than that for a RW. Instead of the expression $\langle R^2 \rangle^{1/2} = a(N)^{1/2}$, in a SAW $\langle R^2 \rangle^{1/2} = a(N)^\nu$ where $\nu > 0.5$

The fact that two polymer segments cannot be in the same place at the same time leads to a repulsive interaction called the excluded volume interaction.

The simplest model was developed by Flory^{6,7} and takes into account both the repulsive interactions due to excluded volume (which swells the chain) and the elastic energy, which makes the polymer adopt the state of maximum entropy (maximum entropy implies collapse of chains). The total free energy of a chain is given by

$$\frac{F_T(R)}{k_B T} = F_{rep} + F_{el} = \nu \frac{N^2}{2R^3} + \frac{R^2}{Na^2}, \quad (2.9)$$

where T is the absolute temperature and ν is the excluded volume constant. By minimizing the total free energy F_T with respect to R we find

$$\langle R \rangle \propto N^{3/5}. \quad (2.10)$$

Polymer coils, which have excluded volume, are said to be 'perturbed' (R_{SAW}) while the assumption of volume-less monomers gives 'unperturbed' dimensions (R_{RW}).⁸ Both dimensions are related to each other by the linear expansion factor α as follows

$$\langle R_{SAW}^2 \rangle^{1/2} = \alpha \langle R_{RW}^2 \rangle^{1/2}. \quad (2.11)$$

2.1.1.4 Self-consistent mean Field Theory

The Flory theory is applicable to isolated polymer chains. In the more complicated case of concentrated solutions, interactions between chains need to be accounted for by a Mean Field Theory (MFT). Such theory is built around the concept of a test polymer, which moves in the mean field generated by the other polymers in the system.

Consider an ideal polymer chain (no excluded volume considered) as a random walk with N steps of statistical length a (Fig. 2.1). For such a chain, a distribution function Γ can be defined in order to know the probability that the chain started at a position R and finished at R' . The distribution function of a random walker in space obeys a diffusion equation,⁹ (a diffusion equation can be written as $\partial\phi/\partial t = D\nabla^2\phi$, where $\phi(r,t)$ is the density of the diffusing material, t is time and D is the constant diffusion coefficient). Consequently for an ideal isolated chain a diffusion expression can be applied as

$$\frac{\partial\Gamma(R,R',N)}{\partial N} = \frac{a^2}{6}\nabla^2\Gamma(R,R',N), \quad (2.12)$$

where the diffusion coefficient given by $a^2/6$ in the right side of the equation, relates to the square of the Kuhn length a .

When the random walk is affected by a spatially dependent potential $U(R)$, eq (2.12) has to be modified since the statistical weights of different possible steps are uneven via a Boltzmann factor. The altered diffusion equation can be written as

$$\frac{\partial\Gamma(R,R',N)}{\partial N} = \frac{a^2}{6}\nabla^2\Gamma(R,R',N) - \frac{U(R)}{k_B T}\Gamma(R,R',N). \quad (2.13)$$

This is the basic equation of the self-consistent field theory and was first developed by Helfand and Tagami in 1972.¹⁰

In an interacting system, each component i.e. each polymer chain positioned at certain R will be under a potential $U_i(R)$ (whose form can be known if the positions of the other polymer chains in the system are known) and have a distribution function Γ_i ; obeying eq (2.13). As a result there are as many differential equations as chains are present in the system, yielding an unsolvable system of coupled equations. However, the system can be simplified by assuming that every polymer chain of the same chemical type experiences an average, mean-field potential $U(R)$.

The assumption of this mean field potential is called mean-field theory and has overcome most of the complexity of eq.(2.13).

2.1.2 Polymers in Solution

2.1.2.1 Good and bad solvent and the theta condition

The conformation of a polymer chain in solution depends on the solvent quality, concentration and temperature. In order to take into account the solvent quality, interaction between polymer segments and neighbouring solvent molecules must be considered. The segment-solvent interaction is conveniently described by the Flory-Huggins interaction parameter^{11,12} χ as

$$\chi = \frac{1}{2k_B T} z(2\varepsilon_{ps} - \varepsilon_{pp} - \varepsilon_{ss}), \quad (2.14)$$

where z is the number of close neighbours for each solvent molecule or polymer segment. ε_{ps} is the energy of interaction between a neighbouring polymer and a solvent segment, and ε_{pp} and ε_{ss} are the energy of interaction between two neighbouring polymers and two solvent molecules respectively. The total interaction energy can be written as a function of the end-to-end chain size as ²

$$U_{\text{int}} = -k_B T 2\nu\chi \frac{N^2}{2R^3} + U_{\text{int}}(0), \quad (2.15)$$

where the dependence on R^3 is equal to that found in the repulsive term F_{rep} of the total free energy given in equation (2.9). Upon combining F_{rep} in eq.(2.9) and eq.(2.15) an expression regarding the excluded volume and solvent interactions attractive energy can be obtained as

$$F_{\text{rep}} + U_{\text{int}} = k_B T \nu(1 - 2\chi) \frac{N^2}{2R^3}. \quad (2.16)$$

The quality of the solvent depends on the value of χ :

a) $\chi < 1/2$: The repulsive free energy dominates in eq.(2.16), therefore the statistical interaction between the units of a polymer chain is repulsive. Chain segments prefer to be surrounded by solvent molecules rather than other polymer segments. In order

to maximise the number of segment-solvent contacts the polymer chain expands with a radius $R \sim N^{3/5}$. This is referred to as 'good solvent' behaviour. In such conditions the expansion factor α (eq (2.11)) is greater than 1. χ may be negative.

b) $\chi=1/2$: The repulsive free energy is the same as the energy due to polymer/solvent interactions and they cancel. The polymer chain is an ideal random walk, with $R \sim N^{1/2}$. This is known as the '*theta condition*'. From eq.(2.11) in theta condition $\alpha=0$.

c) $\chi>1/2$: The attractive term due to polymer/solvent interactions dominates in eq.(2.16) with respect to the repulsive term. The chain segments prefer to be surrounded by other chain segments rather than by solvent molecules. In order to minimize the contact between polymer-solvent segments, the chain collapses to form a globule. This condition is known as '*poor solvent*'. From eq.(2.11) in 'poor solvent' condition $\alpha<1$. In the case of very '*poor solvent*' conditions $R \sim N^{1/3}$.

2.1.2.2 Concentration regimes: dilute, semidilute and concentrated

The interaction between polymer molecules in solution depends strongly on concentration. Concentration regimes can be separated into three categories: dilute, semidilute and concentrated.

In dilute solutions the polymer chains are well separated and they do not interact with each other. Each chain can be considered as a sphere of radius R occupying a finite volume $V \sim R^3$. As the concentration of polymer c is increased, a point is reached where the coils begin to be densely packed and as a result they overlap. This threshold is called the coil overlap concentration c^* . Such a threshold is not sharp; it is more like a region of crossover between the dilute and semidilute regimes.¹ It is expected from c^* to be comparable with the average concentration inside a coil as

$$c^* \approx \frac{N}{R^3} = a^{-3} N^{1-3\nu}, \quad (2.17)$$

where in a good solvent $c^* \approx N^{4/5}$ ($c^* \approx \frac{N}{(N^{3/5})^3}$), while in a theta solvent $c^* \approx N^{1/2}$

($c^* \approx \frac{N}{(N^{1/2})^3}$).¹ It is convenient to express the threshold in terms of the polymer

volume fraction Φ because for a polymer in the absence of solvent $\Phi=1$. As well as in concentration Φ^* is defined as the overlap volume fraction. For large values of N , Φ^* is very small, for instance if $N \sim 1000$ then in a good solvent $\Phi^* \sim 10^{-3}$. Since $\Phi^* \ll 1$, the overlap already occurs at very low polymer fraction.

In semidilute solutions $\Phi^* \ll \Phi \ll 1$, the coils are overlapping and entangled. The existence of the regime of semidilute polymer solutions is a specific polymer feature, for low molecular mass solutions such a regime does not exist because small molecules cannot 'overlap'.

When the chains swell in good solvent above the overlap c^* or Φ^* the solution enters the concentrated regime, where the density fluctuations become very small. As the polymer concentration increases in the region $c > c^*$, the coil swelling gradually diminishes and finally it vanishes in the melt (coils are ideal in the melt, $R \sim N^{1/2}$).

A diagram of polymer chains in dilute, semi-dilute and concentrated solutions is sketched in Fig.2.3.

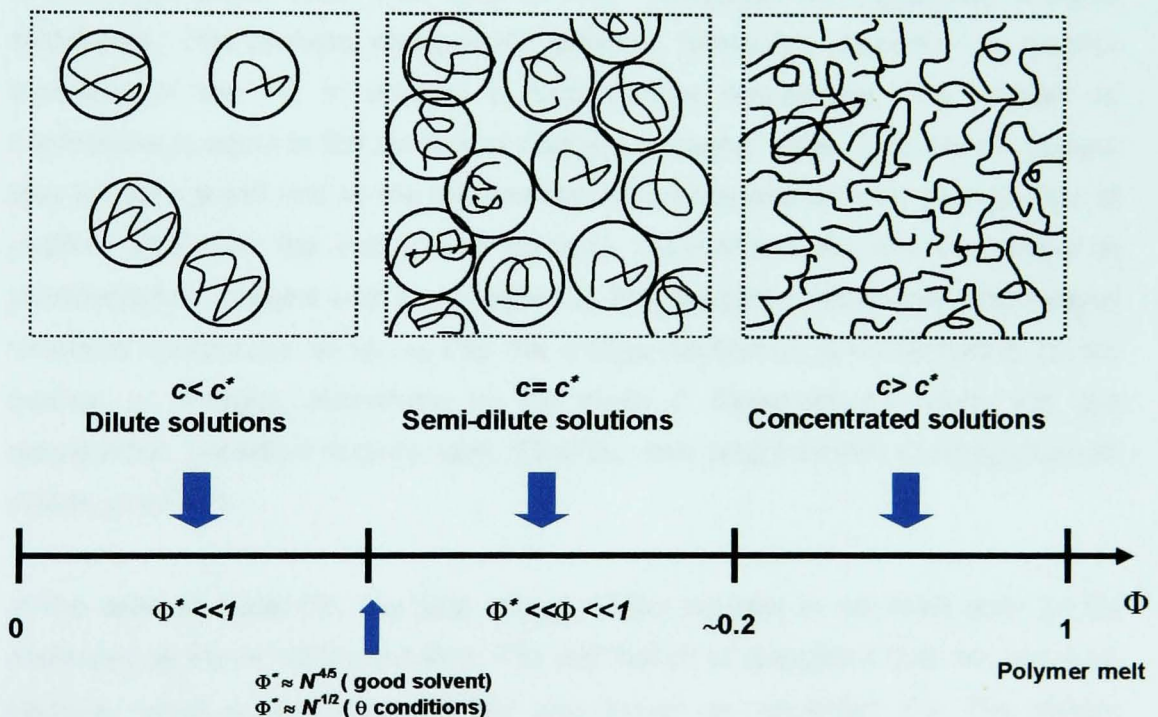


Fig. 2.3 Schematic diagram of the arrangement of polymer chains in different concentration regimes : dilute, semi-dilute and concentrated. The concentration where the polymer coils start to overlap is c^* . It is also shown the crossover between the regimes as a function of polymer volume fraction Φ .

2.2 CHARGED POLYMERS: POLYELECTROLYTES

2.2.1 Introduction.

A polyelectrolyte (PE) is a polymer where a fraction f of its monomers is charged. When PE are dissolved in solution, they dissociate into charged polymer chains and a cloud of free, mobile counterions carrying opposite charges. Such macromolecules appear in numerous industrial applications as well as in biological systems.

When the charge fraction f is not fixed but varies depending on external factors such as the pH of the solution and added-salt concentration, the PE is weakly charged. When the number of charged units f is fixed the polyelectrolyte is strongly charged. This charged structure is referred to as the polyion.¹³

In the case of a strong PE, the total charge as well as its specific distribution along the chain is fixed and imposed by chemistry, i.e. by polymer synthesis. In the polymerisation process strong acidic and neutral monomers are used as building blocks. The acidic monomers dissociate into positively charged protons (H^+) upon contact with water. Such ions bind to water molecules and negatively charged monomers. This process charges the polymer molecules, however the electro-neutrality of the PE in solution is kept by the counterions. The number of counterions is equal to the number of charged monomer units. Typically the solvent also contains a salt and so the total number of counterions is f plus the numbers of positive ions from the salt (called co-ions). Counterions are always present in polyelectrolyte systems and are attracted to the charged polymers via long-ranged Coulomb interactions. In strong PEs the charge distribution is characterized by the fraction of charged monomers in the chain f . Examples of strong PE are poly(styrene sulfonate sodium salt) (PSSNa) and poly(4-vinyl-N-methylpyridinium iodide) (MePVP).

In the case of weak PE, the total charge of the polymer is not fixed and can be controlled by the pH of the solution. The distribution of charges is then an annealed variable, which is why weak PE are also known as 'annealed' PE. The charge distribution along a weak PE is not homogeneous due to chain end-effects and the non-homogeneous distribution of monomers in solution.¹⁴ Examples of weak polyelectrolytes are the polyacid poly(methacrylic acid) (PMAA) and polybase poly((diethylamino)ethyl methacrylate) (PDEAMA).

A schematic picture of a polyelectrolyte molecule in solution is shown in Fig.2.4

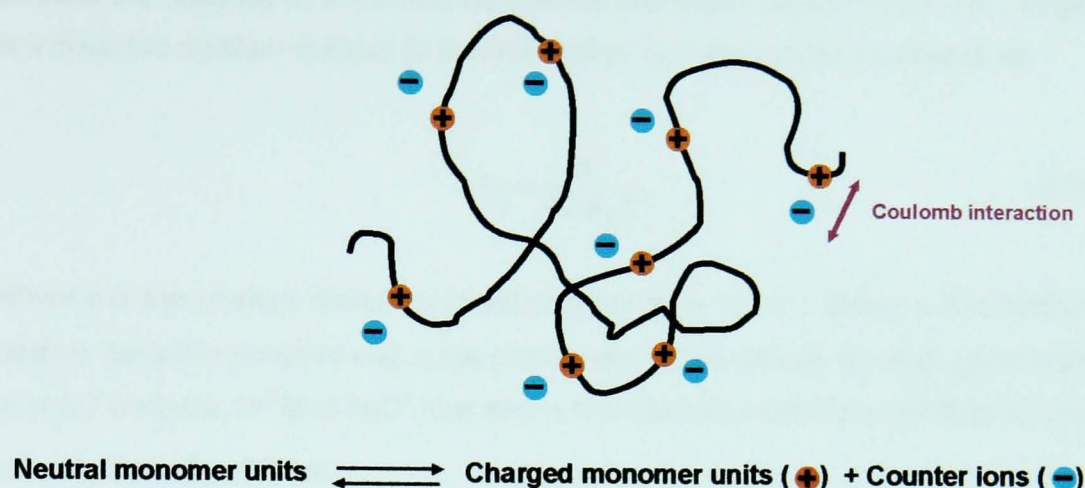


Fig. 2.4 Schematic diagram of a positively charged polyelectrolyte in solution. It is shown a counterion unit for each charged monomer unit

Another classification of PE can be made according to the type of charges. Following this classification there are anionic and cationic PE, and polyampholytes which is a PE containing both anionic and cationic groups.

2.2.2 Interaction between charged objects

In the previous section it has been shown how excluded volume effects are the only important interactions in neutral polymers. The statistics of PE chain conformation is governed by intra-chain Coulomb repulsion between charged monomers, as a consequence the conformation of PE is more extended and swollen than that of neutral polymer chains. In the case of weakly charged PE due to the small fraction of links charged, the Coulomb interactions interplay with van-der-Waals interactions of uncharged links. In strongly charged PEs, the only interaction to consider is the Coulomb interaction due to the large fraction of charged monomers.

In general, the electrostatic interactions $F_{electrostat}$ between two point-like charges separated by a distance r can be expressed as

$$F_{electrostat}(r) = z_1 z_2 V_{el}(r) = z_1 z_2 \frac{\ell_B}{r}, \quad (2.18)$$

where z_1 and z_2 are the valencies or reduced charges in units of the elementary charge e ($e = 1.6022 \times 10^{-19}$ C); $V_{el}(r)$ is the Coulomb interaction between two

elementary charge in units of $k_B T$ and ℓ_B is the Bjerrum length. The Bjerrum length denotes the distance at which the Coulombic interaction between two unit charges in a dielectric medium is equal to thermal energy $k_B T$ and can be expressed as

$$\ell_B = \frac{e^2}{4\pi\epsilon k_B T}, \quad (2.19)$$

where ϵ is the medium dielectric constant given by $\epsilon = \epsilon_0 \epsilon_r$ (ϵ_r being the medium relative dielectric constant and ϵ_0 the permittivity in free space). In water (pure water at pH=7 contains 10^{-7} M of H_3O^+ ions and is therefore an electrolyte solution) at room temperatures $\ell_B \approx 0.7$ nm.

2.2.3 Poisson Boltzmann and Debye-Hückel Theory

A mean field theory approach to describe the distribution of counterions in PE solution results in the Poisson-Boltzmann (PB) equation;¹⁵⁻¹⁷ that is, the local electrostatic potential $\Psi(r)$ at a distance r from the charge point is assumed to satisfy the Poisson equation of electrostatics as

$$\nabla^2 \langle \Psi(r) \rangle = -\frac{e}{\epsilon} \sum_i n_i z_i \exp\left(-\frac{z_i e \langle \Psi(r) \rangle}{k_B T}\right), \quad (2.20)$$

where n_i is the molar concentration of the i -th ion and z_i is the valence or charge of the i -th ion with the convention that $z_i < 0$ for counterions and $z_i > 0$ for co-ions. Solutions of the non-linear PB equation (2.20) have been studied by Chapman¹⁸, Gouy¹⁹ and Debye and Hückel²⁰. Debye and Hückel made an important contribution to the theory of electrolytes by approximating eq (2.20) to a linearized form called the Debye-Hückel equation

$$\nabla^2 \langle \Psi_{DH}(r) \rangle = \frac{1}{(\kappa^{-1})^2} \langle \Psi_{DH}(r) \rangle, \quad (2.21)$$

where Ψ_{DH} is the Debye-Hückel potential and κ^{-1} is the Debye length (also known as screening length). κ is given by

$$\kappa = \left(\frac{8\pi e^2 I}{\epsilon k_B T} \right)^{1/2} = (8\pi \ell_B I)^{1/2}, \quad (2.22)$$

where I is the solution ionic strength expressed as

$$I = \frac{1}{2} \sum_i n_i z_i^2. \quad (2.23)$$

In biological systems, the aqueous solution usually contains mobile salt ions. Salt ions of opposite charge are attracted by the system formed by charged monomers and counterions. The effective (screened) electrostatic interaction $F_{DH}(r)$ between two charges $z_1 e$ and $z_2 e$ in the presence of salt ions and a polarizable solvent can be written as Coulomb interactions (in units of $k_B T$) in the Debye-Hückel approximation as

$$F_{DH}(r) = z_1 z_2 \Psi_{DH}(r) = z_1 z_2 \frac{\ell_B}{r} \exp(-\kappa r). \quad (2.24)$$

The main assumption used in the derivation of Debye-Hückel potential is the relative weakness of the Coulomb interactions. The Debye-Hückel potential becomes inaccurate when the interaction between ions exceeds the thermal energy, at this point non-linear effects become important.

2.2.4 Counterion Condensation

The behaviour of polyelectrolytes in solution is governed by the electrostatic interactions between the polyions and low molecular ions in solution (counterions and ions of added salt). The behaviour exhibited by such polyelectrolyte systems differs from the behaviour of neutral polymers and small electrolytes in solution.

The PB distribution fails qualitatively in highly charged polyelectrolytes due to the long-range character of Coulomb interactions. When the charge density of a rod-like polymer exceeds the critical value of one electron charge e per Bjerrum length ℓ_B , the electrostatic attraction of the polymer to its counterions becomes so strong that a certain fraction of the latter condenses onto the polymer and effectively reduces its charge density. Such a phenomenon was first predicted by Manning and Oosawa^{13,21-23} and it is also named as Manning condensation.

Consider a single rigid PE chain represented by an infinitely long and straight cylinder with a linear charge density ρ . A typical linear charge density reached with synthetic PE is one charge per two carbon bonds, or equivalent one charge per monomer $\rho = e/a$. For example for PMAA $\rho \approx 3\text{nm}^{-1}$ ($a \approx 0.3\text{nm}$). In the initial state the counterions are confined in the cylinder of radius r_1 ; in the final state they are confined with the cylinder of radius r_2 (Fig 2.5). This model does not take in account several effects such as the interaction between polyions, the flexibility degrees of freedom of the polyion and finite size effects.

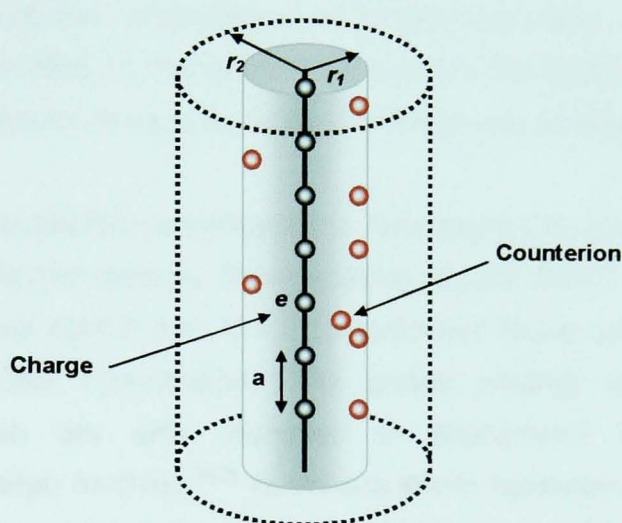


Fig. 2.5 Schematic diagram of a single rigid PE chain represented by an infinitely long and straight cylinder with a linear charge density $\rho = e/a$, where a is the separation between charges and e are the charges. In this model, the counterions (red molecules) go from an initial position r_1 to a final position r_2 . For more clarity added salt ions are omitted in the picture.

The total free energy involved in the process shown in (Fig 2.5) comprises two terms: the decrease in the average energy of attraction of counterions to the charged line given by $\Delta E \approx e \frac{\rho}{2\pi\epsilon} \ln\left(\frac{r_2}{r_1}\right)$ with $r_2 > r_1$ and the gain in the entropy of translation motion as $\Delta S \approx \ln\left(\frac{V_2}{V_1}\right) \approx 2\ln\left(\frac{r_2}{r_1}\right)$. The expression for the total free energy is as follows

$$\Delta F = \Delta E - k_B T \Delta S \approx \left(e \frac{\rho}{4\pi\epsilon k_B T} - 1 \right) 2k_B T \ln\left(\frac{r_2}{r_1}\right) = \left(\frac{\ell_B}{a} - 1 \right) 2k_B T \ln\left(\frac{r_2}{r_1}\right), \quad (2.25)$$

where $\frac{\ell_B}{a}$ is defined as the Manning parameter ξ . When $\xi < 1$ the gain in entropy is the most important contribution in eq. (2.25) and as a result, the counterions go to infinity (in Fig. 2.5 $r_2 \rightarrow \infty$). When $\xi > 1$ the term due to energy of attraction between charges dominates in (2.24), thus the counter ions approach the charge line and 'condense' on it. The condensed fraction is just sufficient to reduce the net charge density until an effective charge density is reached $\rho_{\text{eff}} = e / \ell_B$. When such an effective density is reached, the Manning parameter is at its critical value $\xi = \xi_c = 1$, at this stage the number of 'condensed' counterions neutralizes the charge of the line to such extent that the condensation of counterions stops. All the remaining counterions are floating in the solution. It can be concluded then that in the presence of counterions, there is a threshold in the charge density given by ρ_{eff} .

The concept of counterion condensation is fundamental to our understanding of highly charged polymer systems. Such systems include DNA²⁴ in both its double and single-stranded ($\xi=4.2$ and $\xi=1.7$ respectively) forms and many synthetic polyelectrolytes. DNA hybridization, DNA protein binding, and polyelectrolyte surface adsorption are also examples of phenomena where counterion condensation is deeply involved.^{24,25} Numerous efforts have been made to describe the interactions between polyions and its counterions as well as the distribution function of such counterions in solution based on Manning's theory. The cell model^{26,27} and the cluster model²⁸⁻³¹ are attempts to solve the counterion condensation problem. For example, in the cell model, the total solution can be partitioned into cells, each containing one polyion with the right amount of counterions to render the cell neutral, and probably salt molecules too. Since each cell is neutral, electrostatic interactions between them are neglected. Assuming a homogeneous distribution of polyions, the cells will have approximately the same volume. The cell model approximation consists in restricting the theoretical description of the total system to just one cell. In this way, the many polyelectrolyte problem is replaced by a one-polyelectrolyte problem.

Despite these models accurate analytical solutions have not been obtained (the PB theory is generally considered to be better) and the structure and thickness of the condensate and what precisely distinguishes it from the free (uncondensed) ions remains unsettled. This makes the theoretical understanding of polyelectrolyte systems to be less developed than the understanding of the properties of neutral polymers.

2.2.5 Persistence length in polyelectrolyte solutions

The first breakthrough in treating semiflexible PEs analytically was made by Odijk³² and independently by Skolnick and Fixman³³ by introducing the concept of an “*electrostatic persistence length*” l_e . The notion of persistence length which measures correlations along the chain, is very useful in describing elastic properties of semiflexible polymers in general, and PEs in particular. The Odijk, Skolnick and Fixman theory (OSF) considered a stiff PE chain near the rod limit so that only small excursions from linear conformation are relevant. Electrostatic interactions are treated on a mean-field level and the assumption of uniformly distributed charges on the polymer is made. Within a linearized version of the Poisson-Boltzmann theory, the interaction between any two charges on the rod-like PE is screened and given by the Debye-Hückel expression (eq (2.21)).

According to the OSF theory, the total persistence length of the polymer l_t can be written as a sum of two contributions: the bare persistence length l_o (of the equivalent uncharged chain) and an electrostatic one l_e as

$$l_t = l_o + l_e = l_o + \frac{l_B}{4\kappa^2 a^2}, \quad (2.26)$$

where $\frac{l_B}{4\kappa^2 a^2} = l_{OSF} = l_e$ is the electrostatic persistence length according to OSF theory, a denotes the average distance between charges along the chain, l_B is the Bjerrum length and κ is the inverse of the Debye length. Equation 2.26 is only valid for polymer conformations which do not deviate too much from the rod-like reference state (stiff chains) and for weakly charged polymers; for this expression the electrostatic persistence length decreases inversely proportional with the increase in the solution ionic strength I since $l_{OSF} \sim \kappa^{-2} \sim I^{-1}$.

Many experiments on polyelectrolytes have been interpreted using the OSF theory for intrinsically very stiff polyelectrolytes, like DNA³⁴ and poly(xylylene tetrahydrothiophenium chloride).³⁵ Although it has been claimed that the theory is also valid for long, flexible chains,^{36,37} light scattering experiments on some flexible polyelectrolytes systems do show deviations from the OSF theory pointing towards a linear relation $l_e \sim \kappa^{-1}$.³⁸⁻⁴⁰ An objection to the OSF theory is the neglect of entropy. Taking this into account, Barrat and Joanny⁴¹ (BJ) showed, via computational

calculations,^{42,43} that when the chains are intrinsically flexible, the electrostatic persistence length also yields the linear relation $l_e \sim \kappa^{-1}$.

Since the OSF theory is strictly a mean-field theory, the effective interaction between charges on the polymer is always repulsive.^{44,45} Indeed, eq.(2.26) indicates that the polymer becomes more rigid (favouring a stretched chain conformation) due to electrostatics because $l_{OSF} > 0$. However, under some conditions experiments have shown that electrostatics may cause a reversed effect^{46,47} where enhanced chain flexibility results from a negative electrostatic contribution to the total persistence length. In order to consider such behavior, corrections to linearized Poisson-Boltzmann theory have been considered.^{44,45,48} Such corrections take into account the effect of counterion condensation, the correlations between the ions (which become more significant at lower temperatures) and thermal fluctuations of the counterion density.⁴⁸

The validity of eq.(2.26) for chains that are intrinsically flexible has also been questioned using computer simulations. Such simulations usually show deviations from the OSF theory, and the exponent p in $l_e \sim \kappa^{-p}$ may vary from 1.5,⁴⁹ down to 0.3–0.9.⁵⁰ However results with $p \approx 1$, in agreement with experiment, have also been reported.^{51,52} At the present time there is still not available a simple theory for computing l_e for charged polymer chains with arbitrary stiffness.

2.2.6 Electrostatic Excluded Volume

In this section the self-avoidance of strongly charged polyelectrolyte chains is considered. For short chains where length $L \ll l_t$, the end-to-end radius grows linearly with the length $R \sim L$. In this case of short chains, self-avoidance does not play a significant role.

In the case of long flexible PE, where $L \gg l_t$, the electrostatic total free energy F_T^e can be written as for a neutral chain in eq (2.9) using the Flory expression but considering that for long flexible charged chains $a \approx l_t$ and $N \approx L/l_t$

$$\frac{F_T^e(R)}{k_B T} = F_{rep}^e + F_{el}^e \propto v \frac{(L/l_t)^2}{2R^3} + \frac{R^2}{Ll_t}, \quad (2.27)$$

where F_{rep}^e and F_{el}^e refers to the electrostatic repulsive interactions due to electrostatic excluded volume and the electrostatic elastic energy, which makes the polymer adopt the state of maximum entropy. By minimizing the electrostatic free energy F_{τ}^e in eq. (2.27) the optimal R can be calculated as⁴

$$\langle R \rangle \propto L^{\nu}, \quad (2.28)$$

where $\nu=3/5$ which is the semi-flexible analogue of eq. (2.10).

2.2.7 Dilute polyelectrolyte solutions

As we have discussed for neutral polymer chains in section 2.1.2.3, the dilute regime is defined by $c < c^*$ where c and c^* are polymer concentration and coil overlap concentration respectively. For semi-flexible PEs in dilute regime, the osmotic pressure (in terms of $k_B T$) is given by

$$\Pi = \frac{fc}{z} + \frac{c}{N}, \quad (2.29)$$

where f is the fraction of charged monomers in a polymer chain. The first term in eq.(2.29) is the ideal pressure of non-interacting counterions. The second term relates to the ideal pressure made by the polymer coils and, since this term behaves as $\sim N^{-1}$, it can be neglected for large N . The osmotic pressure in dilute solution of PE comes mainly from counterion entropy; which explains why PEs can be dissolved in water even when their backbone is very hydrophobic.

For neutral polymer chains there are no counterions in solution therefore in dilute conditions, the osmotic pressure is given by the second term in eq (2.29).

REFERENCES

- (1) de-Gennes, P. G. *Scaling Concepts in Polymer Physics*, 5th ed.; Cornell University Press: New York, 1996.
- (2) Jones, R. A. L. *Soft Condensed Matter*, Oxford University Press: Oxford, 2002.
- (3) Grosberg, A. Y.; Khokhlov, A. R. *Statistical Physics of Macromolecules*: New York, 1994.
- (4) Netz, R. R.; Andelman, D. *Physics Reports* **2003**, *380*, 1-95.

- (5) Yu, A.; Grosberg, A. R.; Khokhlov, A. R. *Statistical Physics of Macromolecules*; AIP Press: New York, 1994.
- (6) Flory, P. J. *Statistical Mechanics of Chain Molecules*; Oxford University Press: Oxford, 1989.
- (7) Flory, P. J. *Principles of Polymer Chemistry*; Cornell University Press: New York, 1969.
- (8) Hamley, I. *Introduction to Soft Matter*, 2nd. ed.; J. Wiley: Chichester, 2000.
- (9) Einstein, A. *Annalen der Physik* **1906**, *19*, 371-381.
- (10) Helfand, E.; Tagami, Y. *J. Chem. Phys* **1972**, *56*, 3592-3601.
- (11) Huggins, M. J. *Am. Chem. Soc.* **1942**, *64*, 1712-1719.
- (12) Huggins, M. J. *J. Chem. Phys* **1941**, *9*, 440.
- (13) Oosawa, F. *Polyelectrolytes*; Marcel Dekker: New York, 1971.
- (14) Holm, C.; Joanny, F. J.; Kremer, K.; Netz, R. R.; Reineker, P.; Seidel, C.; Vilgis, T. A.; Winkler, R. G. *Adv. Polym. Sci* **2004**, *166*, 67-111.
- (15) Katchalsky, A.; Alexandrowicz, Z.; Kedem, O. *Chemical Physics of Ionic Solutions*, Conway BE, Barradas RG (eds) ed.; Wiley: New York, 1966.
- (16) Quian, H.; Schellman, J. A. *J. Phys. Chem B* **2000**, *104*, 11528-11540.
- (17) Fixman, M. *J. Chem. Phys* **1979**, *70*, 4995-5005.
- (18) Chapman, D. L. *Philos. Mag* **1913**, *25*, 475-468.
- (19) Gouy, G. *J. Phys(France)* **1910**, *9*, 457-468.
- (20) Debye, P.; Huckel, E. *Phys. Z.* **1923**, *24*, 185-206.
- (21) Manning, G. S. *J. Chem. Phys* **1969**, *51*, 3249.
- (22) Manning, G. S. *J. Chem. Phys* **1969**, *51*, 934.
- (23) Manning, G. S. *J. Chem. Phys* **1969**, *51*, 924.
- (24) Bloomfield, V. A.; Crothers, D. M.; Tinoco, I. J. *Nucleic Acids: Structures, Properties, and Functions*; University Science Press: New York, 2000.
- (25) Gast, F. U.; Hagerman, P. J. *Biochemistry* **1991**, *30*, 4268-4277.
- (26) Yoshida, N. *J. Chem. Phys* **1978**, *69*, 4867-4871.
- (27) Deserno, M.; Holm, C. *Arxiv preprint cond-mat/0112096* **2001**.
- (28) Gueron, M.; Weisbuch, J. *J. Phys. Chem* **1979**, *83*, 1991-1998.
- (29) Kuhn, P. S.; Levin, Y.; Barbosa, M. C. *Macromolecules* **1998**, *31*, 8347-8355.
- (30) Schiessel, H. *Macromolecules* **1999**, *32*, 5673-5680.
- (31) Schiessel, H.; Pincus, P. A. *Macromolecules* **1998**, *31*, 7953-7959.
- (32) Odijk, T. *J. Polym. Sci* **1977**, *15*, 477-483.
- (33) Skolnick, J.; Fixman, M. *Macromolecules* **1977**, *10*, 944-948.
- (34) Maret, G.; Weill, G. *Biopolymers* **1983**, *22*, 2727-2744.
- (35) Mattoussi, H.; O'Donohue, S.; Karasz, F. E. *Macromolecules* **1992**, *25*, 743-749.
- (36) Odijk, T.; Houwaart, A. C. *J. Polym. Sci, Polym. Phys. Ed.* **1978**, *16*, 627-639.
- (37) Khokhlov, A. R.; Khachaturian, K. A. *Polymer* **1982**, *23*, 1742.
- (38) Foster, S.; Schmidt, M.; Antonietti, M. *J. Phys. Chem.* **1992**, *96*, 4008-4012.
- (39) Tricot, M. *Macromolecules* **1984**, *17*, 1698-1704.
- (40) Degiorgio, V.; Mantegazza, F.; Piazza, R. *Euophys. Lett.* **1991**, *15*, 75.
- (41) Barrat, J. L.; Joanny, J. F. *Euophys. Lett.* **1993**, *24*, 333-338.
- (42) Ha, B. Y.; Thirumalai, D. *Macromolecules* **1995**, *28*, 577-581.
- (43) Bratko, D.; Dawson, K. A. *J. Chem. Phys* **1993**, *99*, 5352-5361.
- (44) Fixman, M. *J. Chem. Phys* **1982**, *76*, 6346-6353.
- (45) Bret, M. L. *J. Chem. Phys* **1982**, *76*, 6243-6255.
- (46) Walczak, W. J.; Hoagland, D. A.; Hsu, S. L. *Macromolecules* **1996**, *29*, 7514-7520.
- (47) Hugel, T.; Grosholz, M.; Clausen-Schaumann, H.; Pfau, A.; Gaub, H.; .. M. S. *Macromolecules* **2001**, *34*, 1039-1047.
- (48) Golestanian, R.; Kardar, M.; Liverpool, T. B. *Phys. Rev. Lett* **1999**, *82*, 4456-4459.
- (49) Seidel, C. *Macromol. Theory Simul.* **1994**, *3*, 333-346.

- (50) Micka, U.; Kremer, K. *Phys. Rev. E* **1996**, *54*, 2653-2662.
- (51) Reed, C. E.; Reed, W. F. *J. Chem. Phys* **1991**, *94*, 8479.
- (52) Seidel, C.; Schlacken, H.; Muller, I. *Phys. Chem* **1996**, *100*, 175.

Chapter 3

Polyelectrolyte Systems: Brushes and Hydrogels

Many properties of polyelectrolyte solutions are not dominated by the chain conformations but by the counterions. In this chapter we discuss two examples of this situation: the physics behind polyelectrolyte brushes and polyelectrolyte gels. Together they form the components of our large system under study: polyelectrolyte brush together with polyelectrolyte gel in both good and bad solvent conditions.

For polyelectrolyte brushes, sections containing general approaches for the synthesis of brushes and scaling behaviour of neutral polymer brushes are included for a better understanding of such systems. It follows with the physics behind strong PE brushes and a particularly thorough section of weak PEs, as the study of weak PE brushes is an important component of the present thesis.

As for brushes, for polyelectrolyte gels the present chapter consists of a description of the general physics behind neutral and ionisable (weakly charged) polymer networks. A brief section describing the physical properties of polymer networks is also included.

3.1 INTRODUCTION TO CHARGED SYSTEMS

In both brushes and gels in solution, the polyelectrolyte chains occupy a small region of space surrounded by solvent. This external solvent region acts as a reservoir from which the small ions enjoy the freedom to diffuse in and out of the polyelectrolyte region.

In this scenario of two regions: reservoir and polyelectrolyte a situation of Donnan equilibrium is reached.^{1,2} Donnan equilibrium refers to the unequal distribution of ion species between two ionic solutions separated by a semi permeable membrane or boundary. The boundary layer maintains an unequal distribution of ionic solute concentration by acting as a selective barrier to ionic diffusion e.g. some species of ions may pass through the barrier while others do not.

If the monomer concentration in the polyelectrolyte region is c and the charge fraction is f , then the standard charge density due to the polyelectrolyte is fc . For a salted reservoir solution with ionic strength I the Debye-Hückel screening length is given by κ^{-1} with $\kappa = (8\pi\ell_B I)^{1/2}$. We assume here that the counterion charge $z_i > 0$ (polyion charge < 0 , i.e. a polyacid) is equal to the salt positive ion, consequently the salt negative and positive ion will be confined within the PE and reservoir region respectively.; we call n_+ and n_- the molar concentration of positive and negative ions respectively in the PE region .

There are two parameters that must be considered in charged systems (e.g. PE brushes and gels): the electrostatic potential difference U between the reservoir and the PE section and the chemical potential μ . The chemical potential of a thermodynamic system can be defined as the amount by which the free energy per particle of the system would change if an additional particle were introduced, with the volume kept constant. In the case under study, the system contains more than one species of particle: negative and positive ions, hence there is a separate chemical potential associated with each charge, defined as the change in free energy when the number of particles of that species is increased by one.³

The chemical potential of the ions in the PE region are $\mu_+ = k_B T \ln(n_+) + U$ and $\mu_- = k_B T \ln(n_-) + U$. When these chemical potentials equal the salt chemical potential in the reservoir $\mu = k_B T \ln(n)$ an equilibrium situation is reached. This chemical equilibrium leads to a balance for the ions as $n^2 = n_+ n_-$.

By also considering the electroneutrality of PEs in solutions (section 2.2.1), a second relation can be made as $n_+ = n_- + fc$

The major assumption made here is that the ion densities are uniform. With such an assumption, the electrostatic contribution to the osmotic pressure (eq. (2.29)) is small when compared with the translational entropy of small ions. The osmotic pressure yielded by the Donnan equilibrium is purely entropic and thus independent of the strength of the electrostatic interactions characterised by the Bjerrum length.

3.2 POLYELECTROLYTE BRUSHES

3.2.1 Polymer Brushes: General features.

As discussed above, the term “polymer brush” refers to polymer molecules that are attached by anchor points to a surface in such a way that the graft density of the polymers is high enough that the surface-attached chains become crowded and are stretched away from the surface.⁴ Brushes have received considerable attention in recent years,⁵⁻⁷ due to their totally different behaviour when compared to flexible polymer chains in solution (described in *Chapter 2*) and their wide range of applicability.

We consider a system where the polymers are irreversibly grafted at one of their chain ends to a solid impenetrable substrate. In the presence of solvent, the brush is extended in good solvent conditions. On the contrary, in poor solvents, brushes tend to collapse to exclude solvent; for very poor solvents the system becomes so collapsed that it behaves like a dry polymer brush.

We shall limit our discussion to good solvent conditions. The absence of any attractive interactions between the surface (substrate) and the polymer chains is assumed. The conformation of polymer brushes is dependent upon two parameters: the number of monomers in the chain N and the average distance between polymer chains d . Another important parameter in such systems is the dimensionless grafting density σ , which can be defined as the number of chains grafted in an area the square of the segment size a^2 as

$$\sigma = \frac{a^2}{d^2}. \quad (3.1)$$

Assuming good solvent conditions means that in dilute solutions the chains would have a radius of gyration given by the Flory equation $R_F \sim aN^{3/5}$. According to the grafting density of the attached chains we can have two basic cases:

a) For small grafting densities such that the average distance between anchor points is greater than the radius of gyration ($d > R_F$) the polymer chains will be far apart from each other and not interact. In this case, each chain will be isolated from its neighbours; as a result they adopt a typical random coil that is linked to the surface through a “branch” of varying size. For such a situation, the term “mushroom” conformation is used. The dimensions of such mushrooms are

comparable to the radius of gyration of the free chains as shown schematically in Fig. 3.1(a). The brush can be treated then like an isolated brush (single chain) in a good solvent, such situation is analogous to the regime of dilute solution described in the previous chapter.

b) As the grafting density increases ($R_F > d$) the chains start to overlap. Since we assume that the solvent is good, the monomers repel each other. Being fixed the lateral separation between grafted chains, excluded volume interactions make the polymers extend away from the surface in order to avoid each other. Such an arrangement is similar in shape to a 'brush' of vertical height h which exceeds the unperturbed random walk coil radius.^{4,8} A schematic diagram is shown in Fig.3.1 (b) At relatively low grafting densities the brush in solution is in semi-dilute condition, by a progressive increase of the monomer density the concentrated regime is reached.

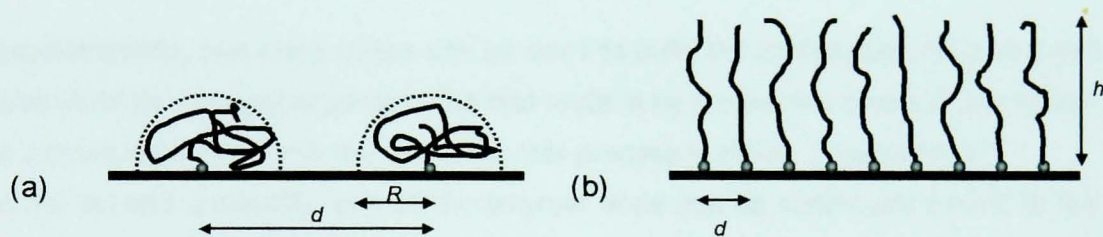


Fig. 3.1 Schematic diagram of the conformation adopted by grafted polymer chains dependent on the distance d between the grafting points: (a) the 'mushroom' conformation where the distance $d \sim \sigma^{1/2}$ between chains is larger than the radius of gyration of the polymer coil. (b) the 'brush' conformation, where the distance between chains is larger than the unperturbed polymer size. The chains are stretched from the surface due to repulsive interactions between monomers reaching a height h .

The limit of low σ after which the polymer chains start to interact (the threshold between a) and b) situations) is simple to find.⁹ Assuming that each chain occupies a hemisphere (Fig. 3.1(a)) with a radius comparable to the Flory radius for a coil in good solvent $R_F \sim aN^{3/5}$, the different coils do not overlap when $R_F < d$, using equation (3.1) we find

$$\frac{R_F}{d} < 1 \Rightarrow \frac{R_F \sigma^{1/2}}{a} < 1 \Rightarrow \sigma < N^{-6/5}. \quad (3.2)$$

The result from eq.(3.2) yields the threshold grafting density as $\sigma^* \sim N^{-6/5}$. Such threshold separates 'mushroom conformation' for $\sigma < N^{-6/5}$ from 'brush conformation' for $N^{-6/5} < \sigma$.

A special case of polymer brushes is brushes formed by charged polymers grafted to a surface, they are called polyelectrolyte or charged brushes and they will be discussed in detail below.

3.2.2 Synthesis of Polymer brushes

A requisite for forcing polymer molecules into brush-like conformations is that the strength of anchoring of the molecules to the interface is sufficiently high that the molecules are connected irreversibly to the surface of the substrate. A second requirement is that the synthetic approach allows the generation of grafting densities high enough to cause sufficient repulsive monomer–monomer interactions within the surface-attached chains to bring them to stretch. The polymer layer can be constructed in several ways depending of the application in mind.

Experimentally, two main routes can be used to build the end-grafted polymer layer (also valid for charged brushes). The first route is by a selective physical adsorption of a block copolymer with the substrate; this process is called 'physisorption'.⁶

In the second possibility, one of the polymer ends can be chemically bound to the grafting surface leading to an irreversible attachment; this process is called 'chemisorption'.¹⁰⁻¹²

3.2.2.1 *Polymer Brushes via Physisorption.*

Physisorption is a reversible process based on the assembly of block copolymers at a solid surface-liquid interface. A copolymer can be defined as a polymer formed when two (or more) different types of monomer are linked in the same polymer chain. Block copolymers can be defined as a type of copolymers that is made up of blocks of different polymerized monomers.

In physisorption one block adsorbs at the surface and acts like an 'anchor' for the second block. This second block has stronger interactions with the solvent than with the surface and so it floats in the solvent forming the brush layer.

The main drawback of the physisorption method is that the chemical variability of the system prepared by this method is restricted as a solvent must be available in which the block copolymer adsorbs to the surface without formation of micelles.

In addition, as the interaction with the surface is based on long range and weak van der Waals interactions, anchoring of the molecules to the substrate is weaker than

those covalently bounded bringing poor control over polymer chain density and decreasing the film stability.

A scheme of brushes prepared by the physisorption method is shown in fig.3.2



Fig. 3.2 Schematic diagram of brushes prepared by physisorption of block copolymers. The grey sections represent the adsorbed 'anchor' block to the substrate surface. The black sections represent the remaining chains floating in the solvent and away from the grafting surface.

3.2.2.2 *Polymer Brushes via Chemisorption*

Covalent attachment of polymer brushes to the solid substrate can be achieved by either "grafting to" or "grafting from" techniques. Both approaches provide short range and strong bonding between adsorbate and substrate.

a) Polymer Brushes via the 'grafting to' technique

This technique involves tethering preformed end-functionalized polymer chains to suitable chemical substrate groups under appropriate conditions (addition or condensation reactions).¹³

The 'grafting to' method often leads to low grafting density and low film thickness, typically 3~5nm as the polymer molecules must diffuse through the existing polymer film to reach the reactive sites on the surface.^{14,15} The grafting density decreases if high molecular weight polymers are employed because of the kinetic and entropic hindrance from surface attached chains to the chains-to-graft. Another restraint encountered by the 'grafting to' approach is the limited choice of end-functionalization for most polymers.

To overcome the low grafting density problem, the "grafting from" approach can be used and has generally become the most attractive way to prepare thick, covalently tethered polymer brushes with a high grafting density.¹⁶

A scheme of brushes prepared by the 'grafting to' technique is shown in Fig.3.3.

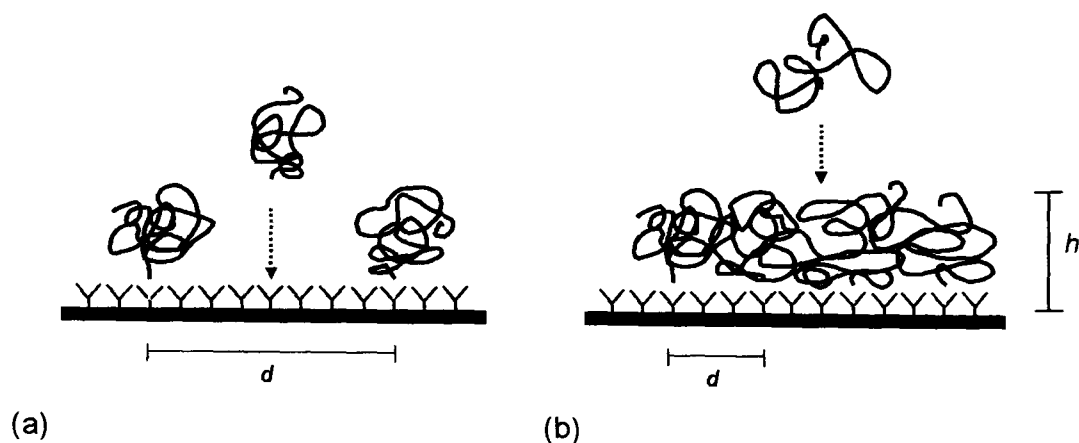


Fig. 3.3 Schematic diagram of the 'grafting to' technique for the attachment of polymer chains, separated by a distance d , to a substrate. (a) Grafting of preformed end-functionalised polymers (black coils with grey ends) to suitable chemical groups located on the substrate surface (Y) (b) Scheme of the hindrance from surface attached chains to the incoming chains, such hindrance increases when polymer film thickness h (\sim molecular weight) increases.

b) Polymer Brushes via the 'grafting from' method

This method provides brushes with high grafting densities and is widely used for making neutral¹⁷⁻²⁰ as well as polyelectrolyte²¹⁻²⁶ brushes. It has been reported that by using a 'grafting from technique', polyelectrolyte brushes can be produced with a grafting density such that the average distance d between high molecular mass neighbouring chains ($M_n > 10^6$ g/mol) is $3 < d < 10$ nm.²¹⁻²³

The "grafting from" approach involves the self-assembly of initiators onto the substrate followed by *in situ* surface initiated polymerization to generate the tethered polymer brush. The initiation of chain growth from the initiators can be performed via free radical polymerisation.^{17-19,21-26} Such surface polymerization can be started thermally either via a chemical process or photochemically.

Recent advances in polymer synthesis techniques has given rise to the importance of controlled "living" free radical polymerization, as it provides several advantages over traditional free radical techniques.²⁷ The main advantage that a "living" free radical system provides for polymer brush synthesis is control over the brush thickness, via control of molecular weight and narrow polydispersities. Numerous "living" free radical techniques have been used to produce polymer brushes. Probably the most common "living" radical technique to produce polymer brushes is atom transfer radical polymerization (ATRP).²⁸⁻³⁰

Biesalski et al have synthesized and characterized strong and weak polyelectrolyte brushes such as poly-*N* methyl-[4-vinylpyridinium]iodide (MePVP)^{21,22} and poly(methacrylic acid) (PMAA) brushes³¹ using an AIBN-analogous initiator system

that can be immobilized on surfaces carrying hydroxyl groups such as silicon wafers and glass substrates.

A schematic diagram of the 'grafting from' method is shown in Fig. 3.4.

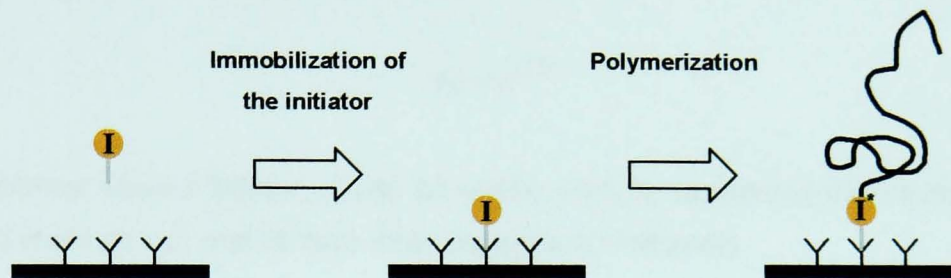


Fig. 3.4 Diagram showing the common synthetic strategy for the generation of polymer brushes via the 'grafting from' approach: surface-initiated polymerization. An initiator molecule (**I**) is deposited on a surface by means of a self-assembly process via the reaction of an anchor group (**Y**) to suitable surface sites, this process is called immobilization of the initiator. After the initiators have been attached, polyelectrolyte chains are grown on the surface from the initiating sites: polymerization process.

3.2.3 The physics of neutral polymer brushes

Consider a polymer brush where the distance between grafted chains is less than its radius of gyration; this is the case of a "brush conformation" as described in section 3.1.1. Considering brushes in good solvent, two regimes can be distinguished: semi-dilute and concentrated solutions.

3.2.3.1 Semi-Dilute conditions and Alexander scaling arguments

In semi-dilute solutions, at relatively low grafting densities, we can use a scaling argument given by Alexander⁸ to find the dependence of the brush height h with the grafting density σ .

A grafted chain may be subdivided into "blobs" of linear size d , each of them containing a number N_b of monomers ($N_b \ll N$). At smaller length scales than the blob size ($r < d$) the sub-chains follow excluded volume statistics, the relation between N_b and d is of the form

$$d = aN_b^{3/5}. \quad (3.3)$$

In the region occupied by the grafted chains, the blobs behave like hard spheres and fill space densely (Fig.3.5). The polymer volume fraction ϕ_b inside the brush is as

$$\phi_b \approx N_b \frac{a^3}{b^3}. \quad (3.4)$$

Inserting eq (3.3) and eq (3.1) into eq (3.4) we obtain

$$\phi_b \approx \sigma^{2/3}. \quad (3.5)$$

The polymer volume fraction ϕ_b can be written also by expressing the volume per grafted chain as hd^2 , and as each chain contains N monomers

$$\phi_b = N \frac{a^3}{hd^2} = N \frac{a}{h\sigma^{-1}}. \quad (3.6)$$

The thickness of the grafted layer h can be derived from equating eq (3.5) and (3.6) as

$$h \approx Na\sigma^{1/3}. \quad (3.7)$$

In semi-dilute solutions the brush height h depends linearly on the number of monomers in the brush N instead the square root dependence as for ideal chains or the 3/5 power for isolated chains in good solvent condition.

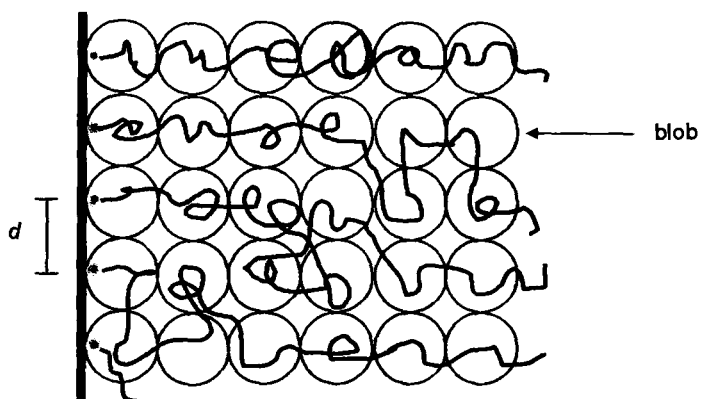


Fig. 3.5 Diagram of stretched situation for a grafted layer in good solvent condition in the semi-dilute regime. Each grafted chain can be subdivided into blobs of linear size d .

3.2.3.2 Concentrated conditions and Flory calculation

A concentrated solution may be considered as one in which the brush chains strongly overlap. In such case the grafting density is $\sigma > a^2 \langle R_F^2 \rangle$, which means that the projected area of a tethered chain on the substrate is smaller than the cross-sectional area of an unattached chain in the solvent.³²

For concentrated solutions, a slightly more general analysis is used to find the brush height. We achieve this by considering excluded volume, in which manner the affinity of the chains for the solvent is taken into account besides the polymer-polymer interaction. Thus, the same argument employed by Flory³³ for single chains in good solvent condition (*Chapter 2 section 2.1.1.3*) is employed for a concentrated brush layer. The starting point is a form of the free energy $F_{T,chain}$ (per N chains) containing two physical contributions: a repulsive term due to the excluded volume interaction and an entropic free-energy loss due to the stretching of the chain up to the height of the brush h as

$$\frac{F_{T,chain}(h)}{k_B T} \approx \nu \frac{N^2 \sigma}{h a^2} + \frac{h^2}{N a^2}, \quad (3.8)$$

where, taking as a reference eq.(2.9) the term $1/R^3$ in the repulsive component of the free energy $F_T(R)$ has been replaced by the volume associate with a single grafted chain $\sigma/(h a^2)$ which using eq.(2.1) equals to $1/(h d^2) \approx 1/R^3$.

The equilibrium height h is obtained by minimizing eq.(3.8) with respect to h giving

$$h \approx N(\nu \sigma)^{1/3}. \quad (3.9)$$

From eq.(3.8) we find the same grafting density and chain length linear dependence as in the semi-dilute regime (eq.(3.7)). It is important to state that the physics involved in semi-dilute and concentrate solutions is not the same; in the concentrated regime the extension of the brush is caused by the osmotic pressure difference between brush and solvent. Such osmotic pressure drives solvent into the brush, stretching out the chains until a balance between stretching energy and excluded volume interaction is reached.³⁴ The above scaling calculation has been confirmed by experiments^{10,35-38} and computer simulations.^{39,40}

At the overlap threshold $\sigma^* \sim N^{-6/5}$ (below which the mushroom conformation is present) the height given by eq.(3.9) scales as $h \sim N^{3/5}$ and thus agrees with the scaling of an unperturbed chain radius in good solvent (eq.(2.10)).

3.2.3.3 Parabolic Brushes and Self-Consistence Theory.

Both the Flory and scaling arguments presented above assume that all chains are stretched to exactly the same height (each chain behaves in a manner identical with every other), leading to a step profile for the monomer density. Monte Carlo⁴¹ or

molecular dynamics simulations⁴² have been used to confirm this general scaling of the brush height but yielded a more rounded monomer density profile which goes continuously to zero in the outer perimeter of the brush. In order to understand the segment profile given by such simulations a 'classical path' theory was used for strongly stretched polymer systems.⁴³ The classical path can be understood as the most probable path that a polymer takes (for a given start and end position) to minimize the free energy. It is expected that this classical path is a good approximation in the strong-stretching limit, since in such regimes random walk fluctuations around the classical path can be neglected.⁴⁴ Based on this assumption, numerical and analytical self-consistent field theories (SCF) have been proposed for such systems in the infinite-stretching limit.^{5,44,45} In such SCF models; the monomer interactions are replaced by a position-dependent monomer chemical potential arising self-consistently from the calculated monomer density profile. The classical SCF equations yield a simple, analytical solution: the monomer volume-fraction profile depends on the vertical distance y from the grafting surface and has a parabolic profile,⁴⁴ however the brush height has the same functional dependence as that predicted by the Flory energy balance argument that yielded eq.(3.9): $h \sim N(\sigma \nu)^{1/3}$. A diagram of the segment density profile (normalized to unity) of polymer brushes $\phi = \phi(y)$ in different regimes is shown in Fig. 3.6.

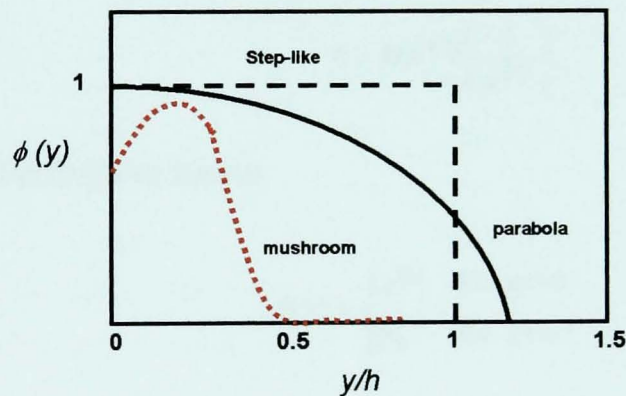


Fig. 3.6 Schematic diagram of the monomer volume fraction profile $\phi(y)$ versus height (y/h) at different regimes. The typical profile given by 'mushroom conformation' ($d > R_F$) is plotted in red dotted lines. The step profile as a result of the Alexander and Flory arguments (where $y=h=\text{constant}$) for 'brush conformation' ($d < R_F$) in the semidilute and concentrated regimes respectively is shown in black dotted lines. The parabolic profile describes the strongly stretched brush using self-consistent-field (SCF) theory.

Deviations from the parabolic profile become progressively important as the length of the polymers N (\sim molecular weight) decreases. With respect to the grafting density σ this law also fails at both very low graft densities (by predicting a

vanishingly small thickness of the brush) as well as at very high graft densities (by predicting a brush thickness larger than the length of the grafted polymer).⁴⁶

It should be noted that, although the “parabolic field” was derived by assuming a high stretching of the polymers chain, it provides a better description of polymer brushes in the intermediate-stretching regime (good solvents and moderate graft densities).⁴⁷

3.2.3.4 Poor solvent conditions

So far, we have assumed that the polymer-grafted layer is in contact with good solvent. In such a case the grafted chains try to minimize their mutual contact by stretching out into the solvent.

When the solvent is bad, brushes tend to collapse to exclude solvent; the height reached by the grafted chains is lower than that reached in good solvent conditions. The Flory energy balance treatment employed in the concentrated regime (section 3.2.3.2) can be extended through the theta point into the bad solvent condition by modifying the stretching energy term in eq (3.8). The new stretching energy would include the energy cost of brush compression,³⁴ this can be expressed in terms of the reduced temperature $t \equiv (T - T_\theta) / T_\theta$ where T_θ is the theta temperature. The brush height is then (as shown in section 3.1.3.2)

$$h = N\sigma^{1/2} f\left(\frac{t}{\sigma^{1/2}}\right), \quad (3.10)$$

where the function $f(x)$ is as follows

$$f(x) = \begin{cases} x^{1/3} & \text{for } x \gg 1 \\ |x|^{-1} & \text{for } x \ll -1. \end{cases} \quad (3.11)$$

In conditions of very poor solvent ($t \ll -1$) by using eq.(3.10) and eq.(3.11) the height of the collapsed layer scales linearly in $h \sim \sigma N$ (the same dependence as that obtained for a dry polymer layer), in agreement with experiments.⁴⁸ In conditions of good solvent, eq.(3.10) still yields the same dependence $h \sim N(\sigma v)^{1/3}$. For theta solvents using an Alexander approach similar to that yielding eq.(3.9), the brush height is predicted to scale as $h \sim N\sigma^{1/2}$ in good agreement with computer simulations.⁴⁹ The SCF theory can also be applied to theta and poor solvent conditions.

3.2.4 The physics of polyelectrolyte brushes

The physics of polymer brushes becomes more complex when ionic charges are included in the brush system. In this case of charged brushes, the swelling behaviour is mainly governed by electrostatic interactions and the osmotic pressure of the counterions within the brush predominates over the osmotic pressure of the macromolecular segments.

As with single polyelectrolyte chains, polyelectrolyte brushes can be divided into strong and weak PE brushes. In strong PE brushes, PE chains with fixed charge are grafted onto the substrate. In weak PE brushes, PE chains with no fixed charge are tethered on the substrate and the degree of dissociation depends on the local pH. Little is known from experiments on the scaling behaviour of PE brushes when compared with neutral brushes. Grafted PE layers have been the focus of theoretical⁵⁰⁻⁵⁴ and experimental⁵⁵⁻⁵⁷ studies.

We follow here the lines of the original work of Pincus⁵⁰ which assumes that the polymer concentration is uniform through the height of the brush h , similar to the approximation Alexander⁸ made for neutral polymer brushes. Pincus presented scaling theories for PE brushes, in salt-free good solvent conditions, in the so-called *osmotic brush regime (OB)*. In this regime, the brush height h is the end result from the balance between the repulsive osmotic counterion pressure (which tends to increase the brush height) and the chain elasticity (which tends to decrease the brush height). This work has been lately generalized to poor solvent conditions^{51,58} and to the regime where excluded volume interactions cannot be neglected: the *quasi-neutral (QNB) or Alexander regime* introduced by Borisov et al.⁵⁹ In this regime, the excluded volume interactions between non-charged units at certain positions dominate over the electrostatic interactions. In the following, the strong PE brush with no added salt will be described.

3.2.4.1 Strong PE brushes

In our arguments we assume that two length scales characterize the charged brush: the average vertical stretching of the grafted PE chains h and the extent of the counterion cloud, denoted by C . In addition we make the assumption that the grafted PE chains are ideally flexible and a fraction f of their monomers possesses charge. The presence of additional salt is neglected in our PE brush system for simplicity.

Two cases must be considered: when the counterions extend outside the brush $C \gg h$ and the brush becomes charged, and the case in which the counterions are confined inside the grafted layer $C \approx h$ yielding a neutral brush. The case of $C \gg h$ is indicative of weakly charged brushes while when $C \approx h$, the strongly charged limit is reached.

A schematic picture of both scenarios is shown in Fig. 3.6.

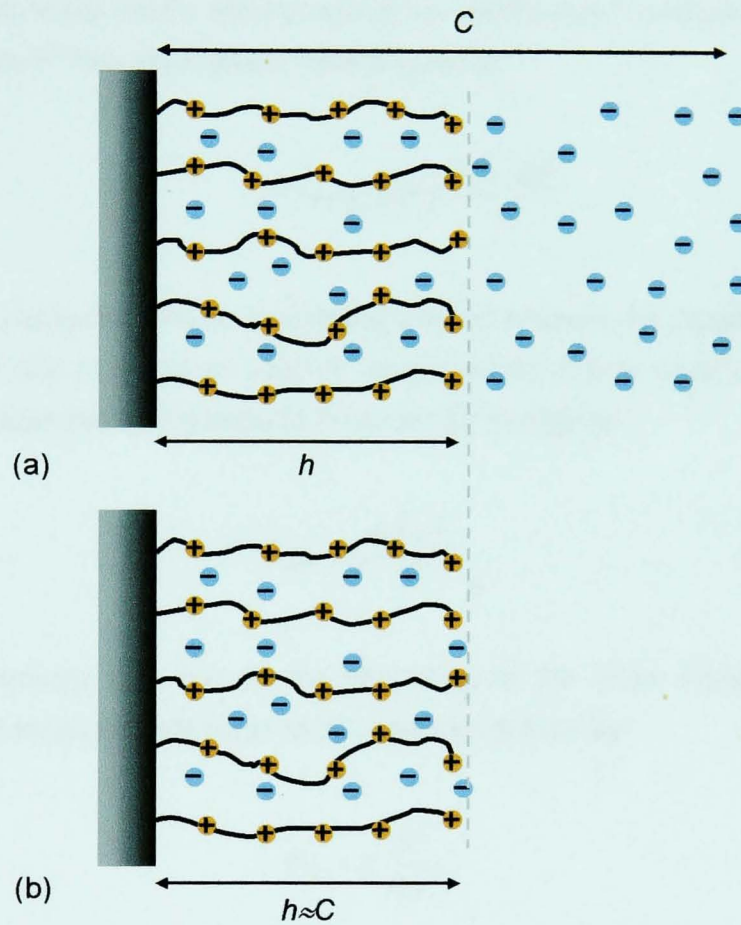


Fig. 3.6 Schematic diagram of a strong PE brush in good solvent conditions in the absence of added salt. (a) It is shown the weak-charge limit where the thickness of the counterion cloud is greater than the brush thickness $C \gg h$. (b) The case of strong-charge limit is shown here, where the thickness of counterion cloud and PE brush are roughly the same $C \approx h$.

(a) Counterions extended over the brush height: $C \gg h$ (weak-charged limit)

The total free energy density (per unit area in units of $k_B T$) for a PE brush $F_{T,PE \text{ brush}}$ when $C \gg h$ contains four contributions.

The osmotic free energy F_{os} associated with the entropy cost of confining the counterions to a layer of fixed thickness C is given by

$$F_{os} \approx \frac{Nf\sigma}{z} \ln\left(\frac{Nf\sigma}{zC}\right), \quad (3.12)$$

where the grafting density of PE is σ , z is the counterion valence, N the polymerization index of the grafted PE chains and f the charge fraction. The charge density of the grafted PE layer $\rho_{PE\ brush}$ is due to the monomer charges and can be expressed as $\rho_{PE\ brush} = \sigma Nf$.

Since the brush is not locally electro-neutral an electrostatic contribution has to be taken into account. This electrostatic term is given by

$$F^e \approx \ell_B (Nf\sigma)^2 \frac{(C-h)^2}{h}. \quad (3.13)$$

As for neutral polymer brushes, in charged grafted systems the repulsion between the monomers due to excluded volume (contributions due to counterions are not taken into consideration) contribute to the total free energy as

$$F_{rep} \approx \nu \frac{N^2 \sigma^2}{h}. \quad (3.14)$$

The entropic energy cost due to the stretching of the chain (strictly, this is a conformational entropy) contributes to the total free energy as

$$F_{st} \approx \sigma \frac{h^2}{Na^2}, \quad (3.15)$$

These two contributions given by eq.(3.14) and eq.(3.15) are general for the total free energy of non-charged brushes (section 3.1.3.2) as well as real polymer chains (section 2.1.1.3).

As we have shown $F_{T,PE\ brush} = F_{T,PE\ brush}(h, C) = F_{os} + F^e + F_{rep} + F_{st}$; minimization of $F_{T,PE\ brush}(h, C)$ with respect to C will yield the counterion cloud height C as

$$\frac{\partial F_{T,brush}(h, C)}{\partial C} = \frac{\partial (F_{os} + F^e)}{\partial C} = 0 \Rightarrow C \approx \frac{1}{z\ell_B Nf\sigma}, \quad (3.16)$$

which has the same scaling behaviour as the Gouy-Chapman length λ_{GC} . The Gouy-Chapman length defines the characteristic thickness of the counterions cloud

above a charged surface.^{60,61} In the case of a PE brush, the surface charge density is given by $\rho_{PE\ brush} = \sigma N f$.

In order to get the so-called *Pincus* brush height⁴⁷ h_{Pincus} , we must balance the PE stretching and electrostatic energy as

$$\frac{\partial(F_{st} + F^e)}{\partial h} = 0 \Rightarrow h_{Pincus} \approx N^3 \sigma a^2 \ell_B f^2, \quad (3.17)$$

corresponding to the *Pincus brush regime (PB)*, which results from the electrostatic attraction between the charged monomers and the counterions cloud. Note the unusual dependence of h_{Pincus} with N^3 , meaning that the layer thickness grows faster than linearly with molecular weight, as well as h_{Pincus} dependence on grafting density σ .

(b) Counterions confined within the brush height: $C \cong h$ (strong -charged limit)

When counterions are trapped inside the grafted polymer layer the brush can be considered neutral and hence the electrostatic energy F^e contribution to the system total free energy disappears: $F_{T,PE\ brush} = F_{T,PE\ brush}(h \cong C) = F_{os} + F_{rep} + F_{st}$.

There are two ways of balancing $F_{T,PE\ brush}(h)$. By comparing the osmotic energy of counterion confinement with the PE stretching term the brush height can be obtained as

$$\frac{\partial(F_{os} + F_{st})}{\partial h} = 0 \Rightarrow h_{osmotic} \approx \frac{N a f^{1/2}}{z^{1/2}}, \quad (3.18)$$

constituting the *osmotic brush regime (OB)*. In such a regime, the driving force for chain stretching is the osmotic pressure of the counterions; $h_{osmotic}$ given by eq. (3.18) does not depend on the grafting density.

The second way to balance $F_{T,PE\ brush}(h)$ is by comparing the free energy due to excluded volume interactions with the polymer stretching energy. This approach is usually made for brushes with high grafting density where excluded volume interactions can no longer be neglected. By balancing these two contributions to the total free energy we obtain

$$\frac{\partial(F_{rep} + F_{st})}{\partial h} = 0 \Rightarrow h_{q-neutral} \approx Na \left(\frac{\nu\sigma}{a} \right)^{1/3}, \quad (3.19)$$

where the brush height h is called $h_{q-neutral}$ because its dependence with N, ν and σ is identical at that obtained for a neutral brush in eq.(3.7) and (3.9). This regime is called the *quasi-neutral brush regime (QNB)*.⁵⁹

By constructing an equation system with the PE brush heights in the three regimes: h_{Pincus} , $h_{osmotic}$ and $h_{q-neutral}$ given by eq. (3.17), (3.18) and (3.19) respectively, the characteristic charge fraction f_c and grafting density σ_c at which the three scaling regimes coexist can be found as

$$f_c \approx \left(\frac{z\nu}{N^2 a^2 \ell_B} \right)^{1/3}, \quad (3.20)$$

and

$$\sigma_c \approx \frac{1}{N \ell_B^{1/2} \nu^{1/2}}. \quad (3.21)$$

As in the case of neutral brushes, the scaling laws for PE brushes can be extended to theta and poor solvent conditions if the additional contributions to the total free energy given by PE brushes (F_{os} and F^e) are considered.⁵⁸ Table 3.1 shows the scaling behaviours of neutral polymer brushes and strong PE brushes at good, theta and poor solvent conditions.

Solvent quality	Neutral brush	PE brush
good	$h \approx N\sigma^{1/3}$	$h \approx N$ (OB) $h \approx N^3\sigma$ (PB) $h \approx N\sigma^{1/3}$ (QNB)
theta	$h \approx N\sigma^{1/2}$	$h \approx N\sigma^{1/2}$
poor	$h \approx N\sigma$	$h \approx N\sigma$

Table 3.1 Comparison of the scaling behaviour of neutral polymer brushes and strong PE brushes in different solvents.

3.2.4.2 Weak PE brushes

The properties of weak PE brushes become more complex⁶²⁻⁶⁵ than those of strong PE brushes. Weak PE brushes involve two major complications: the charge density can be controlled by external parameters such as pH or the addition of salt, and conversely non fixed charges means that the ions can move via dissociation and association processes.⁶⁰

We follow the work of Israëls et al⁶² for the SFC theoretical description presented in this section. A polyacid brush will be used as an example for the swelling behaviour of weak PE brushes.

In the SCF model we assume that the half-space next to the surface (formed by PE region and part of the reservoir region) can be separated into discrete parallel layers at vertical distance y from the surface being $y=1,2\dots M$ where M is sufficiently large. A new parameter must be introduced that defines the statistical probability of finding a segment of the type A in a certain layer y . This parameter is called the weighting factor $G_A(y)$ and is given by

$$G_A(y) = e^{-u_A(y)/k_B T}, \quad (3.22)$$

where $u_A(y)$ denotes the potential of mean force, with respect to a reference state that we take to be the bulk solution: u_A^b .

As grafted PE chains are considered, all allowed conformations must have their first segment in $y=1$ and the total number of polymer units in the system fixed.⁶⁶ In each layer there are three components allowed: water, positively charged ions, and negatively charged ions that are free to leave the PE region.

The dissociation of a proton from a polyacid-grafted chain yields a COO^- group and thus a negative charge. The total number of charges along the chain is not fixed but the solution pH imposes the chemical potential of H^+ and thus the charges chemical potential. The non-constant charge density is governed by the acid-base equilibrium



where HA is the uncharged brush segment (carboxylic acid), A^- is the negatively charged brush segment (carboxylate ion) and H^+ is the proton. This equilibrium is characterized by a constant K_a . We have to include the equilibrium in each of the y layers, so we express

$$K_a(y) = \frac{[A^-](y) \cdot [H^+](y)}{[HA](y)}, \quad (3.24)$$

where the square brackets denotes concentration. The degree of dissociation $\alpha(y)$ as a function of local concentration is expressed as

$$\alpha(y) = \frac{[A^-](y)}{[A^-](y) + [HA](y)}. \quad (3.25)$$

Eq.(3.22), (3.23) and (3.24) are valid for local concentration, but it is also important to find the degree of dissociation of a polyacid segment in the bulk α^b (the reference state). By using eq.(3.24) and eq.(3.25) this can be obtained

$$\alpha^b = \frac{K_a}{K_a + [H^+]} = \frac{[A^-]_b}{[A^-]_b + [HA]_b}, \quad (3.26)$$

where $[H^+]$ and K_a are respectively the concentration of protons and the dissociation constant in the bulk. The subscript b refers to the bulk reference state.

In the two state model, each segment A can be in two states: the protonated HA or the deprotonated A^- . According to this model the statistical weight $G_A(y)$ given by eq. (3.22) can also be expressed as a function of concentration^{67,68} as

$$G_A(y) = \frac{[A](y)}{[A]_b} = \frac{[A^-](y) + [HA](y)}{[A^-]_b + [HA]_b}, \quad (3.27)$$

where the weighting factors of HA and A^- segments are

$$G_{A^-}(y) = \frac{[A^-](y)}{[A]_b} \quad \text{and} \quad G_{HA}(y) = \frac{[HA](y)}{[HA]_b}. \quad (3.28)$$

Introducing eq(3.26) and eq.(3.28) into eq.(3.27) we obtain

$$G_A(y) = \alpha^b G_{A^-}(y) + (1 - \alpha^b) G_{HA}(y). \quad (3.29)$$

Inserting eq.(3.27) and eq.(3.28) into eq.(3.25) the local degree of dissociation can be written as

$$\alpha(y) = \alpha^b \frac{G_{A^-}(y)}{G_A(y)}, \quad (3.30)$$

where substituting equation (3.29) gives

$$\alpha(y) = \frac{\alpha^b}{\alpha^b + (1 - \alpha^b) e^{-E(y)}}, \quad (3.31)$$

where $e^{-E(y)} = G_{A^-}(y)/G_{HA}(y)$ is defined as the Boltzmann factor of the local electrostatic potential $E(y)$ (in units of $k_B T$). For a polyacid brush $E(y) < 0$ with respect to the bulk solution ($G_{A^-}(y) < G_{HA}(y)$). By using eq.(3.26) and eq.(3.31) we finally obtain

$$\alpha(y) = \frac{K_a}{K_a + [H^+] e^{-E(y)}}. \quad (3.32)$$

The attractiveness of this model is in its simplicity: the local degree of dissociation $\alpha(y)$ given by eq.(3.32) has the same form as that in the bulk α^b given by eq.(3.26) except that the bulk proton concentration $[H^+]$ is replaced by the local proton concentration $[H^+] e^{-E(y)}$.

In order to derive the weak PE brush height in a monovalent salt solution, we make a simplification in the above proposed model. We consider the brush as a homogeneous region with degree of dissociation α in equilibrium with the bulk solution degree of dissociation α^b and assume that the PE brush is uniform in segment density and electrostatic potential (the step-like model). This is the same assumption Alexander made to describe neutral brushes⁸ (shown in *section 3.2.3.*) and Pincus⁵⁰ took to illustrate charged brushes with constant charge density (*section 3.2.4.1*) and seems to predict correctly the behaviour of weak PE brushes.⁶⁹ The y dependence in eq. (3.32) can then be neglected and written as

$$\alpha(y) = \frac{K_a}{K_a + [H^+] e^{-E}}, \quad (3.33)$$

where the electrostatic potential (y -independent) in the brush with respect to the bulk solution can be expressed as the ratio between counterions inside the brush region n_{ci} (since it is a polyacid its counterions are rendered positive) and those in the bulk solution n_s as

$$e^{-E} \approx \frac{n_{ci}}{n_s}. \quad (3.34)$$

We identify now different brush regimes for different bulk salt concentrations n_s .

(a) At high salt concentrations $n_{ci} \approx n_s \Rightarrow E=0$ and by eq.(3.33) $\alpha \approx \alpha^b$, meaning that the dissociation degree is constant which is equivalent to say that the charge fraction f can be replaced by α^b and be controlled by the pH of the solution. This regime is known as *salted brush regime (SB)*. In this regime weak PE brushes behave in a very similar way as strong PE brushes. Using mean field theory⁷⁰ the scaling behaviour of weak PE in this regime is found to be

$$h_{\text{salted,w}} \approx N(\alpha^b)^{2/3} \sigma^{1/3} n_s^{-1/3}. \quad (3.35)$$

where the height of the PE brushes (both strong and weak) decreases with increasing salt concentration, due to electrostatic screening.

(b) At lower salt concentrations $n_{ci} \gg n_s$ we are in the OB regime and using the electroneutrality condition n_{ci} is given by

$$n_{ci} = \alpha c = \alpha \frac{N\sigma}{h}. \quad (3.36)$$

In the OB regime from eq.(3.18) we see that $h/N \propto \alpha^{1/2}$, and with eq.(3.34) and eq (3.36) we obtain

$$e^{-E} \propto \frac{\sigma \alpha^{1/2}}{n_s}, \quad (3.37)$$

Inserting eq.(3.37) and eq.(3.26) in eq.(3.33) it yields

$$\alpha^{3/2} \approx \frac{K_a}{[H^+]} \sigma^{-1} n_s, \quad (3.38)$$

where it is implicit that the degree of dissociation in the brush region α decreases with decreasing salt concentration n_s . This equation (3.38) cannot be solved easily except with the approximation employed (low salt concentrations). By replacing f

with α and using eq.(3.38) in the expression for $h_{osmotic}$ given in eq.(3.18) we obtain the brush height in the OB regime for a weak PE brush as

$$h_{osmotic,w} \approx N\sigma^{-1/3}n_s^{1/3}, \quad (3.39)$$

where $h_{osmotic,w}$ refers to the brush height in the OB regime for a weak PE brush. The final result yielded by eq.(3.39) shows that the brush height increases with increasing salt concentration. When external salt is added to the system there is an increase in the degree of dissociation of the acidic groups, as a consequence charge build up along the PE chains leading to an increased stretching caused by coulombic repulsions.

As we have previously said, we are considering the case of polyacid brushes, for polybase ones the treatment would be equivalent to that presented here. The equilibrium constant would be that of a base K_b , and the uncharged brush segment B . The dissociation of an OH group from the polybase-grafted chain yields HB^+ ions, thus the brush segments become positively charged.

In the limit of $n_s \rightarrow 0$, according to eq.(3.38) $\alpha \approx 0$, and then the weak PE enters a QNB regime. Although the lowest level of ionic strength is given by the dissociation of water when it is in contact with the weak PE chains.

3.3 POLYELECTROLYTE HYDROGELS

3.3.1 Hydrogels: general features

A hydrogel can be defined as a three-dimensional, water-swallowable network connected by chemical or physical cross-link points (points where at least three chains emanate⁷¹) and immersed in an aqueous medium.⁷² A hydrogel is a form of matter intermediate between a solid and a liquid: the liquid inside the gel prevents the polymer network from collapsing into a compact mass, whereas the network prevents the liquid from flowing away, both network and liquid coexist in a thermodynamic equilibrium. In order to understand gel systems two types of statistical information are needed: the situation at the moment of preparation and at the moment of study (solvent, temperature etc.). Thus, gels are described in terms of the 'preparative ensemble' and the 'final ensemble', which give them a more complex behaviour than usual equilibrium system where a single ensemble (ruled by Boltzmann exponentials) is required.

A sol (solution) is defined as a stable suspension of colloidal solid particles in a liquid. For sol to exist must be small enough for the dispersion forces to be greater than those of gravity. A gel forms when the homogeneous dispersion in the initial sol rigidifies. This process is called gelation. A sol can be transformed into a polymeric gel by going through the gel-point. The gel-point is the threshold where the sol abruptly changes from a viscous liquid state to another phase called gel.⁷³ Fig. 3.7 shows a simplified scheme of the formation of a polymeric network.

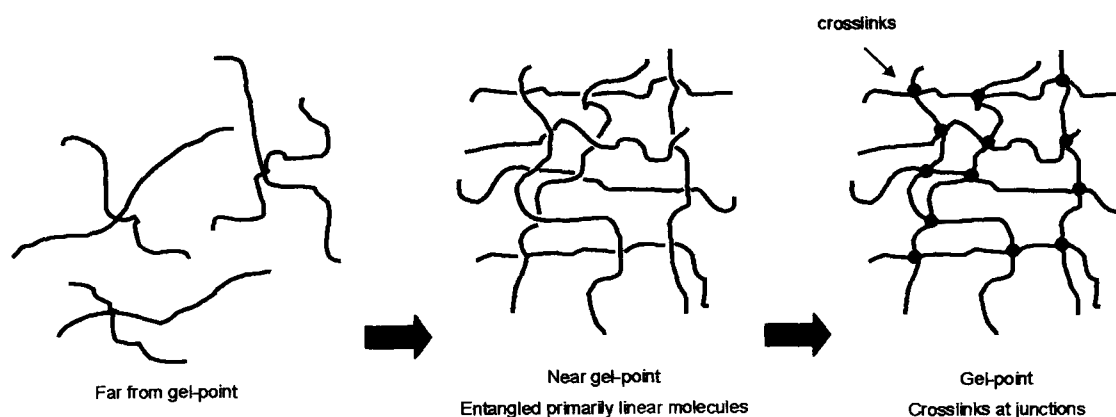


Fig. 3.7 Schematic diagram of the formation of a polymer network (hydrogel).

As a whole, a polymer gel is actually one single giant three-dimensional molecule since all the monomer units in the gel are linked to each other to form a large molecule on a macroscopic scale. In fact such macroscopic scale confers gels an

important advantage when compared to dilute polymer solutions: the possibility of direct visual observation of conformational transitions. In contrast, the main disadvantage is the very slow equilibration time associated with gels.

Generally, hydrogels can be divided into two classes: neutral and charged. In neutral hydrogels (e.g. polyethylene glycol (PEG)), the swelling properties can be explained as a balance of two effects: the osmotic pressure due to polymer-solvent interactions and the elastic contributions (stretching energy) of the crosslinked polymer chains.⁷⁴ It has been demonstrated that the osmotic pressure of neutral gels may differ from that of the un-crosslinked polymer solution at the same concentration and that the degree of crosslinking may determine the quality of polymer-solvent interaction.⁷⁵⁻⁷⁷ But, if the gel is not too heterogeneous the conformational properties of the elastic chains are basically the same as for isolated linear polymer chains of the same molecular weight.⁷⁸

As for charged chains and brushes, the physics of charged gels is more complex than that of neutral gels. Being charged, the dominant force for swelling in PE gels is the electrostatic repulsion between gel charges. In addition the counterions have also a dominant effect on the osmotic pressure. Consequently swelling of PE gels can be induced through stimuli as changes in pH and salinity.^{72,79-81}

Important parameters used to characterize the network structure of hydrogels are: the water and polymer volume fraction in the swollen state, ν_1 and ν_2 respectively (we will use 1 as subscript to refer to water and 2 to refer to polymer). The average molecular weight of the polymer chain between two neighbouring crosslinking points M_c , that is inversely proportional to the crosslinking density of the gel ρ_c^{gel} . M_c is calculated in average values due to the randomness of the gelation process. The mesh size R_c^{gel} is another important parameter that measures the average linear distance between adjacent crosslinks providing the space accessible for particle diffusion in the network.⁸¹

Another subdivision that can be made in gels depending on the nature of the crosslinks that connect the units are: physical and chemical gels. Both neutral and charged gels can be of a physical or chemical nature.

3.3.1.1 Physical gels (reversible)

In this type of gels the bonds linking the subunits are due to physical interactions (i.e. dipole-dipole interactions, traces of crystallinity). Such systems are generally thermoreversible as the bonds break at high temperature and reform again at lower

temperature. We discuss in turn gels due to microcrystalline region and microphase separation.

(a) Microcrystalline regions.

In polymer solutions there are regions where polymer chains meet, as a result they can form small crystalline regions linking more than one chain. Given the thermoreversible property, such crosslinks will break when the solution is heated above the crystallite melting point and form again when low temperatures are reached (Fig. 3.8). An example of this physical gel type is the familiar gelatin dessert, which is the product of dissolution in water at high temperature of collagen (which has helix structure in its native state). In this case, a solution of long chain polymers undergoes a phase transition on cooling which results in aggregation of individual chains into clusters through helix formation or crystallization.⁸²

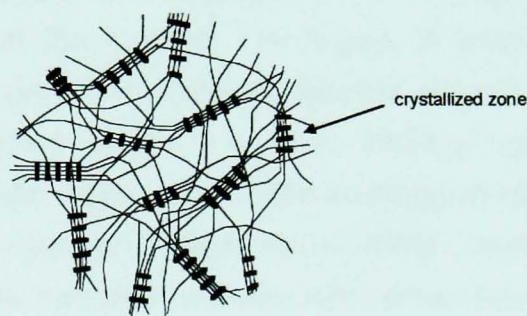


Fig. 3.8 Schematic diagram of the thermoreversible gelation by the formation of microcrystals.

(b) Microphase separation.

This mechanism occurs for block copolymer gels. In this case and under certain conditions (i.e. solvent types) block copolymers can microphase separate. We illustrate this example with triblock copolymers formed by hydrophilic and hydrophobic sections. Fig.3.9 shows the conformations that these copolymers adopt in presence of water, in this case the hydrophobic regions are the crosslinking points.

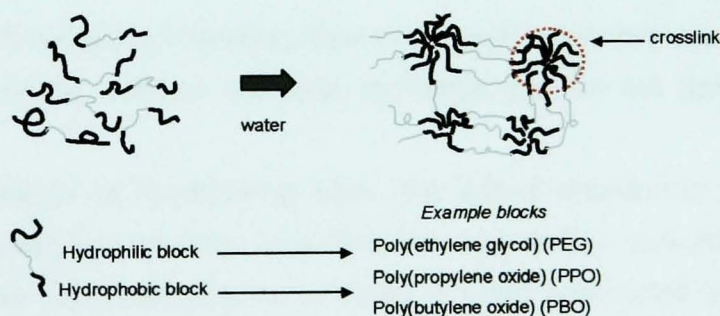


Fig. 3.9 Schematic diagram of the formation of a physical gel by microphase separation between hydrophilic and hydrophobic parts in triblock copolymers. Examples of copolymers able to provide this type of networks are also given.

3.3.1.2 Chemical gels (irreversible)

Chemical gels are formed by multi-functional units that can be covalently linked to make three-dimensional networks. A standard recipe starts from a dilute (1–10%) aqueous solution of the desired monomer, crosslinking agent, and an initiator that will start the polymerisation reaction. Common crosslinkers are poly(ethylene glycol) dimethylacrylate (PEGDMA), ethylene glycol dimethylacrylate (EGDMA) and bis-acrylamide. The crosslinking density depends on the ratio of crosslinking agent to monomer and the functionality of the crosslinker (number of chains that emanate from a crosslink point).

Almost any water-soluble polymer can be prepared as a gel by performing the polymerisation in the presence of a cross-linking agent or by carrying out a cross-linking reaction on a solution of the polymer. The degree of cross-linking will determine the properties of the gel.⁸³ The chemical networks undergo swelling in analogy to dilution of free polymer chains in solution. Chemical gels are not homogeneous. They usually contain regions of low water swelling and high crosslink density, called ‘clusters’, that are dispersed within regions of high swelling and low crosslink density. In chemical gels, free chain ends are seen as network defects that do not contribute to the elasticity of the network. Other network defects are chain loops and entanglements.⁸⁴

Examples of chemical gels are: vulcanized rubbers where natural rubber (linear polyisoprene) is crosslinked using sulfur to yield an elastic material.⁸² Many more examples of chemical gels are found in hydrogels used for biomedical applications (generally methacrylates), where they have been chemically tailored in order to obtain biological recognition.^{81,84}

3.3.2 The physics of neutral gels

In order to derive the equilibrium swelling theory of ionisable (weakly charged) gels we start with the simple case of chemical hydrogels that do not contain ionic moieties.

For a low concentration of crosslinking sites, the strand end-to-end vector R_c distribution function can be described by a Gaussian distribution; excluded volume effects make a minor contribution to the entropic changes associated with strand deformations.⁷³ To a good approximation, the macroscopic dimensions of the system determine the mean link positions. For networks under strain and for sufficiently long strands, different models have been proposed to describe

fluctuations of R_c , the “affine” model^{73,85} or the “phantom” model⁸⁶ are examples of such models. In the phantom model, the network junctions can freely move and are not influenced by stretched chains; in the affine model, the junctions move ‘affinely’ under swelling. This means that the relative position of the junctions remains unchanged under swelling. Both models are likely to fail at high crosslinking densities, where excluded volume effects play a significant role both on the conformational properties and entropy of the strands and on the fluctuations of R_c which can no longer be described by a Gaussian distribution.⁸⁶

Assuming that the network is homogeneously swollen ($\beta_{gel,x}=\beta_{gel,y}=\beta_{gel,z}=\beta_{gel}$), neglecting excluded volume interactions and at relatively low crosslinking density the Flory-Rehner theory⁷⁴ expresses the total free energy of a swollen polymer network as

$$\Delta F_{total} = \Delta F_{elastic} + \Delta F_{mixing}, \quad (3.40)$$

where $\Delta F_{elastic}$ is given by the elastic retractive forces inside the gel and is described by classical rubber elasticity; using the simplest phantom network model⁷³ which assumes that the junctions of a network undergo Brownian motion about their mean positions, we obtain

$$\Delta F_{elastic} = \frac{3}{2} k_B T N_c^{gel} (\beta_{gel}^2 - 1 - \ln \beta_{gel}), \quad (3.41)$$

where N_c^{gel} is the number of ‘effective’ (tethered at both ends) subchains in the network and β_{gel} is the gel expansion or deformation factor

$$\beta_{x,gel} \beta_{y,gel} \beta_{z,gel} = \beta_{gel}^3 = \frac{V}{V_0}, \quad (3.42)$$

where V and V_0 are the total volume of a swollen and relaxed hydrogel respectively. The mixing term in eq. (3.40) is given by the Flory-Huggins lattice model⁷³. In the phantom model, there is no contribution from number of polymer chains ϕ_2 in ΔF_{mix} . Although the network itself has a mass that should be considered infinite, the network strands can have entropy between two fixed junctions because they have a certain conformational freedom. If the junctions are not fixed in space, as in the phantom theory, then the entropy does not contribute in ΔF_{mix} .⁸⁷ The expression for ΔF_{mix} is

$$\Delta F_{mix} = k_B T [\phi_1 \ln v_1 + \chi \phi_1 v_2], \quad (3.44)$$

where ϕ_1 is the number of solvent molecules in the swollen gel; v_1 and v_2 are the volume fractions of solvent and polymer respectively and χ is the Flory-Huggins parameter related to segment-solvent interactions, previously introduced in eq.(2.14). The volume fraction of the polymer in the swollen gel v_2 can be expressed as $v_2 = V_0/V$; incorporating the molar volume of the solvent ϕ_1 to compute the solvent contribution to the volume yields

$$\beta_{gel}^3 = \frac{1}{v_2} = \frac{(V_0 + (\phi_1 \phi_1 / N_A))}{V_0}, \quad (3.45)$$

where N_A is Avogadro's number. By introducing eq.(3.45) into the successive following expressions everything will become molar instead of per lattice site.

At equilibrium, the difference between the chemical potential of the solvent outside and inside the gel must be zero.

$$\mu_1 - \mu_1^0 = 0, \quad (3.45)$$

where μ_1^0 and μ_1 are the chemical potential of solvent outside (pure water in standard state) and inside the gel respectively. Thus, the changes of the chemical potential due to mixing and elastic forces must balance each other as

$$0 = (\Delta\mu_1)_{total} = N_A \left(\frac{\partial(\Delta F_{total})}{\partial \phi_1} \right) = (\Delta\mu_1)_{mixing} + (\Delta\mu_1)_{elastic}. \quad (3.46)$$

Inserting in ΔF_{mixing} given by eq.(3.44) the relation $v_2 = \frac{V_0}{V_0 + (\phi_1 \phi_1 / N_A)}$ given by eq.(3.45) and $v_1 = 1 - v_2$, we obtain $\Delta F_{mixing} = \Delta F_{mixing}(\phi_1, v_2(\phi_1))$ where

$$(\Delta\mu_1)_{mixing} = N_A \left(\frac{\partial(\Delta F_{mixing})}{\partial \phi_1} \right) = RT [\ln(1 - v_2) + v_2 + \chi v_2^2]. \quad (3.47)$$

and using eq.(3.41) for $\Delta F_{elastic}$, and eq.(3.45) for β_{gel}

$$(\Delta\mu_1)_{elastic} = N_A \left(\frac{\partial(\Delta F_{elastic})}{\partial \phi_1} \right) = N_A \left(\frac{\partial(\Delta F_{elastic})}{\partial \beta} \right) \left(\frac{\partial \beta}{\partial \phi_1} \right) =$$

$$= RT\phi_1 \frac{N_c^{gel}}{V_0} \left(v_2^{1/3} - \frac{v_2}{2} \right). \quad (3.48)$$

Using eq.(3.47) and eq.(3.48) we can now evaluate the equilibrium situation given by eq.(3.46) as

$$0 = \Delta(\mu_1)_{total} = RT \left(\ln(1-v_2) + v_2 + \chi v_2^2 + \phi_1 \frac{N_c^{gel}}{V_0} \left(v_2^{1/3} - \frac{v_2}{2} \right) \right), \quad (3.48)$$

yielding

$$-[\ln(1-v_{2m}) + v_{2m} + \chi v_{2m}^2] = \phi_1 \frac{N_c^{gel}}{V_0} \left(v_{2m}^{1/3} - \frac{v_{2m}}{2} \right), \quad (3.49)$$

where v_{2m} is the volume fraction of polymer at swelling equilibrium (with the subscript m indicating maximum). The left hand member in eq. (3.49) represents the lowering of the chemical potential due to the mixing of polymer and solvent; the right side yields the increase from the elastic reaction of the network. Another term we can include in the right side of eq.(3.49) is a multiplying factor $(1-2M_c/M)$ where M is the molecular weight of the polymer chains prepared under identical conditions but in the absence of the crosslinking agent. Such a term expresses the corrections for the network imperfections resulting from chain ends, for a perfect network $M=\infty$, then the correction term is one. We assume ideal perfect networks.

Specific volume \tilde{v} can be defined as the volume of a unit of mass of a material. It is equal to the inverse of density (units of the specific volume are m^3/kg). We can rewrite N_c^{gel}/V_0 in terms of the specific volume of the polymer \tilde{v} and the molecular weight between crosslinks M_c as

$$\frac{N_c^{gel}}{V_0} = \frac{1}{\tilde{v}M_c} = \rho_c^{gel}, \quad (3.50)$$

where ρ_c^{gel} is the gel crosslinking density. Inserting eq.(3.50) into eq.(3.49) we obtain the crosslinking density of the polymer network as

$$\frac{1}{\tilde{\nu}M_c} = \rho_c^{gel} = -\frac{RT[\ln(1-\nu_{2m}) + \nu_2 + \chi\nu_{2m}^2]}{\phi_1\left(\nu_{2m}^{1/3} - \frac{\nu_{2m}}{2}\right)}, \quad (3.51)$$

The swelling ratio q is given by the ratio of the swollen and unswollen network V/V_0 , therefore $q=1/\nu_2$. At swelling equilibrium we can calculate q_m (maximum swelling ratio at equilibrium) by replacing $1/\nu_{2m}$ by q_m in eq.(3.49). As an approximation, consider low degree of crosslinking=high degree of swelling, implying large M_c values, i.e. 10,000 or more, then q_m in a good solvent situation will exceed 10, which means small ν_{2m} .⁷³ As a result $\nu_{2m}^{1/3} \gg \nu_{2m}$, then as an approximation we neglect $\nu_{2m}/2$ and higher terms in the series expansion of $\ln(1-\nu_{2m})$ in eq.(3.49) resulting⁸⁵

$$q_m^{3/5} \cong \frac{V_0}{N_c^{gel}} \left(\frac{1}{2} - \chi\right) \frac{1}{\phi_1}. \quad (3.52)$$

Equation (3.52) shows the dependence of the equilibrium-swelling ratio of a polymer network on the quality of solvent (χ) and density of cross-linking ($V_0/N_c^{gel}=1/\rho_c^{gel}$)

The mesh size of the network can be calculated as $R_c^{gel} = \beta_{gel} \langle (R_o^{gel})^2 \rangle^{1/2}$ where $\langle (R_o^{gel})^2 \rangle$ is the mean square unperturbed end-to-end distance of the polymer chains between two neighbouring crosslinks and β_{gel} is given by eq.(3.45). In the original Flory theory⁷³ $\langle (R_o^{gel})^2 \rangle$ is gaussian and is given by eq.(2.1) that for polymer networks becomes $\langle (R_o^{gel})^2 \rangle = a^2 N_c^{gel}$.

3.3.3 The physics of ionisable (weak polyelectrolyte) gels

Electrostatic interactions modify profoundly the behaviour of polymeric gels. Perhaps one of the most striking properties of charged gels is their ability to swell. Polyelectrolyte gels can exhibit a swelling degree in water as high as 1000, which can be controlled by changing the ionic strength of the solution.⁸⁰

In a salt free solution, for any charge located on a monomer there is a counterion to maintain the neutrality of the hydrogel. For the counterions, it is thermodynamically advantageous to abandon the gel and travel in the external volume (reservoir), because by doing this, they gain significant entropy of translational motion. However, this is impossible because the condition of macroscopic electroneutrality of the gel must be kept. The counterions are thus forced to be confined within the

gel, producing a significant osmotic pressure providing more space for the transactional motion of every other counterion. This explains why counterions have a dominant effect on the osmotic pressure of ionisable gels.

The swelling behaviour of weakly charged gels has been described by Katchalski et al.^{88,89} and Flory and Rehner⁷⁴ as resulting from a balance between the elastic energy of the network (as for neutral gels) and the osmotic pressure of the ions. In salt free solutions, this osmotic pressure is due to the counterions that are confined inside the gel in contact with the system reservoir. In the presence of salt, the osmotic pressure is associated with the establishment of the Donnan equilibrium.⁷³

Consider a flexible polyelectrolyte network immersed in water with added salt (monovalent salt). We assume low salt concentration (i.e. weak screening limit), where the Debye-Hückel screening length κ^{-1} is larger than the network mesh size. In such a case, according to the model proposed by Barrat et al, the equilibrium swelling of the gel does not depend on the strength of the electrostatic interaction but just on the osmotic pressure of the counterions.⁷⁸ The tension created by this pressure is transmitted through the crosslinks to the elastic chains, which behave as isolated chains with applied forces at their end points.⁸⁰ Such a model predicts a simple scaling behavior of equilibrium swelling degree as a function of the ionization degree α . We restrict ourselves here to consider the model presented by the Flory Rehner theory^{73,74,85} for describing the swelling behaviour of weakly charged gels.

For instance, if we consider a PMAA network the monomers carry acrylic acid as ionisable group. For simplicity we will assume that only one type of ion can bind chemically to the network-fixed carboxylate, in this case hydrogen ions (counterions). The electrostatic repulsions between the fixed carboxylate ions are screened by the presence of other ions (ions from the solvent i.e. H^+ and OH^- for water, and ions from the salt) thus reducing such repulsions. A schematic diagram of an ionisable network (e.g. an acrylic acid network) in a pH solution is shown in Fig. 3.10

In Fig. 3.10 the equilibrium between the swollen ionic gel and its surroundings resembles Donnan membrane equilibria. In such a system, the polymer acts as its own membrane preventing diffusion of the fixed charged substituents into the outer solution.⁷³ Equilibrium is reached when the chemical potentials of mobile components within the gel are equal to those in the reservoir (osmotic equilibrium) and simultaneously, the chemical potential of free hydrogen ions in the gel equals that of counterions (chemical equilibrium).⁷⁹

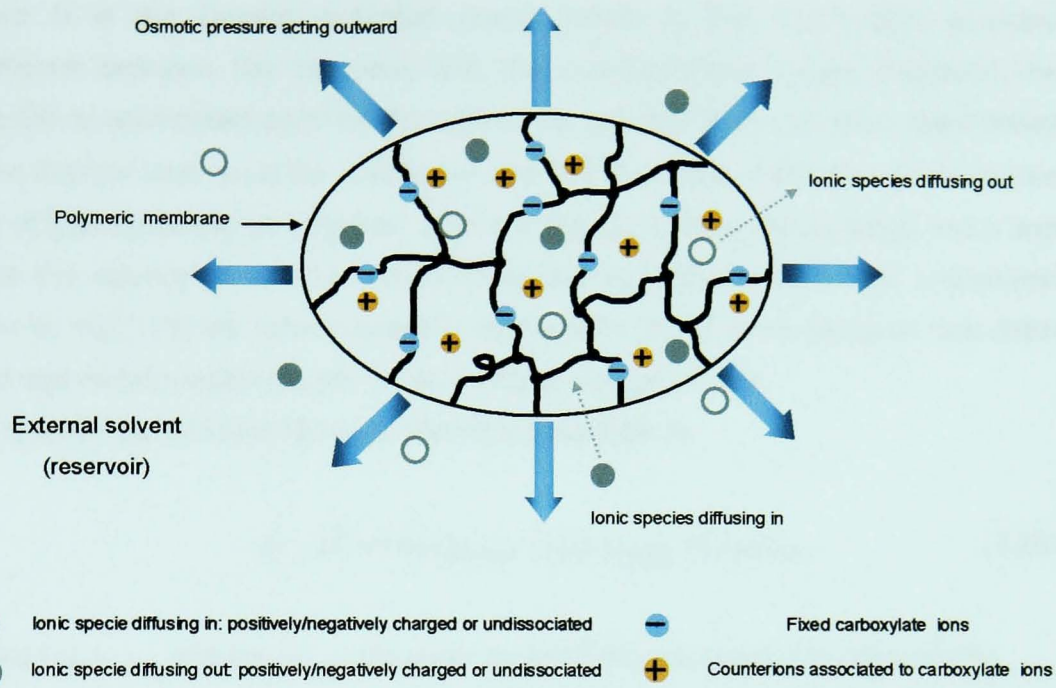


Fig. 3.10. Schematic diagram of the swelling of an ionisable hydrogel in a pH solution. The blue arrows represent the osmotic pressure mainly due to the counterions inside the gel. The outer part of the gel acts like a polymeric membrane that allows free ionic species diffuse in and out of the network but prevent the diffusion of the fixed charges (carboxylate ions) in the external solvent. The distribution of the ions between the gel and the reservoir is obtained from Donnan equilibrium.

To obtain the equilibrium conditions we express the free energy of the ionisable gel as

$$\Delta F_{total} = \Delta F_{elastic} + \Delta F_{mixing} + \Delta F_{ion}, \quad (3.53)$$

where the first two terms are common for neutral networks (as described in the previous section) and ΔF_{ion} is the free energy term due to the ionic nature of the polymer network and can be written as⁷⁹

$$\Delta F_{ion} = \Delta F_{dis} + \Delta F_{Coul}, \quad (3.54)$$

where ΔF_{dis} is introduced to account for the dissociation of the acid groups. They are assumed to be far apart in the chains thus interactions between them are neglected; ΔF_{Coul} is the free energy contribution associated with Coulombic interactions within the system and can be expressed as

$$\Delta F_{Coul} = \sum_i \phi_i z_i U + \phi_a z_a U, \quad (3.55)$$

where U is the Donnan potential energy which is the electrostatic potential difference between the reservoir and the polyelectrolyte region (network). The potential is considered constant throughout the gel and does not affect the mobility of the internal ions; ϕ_i is the number of ions in the gel (the subscript i refers to free ions of type i (positive or negative) and a to the dissociated acrylic acid), and z and e are the valency of ions and elementary charge respectively. In the expression given by eq.(3.55) we have neglected electrostatic interactions between ions (both fixed and mobile) within the gel for simplicity in our arguments.

We express eq. (3.53) in terms of chemical potentials as

$$\mu_1 - \mu_1^0 = (\Delta\mu_1)_{elastic} + (\Delta\mu_1)_{mixing} + (\Delta\mu_1)_{ion}, \quad (3.56)$$

where $(\Delta\mu_1)_{mixing}$ and $(\Delta\mu_1)_{elastic}$ are given by eq.(3.47) and eq.(3.48) respectively.

In the neutral gels section μ_1^0 and μ_1 are the chemical potential of solvent outside and inside the gel respectively, the solvent outside being pure water. In the case of charged gels, the chemical potential of the solvent outside the gel contains ions and so differs from the chemical potential of pure water. We name μ_1^* to the chemical potential of external solution (containing ions).⁷³

For the swelling equilibrium, fulfilment of $\mu_1^* = \mu_1$ is required so $\mu_1 - \mu_1^0 = \mu_1^* - \mu_1^0$, taking this into account we can write eq. (3.56) as

$$(\Delta\mu_1^*)_{ion} - (\Delta\mu_1)_{ion} = (\Delta\mu_1)_{elastic} + (\Delta\mu_1)_{mixing}, \quad (3.57)$$

where $(\Delta\mu_1^*)_{ion} = \mu_1^* - \mu_1^0$. In general $(\Delta\mu_1^*)_{ion} = \mu_1^* - \mu_1^0 = gRT \ln N_1^*$ where g is a constant, known as the osmotic coefficient and N_1^* the mole fraction of solvent in the reservoir. In dilute solutions $g \approx 1$ and $\ln N_1^* \cong -\phi_1 \sum_i n_i^*$, where $\sum_i n_i^*$ is the concentration of all ionic solute species in the reservoir.⁷³ Hence

$$(\Delta\mu_1^*)_{ion} \approx -\phi_1 RT \sum_i n_i^*, \quad (3.58)$$

Similarly with the gel

$$(\Delta\mu_1)_{ion} \approx -\phi_1 RT \sum_i n_i, \quad (3.59)$$

where the summation includes all mobile species only. Substitution of the expressions given by eq.(3.58) and (3.59) together with those given by eq.(3.47) and (3.48) into eq.(3.57) we obtain

$$RT \sum_i (n_i - n_i^*) = \frac{RT}{\varphi_1} \left(\ln(1 - \nu_{2m}) + \nu_{2m} + \chi \nu_{2m}^2 + \varphi_1 \frac{N_c^{gel}}{V_0} \left(\nu_{2m}^{1/3} - \frac{\nu_{2m}}{2} \right) \right), \quad (3.60)$$

where $\sum_i (n_i - n_i^*) = (n_+ + n_- - n_+^* - n_-^*)$

More relationships are needed for the Donnan equilibrium, these include

$$\frac{n_{neutral}}{n_{neutral}^*} = 1, \quad (3.61)$$

where $n_{neutral}$ and $n_{neutral}^*$ refers to the concentration of neutral solute (undissociated electrolyte) in the gel and external solution respectively. The other two important relations that need to be introduced are

$$\frac{n_i}{n_i^*} = \exp\left(-\frac{z_i U}{k_B T}\right) = K^{z_i}, \quad (3.62)$$

and

$$\frac{n_a n_h}{n_{ah}} = \frac{[A^-][H^+]}{[AH]} = K_a, \quad (3.63)$$

where we have introduced the Donnan ratio K in eq.(3.62) which describes the distribution of mobile ions of type i between the gel and the solution ; the term

$\frac{n_i}{n_i^*}$ can be $\frac{n_i}{n_i^*} = \frac{n_+}{n_+^*} = \frac{n_-}{n_-^*}$. Eq. (3.63) describes the dissociation equilibrium of the

fixed acid groups introducing dissociation constant in the gel: K_a . We make the assumptions that only hydrogen ions of molar concentration $n_h=[H^+]$ can associate with the carboxylate of molar concentration $n_a=[A^-]$; $[AH]=n_{ah}$ refers to the concentration of ionisable repeat units on polymer chains.

We derive now equations for the free mobile ions inside and outside the anionic gel due to the added monovalent salt (e.g. NaOH or HCl)

$$n_+ = \nu_+ n_{neutral} \text{ and } n_- = \nu_- n_{neutral} + \alpha \frac{n_2}{z_-}$$

implies that

$$n_+ + n_- = (\nu_+ + \nu_-) n_{neutral} + \alpha \frac{n_2}{z_-} = \bar{\nu} n_{neutral} + \alpha \frac{n_2}{z_-}, \quad (3.64)$$

$$n_+^* = \nu_+ n_{neutral}^* \text{ and } n_-^* = \nu_- n_{neutral}^* \Rightarrow n_+^* + n_-^* = (\nu_+ + \nu_-) n_{neutral}^* = \bar{\nu} n_{neutral}^* \quad (3.65)$$

where stoichiometric coefficients ν_i are coefficients that represent the degree to which a chemical species participates in a reaction $\nu_+ = \nu_-$; n_2 ($n_2 = n_{ah}$) refers to the molar concentration of fixed ionizable repeat units in the gels; αn_2 is the concentration of fixed ions in the gel in equilibrium, where α is the degree of dissociation and can be expressed as

$$\alpha = \frac{[A^-]}{[AH] + [A^-]} = \frac{k_a}{K_a + [H^+]} = \frac{K_a}{K_a + 10^{-pH}}. \quad (3.66)$$

Introducing in the left side of eq.(3.60) the relations given by eq.(3.64) and (3.65) we obtain

$$RT \sum_i (n_i - n_i^*) = RT(n_+ + n_- - n_+^* - n_-^*) = RT \left[\frac{\alpha n_2}{z_-} - \bar{\nu} (n_{neutral} - n_{neutral}^*) \right], \quad (3.67)$$

and introducing this new expression in the swelling equilibrium given by eq. (3.60)

$$\begin{aligned} \frac{\alpha n_2}{z_-} - \bar{\nu} (n_{neutral} - n_{neutral}^*) = \\ = \frac{1}{\varphi_1} \left(\ln(1 - \nu_{2m}) + \nu_{2m} + \chi \nu_{2m}^2 + \varphi_1 \frac{N_c^{gel}}{V_0} \left(\nu_{2m}^{1/3} - \frac{\nu_{2m}}{2} \right) \right), \end{aligned} \quad (3.70)$$

which has to be resolved for $(n_{neutral} - n_{neutral}^*)$ and is not a simple task without approximations. A good approximation is to consider that the external free ions concentration is small when compared to that of the dissociated fixed anions. In such case $n_{neutral}^* \ll \alpha n_2 / z_-$, and then we can neglect the term $\bar{\nu} (n_{neutral} - n_{neutral}^*)$ in the left hand side of eq.(3.70).

In addition, we make the same approximation as we have made for neutral gels in the previous section: consider low degree of crosslinking \equiv high degree of swelling which implies high q_m in a good solvent situation and small ν_{2m} .⁷³ As a result $\nu_{2m}^{1/3} \gg \nu_{2m}$, then as an approximation we neglect $\nu_{2m}/2$ and higher terms in the series expansion of $\ln(1-\nu_{2m})$ in eq.(3.70) resulting⁷³

$$\frac{\alpha n_2}{z_- \varphi_1} = \frac{1}{\varphi_1} \left(\chi - \frac{1}{2} \right) \nu_{2m}^2 + \frac{N_c^{gel}}{V_0} \nu_{2m}^{1/3}, \quad (3.71)$$

and expressing the concentration of fixed acid groups in the polymers as

$$n_2 = \frac{\nu_{2m}}{V_{monomer}}, \quad (3.72)$$

where $V_{monomer}$ is the molar volume of the monomer unit of the polymer ($=\tilde{v}M_{monomer}$)
Introducing eq.(3.72) into eq.(3.71) we obtain the swelling equation as a function of ν_{2m} as

$$\frac{\alpha \nu_{2m}}{z_- V_{monomer} \varphi_1} = \frac{1}{\varphi_1} \left(\chi - \frac{1}{2} \right) \nu_{2m}^2 + \frac{N_c^{gel}}{V_0} \nu_{2m}^{1/3}, \quad (3.73)$$

and from this final expression the ratio of swelling can be calculated by substituting ν_{2m} for $1/q_m$ as we have done previously for neutral networks; this ratio will have a strong dependence on the degree of dissociation.⁷³

3.3.4 Physical properties of hydrogels

3.3.4.1 Mechanical properties

Hydrogels resemble natural rubbers in their ability to elastically respond to applied stress. A hydrogel subjected to a relatively small deformation, less than 20% will fully recover to its original dimension in a rapid fashion. Accordingly, hydrogels can be mechanically characterised by an elastic shear modulus⁸¹ G which can be defined as the ratio of shear stress to the shear strain.

The Young modulus E is defined as the limit, for small strains, of the rate of change of stress with linear strain. Flory and Rehner⁸⁵ recognized the swelling phenomenon

exhibited by cross-linked polymers when exposed to certain solvents and derived an expression for the elastic modulus of a swollen (isotropic) polymer network as

$$E = \left(\frac{RT\rho_c^{gel} \nu_{2m}^{1/3}}{M_c} \right) \left(1 + \frac{2}{\beta_{gel}^2} \right), \quad (3.74)$$

where all the terms have been defined in the previous section. For a chemically cross-linked gel in a good solvent for the polymer, the elastic modulus would be expected to be less than that of a rubbery polymer, below 10 MPa.⁸³

3.3.4.2 Diffusion properties

The swelling kinetics of hydrogels can be classified as diffusion controlled (Fickian) and relaxation-controlled (non-Fickian) swelling.⁸¹ When water diffuses into the hydrogels much faster than the relaxation time employed by the polymer chains, the swelling kinetics is diffusion controlled. We focus on the case where the expansion and contraction of hydrogels depends on the diffusion of water or solvent into and out of the matrix.⁹⁰ The type of diffusion present in polymer networks in the presence of solvent is called collective diffusion, defined as the cooperative diffusion of a large number of particles, most often within a solvent. The diffusion coefficients of solutes in gels have been measured and do not differ dramatically from those in solution.⁹¹ Accordingly, by extending descriptions developed for long polymer chains in solution, diffusion constants in terms on the Flory radius and viscosity can be given.

The arguments presented here are obtained from a two fluid model.⁹² We introduce a displacement vector $u=u(r,t)$ which represents the displacement of a point r of a polymer network from its average location at time t . Such a displacement for every point in the gel results from a balance between the the elastic restoring force and a viscous force due to the solvent resistance.^{3,46,92} The elastic force per unit volume of the gel is $G\nabla^2 u(r,t)$ where G is the elastic shear modulus. The viscous force exerted by a solvent flowing through a porous medium of pore size R_c^{gel} (mesh size) is given by the Brinkman equation⁹³ and is of the order of $\eta(R_c^{gel})^{-2} \frac{\partial u(r,t)}{\partial t}$, where η is the solvent viscosity. Thus, the force balance in the gel can be written as

$$\frac{\partial u(r,t)}{\partial t} = \frac{G(R_c^{gel})^2}{\eta} \nabla^2 u(r,t), \quad (3.75)$$

which is Fick's Second Law of diffusion used for non-steady or continually changing state diffusion,⁹⁴ i.e. when the concentration within the diffusion volume changes with respect to time; the diffusion constant D in eq.(3.75) is

$$D = \frac{G(R_c^{gel})^2}{\eta}, \quad (3.76)$$

where R_c^{gel} is given by eq.(3.50). This diffusion constant assumes that all chains interact

A thorough discussion of the mathematics involved in diffusion processes in polymer network systems is given by Crank.⁹⁵

REFERENCES

- (1) Donnan, F. Z. *Physik. Chem.A* **1934**, *168*, 369.
- (2) Donnan, F.; Guggenheim, E. Z. *Physik. Chem.A* **1932**, *122*, 346.
- (3) Barrat, J. L.; Joanny, J. F. *Advances in Chemical Physics* **1996**, *81*.
- (4) Advincula, R. C.; Brittain, W. J.; Caster, K. C.; R ue, J. *Polymer Brushes: Synthesis, Characterization and Applications*; John Wiley & Sons Inc, 2004.
- (5) Miiner, S. T. *Science* **1991**, *251*, 905.
- (6) Halperin, A.; Tirrell, M.; Lodge, T. P. *Adv. Polym. Sci* **1992**, *100*, 131.
- (7) Szleifer, I.; Carignano, M. A. *Adv. Chem. Phys* **1996**, *94*, 165.
- (8) Alexander, S. J. *Phys(France)* **1977**, *38*, 983-987.
- (9) de-Gennes, P. *Macromol* **1980**, *13*, 1069-1075.
- (10) Auroy, P.; Auvray, L.; Leger, L. *Macromolecules* **1991**, *24*, 2523-2528.
- (11) Krenkler, K. P.; Laible, R.; Angew, K. H. *Angew. Makromol. Chem.* **1953**, *53*, 101.
- (12) Laible, R.; Hamann, K. *Adv. Colloid Interface Sci* **1980**, *13*, 65.
- (13) Mansky, P.; Liu, Y.; Huang, E.; Russell, T. P.; Hawker, C. *Science* **1997**, *275*, 1458.
- (14) Zajac, R.; Chakrabarti, A. *Phys. Rev. E* **1995**, *52*, 6536.
- (15) Kopf, A.; Baschnagel, J.; Wittmer, J.; Binder, K. *Macromolecules* **1996**, *29*, 1433-1441.
- (16) Zhao, B.; Brittain, W. J. *Prog. Polym. Sci.* **2000**, *25*, 677.
- (17) Prucker, O.; Ruehe, J. *Langmuir* **1998**, *14*, 6893-6898.
- (18) Prucker, O.; Ruehe, J. *Macromolecules* **1998**, *31*, 602.
- (19) Prucker, O.; Ruehe, J. *Macromolecules* **1998**, *31*, 592.
- (20) Jordan, R.; West, N.; Ulman, A.; Chou, Y. M.; Nuyken, O. *Macromolecules* **2001**, *34*, 1606-1611.
- (21) Biesalski, M.; Ruehe, J. *Macromolecules* **2002**, *35*, 499-507.
- (22) Biesalski, M.; Ruehe, J. *Langmuir* **2000**, *16*, 1943.
- (23) Biesalski, M.; Ruehe, J. *Macromolecules* **1999**, *32*, 2309-2316.
- (24) Biesalski, M.; Ruehe, J.; Kuegler, R.; Knoll, W. *Polyelectrolytes at solid surfaces: multilayers and brushes, in Handbook of Polyelectrolytes*; Am. Sci. Publ.: San Diego, 2002; Vol. 1.
- (25) Guo, X.; Ballauff, M. *Langmuir* **2000**, *16*, 8719-8726.

- (26) Guo, X.; Weiss, A.; Ballauff, M. *Macromolecules* **1999**, *32*, 6043-6046.
- (27) Matyjaszewski, K. *ACS Symposium, American Chemical Society, Washington 2000*, *768*, 82-92.
- (28) Matyjaszewski, K.; Miller, P.; Shukla, N.; Immaraporn, B.; Gelman, A.; Luokala, B. B.; Siclovan, T. M.; Lickelbick, G.; Vallant, T.; Hoffmann, H.; Pakula, T. *Macromolecules* **1999**, *32*, 8716-8724.
- (29) Ejaz, M.; Yamamoto, S.; Ohno, K.; Tsujii, Y.; Fukuda, T. *Macromolecules* **1998**, *31*, 5934-5936.
- (30) Ejaz, M.; Ohno, K.; Tsujii, Y.; Fukuda, T. *Macromolecules* **2000**, *33*, 2870-2874.
- (31) Biesalski, M.; Johannsmann, D.; Ruhe, J. *Journal Chem. Phy* **2002**, *117*, 4988-4994.
- (32) Kelsall, R.; Hamley, I. W.; Geoghegan, M. *Nanoscale science and Technology*, Wiley, 2005.
- (33) Flory, P. J. *Statistical Mechanics of Chain Molecules*; Oxford University Press: Oxford, 1989.
- (34) Jones, R. A. L.; Richards, R. W. *Polymers at Surfaces and Interfaces*; Cambridge University Press: Cambridge, 1999.
- (35) Auroy, P.; Auvray, L.; Leger, L. *Phys. Rev. Lett* **1991**, *66*.
- (36) Auroy, P.; Auvray, L.; Leger, L. *Macromol* **1991**, *24*, 5158-5168.
- (37) Taunton, H. J.; Toprakcioglu, C.; Fetters, L. J.; Klein, J. *Macromol* **1990**, *23*, 571-579.
- (38) Taunton, H. J.; Toprakcioglu, C.; Fetters, L. J.; Klein, J. *Nature* **1988**, *332*, 712.
- (39) Murat, M.; Grest, G. S. *Macromol* **1989**, *22*, 4054-4059.
- (40) Chakrabarti, A.; Torai, R. *Macromol* **1990**, *23*, 2016-2021.
- (41) Muthukumar, M.; Ho, J. S. *Macromolecules* **1989**, *22*, 965.
- (42) Seidel, C. *Macromolecules* **2003**, *36*, 2536.
- (43) Semenov, A. N. *Sov. Phys. JETP* **1985**, *61*, 733.
- (44) Milner, S. T.; Witten, T. A.; Cates, M. E. *Macromolecules* **1988**, *21*, 2610-2619.
- (45) Skovortsov, A. M.; Pavlushkov, I. V.; Gorbunov, A. A.; Zhulina, Y. B.; Borisov, O. V.; Pryamistyn, V. A. *Pol. Sci* **1988**, *30*, 1706.
- (46) de-Gennes, P. G. *Scaling Concepts in Polymer Physics*, 5th ed.; Cornell University Press: New York, 1996.
- (47) Pincus, P. *Macromolecules* **1991**, *24*, 2912-2919.
- (48) Auroy, P.; Auvray, L. *Macromolecules* **1992**, *25*, 4134-4141.
- (49) Grest, G. S.; Murat, M. *Macromolecules* **1993**, *26*, 3108.
- (50) Pincus, P. *Macromolecules* **1991**, *24*, 2912-2919.
- (51) Zhulina, E. B.; Borisov, O. V.; Birshtein, T. M. *J. Phys. II* **1992**, *2*, 63.
- (52) Miklavic, S.; Marcelja, S. *J. Phys. Chem* **1988**, *92*, 6718-6722.
- (53) Misra, S.; Varanasi, S.; Varanasi, P. *Macromolecules* **1989**, *22*, 5173.
- (54) Zhulina, E. B.; Borisov, O. V. *J. Chem. Phys* **1997**, 5952.
- (55) Mir, Y.; Auvroy, P.; Auvray, L. *Phys. Rev. Lett* **1995**, *75*, 2863.
- (56) Ahrens, H.; Forster, S.; Helm, C. A. *Phys. Rev. Lett* **1998**, *81*, 4172-4176.
- (57) Ahrens, H.; Forster, S.; Helm, C. A. *Macromolecules* **1997**, *30*, 8447-8452.
- (58) Ross, R. S.; Pincus, P. A. *Macromolecules* **1992**, *25*, 2177-2183.
- (59) Borisov, O. V.; Birstein, T. M.; zhulina, E. B. *J. Phys II (France)* **1991**, *1*, 521.
- (60) Zhulina, E. B.; Borisov, O. V. *Macromolecules* **1996**, *29*, 2618-2626.
- (61) Israelachvili, J. N. *Intermolecular and Surface Forces*; Academic London, 1985.
- (62) Israels, R.; Leermakers, F. A. M.; Fler, G. J. *Macromolecules* **1994**, *27*, 3087-3093.
- (63) Lyatskaya, Y. V.; Leermakers, F. A. M.; Fler, G. J.; Zhulina, E. B.; Birshtein, T. M. *Macromolecules* **1995**, *28*, 3562-3569.
- (64) Zhulina, E. B.; Borisov, O. V.; Birshtein, T. M. *Macromolecules* **1999**, *32*, 8189-8196.

- (65) Borisov, O. V.; Boulakh, A. B.; Zhulina, E. B. *Eur. Phys. J. E* **2003**, *12*, 543-551.
- (66) Cosgrove, T.; Heath, T.; Lent, B. v.; Leemarkers, F. A. M.; Scheutjens, J. M. H. M. *Macromolecules* **1987**, *20*, 1692-1696.
- (67) Hurter, P. N.; Scheutjens, J. M. H. M.; Hatton, T. A. *Macromolecules* **1993**, *26*, 5030-5035.
- (68) Bjorling, M.; Linse, P.; Karlstrom, G. *J. Phys. Chem* **1990**, *94*, 471.
- (69) Zhulina, E. B.; Borisov, O. V.; Priamitsin, V. A.; Birshtein, T. M. *Macromolecules* **1991**, *24*, 140-145.
- (70) Zhulina, E. B.; Birshtein, T. M.; Borisov, O. V. *Macromolecules* **1995**, *28*, 1491-1499.
- (71) Jenkins, A. D.; Kratochvil, P.; Stepto, R. F. T.; Suter, U. W. *IUPAC, Glossary of Basic Terms in Polymer Science. Pure Appl. Chem* **1996**, *68*, 2287.
- (72) Ostroha, J.; Pong, M.; Lowman, A.; Dan, N. *Biomaterials* **2004**, *25*, 4345-4353.
- (73) Flory, P. J. *Principles of Polymer Chemistry*, Cornell University Press: New York, 1969.
- (74) Flory, P. J.; Rehner, J. J. *J. Chem. Phys* **1944**, *12*, 412-414.
- (75) Horkay, F.; Zrinyi, M. *Macromolecules* **1982**, *15*, 1306-1310.
- (76) Geissler, E.; Hecht, A. M.; Horkay, F.; Zrinyi, M. *Macromolecules* **1988**, *21*, 2594-2599.
- (77) Mallam, S.; Horkay, F.; Hecht, A. M.; Geissler, E. *macromolecules* **1989**, *22*, 3356-3361.
- (78) Barrat, J. L.; Joanny, J. F.; Pincus, P. *J. Phys II (France)* **1992**, *2*, 1531-1544.
- (79) Ricka, J.; Tanaka, T. *Macromolecules* **1984**, *17*, 2916-2921.
- (80) Skouri, R.; Schosseler, F.; Munch, J. P.; Candau, S. J. *Macromolecules* **1995**, *28*, 197-210.
- (81) Peppas, N. A.; Bures, P.; Leobandung, W.; Ichikawa, H. *Eur. J. Pharmaceutics and Biopharmaceutics*. **2000**, *50*, 27-46.
- (82) Jones, R. A. L. *Soft Condensed Matter*, Oxford University Press: Oxford, 2002.
- (83) Calvert, P. *Electroactive Polymer (EAP) Actuators as Artificial Muscles: Reality, Potential, and Challenges. Chapter 5, Electroactive Polymer gels*, Second ed.; Press Monograph PM136, 2004.
- (84) Hoffman, A. S. *Adv. Drug. Del. Rev* **2002**, *43*, 3-12.
- (85) Flory, P. J.; Rehner, J. J. *J. Chem. Phys* **1943**, *11*, 521-526.
- (86) James, H. M.; Guth, E. J. *J. Chem. Phys* **1943**, *11*, 455.
- (87) Russ, T.; Brenn, R.; Geoghegan, M. *Macromolecules* **2003**, *36*, 127-141.
- (88) Katchalsky, A.; Lifson, S.; Heisenberg, H. *J. Polym. Sci* **1951**, *7*, 571.
- (89) Katchalsky, A.; Michaeli, J. *J. Poly. Sci* **1955**, *9*, 69.
- (90) Peppas, N. A.; Colombo, P. J. *Control. Release* **1997**, *45*, 35-40.
- (91) Pavesi, L.; Rigamonti, A. *Phys. Rev. E* **1995**, *51*, 3318-3323.
- (92) Tanaka, T.; Hocker, L. O.; Benedek, G. B. *J. Chem. Phys* **1973**, *59*, 5151-5159.
- (93) Brinkman, H. C. *Appl. Sci. Res* **1947**, *A1*, 27.
- (94) Fick, A. *Philos. Mag* **1855**, *10*, 30.
- (95) Crank, J. *The Mathematics of Diffusion*; Oxford University Press: Oxford, 1975.

Part II

Experimental

Chapter 4

Experimental Techniques

We present in this chapter the experimental techniques employed in this thesis. The chapter is divided into three major sections concerning three separated areas: single poly(methacrylic) acid chains, polyacid and polybase brushes and adhesion measurements on poly(methacrylic) acid gel/brush systems.

Sample preparation, instrumentation and analysis are presented in each section.

4.1 LABELLED POLY(METHACRYLIC) ACID

The behaviour of single poly(methacrylic) acid chains will be studied mainly via fluorescence techniques. Thus, the polyacid chains used are labelled with fluorescent chromophores.

4.1.1 Sample preparation

The monomer used was methacrylic acid, MAA (Aldrich-99%) distilled under vacuum and stored below 0°C in a stoppered vessel. In order to be able to screen the pH dependent behaviour of MAA the following fluorescent chromophores were employed: acenaphthalene (N) and (9-anthryl) methyl methacrylateanthracene (A). Acenaphthalene (N) (Aldrich-85%) was purified by precipitation liquid chromatography; a mixture (60/40 volume %) of acetonitrile and water was used as the eluent at a flow rate of 1 ml/min. The monomer solution collected from the column was evaporated and dried in a vacuum oven overnight at room temperature. (9-Anthryl) methylmethacrylate anthracene (A) synthesis was performed by Dr Ramune Rutkaite as discussed elsewhere.¹ The initiator used was 2,2'-azobisisobutyronitrile (AIBN) recrystallized from NaOH or EtOH (three times). The

recrystallised material was washed with a small amount of methanol, filtered under vacuum and dried in a vacuum oven overnight at room temperature. The purified reagent was stored at -10°C .

Poly(methacrylic) acid (PMAA) was synthesized by copolymerization of MAA with the single comonomer N (label) 0.5mol% in feed, A (label) 1.5 mol% and the double label NA 0.5mol%/1.5mol% in the feed, yielding N-PMAA,A-PMAA and NA-PMAA respectively. The polymerization was performed by free radical polymerization using AIBN as initiator in benzene solution. Fig. 4.1 shows a diagram of the structure of NA-PMAA and rotation of both chromophores N and A when excited.

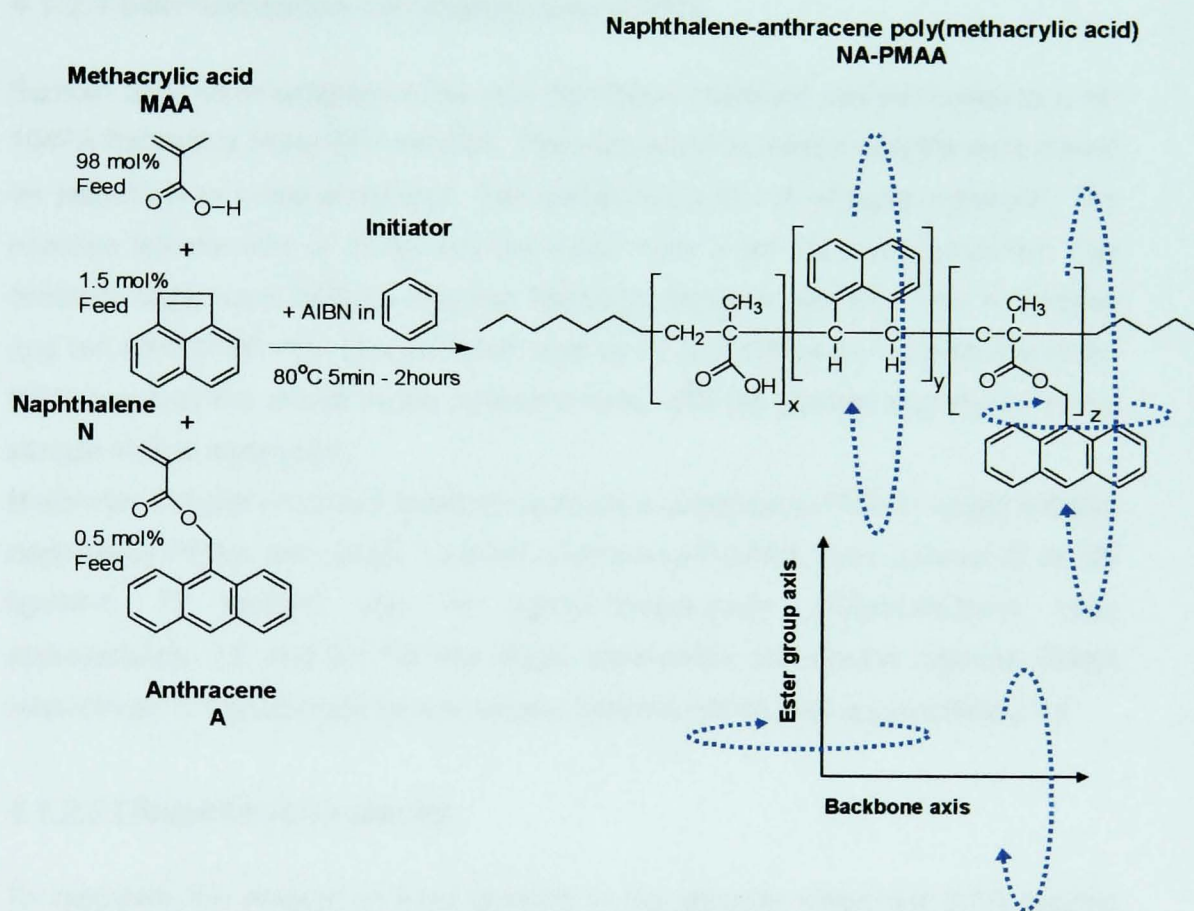


Fig 4.1 Chemical structure of labelled NA-PMAA polymer chains. It is also shown the rotation axis of excited naphthalene and anthracene chromophores

Before use, the samples were thoroughly degassed (oxygen inhibits free radical polymerisation), three times freeze pumped and sealed under high vacuum (ca 10^{-4} mbar). After the degassing process the samples were polymerised at 60°C for 48 hours. In order to ensure a truly random distribution of fluorescent chromophores along the length of the polymer most samples were only allowed to proceed to 10-20% conversion (full conversion leads to branching and problems due to the

reactants no longer being in excess). The polymers were purified by multiple dissolution (five times) in methanol followed by precipitation into diethyl ether. As shown in Fig.4.1 the final product is a polymer bearing a naphthyl chromophore rigidly bound to the chain backbone through two single covalent bounds, such that polymer segment-independent motion is not possible; and an anthracene chromophore bound via a methacrylate group (i.e. limited to only the carbon backbone). The anthracene probe can then rotate around two different axes.

4.1.2 Sample characterisation

4.1.2.1 Gel-Permeation Chromatography (GPC)

Sample GPC chromatogram of the labelled PMAA materials was performed in a HP 1047A Refractive Index (RI) detector. The calculated molecular weights were based on polyethylene oxide standards. The conditions were of ~1mg/ml solutions. The injection volume was of 200 μ l and the eluant was a pH 7.0 aqueous buffer. The columns used were 2x30cm Viskotec Viskogel columns with flow rate of 1ml/min and run time of 40 min. The detection was by RI (the difference in refractive index (dRI) between the eluent in the reference side, and the sample and eluent in the sample side is measured).

Molecular weights of double labelled naphthalene-anthracene-PMAA, single labelled naphthalene-PMAA and single labelled anthracene-PMAA were measured as 80 kgmol⁻¹, 72 kgmol⁻¹ and 74 Kgmol⁻¹ respectively. Polydispersities were approximately 2.9 and 2.7 for the single naphthalene and double labelled PMAA respectively. Polydispersity for anthracene labelled PMAA was approximately 2.6.

4.1.2.2 Ultraviolet (UV) spectra.

To calculate the amount of label present in the polymer Ultraviolet (UV) spectra were recorded with a Hitachi U-2010 spectrometer scanning from 200 to 400nm. The wavelengths where there was maximum absorption were estimated from the absorption spectra. Polymer solutions (0.01 wt%) in methanol (spectroscopic grade) were prepared and measured at room temperature. For NA-PMAA the concentration of anthracene was calculated first with the amount of naphthalene calculated from the absorption at 290 nm after correction for anthracene absorption. A detailed explanation of the method employed is given at the appendix 2. For NA-PMAA the amount of naphthalene and anthracene was 0.56 mol% and 0.23 mol% respectively (i.e. there is 1 naphthalene per 221 units of monomer MAA and 1 anthracene per

440 units of MAA). For the single labelled N-PMAA the calculated amount of naphthalene chromophores was 0.82 mol% or 1 unit of naphthalene every 130 units of MAA. For the single labelled A-PMAA the calculated amount of anthracene chromophores was 1 unit of anthracene every 330 units of MAA. UV absorption spectra of N-PMAA, A-PMAA and NA-PMAA are shown in Fig. 4.2.

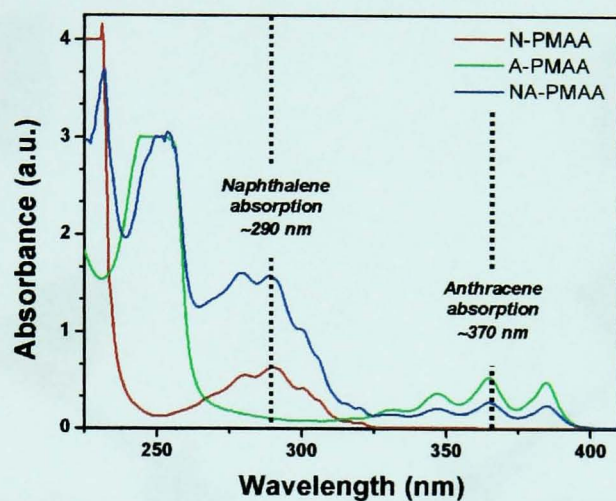


Fig 4.2. UV absorption spectra of N-PMAA, A-PMAA and NA-PMAA in methanol 0.01 wt % scanning from 200 to 400nm.

In order to monitor single molecule behaviour via fluorescence techniques, aqueous dilute solutions of 0.01wt% were prepared with N-PMAA, NA-PMAA and A-PMAA samples.

4.1.3 Fluorescence measurements: Instrumentation and Analysis

4.1.3.1 Steady State measurements

The Steady State Measurements were performed in a LS-50B Perkin-Elmer luminescence spectrometer equipped with a 20kW/ 8 μ s-equivalent xenon discharge lamp (FL WinLAB Software). Pulse width at half height is better than 10 μ s. The optical system consists of two reflection grating monochromators (excitation and emission), two polarisers (excitation and emission) and the reference and sample photomultiplier detectors. Fig. 4.3 shows a schematic diagram of the LS-50B Perkin-Elmer luminescence spectrometer.

In the present study single labelled (N-PMAA) and double labelled (NA-PMAA) samples have been excited at the characteristic excitation wavelength of the donor

(N) 290nm. Emission intensity was recorded over a range of wavelengths including the characteristic emission wavelengths of naphthalene and anthracene, 340 and 420 nm respectively. It is important to state that the dilute condition of our experiment allows us to study the (average) behaviour of single polymer chains.

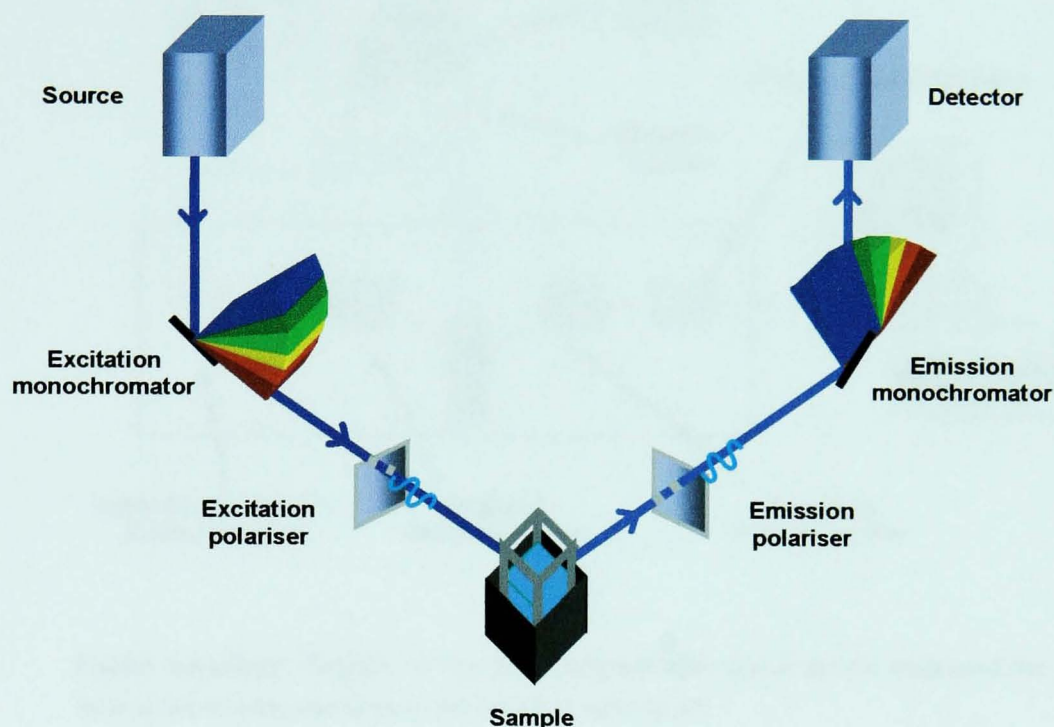


Fig.4.3 Layout of the LS-50B Perkin-Elmer luminescence spectrometer used for steady state measurements.

Energy Transfer efficiencies were characterized by the ratio of the emission intensities of anthracene and naphthalene I_A/I_N at 420 and 340 nm respectively.

In order to study the acceptor (A) behaviour in NA-PMAA, excitation scans have been recorded (at a fixed emission wavelength of 420nm) over a range of wavelengths including the characteristic excitation wavelengths of naphthalene and anthracene: 290 and 370 nm respectively.

The data were obtained using a steady state fluorimeter combined with a flow cell/peristaltic pump system, such that liquid from a stirred vessel (the pH of which was accurately adjusted by means of a burette containing acid or base) was constantly circulated through the flow cell. Drops of HCl or NaOH are added to the solution to change the pH, which is recorded as soon as the solution stabilizes. Fig. 4.4 shows a schematic diagram of the flow cell/peristaltic pump set-up employed for this experiment.

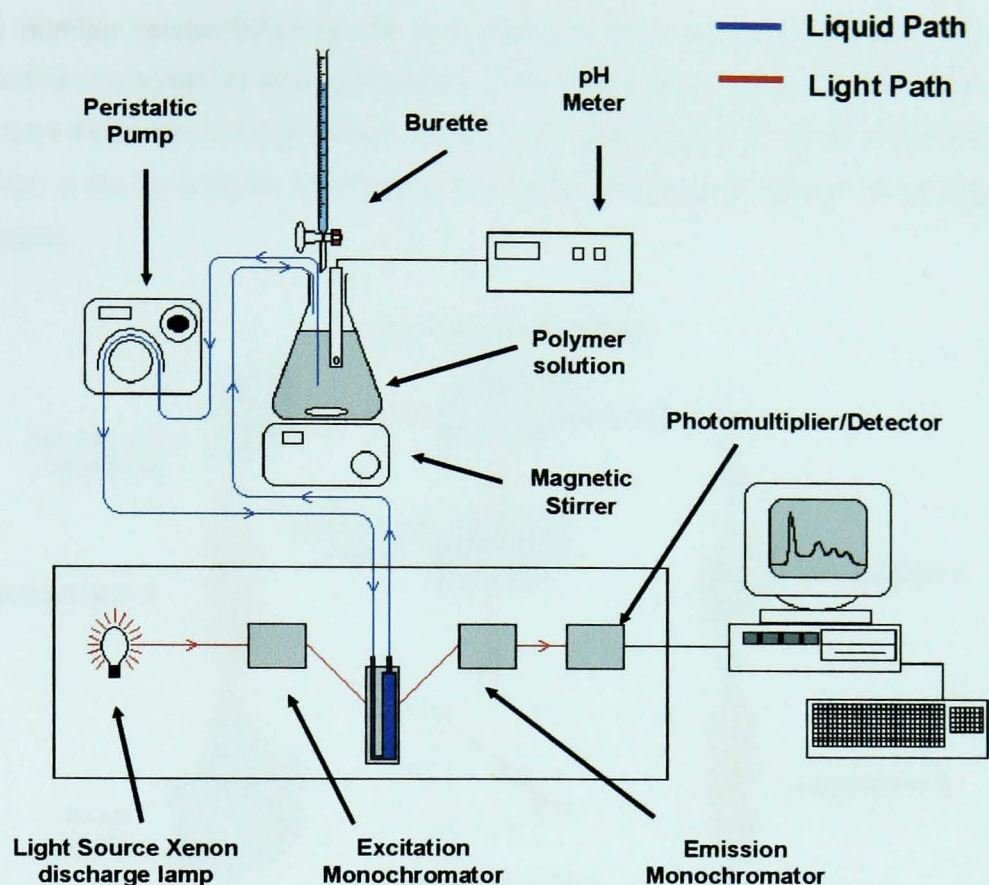


Fig.4.4 Schematic diagram of the flow cell/peristaltic pump set-up employed for fluorescence measurements in NA-PMAA at various pH.

4.1.3.2 Lifetime measurements

Measurements were carried out on a spectrometer, equipped with an IBH System 5000 coaxial nanosecond flash lamp and a single photon counting photomultiplier connected to a time to amplitude converter (TAC) and multichannel analyser (MCA). A schematic diagram of the IBH system 5000 is shown in Fig.4.5.

Each lamp flash (red path) is viewed directly by photomultiplier 1 through a fibre optic cable (Fig.4.5). The output from photomultiplier 1 passes through a discriminator to the start input of the time-to-amplitude converter (TAC), where it initiates a voltage ramp linear with time. Simultaneously, the optical pulses (dark blue path) travel through the excitation monochromator, where the excitation wavelength is selected. The emission (bright blue path) passes through the emission monochromator where the analysis wavelength is selected and detected by photomultiplier 2, which is connected, via a constant fraction discriminator, to the "stop side" of the TAC. When a photon is detected, a signal is sent from the stop multiplier to the TAC, which stops the voltage ramp charging. The output from TAC,

yields a number (proportional to the time between start and stop pulses) and is stored in the multichannel analyser (MCA). After many start cycles, a histogram of various time intervals and the frequency at which they occur is built up in the MCA unit.² Such a set-up enables fluorescent decays in the range of 10's of ns to 1-2 μ s to be studied .

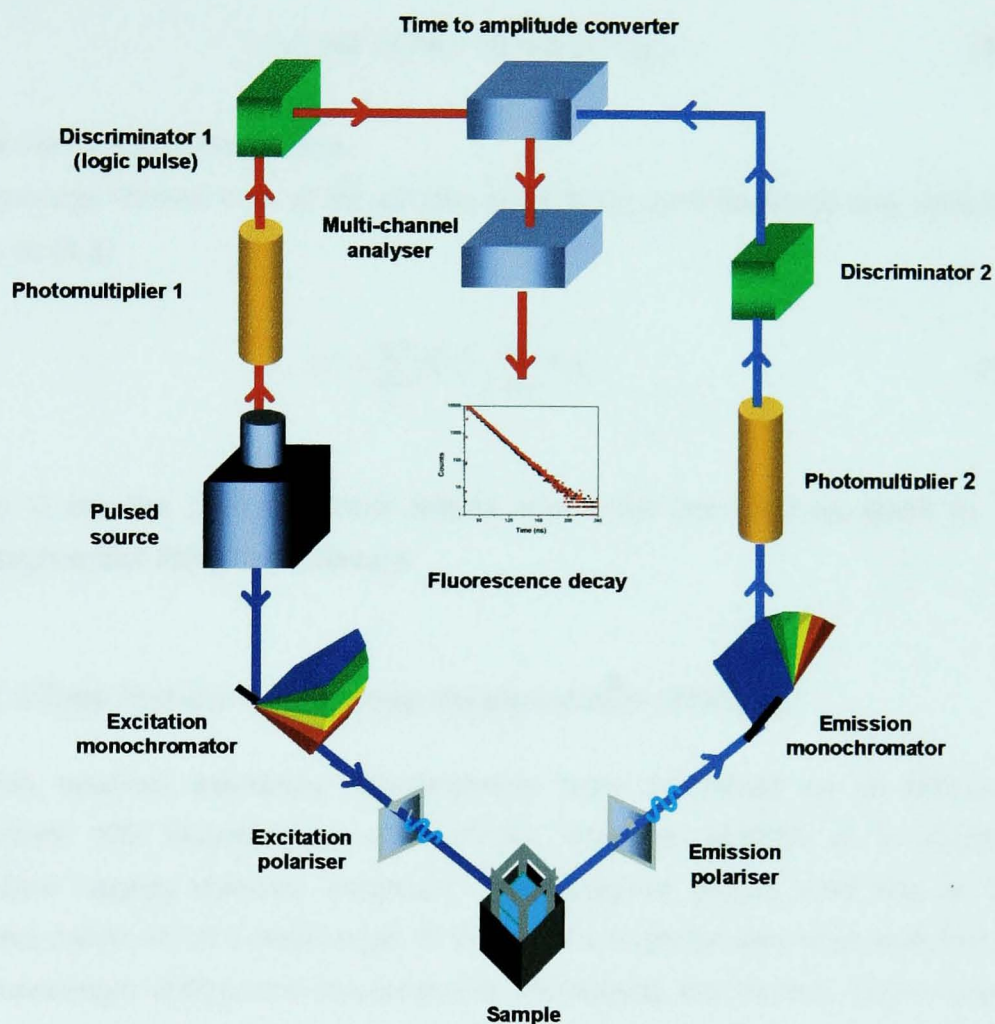


Fig 4.5 Schematic diagram of the IBH System 5000.

Naphthalene and anthracene fluorescence decays were collected at the "magic angle" of 54.7° with respect to that of vertically polarized excitation. The use of the "magic angle" results in an intensity signal proportional to the total intensity I_T , not one proportional to vertically polarized light, horizontally polarized light or a combination of both.³

Excitation and emission wavelengths of 290 and 340nm respectively were employed in N-PMAA and NA-PMAA to study acceptor decays and energy transfer. Excitation and emission wavelengths of 370 and 420nm respectively were employed in A-PMAA to study acceptor decays. Sampling was carried out using the same method comprising a pump/flow cell pH meter combination as illustrated in Fig. 4.4

The Edinburgh Instruments analysis software was used to analyse fluorescence decay curves. The use of just one exponential to fit the decays was insufficient. The decays were fitted to triple eq (4.1) or double exponential eq (4.2),

$$I = A_1 \exp(-t/\tau_1) + A_2 \exp(-t/\tau_2) + A_3 \exp(-t/\tau_3), \quad \text{or} \quad (4.1)$$

$$I = A \exp(-t/\tau_A) + B \exp(-t/\tau_B), \quad (4.2)$$

where I is intensity and t is time.

The average lifetime $\langle \tau \rangle$ of the excited state of the chromophores was estimated using eq (4.3)

$$\langle \tau \rangle = \frac{\sum_i A_i \tau_i^2}{\sum_i A_i \tau_i}, \quad (4.3)$$

where A_i are the pre-exponential factors and τ_i are the lifetimes given by the multiexponential fitting to the decays.

4.1.3.3 Time Resolved Anisotropy measurements (TRAMS)

All time resolved anisotropy measurements were performed on an Edinburgh instrument 199 Fluorescence spectrometer with the addition of a computer controlled toggling polariser accessory. The excitation source used was an IBH nanoled, model-03 at a wavelength of 370nm. The emission was fixed at 450nm. At this wavelength anthracene chromophores (acceptors) are excited. Time resolved data were obtained using time correlated single photon counting (Fig.4.5). Components of the time dependent emission intensity were collected with the emission polariser in the vertical and horizontal positions ($I_{||}(t)$ and $I_{\perp}(t)$ respectively) using a "toggling" procedure. In this procedure the analyser was rotated sequentially through 90° with simultaneous switching from the two separate detection systems (vertical and horizontal) in the Multi-channel Analyser (MCA).

In the TRAMS experiment, vertically polarized radiation is used to photoselect (via absorption) those chromophores whose transition vectors (dipole moments) are in a parallel plane to that of the incident radiation at the instant of photon incidence. If the luminescent molecule remains stationary during its excited state lifetime, the resultant radiation will remain highly polarised, characteristic of the intrinsic anisotropy r_0 of that particular species. The light emitted from the molecules that changed their orientation while they were excited will be polarised differently to the

exciting radiation. A schematic diagram in Fig.4.6 illustrates these processes taking place in TRAMS measurements.

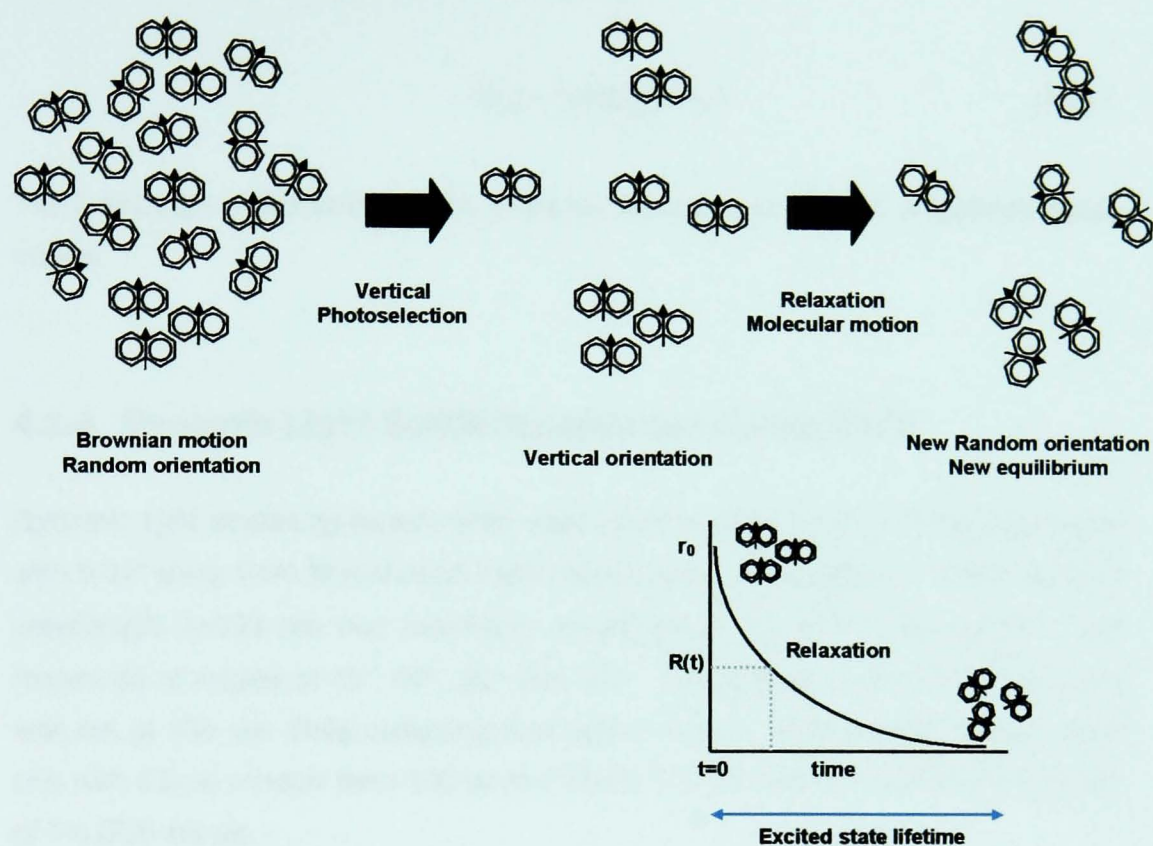


Fig.4.6 Diagram of the processes taking place in TRAMS measurements: photoselection and relaxation. Initially the chromophores are in Brownian motion. Vertically polarized radiation photoselects the chromophores whose dipole moments (represented as little black arrows in the chromophores) are vertical: vertical photoselection. After the photoselection, the molecules return to a relaxed state via light emission (during their excited state lifetime). In the new equilibrium, the orientation of the dipole moments is again random. The degree of orientation within the sample can be quantified by the anisotropy $R(t)$.

Information regarding molecular motion is contained within the relative time dependent intensities $I_{\perp}(t)$ and $I_{\parallel}(t)$ of luminescence observed in parallel and perpendicular planes to that of photoselection. To decode this information we make use of the anisotropy function $R(t)$ defined as follows:

$$R(t) = \frac{I_{\parallel}(t) - I_{\perp}(t)}{I_{\parallel}(t) + 2I_{\perp}(t)}. \quad (4.4)$$

Using eq (4.4) anisotropy decays were collected as a function of pH in NA-PMAA samples exciting anthracene. Different procedures of analysis have been discussed elsewhere.⁴ In the present studies, the raw anisotropy data $R(t)$ were directly fitted to a function (without deconvolution with the response function) which is assumed to

model the decay of true anisotropy data. Assuming the dyes behave like an isotropic rotor in a fluid environment, the anisotropy could be modelled with just one rotational correlation time τ_c using the following equation:

$$R(t) = r_0 \exp(-t/\tau_c). \quad (4.5)$$

The Edinburgh Instrument analysis software was used to analyse anisotropy decay curves.

4.1.4 Dynamic Light Scattering measurements (DLS)

Dynamic light scattering experiments were performed on a BI-200 SM goniometer with 0.01° steps from Brookhaven Instruments Corporation using a He-Ne-Laser (of wavelength $\lambda=633$ nm and maximum power output 75 mW). Each sample was measured at angles of 40° , 60° , 90° and 120° . The pinhole in front of the detector was set at $400 \mu\text{m}$. Data collecting time was 5 min for each experiment (i.e. each pH) with a time window from 100 ns to 100 ms. Fig 4.7 shows a schematic diagram of the DLS set-up.

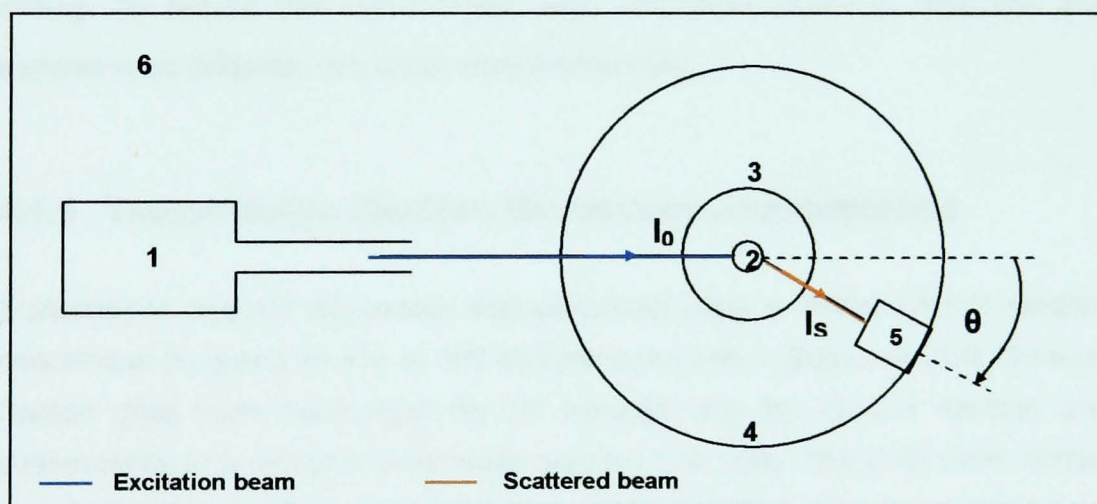


Fig. 4.7: Schematic diagram of the DLS set-up, 1: Laser, 2: Sample tube, 3: Sample bath (decaline), 4: Circular base, 5: Detector, 6: Housing.

The measured correlation functions were analysed using cumulant analysis by polynomial fit.⁵ The linear relaxation rate $\Gamma=1/\tau_d$ (where τ_d is a time constant representing the temporal decay in light scattering intensity) was plotted as a function of the squared scattering vector q^2 ($q=(2\pi/\lambda)\sin\theta$) with the linear fit to the

data forced through the origin, yielding the diffusion coefficient D_t as the slope ($\Gamma = D_t q^2$).⁶ The hydrodynamic radius R_H was determined using the Stokes-Einstein relation^{7,8}

$$R_H = \frac{k_B \cdot T}{6 \cdot \eta \cdot D_t}, \quad (4.6)$$

with k_B = Boltzmann's constant, T = absolute temperature and η = viscosity.

For dynamic light scattering, it is important to increase the concentration of the PMAA in order to increase signal intensity. Too great an increase in concentration, results in aggregation, which can be detected by a *slow mode* (interchain effects) in the DLS experiments.^{9,10} This slow mode can be inhibited by adding salt to shield the charges. However, too much salt will affect the conformational transition. The best compromise between shielding interchain forces and minimizing intrachain forces is found at a concentration of 0.1 wt% of polymer and 0.01 M of NaCl. Solutions were prepared by dissolving the same labelled PMAA used in fluorescence analysis in previously filtered 0.01 M NaCl water solution. The pH was adjusted by adding 0.5 M HCl and 1 M NaOH. Samples were prepared at least 16 h prior to the experiment in order to ensure the complete dissolution of the polymer and to equilibrate the pH, which was measured using a pH meter under constant stirring. To ensure that the samples were completely dust-free, solutions and samples were prepared in a clean room environment.

4.1.5 Transmission Electron Microscopy measurements

Transmission electron microscopy was performed using a Philips CM100 electron microscope (tungsten source at 100 kV) equipped with a Gatan 1k CCD Camera. Carbon grids were submerged for 20 seconds into the sample solution and subsequently in a uranyl acetate water solution (2% w/w). The grids were blotted and dried under vacuum (uranyl acetate is a highly efficient staining agent for many polymers, freezing the structure in several ms).¹¹

4.2 POLYELECTROLYTE BRUSHES

The polyelectrolyte brushes presented in this thesis were prepared by Dr Collin J. Crook, Dr Paul D. Topham, Andrew J. Parnell and Dr Jonathan R. Howse.¹²

4.2.1 Brush preparation

Polymer brushes, comprising polyacid (PMAA) or polybase poly[(diethylamino) ethyl methacrylate] (PDEAMA) chains, were grown from functionalized surfaces by atom transfer radical polymerization (ATRP). The polyacid was formed by hydrolyzing a poly(*tert*-butyl methacrylate) brush whereas the polybase brush was grown directly (ATRP is not suitable for growing PMAA chains directly). These samples were required for neutron reflectivity experiments and so were prepared on large silicon blocks to provide a large surface area and suitable thickness for the reflection geometry.

Small pieces of silicon wafers (Mitsubishi Research and Crystran Ltd., 30x30x20 mm, polished to the (100) surface with a native SiO₂ layer of 1.5 nm) were then used as substrates. These substrates were rendered hydrophilic by a two step process, first cleaning in oxygen plasma for 10 min and then immersion in an aqueous solution of ammonia (5% v/v) and hydrogen peroxide (3% v/v) at 80 °C for 10 min (details of the method are given elsewhere¹³). The sample was then repeatedly washed with clean water. The silicon was then dried under a nitrogen atmosphere for several minutes to remove all traces of water. After preparing the substrates the synthesis of bushes is based in two differentiated steps: (a) surface functionalization and (b) polymerisation.

4.2.1.1 Polyacid brushes.

(a) The clean silicon block was transferred to a refluxing environment of 5% (v/v) 3-aminopropyltriethoxysilane (1) in toluene. The sample was held in place for 16 h using a specially designed PTFE holder at a height just above the condensing region. Once removed, the sample was placed in a reaction vessel containing a solution of 2-bromo-2-methylpropionic acid (2) (33.4 mg, 0.20 mmol) and *p*-(dimethyl amino) pyridine (3) (6 mg, 0.05 mmol) in 10 ml of dry dichloromethane.¹⁴ The solution was cooled to 0°C before adding dicyclohexylcarbodiimide (51.6 mg, 0.25 mmol). The wafers were left at room temperature overnight before being washed with toluene and acetone. Finally the wafers were dried with nitrogen before

proceeding to following polymerisation step. A scheme of the chemical reaction is shown in Fig. 4.8.

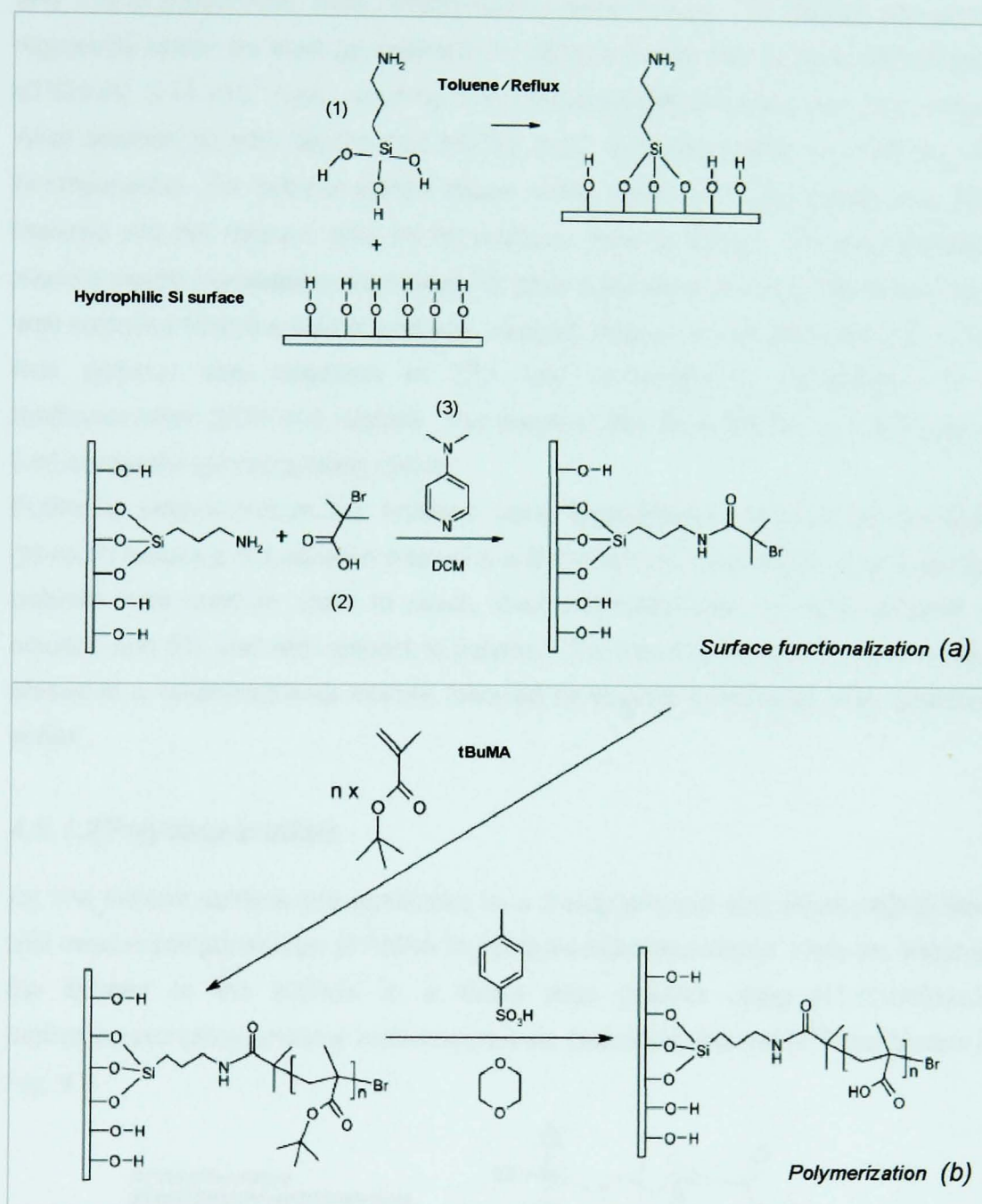


Fig.4.8 Formation of poly(methacrylic) acid brushes . Adapted from ref. (11)

(b) The chemicals employed in the synthesis were purified as follows: *tert*-butyl methacrylate (tBuMA) (Aldrich, 98%) was stirred over CaH_2 overnight before being distilled under reduced pressure. *N,N,N',N',N''*-pentamethyldiethylene-triamine (PMDETA) (Aldrich 99%) was used as received. $\text{Cu}(\text{I})\text{Br}$ (Aldrich, 98%) was stirred with glacial acetic acid overnight, before being filtered and thoroughly washed with

ethanol and acetone, and then dried under vacuum. Benzonitrile (Aldrich, 98%) was used as supplied.

Methyl-2-bromopionate (0.103 ml, 9.25×10^{-4} mol), Cu(I)Br (133 mg, 0.925 mmol) and 1 ml of benzonitrile, were introduced to a reaction tube. The mixture was stirred vigorously under an inert atmosphere for 20 min before the addition of PMDETA (0.579 ml, 2.78×10^{-3} mol), resulting in the development of an intense green colour. After another 20 min, tBuMA (15 ml, 9.2×10^{-2} mol) was added and stirred until homogeneous. An initiator-coated silicon wafer held in a wire cradle was then lowered into the mixture, and the temperature rose to 100°C. The polymerisation mixture rapidly increased in viscosity and, after a period of an hour, the silicon wafer was removed from the vessel and was washed clean in tetrahydrofuran (THF). The free polymer was dissolved in THF and recovered by precipitation in a methanol/water (95/5 v/v) mixture. The polymer was then filtered and cleaned by further dissolving/precipitating cycles.

Following polymerisation the brushes were hydrolysed to remove the *tert*-butyl group by refluxing in a solution *p*-toluene sulfonic acid in 1,4 dioxane. Sacrificial free polymer was used in order to reach ideal concentrations, i.e. 20% polymer in solution and 5% acid with respect to polymer. The brushes were then removed and placed in a water/methanol mixture followed by several wash steps with deionised water.

4.2.1.2 Polybase brushes

(a) The initiator surface was generated by a 2-step process and differs slightly from that used in the generation of PMAA brushes as described above. Here we attached the initiator to the surface in a single step transfer using (11-(2-bromo-2-methyl)propionyloxy)undecyl trichlorosilane as described elsewhere¹⁵ and shown in Fig. 4.9.

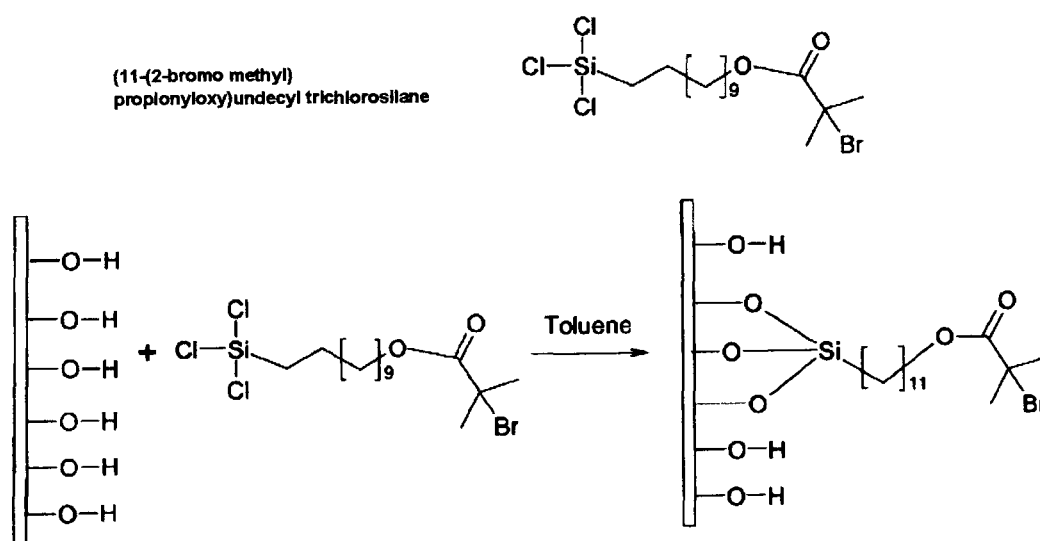


Fig. 4.9 Formation of the initiator surface for polybase brushes. Adapted from ref. (11)

The silicon surface was placed in a PTFE beaker with a tight fitting lid containing 20 ml of a $1.5 \mu\text{l ml}^{-1}$ solution of trichlorosilane initiator in dry toluene. After the required period the silicon block was removed and subjected to washings with toluene twice, acetone, and ethanol before finally dried under nitrogen. The blocks were stored under vacuum until required for the brush synthesis (Fig.4.9)

(b) (Diethylamino) ethyl methacrylate (DEAMA) (Aldrich, 99%) was stirred over calcium hydride overnight before being distilled under high vacuum at 70°C . PMDETA (Aldrich 99%) was used as received. Cu(I)Br (Aldrich, 98%) was stirred with glacial acetic acid overnight, before being filtered and thoroughly washed with ethanol and acetone, and then dried under vacuum. THF was distilled over sodium/potassium benzophenone and stored under vacuum before use.

Copper (I) bromide (163 mg, 1.14 mmol) and PMDETA (270 ml, 1.29 mmol) were added to 15 ml of stirred THF. The reagents were purged with nitrogen and thoroughly mixed, to which the DEAMA monomer (25 ml, 124 mmol) was subsequently introduced. After 20 min of further stirring, whilst maintaining the flow of nitrogen, the suspended initiator was lowered into the bright blue solution at 75°C . After 17 h, the silicon-based polymer brushes were withdrawn from the solution (now dark green) and purified using a THF soxhlet reflux system for 24 h. A reference wafer with a saturated initiator surface of dimensions $10 \times 10 \times 0.625 \text{ mm}$ was also used for each polymerisation bath to assess the consistency of polymer chain growth. With the absence of any direct means of measuring the polymer chain molecular weight the use of a reference wafer allows for some assessment of the molecular weight of the polymer chains on the dilute brush under study. Fig. 4.10 illustrates the process described in this subsection.

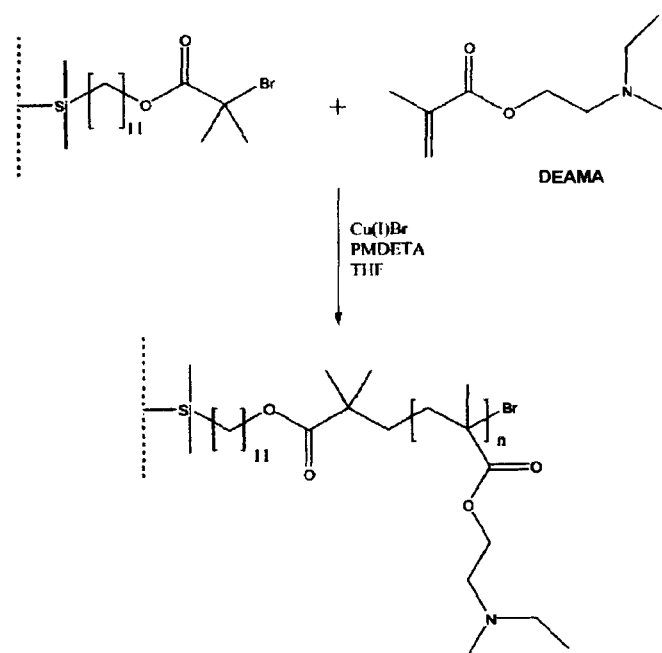


Fig. 4.10 Preparation of polybase brushes. Adapted from ref. (11)

4.2.2 Neutron Reflectivity measurements: Instrumentation and Analysis

4.2.2.1 Instrumentation.

Neutron Reflectometry is a key technique in the study of soft matter, complex fluids, surfaces, interfaces, and thin films. Neutrons scatter from material via a nuclear interaction. This interaction is such that the scattering power of an atom is not related to its atomic number but to what is called the scattering length of the nucleus, which varies seemingly randomly with atomic mass. This property makes neutrons a very important technique for studying polymeric systems since it allows the detection of isotopes of the same element in a distinct manner. Deuterium has a greater scattering length than hydrogen and so is used to label one of the components of the system under study. This labelling method allows materials that cannot be investigated by X-ray reflection to be studied.¹⁶ In addition, neutron reflectivity is non-destructive to delicate systems and has the ability to study buried interfaces that be used to look at samples in shear cells, pressure cells, cryostats and furnaces for example.

In the present work neutron reflectivity (NR) is used as a complementary technique to the luminescence techniques previously described. NR will provide us with information about the swelling or coiling of the PDEAMA and PMAA brushes when the pH of the medium in which it is dissolved changes. In addition it can yield information about the kinetics of the swelling/collapse processes.

In any spectrometer, which uses radiation to investigate organization or motion at a molecular level several components in common can be identified:

(a) First a source of radiation is required. There are two types of sources of interest: reactors and pulsed (spallation) sources. In the reactor source a nuclear chain reaction produces a continuous flux of neutrons. The reflectivity profile is often (but not always) obtained by changing the angle of incidence θ_0 simultaneously with angle of detector 2θ at a constant wavelength. In pulsed sources high energy protons from a synchrotron hit a heavy metal target, such as tantalum, and expel neutrons from the nuclei, which come in sharp bursts (the protons are diverted from the synchrotron onto the target at a fixed frequency). For such sources measurements are performed at fixed angle of incidence and analysed by a *Time-of-Flight* method in which neutrons are velocity (wavelength) selected using typically a chopper and filters so that a spectrum can be obtained at constant angle θ . For both reactor/spallation sources the neutrons have to be moderated.

(b) When the neutrons emerge from the nuclei that produce them they have a large energy that needs to be “slowed down”. A moderator is used to decrease this energy. In the moderator the neutrons are scattered many times within a suitable medium (usually liquid hydrogen) exchanging energy at each collision. This process is stopped when the neutrons reach thermal equilibrium with the nuclei of the moderator. The moderator temperature determines the spectral distribution of neutrons produced, so for a liquid hydrogen moderator the neutrons have a Maxwell Boltzmann velocity distribution for a temperature of 20K.

(c) After the cold moderator, the energy (and hence wavelength) of the beam needs to be defined before it reaches the sample object of our study. For this purpose a chopper (and some filters) is used as a wavelength selector.

(d) After the wavelength distribution of the incident neutrons has been defined, scattering detectors will identify changes in direction and energy, which have occurred. The neutrons are detected before the sample and that is used to normalize the signal at the sample. In *Time-of-Flight* spectrometers, the wavelength comes from the de Broglie relation $\lambda = h/mv$, where λ is the neutron's wavelength, h is the Planck constant, m is the neutron's rest mass and v is the neutron's velocity. Thus longer wavelength neutrons come after short wavelength ones. The velocity of the neutrons will be dependent upon their energy, with the more energetic neutrons travelling at a higher velocity (and smaller wavelength). Since the distance from the source to the detector is known, then the time at which a neutron hits the detector (relative to their timing pulse) will provide its velocity and therefore its energy (kinetic energy). Such energy can be converted into wavelength by the de Broglie relation and the neutrons intensity varies with wavelength. In other words, detectors measure intensity as a function of time.

Traditionally reflectivity profiles are recorded either as a function of θ or λ however is convenient to use the scattering vector $Q = (4\pi/\lambda) \sin\theta$. Measurements can be either specular or off specular. Specular measurements are those where the angle of incidence relative to the normal between the two interfaces is equal to the relative angle of reflection, whereas off specular reflection involves different incident and reflection angles including those out of plane. Variation in the refractive index normal to the surface is monitored. A specular neutron reflectivity measurement provides information on concentration or composition perpendicular to the surface or interface, in particular the surface and interface roughness.¹⁶

The data presented in this thesis were obtained at the EROS *Time-of-flight* neutron reflectometer (Orphée reactor) at the Laboratoire Léon Brillouin at Saclay in France. The reflectometer is composed of a chopper that defines the neutron bursts. Then, a 3.9 m evacuated collimator defines a very narrow neutron beam. Inside the collimator, a neutron supermirror deflects neutrons of the wrong energies away and allows the use of liquid measurements by allowing the liquid surface to remain flat. The samples are installed on a goniometer head for alignment purpose. Changing the height and angle of the sample via the goniometer will ensure that incident and reflected angles are equal (specular measurements). Measurements of PDEAMA and PMAA brushes were performed in air (dry) at 1° angle and in a liquid cell at an angle of 1.4° . The reflected intensity is measured at a 2 to 4 m distance by single ^3He counter. A diagram of EROS is shown in Fig. 4.11.

Preliminary measurements were performed on the SURF reflectometer at the ISIS source, Rutherford-Appleton laboratory, Chilton, Didcot, Oxfordshire. The ISIS source relies on the spallation process in which pulsed neutrons are produced as a result of the collision of highly energetic protons from a source with a heavy metal target. The result is a "white beam" consisting of a continuous distribution of neutron wavelengths which is analyzed with the time of flight method, under a fixed angle.

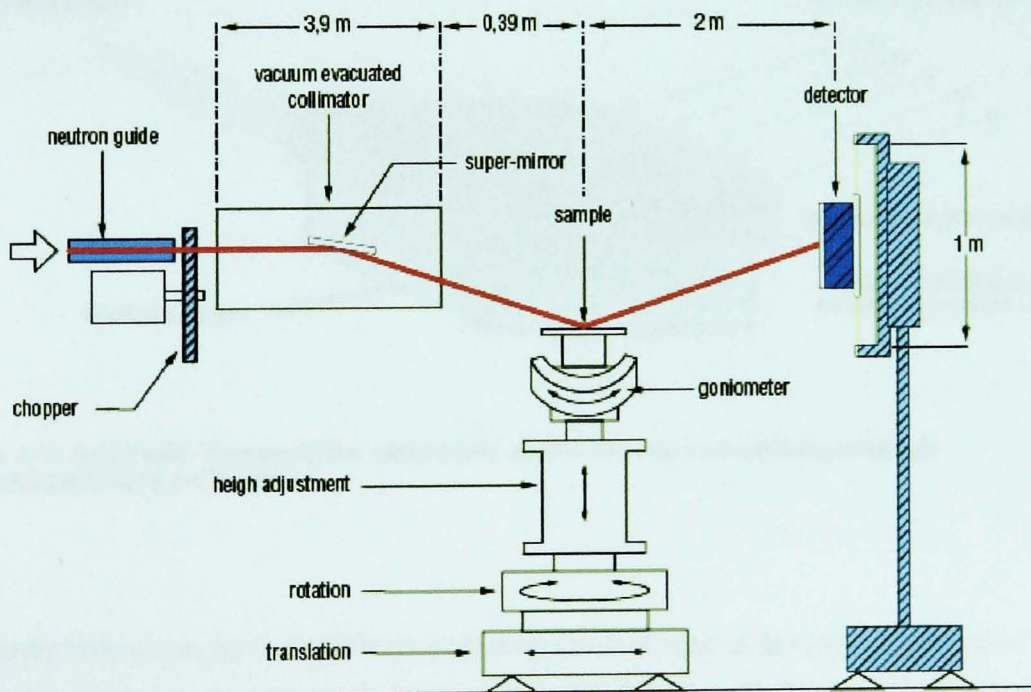


Fig. 4.11 Schematic diagram of EROS time-of-flight neutron reflectometer (Orphée reactor) at the Laboratoire Léon Brillouin at Saclay in France. Adapted from <http://www-llb.cea.fr/spectros/pdf/eros-llb>.

The object of our study is a semi-infinite system, single film of thickness d (the PDEAMA/PMAA brush is the single film). Each sample is clamped into a polytetrafluoroethylene (PTFE) sample cell via a rubbed ring. The geometry in the sample cell is an inverted one, with neutrons incident on the brush through the silicon. After impinging the silicon, the beam undergoes successive reflections and transmissions along the brush. Heavy water (at various pHs by addition of NaOH or HCl as appropriate) is used for contrast with the hydrogenous polybase/polyacid brush placed in the sample cell. D_2O scatters neutrons very well whereas H_2O does not, and so swollen brushes reflect less efficiently neutrons than collapsed ones. This is due to the fact that when the brush is swollen, some D_2O molecules are within the hydrogenous brush region and so the interface between brush and external solution can be considered diffuse. In this case, the difference in Nb values of the brush region with respect to the external solution is not large. In collapsed brushes a sharp interface is formed between the brush and the heavy water regions, such interface is highly reflective for neutrons

Details of the sample cell and orientation can be seen in Fig. 4.12

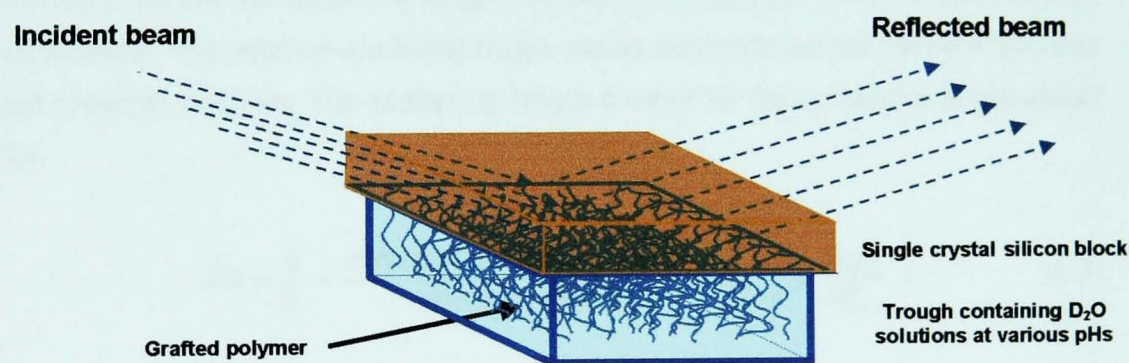


Fig. 4.12 Schematic diagram of the sample cell used in NR measurements to measure swelling/collapse on brushes

The experiments we performed from a starting point of neutral pH (plain D_2O), after which the pH was progressively increased till reaching pH ~ 10 . Further experiments were performed decreasing gradually the pH. After each measurement of the reflectivity of a given swelling (*i.e.* pH value), the silicon wafer with the brush was removed from the sample cell and washed before the next solution was added. In some runs, the brush usually needed circa 30 minutes to equilibrate from the new pH (the reflectivity profile changed during the first stages of the run). In order to

obtain the most accurate reflectivity profile typically three scans were measured at each pH, scans for which the data unchanged were added together to produce the data presented here.

4.2.2.2 Theoretical background and analysis

If the radiation used to study a material consists of neutrons then the refractive index for this material is usually slightly less than unity (order of 10^{-6}) and can be expressed as:

$$n_{mat} = 1 - \lambda^2 A + i\lambda B, \quad (4.7)$$

where λ is the neutron wavelength (in vacuum); A and B are constants and represent the effects of scattering and absorption respectively:

$$A = \frac{Nb}{2\pi}, \quad B = \frac{N(\sigma_c + \sigma_i)}{4\pi}. \quad (4.8)$$

Where N represents the atomic number density, b is the scattering length and Nb and $N(\sigma_c + \sigma_i)$ are the scattering length density and absorption cross section density respectively. The neutron scattering length varies randomly across the periodic table and between isotopes. The scattering length density Nb for a material is calculated like:

$$Nb = \frac{b}{V} = \frac{\text{coherent scattering length}}{\text{specific volume}} = N_A \sum_i \phi_i \frac{b_i \rho_i}{M_{wi}}, \quad (4.9)$$

where N_A is Avogadro's constant and the summation is over all the molecules contained in the material. ϕ_i , b_i , ρ_i and M_{wi} are the volume fraction, scattering length, density and molecular weight of the molecule i respectively. The scattering length density of a single molecule $Nb_{molecule}$ (of molecular weight M_w) is the sum of the scattering lengths of each atom b_a present in the molecule

$$(Nb_{molecule} = \frac{\rho N_A}{M_w} \sum_a b_a, \text{ where } \rho \text{ is the density of the molecule}).$$

From eq.(4.8) σ_c and σ_i are the coherent and incoherent scattering cross sections respectively, the sum of both is the total scattering cross section σ_s which is related to the scattering length b by $\sigma_s = 4\pi|b|^2$

Given A and B in (4.8) and using (4.7) it can be seen that the “refractive index” for neutrons is related to the scattering length density. Neglecting absorption effects (no significant absorption phenomena is observed for most polymeric materials of interest), the refractive index for neutrons is a real number that can be expressed as:

$$n = 1 - \frac{\lambda^2 Nb}{2\pi} \quad (4.10)$$

The refractive index for neutrons is very close and usually slightly less than unity, so there will be a critical glancing angle below which there is total external reflection. For incident angles above the critical angle, the reflectivity falls away very rapidly. The sharp change in the reflectivity marks what is generally referred to as the “total reflection edge”. A detailed explanation of the critical angle is given below.

Consider an interface separating two media with refractive indexes n_0 and n_1 respectively and a neutron beam incident on the surface at an angle α_0 . As neutron can be treated in similar way to electromagnetic radiation, a parallel to Snell's law of refraction can be developed. Snell's law for classical optics is:

$$n_0 \sin \alpha_0 = n_1 \sin \alpha_1 \quad (4.11)$$

where n_i is the refractive index of the medium and α_i is the angle of incidence relative to the normal between the two interfaces. For neutron reflectivity the angle of incidence is usually defined as the angle relative to the surface, which the beam is incident, resulting in:

$$n_0 \cos \theta_0 = n_1 \cos \theta_1 \quad (4.12)$$

where $\theta = 90 - \alpha$. Reflection and refraction of an electromagnetic beam is shown in Fig. 4.13 for incidence on a single layer.

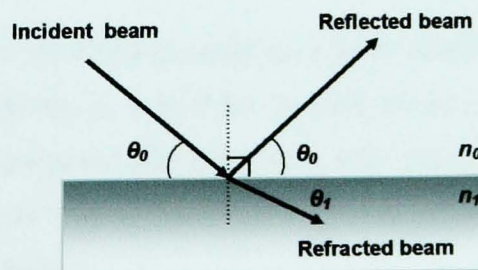


Fig. 4.13 Diagram illustrating reflection (at an angle θ_0) and refraction (at an angle θ_1) of a neutron beam incident to an interface between air and a medium of refractive indexes n_0 and n_1

When the angle of incidence is equal to the critical angle $\theta_i = \theta_c$, the angle of refracted beam is zero and the neutron beam is propagated along the surface. In this situation $\theta_r = 0$ so $\cos \theta_r = 1$ in eq.(4.12).

Total Internal Reflection (instead of refraction) will occur for a beam incident upon an interface where $n_1 < 1$ (as the medium 0 is air, $n_0 = 1$). From eq.(4.12) $n_1 < 1$ implies that $\cos \theta_0 < \cos \theta_1$, then $\theta_1 < \theta_0$ and there is a real angle of refraction for values of $\theta_0 > \theta_c$ where:

$$\cos \theta_c = \frac{n_1}{n_0} = n_1. \quad (4.13)$$

The cosine function can be expressed as an expanded series such as follows;

$$\cos \theta = 1 - \frac{\theta^2}{2!} + \frac{\theta^4}{4!} - \frac{\theta^6}{6!} + \dots \quad (4.14)$$

For small angles only the first two parts of the above expression need to apply so be obtained

$$\cos \theta = 1 - \frac{\theta^2}{2} \dots \quad (4.15)$$

An approximation for the critical angle θ_c can be obtained using eq.(4.15), neglecting absorption (the imaginary part of refractive index is ignored) and combining eq.(4.10) and (4.13) as :

$$\theta_c = \lambda \sqrt{\frac{Nb}{\pi}}. \quad (4.16)$$

Where θ_c is expressed in radians and Nb and λ are in \AA^{-2} and \AA respectively.

If we consider a beam of neutrons incident on a semi-infinite block of material, then at small angles of incidence $\theta_0 < \theta_c$ there is total external reflection and only an evanescent wave propagates into the specimen. The reflectivity $R(\theta) \cong 1$.

For incident angles greater than θ_c the beam begins to penetrate the sample and the reflectivity falls off very rapidly.

The extent to which radiation is reflected at an interface depends upon difference in the wavevector on both sides and the interface. In vacuum, the z component of the wavevector (normal to the interface) can be written as:

$$K_{z,0} = \left(\frac{2\pi}{\lambda} \right) \sin \theta_0, \quad (4.17)$$

or as a momentum transfer:

$$Q_{z,0} = \left(\frac{4\pi}{\lambda} \right) \sin \theta_0. \quad (4.18)$$

Since the geometry is such that the incident and detection angles are equal, the only component of interest of K or Q is the z-component.

In a medium 1, $K_{z,1}$ propagates following

$$K_{z,1} = \sqrt{K_{z,0}^2 - K_{c,1}^2}, \quad (4.19)$$

where $K_{c,1}$ is the critical value of $K_{z,1}$ below which total reflection occurs.

Consider an infinitely sharp interface separating two media, air and a film. The reflection coefficient is the same as that for Fresnel reflection of electromagnetic waves and is given by¹⁶

$$r_{0,1} = \frac{K_{z,0} - K_{z,1}}{K_{z,0} + K_{z,1}}, \quad (4.20)$$

and the reflectivity by

$$R = r_{0,1} r_{0,1}^*. \quad (4.21)$$

where the asterisk denotes the complex conjugate. Combining eq.(4.19) and eq.(4.20), eq.(4.21) can be written as:

$$R(K_{z,0}) = \frac{\left| 1 - \left[1 - \left(\frac{K_{c,1}}{K_{z,0}} \right)^2 \right]^{\frac{1}{2}} \right|^2}{\left| 1 + \left[1 - \left(\frac{K_{c,1}}{K_{z,0}} \right)^2 \right]^{\frac{1}{2}} \right|^2}, \quad (4.22)$$

where

$$R(K_{z,0}) \propto \left(\frac{K_{c,1}}{K_{z,0}} \right)^4. \quad (4.23)$$

For an infinitely sharp interface eq.(4.23) implies that

$$R(K_{z,0}) K_{z,0}^4 = \text{constant}, \quad (4.24)$$

Which is known as Porod's Law^{17,18} by which it can be assumed that the reflectivity will vary with $K_{z,0}^{-4}$ at high values of $K_{z,0}$.

When the interface is not sharp is due to roughness at the air interface. In such case the measured reflectivity will not follow Porod's law, instead the reflectivity will fall faster than $K_{z,0}^{-4}$.¹⁹ The reflectivity expression has to be modified which is usually done by giving the interface a Gaussian smoothing function¹⁶.

$$R = |r_{0,1}| \exp(-4K_{z,0}K_{z,1}\sigma_{0,1}^2), \quad (4.25)$$

where σ is the width of the Gaussian function. Using eq.(4.25), the deviation of the actual interface from its mean position can be described by Gaussian statistics.

The roughness in an interface produces an overall reduction of the reflected intensity while maintaining the features of the reflectivity profile (Fresnel reflectivity).

When the system under study has more than one interface between media different methods are employed. *Optical matrix methods* are particularly useful for either discrete layers or continuous interfaces which can be broken up into series of discrete layers by treating each one with its own defined thickness and scattering length density. The *Optical matrix method* is often referred to as dynamic optics approximation. Another method for modelling reflectivity data is the *kinematic approximation* in which the reflectivity is related to the Fourier transform of the

scattering length density normal to the interface. We will not refer to this model in the present study.

Consider the example of a semi-infinite system, for example a single film of thickness d_1 , with sharp interfaces and constant refractive index situated above a bulk substrate of thickness d_2 (Fig 4.14).

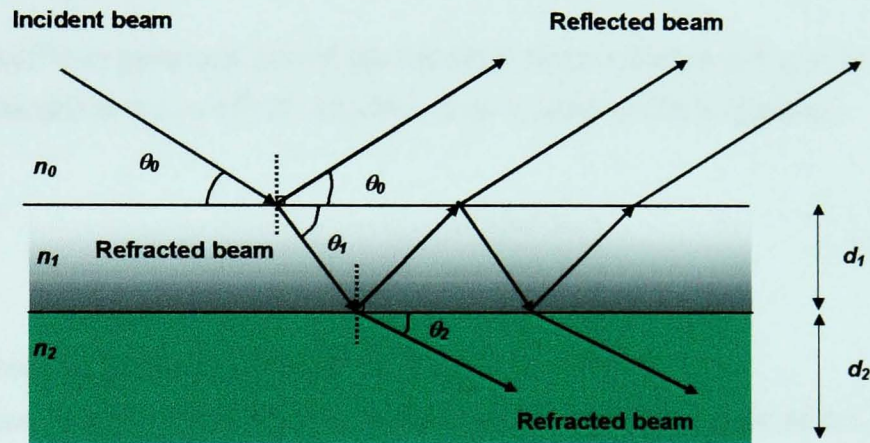


Fig. 4.14 Diagram showing incident, reflected and refracted beams for a single film of thickness d_1 on substrate of thickness d_2

The expression to calculate the reflectivity is given by standard optical methods as:

$$R = \left| \frac{r_{01} + r_{12} \exp(2i\beta)}{(1 + r_{01}r_{12} \exp(2i\beta))} \right|^2, \quad (4.26)$$

where r_{ij} is the (Fresnel) reflection coefficient between medium i and j and β is the optical path length for neutrons in the film defined as:

$$\beta = \left(\frac{2\pi}{\lambda} \right) n_1 d_1 \sin \theta_0. \quad (4.27)$$

With a single layer multiple reflection and refraction are likely to occur and so interference patterns occur. For interference to occur the Bragg condition needs to be satisfied:

$$m\lambda = 2n_1 d_1 \sin \theta \quad (4.28)$$

Where d_1 is the distance between scattering centers (film thickness) and m is an integer known as the *order* of the diffracted beam. Combining eq.(4.28) with $Q = (4\pi/\lambda)\sin\theta$ the peak to peak distance ΔQ in Q space can be calculated for our pattern as:

$$\Delta Q = \frac{2\pi}{d_1}. \quad (4.29)$$

Consider a multi-layer generalisation of the two-layer system shown in Fig. 4.14. The reflection coefficient of the $(n-1)^{th}/n^{th}$ interface in an n layered film is given by

$$r_{n-1,n} = \frac{r'_{n-1,n} + r'_{n,n+1} \exp(2id_n K_n)}{1 + r'_{n-1,n} r'_{n,n+1} \exp(2id_n K_n)}, \quad (4.30)$$

where the prime designates the reflectance given from eq.(4.20)

This reflectance given in eq.(4.30) is used to calculate the reflectance at the next interface

$$r_{n-2,n-1} = \frac{r'_{n-2,n-1} + r_{n-1,n} \exp(2id_{n-1} K_{n-1})}{1 + r'_{n-2,n-1} r_{n-1,n} \exp(2id_{n-1} K_{n-1})}. \quad (4.31)$$

In this manner, the calculation can continue recursively until the air-film interface is reached.

For the treatment of the data, the data for the various angles were normalised to total reflection. Neutron reflection data were analysed using the *slab fit* program, created by Dr Devinderjit S. Sivia (Rutherford Appleton Laboratory). The *slab fit* program attempts to carry out an *ab initio* search for a density-profile in good agreement with the reflectivity data, using a combination of trial-and-error slab-splitting and initialisation steps and local optimisation using the downhill simplex algorithm.

The sum of several (up to 20) uniform layers of material (or slabs) and three Gaussian roughness parameters: one each for the outer and innermost interfaces, and the third for all the internal ones, are assumed to describe satisfactorily the density profile. The fitting was repeated for various thickness limits to allow different levels of swelling with the brush thickness used to calculate the conserved volume fraction for each of these thickness ranges. Regardless of the different thicknesses

used, the total volume fraction of brush was conserved, although it was allowed to float to within $\pm 10\%$. A total thickness d was chosen for the fitting procedure.

The first iteration of the fitting routine is a single layer whose volume fraction is given by the dry brush thickness divided by the total thickness of the layer d (to conserve mass). A failure to fit the neutron data to this profile by varying volume fraction, thickness (volume fraction and thickness were allowed to vary within 10%) or roughness parameters is followed by the layer being divided into two, yielding a new volume fraction profile. The thicknesses of the two layers are allowed to float (again within the 10% tolerance limit), such that the total thickness continues being the same as the first (single) layer. Three layers follow. If fitting continued inadequate, the number of layers increased to a maximum of 20, where the internal roughnesses of each layer is kept constant (in order to keep the number of fittings parameters low).

Fitting was ended when (the normalized) $\chi^2 < 1$. The choice of d for the fittings is rather arbitrary, but is a predetermining factor in the quality of the fits so, the entire procedure was repeated for various thicknesses. In order to differentiate between different high-quality fits of similar χ^2 , we spared physically unrealistic profiles (brush layer detached from the substrate, negative volume fraction) and chose the fit requiring the fewest number of layers. The silicon oxide and initiator layer were not present in these fits, perhaps because they often are imprecise and can be subsumed into the brush-substrate roughness.

4.3 PMAA HYDROGELS

4.3.1 Hydrogels preparation

The pH responsive gels were synthesised via a free-radical mechanism. The synthesis was performed in an aqueous environment using MAA as the monomer, 2,2'-azobis(2-methylpropionamide) dihydrochloride (AMPA) as the initiator and N,N'-methylene bisacrylamide (MBA) as the crosslinking agent. Fig.4.15 shows the chemical structure of such reactants.

The polymerisations were carried out in a water solution containing MAA 47% w/v, AMPA 0.9wt% and MBA 1.1% w/v. (relative amount of crosslinker MBA with respect

of monomer MAA is 3.2wt%). Different amounts of reagents were tested but those chosen allowed the gels to fully swell at high pHs while still maintaining their shapes

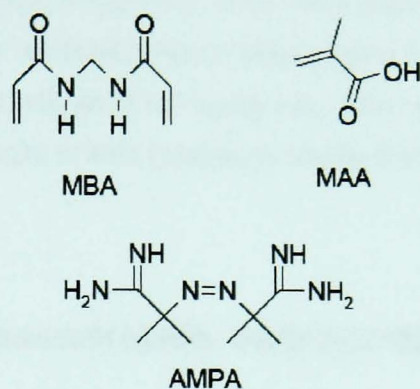


Fig. 4.15 Reactants used for the synthesis of cross-linked PMAA gels

The aqueous solution containing MAA, AMPA and MBA was degassed under a nitrogen atmosphere for approximately 10 minutes. The polymerisation was then initiated thermally at 80°C and gelation occurred in an hour. In order to obtain gels with the desired shape (hemispherical shape of radius ~3mm) a glass mould was used, allowing three hemispherical gels to be made at the same time (under identical conditions). This mould was placed in a bottled sealed with a rubber septum so the degassing and polymerisation processes could be performed *in situ* (Fig.4.16).

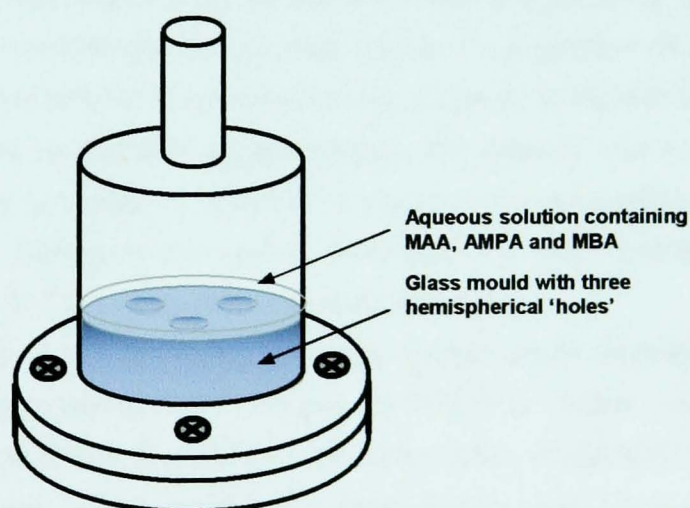


Fig. 4.16 Scheme of the system used to make hemispherical-shape gels. The aqueous solution containing monomer MAA, initiator AMPA and crosslinker MBA rests on a glass mould built in order to obtain gels of the desired hemispherical shape when gelation occurs. The three hemispherical 'holes' of radius ~3mm allowed three gels of that dimension to be prepared at the same time under identical conditions. The polymerisation process was performed *in situ*.

The percentages used for the different reactants yielded a network with a high crosslink density of one crosslinker unit every 60 chains of PMAA.

The three gels were weighed after being removed from the mould where gelation took place, yielding an average weight w_1 . They were then placed in a water bath overnight in order to remove residual solution (free chains in the gel) and left to dry in open air for about 4 hours and weighed again (w_2). The ratio w_2/w_1 allowed us to know approximately the amount of free (residual) chains that did not form part of the final gel.

4.3.2 Contact area measurements: Instrumentation and Analysis

In order to probe the existence of adhesion between the PMAA gel and PMAA brush in basic conditions, hemispherical gels (lenses) were made as described previously. The adhesion properties could be preliminary observed by measuring the contact area between the two components of the system at various pHs.

Various methods were tested to measure the contact area between gel and brush in aqueous solution. Such a task might seem relatively trivial but the fact that the system is immersed in an aqueous solution creates problems of contrast between the gel and water. The first attempt was to use a reflection microscope to observe from above the contact area between the gel and the brush on silicon when immersed in water. Several problems were faced; for example the gel could not be distinguished from the water (due to their similar refractive indexes). In order to resolve this problem the water was coloured but, as expected, after a short period of time it diffused into the gel. Alternatively the gel was coloured via addition of a chromophore in the synthesis but still not much contrast was provided. In addition to this problem, the unavoidable air bubbles trapped during the gelation and the heterogeneities present in the gel made it unviable to observe any well-defined contact area from above. By looking at the contact area from the side, reliable information was obtained despite the air bubbles and heterogeneities.

Preliminary measurements were then performed using a contact angle machine equipped with a high-resolution Watec CCD camera, WAT-902 B model. The camera was connected to the computer via a Belkin USB-video driver, F5U228 FCC standard. Pictures were constantly taken at different frames of time using Capture Studio Professional v.4.05 software, video format 720x565 resolution. The pH meter was a Mettler Toledo, SevenEasy S20K model (inserted permanently in the system), which allowed us to monitor the pH constantly via an external driver connected to the computer, and the software used was Balink software.

The brush was placed in a petri-dish covered in water (glass containers caused distortion in the images obtained). Three hemispherical lenses were positioned onto the brush forming a triangle, distant enough so they did not overlap when fully swollen. A glass slide was positioned on top of the three lenses so they were kept in place during the processes of changing pHs (Fig.4.17). The weight of the glass slide was not considered as the same glass slide was used in all experiments. Solutions of HCl and NaOH, 1M and 2.5 M respectively were prepared and added to the system in order to obtain the desired pH. Fig. 4.18 shows a picture of the set-up used to perform these experiments.

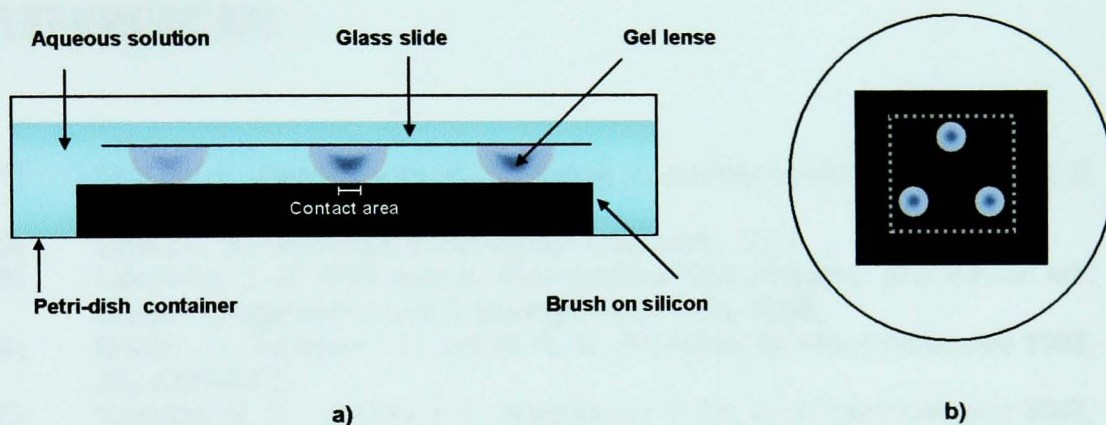


Fig.4.17 Diagram of the brush-gel system used to study adhesion; a) View from the side b) View from the top

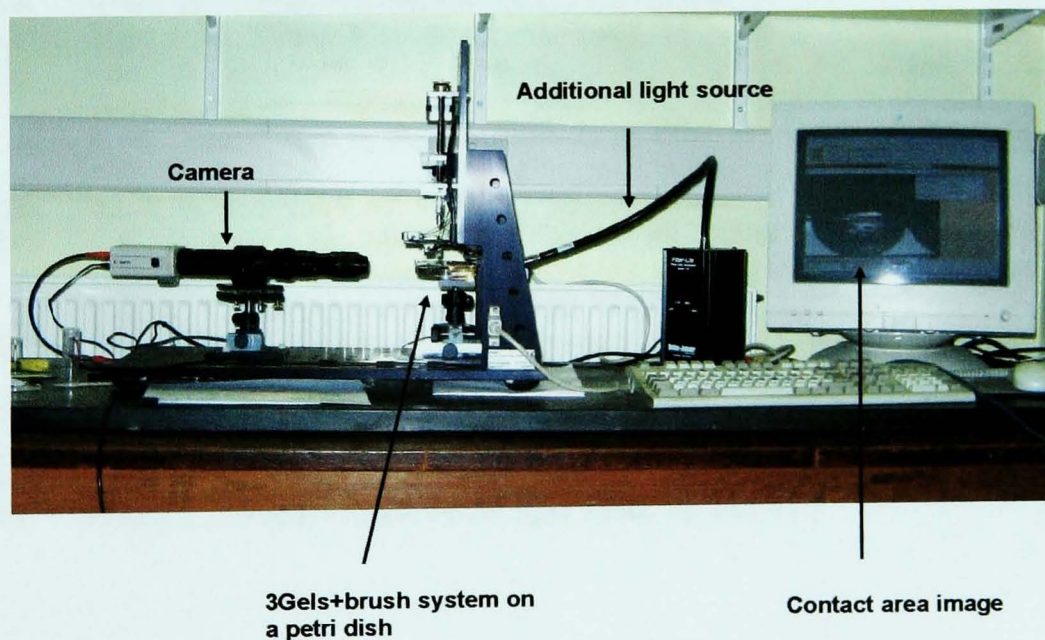


Fig. 4.18 Picture of the set-up used to measure contact area between gel and brush system at different pHs For more clarity the pH meter is not included in this picture

After contact area measurements of the gels in contact with the brush were performed, contact areas of the gel in contact with blank silicon were also measured in order to provide a reference for the polymer-coated silicon. The idea behind this experiment is to observe how fast the gel spreads over the surface (with and without brush) when the solution is driven from poor to good solvent conditions. Short timescales should imply small interactions between gel and surface. In contrast, retarded timescales employed for the gels to fully spread over the surface should entail significant interactions (adhesion) between gel and surface.

REFERENCES

- (1) Flint, N. J.; Gardebrecht, S.; Swanson, L. *Journal of Fluorescence* **1998**, *8*, 343-353.
- (2) Chee, C. K.; University of Lancaster: Lancaster, 2001.
- (3) Lakowicz, J. R. *Principles of Fluorescence Spectroscopy*, 2nd Edition ed.; Kluwer Academic/Plenum Publishers: New York, 1999.
- (4) Soutar, I.; Swanson, L.; Imhof, R. E.; Rumbles, G. *Macromolecules* **1992**, *25*, 4399-4405.
- (5) Kazakov, S. V.; Galaev, I. Y.; Mattiasson, B. *Int. J. of Thermophysics* **2002**, *23*, 161-173.
- (6) Berne, B.; Pecora, R. *Dynamic Light Scattering*; Wiley: New York, 1976.
- (7) Kirkwood, J. G.; Riseman, J. *J. Chem. Phys* **1948**, *16*, 565-573.
- (8) Zimm, B. H. *J. Chem. Phys* **1956**, *24*, 269-278.
- (9) Sedlak, M. *J. Chem. Phys* **1997**, *107*, 10140-10144.
- (10) Reed, W. F. *Macromolecules* **1994**, *27*, 873-874.
- (11) Zhao, F.-Q.; Craig, R. *J. Struct. Biol.* **2003**, *141*, 43-52.
- (12) Ryan, A. J.; Crook, C. J.; Howse, J. R.; Topham, P.; Jones, R. A. L.; Geoghegan, M.; Parnell, A. J.; Ruiz-Pérez, L.; Martin, S. J.; Cadby, A.; A, M.; Webster, J. R. P.; Gleeson, A. J.; Bras, W. *Faraday Discuss.* **2005**, *128*, 55-74.
- (13) Iscoff, R. *Semicond. Int.* **1993**, *16*, 58-63.
- (14) Matyjaszewsky, M.; Miller, P. J.; Shukla, N.; Immaraporn, B.; Gelman, A.; Luokala, B. B.; Siclovan, T. M.; Kickelbick, G.; Vallant, T.; Hoffmann, H.; Pakula, T. *Macromolecules* **1999**, *32*, 8716-8724.
- (15) Beers, K. L.; Gaynor, S. G.; Matyjaszewski, K.; Sheiko, S. S.; Moller, M. *Macromolecules* **1998**, *31*, 9413-9415.
- (16) Russell, T. P. *Mater. Sci. Rep* **1990**, *5*, 171-271.
- (17) Porod, G. *kolloid-Z* **1951**, *124*.
- (18) Porod, G. *kolloid-Z* **1952**, *125*.
- (19) Nevot, L.; Croce, P. *Rev. Phys. Appl* **1980**, *15*, 761-779.

Chapter 5

Poly (methacrylic) acid in Solution

5.1 INTRODUCTION

The behaviour of polyelectrolytes in solution remains an active area of research. The areas of potential application of these polymers are very extensive and include semiconductor devices, molecular sensors, nanoscale pumping devices, switchable adhesion systems, new optics, microelectronics, drug delivery, flocculants, super-absorbants, etc.¹ Knowledge of the processes taking place in simple polyelectrolyte systems when exposed to different external stimuli, particularly their magnitude, the extent and range over which they occur, together with an understanding of the forces arising from changes in shape, will assist in elucidating the roles that complex biological polyelectrolytes such as DNA play in biochemical processes.^{2,3}

In particular, poly (methacrylic acid) (PMAA) is a weak polyacid of interest because it exhibits a marked pH-induced conformational transition. This transition has been studied by different techniques such as: potentiometry titration,⁴⁻⁷ viscosimetry measurements,⁸⁻¹¹ solubilization of hydrophobic molecules in aqueous PMAA,¹²⁻¹⁸ calorimetry,^{15,19-21} Raman spectroscopy²² and scattering methods.²³⁻²⁸ The results obtained from these different techniques have indicated that at low pH the PMAA chains exist as hypercoils with most of the methyl groups in the interior due to hydrophobic interactions. At higher pH the chains stretch to a more open conformation due to coulombic repulsions between ionized carboxylic groups. The conformational transition between the two states occurs at pH 4-6, but the origin of this transition is not well understood. Besides the issue of the origin of the process, some studies suggests that the conformational change is cooperative (affine) and occurs in one step analogue to the helix-coil transition of polypeptides.²⁹ Contrary to

this suggestion, data from Raman spectroscopy indicate the presence of a multiplicity of structures suggesting the transition happening as a progressive rather than a cooperative change.²²

Techniques with resolution in a range from 2 to 100Å are needed to observe the transition on the single molecule level. Fluorescence spectroscopy measurements offer such resolution and they allow *in situ* monitoring of processes occurring within the polymer chains when changing pH. In order to screen such processes it is necessary to attach a small amount of fluorescent dyes to the polymer under study. These chromophores are introduced as a dispersed molecular probe or covalently bond label in extremely low levels of concentration (10^{-5} – 10^{-6} M) in the expectation that minimal perturbation of the system will result. Different probes have been used in order to study the conformational transition in PMAA. For example pyrene has been used to investigate the kinetics of polymer coil expansion,^{14,15} transitions from hypercoil to rod-like structures¹⁵ and structural microdomains in polyelectrolytes,^{14,30,31} restrictions of movement of reactive molecules by the polymer³² etc. Other probes commonly used to study PMAA are dansyl label,¹⁷ anthracene³³ and 1-vinyl naphthalene.³⁴

Combination of chromophores in polymeric systems is a common procedure used in order to investigate molecular distances. For this purpose non-radiative energy transfer (NRET) measurements are performed in donor–acceptor labelled polymers. NRET observed when the emission spectra of the donor fluorophore overlaps the absorption spectra of the acceptor fluorophore depends on the relative orientation and separation distance R between the pairs. Since the chromophores are attached to the polymer chains, changes in chain conformation reveal changes in the distance between donor-acceptor dyes.^{35,36} Such variation in distances is monitored as a greater or lower efficiency in transfer of energy from the donor to the acceptor. For such reason NRET is commonly referred to as a 'spectroscopic ruler'.³⁷

One of the most popular combinations of chromophores used for NRET measurements is naphthalene as a donor and anthracene as an acceptor. This particular pair has some advantages: there is a range of wavelengths (290–320nm) where naphthalene can be excited with minimal direct excitation of anthracene, naphthalene monomer and anthracene fluorescence bands are quite different and easy to distinguish and the anthracene chromophore can be covalently bound to polymers containing naphthalene in different ways.³⁸

In the present study we use naphthalene (N) and anthracene (A) labels covalently bound to the PMAA chains. The chromophores are randomly distributed along the chain. NRET measurements were performed in the donor (N)-acceptor (A) pair upon steady state fluorescence intensity and emission decay measurements at different pHs. Fig 5.1 illustrates how the 'spectroscopic ruler' concept, based on NRET measurements, can reveal information about the conformational changes in PMAA as function of pH.

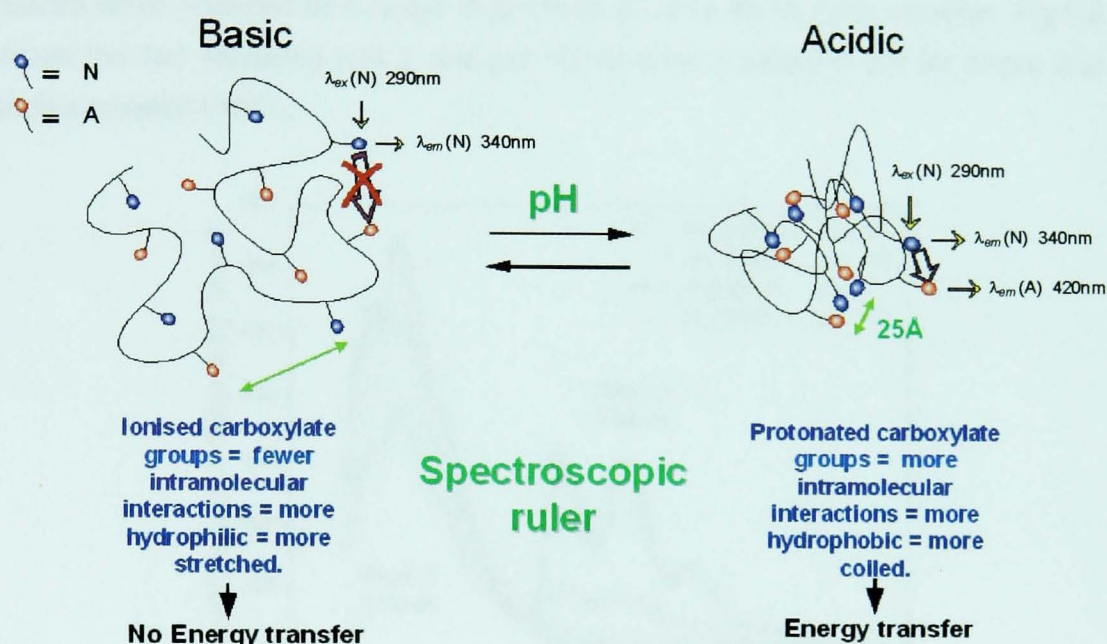


Fig. 5.1 Scheme of the Energy Transfer process between naphthalene (N) donor and anthracene (A) acceptor as a function of their relative distance. On the left hand side energy transfer does not occur due to the great average distance between donors and acceptors (stretched conformation at high pHs). On the right hand side the average distance between donors and acceptors is enough for energy transfer to occurs (coiled conformation at low pH).

In addition to these measurements we employed time resolved anisotropy measurements of the labelled polymers for information on molecular segmental dynamics.

Although other authors have studied naphthalene–anthracene labelled PMAA, prior work has emphasized generally the combination of two techniques: Steady State combined with lifetime measurements^{33,39,40} or time resolved anisotropy measurements (TRAMS) combined with lifetime measurements in the case of single labelled naphthalene-PMAA.^{34,41} We report here a complete characterisation of the pH-dependent conformational changes occurring in PMAA in dilute solution upon combination of the three fluorescence techniques. In addition, complementary data were obtained from dynamic light scattering (DLS) and transmission electron microscopy (TEM) measurements. Such techniques allow an estimation of the polymer chain size at different degrees of ionization.

5.2 FLUORESCENCE MEASUREMENTS

5.2.1 Steady State measurements in aqueous solution

5.2.1.1 Donor and donor-acceptor labelled PMAA comparison

In the current work NA-PMAA and N-PMAA were dissolved in water (0.01wt%, which is dilute enough to observe single molecule behaviour, see *Appendix*). Emission spectra were recorded at a range of pH from pH 2 to 10 for both samples. Fig.5.2 shows the two extremes (pH 2 and pH 10) of such a range of pH for single and double-labelled PMAA.

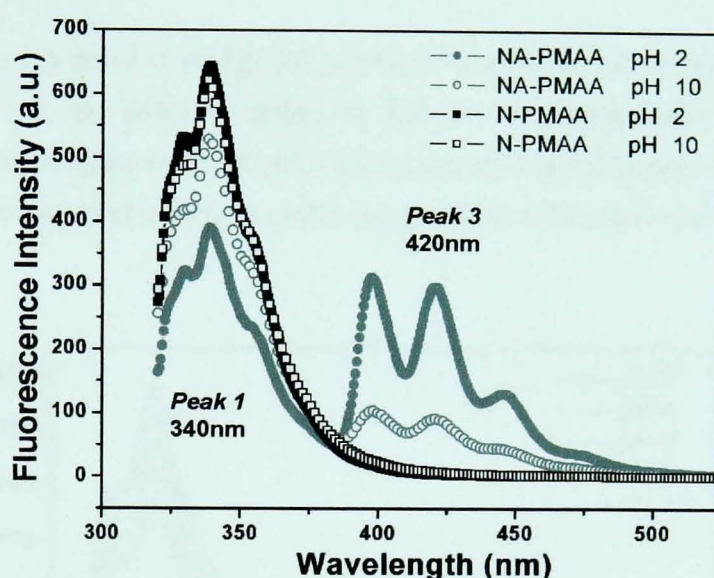


Fig. 5.2 Steady-State spectra of both single (N-PMAA) and double (NA-PMAA) labelled PMAA in aqueous solution (10^{-2} wt%) at different pH. The Emission wavelength was $\lambda_{em}=310-550$ nm, the excitation wavelength was $\lambda_{ex}=290$ nm

In the curve for N-PMAA, no difference in the spectra is observed when the pH of the solution is changed. There is no significant dependence in the emission of the naphthalene chromophore with the structural conformation of the polymer backbone to which it is attached. Naphthalene monomer emits at 340 nm after direct excitation, monomer and excimer emit from 350nm to approximately 410 nm. For NA-PMAA the naphthalene (donor) and anthracene (acceptor) emit at 340 and 430nm respectively. At high pH the donor emission peak appears slightly decreased with respect to that of the N-PMAA. Anthracene emission is observable at ~ 420 nm. This emission may be due to both some absorption of excitation at ~ 290 nm sufficient for its emission and some low transfer of excitation from naphthalene.

In acidic conditions (below pH 6) the naphthalene emission peak for NA-PMAA decreases due to de-excitation to the anthracene chromophore whose emission increases as a result of ET.

5.2.1.2 Donor-acceptor labelled PMAA and Energy Transfer.

From emission spectra of NA-PMAA over a whole range of pH the enhancement of anthracene emission allows the calculation of the ET efficiency as

$$\frac{\text{Increased anthracene emission}}{\text{Quenched naphthalene emission}} = \frac{I(\lambda_{em} = 420\text{nm})}{I(\lambda_{em} = 340\text{nm})} \quad (5.1)$$

Fig 5.3 shows such spectra. In Fig 5.4 (a) the enhancement of anthracene emission from Fig. 5.3 can be seen in detail as the pH is progressively lowered. The behaviour was reversible when pH was increased from pH 2 to pH 10. In Fig.5.4 (b) we show the efficiency of energy transfer (eq.(5.1)) as a function of pH.

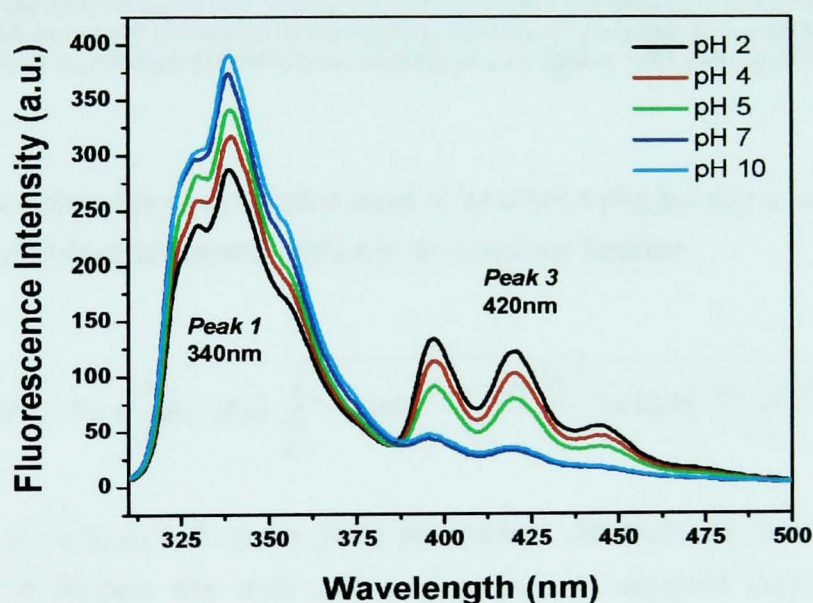


Fig. 5.3 Emission spectra for NA-PMAA at different pHs. The excitation was fixed at $\lambda_{ex}=290\text{nm}$ (naphthalene characteristic), and the emission was $\lambda_{em}=310\text{-}500\text{nm}$. Peak 1 and peak 3 are the donor and acceptor emission peaks at 340nm and 420nm respectively.

The transition curve in Fig.5.4 (b) has the same pattern as those observed by other authors using different chromophores attached or dispersed in polyelectrolyte systems.^{33,42}

The ratio of peak 3 and peak 1, I_{420}/I_{340} (Fig.5.4 (b)) increases as the polymer collapses from a stretched (at high pH) to a coiled conformation (at low pH). The

phenomenon is reversible within the pH cycle and the same data are obtained when the chain swells. In the $6 \leq \text{pH} < 10$ region I_{420}/I_{340} remains approximately constant indicating no major changes in the chain conformation when becoming more basic. In the $\text{pH} < 6$ region the process changes dramatically and depends strongly of the acidity of the solution.

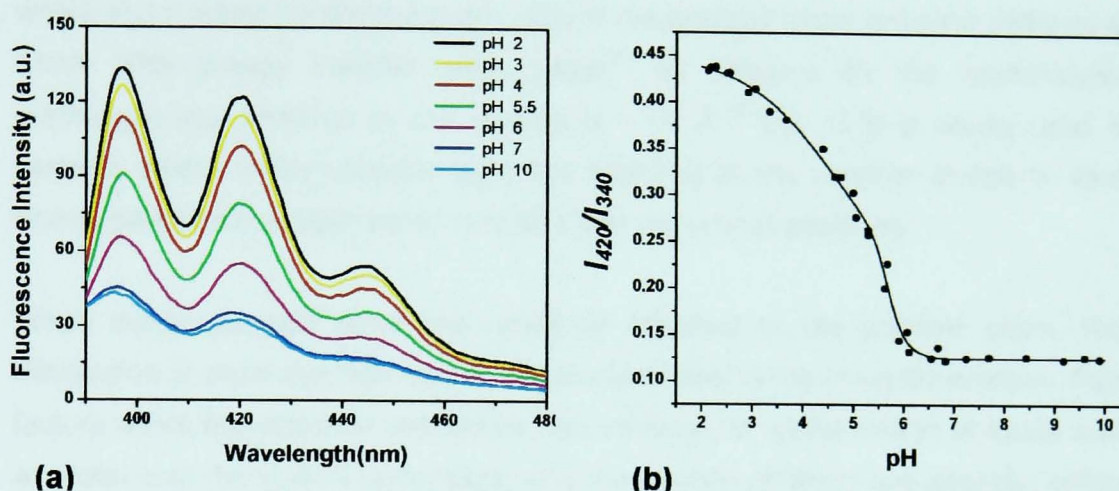


Fig.5.4 (a) Detailed acceptor anthracene enhancement as a consequence of ET from naphthalene in NA-PMAA as the pH is lowered (from Fig.5.3). (b) Ratio of emission at $\lambda_{em}=420\text{nm}$ (anthracene) to emission at $\lambda_{em}=338\text{nm}$ (naphthalene) exciting at $\lambda_{ex}=290\text{nm}$ with varying pH for a NA-PMAA sample.

In order to obtain the neutralization point of NA-PMAA (Fig.5.4 (b)) we fitted the data using a Levenberg-Marquardt routine to an empirical function

$$f(\text{pH}) = h_2 + \frac{1}{2}(h_1 - h_2) \cdot \sqrt{\left(1 + \tanh\left(\frac{\Delta_1 - \text{pH}}{\sigma_1}\right)\right) \cdot \left(1 + \tanh\left(\frac{\Delta_2 - \text{pH}}{\sigma_2}\right)\right)} \quad (5.2)$$

where $h_1, h_2, \Delta_1, \Delta_2, \sigma_1$ and σ_2 are fitting parameters. Although this function is wholly empirical it models the data well and allows an accurate estimation of the neutralization point (inflection point) by differentiation. The neutralization pH for PMAA is thus calculated to be 5.7

At pH 2 the ratio is at a maximum ~ 0.45 indicating $\sim 45\%$ efficiency of energy transfer in the hypercoiled form of PMAA. It has been demonstrated that this maximum ratio increases when M_w or polyelectrolyte concentration in solution is increased.^{42,43} Understandably, when M_w increases the greater probability of having donor and acceptor in the same chain results in greater ET efficiencies; in the same way, when the concentration of PE in solution is increased the probability of interchain ET is also augmented and thus the ET efficiency.

The energy transfer efficiency E_r is a function of the distance r between the donor and acceptor

$$E_r = \frac{1}{1+(r/R_0)^6}, \quad (5.3)$$

where R_0 for rotational chromophore pairs is the average donor-acceptor distance at which 50% energy transfer takes place.³⁶ R_0 distance for the naphthalene-anthracene pair involved in our studies is $\sim 25 \text{ \AA}$.³⁸ Eq. (5.3) is widely used in systems where donor-acceptor pairs are attached to the polymer chains at fixed known positions (i.e. chain ends, or middle and chain ends positions).

When donor-acceptor pairs are randomly attached to the polymer chain, the distribution of distances between such pairs is related to the chain dimensions. Two factors affect this distance distribution: the variation of concentration of donor and acceptor over the system under study and the location of donor and acceptor within the chain (i.e. whether it is located at the centre of a coil, or at the extremities).⁴⁴ For several acceptors per chain, the probability of ET in optimum conditions (low pH) increases because it is likely that one acceptor chromophore will be closer to the donor than the average distance between all the possible donor-acceptor pairs present in the system. Steady State data cannot be used to determine the distance distribution and will not even reveal the presence of any distribution in the system. Distance distributions have been expressed as Lorentzian functions.⁴⁵ End-to-end-distances (size of the polymer chain) have been calculated assuming a Gaussian distribution function to model the energy transfer efficiency.⁴⁶ All of these theoretical treatments are postulated assuming that segmental diffusion does not occur on the timescale of the energy transfer. However, no such assumption is necessary for DLS and this is used (see below), along with TEM, to estimate an approximate size of the conformation adopted by PMAA in both acidic and basic conditions.

5.2.2 Fluorescence Lifetime measurements in aqueous solution

5.2.2.1 Comparison between donor and donor-acceptor labelled PMAA

In Fig. 5.5 we show fluorescence decay data for NA-PMAA and N-PMAA at pH 2 and pH 10. From the data it can be observed that at high pH, naphthalene chromophores have the same fluorescence decay behaviour regardless of whether the polymer also has an anthracene label. In acidic conditions such decays become

slower than those of basic conditions since the polymer chains are coiled due to hydrophobic interactions. It is worth noting that in acidic situations the donor decay in NA-PMAA deviates away from the decay of N-PMAA, indicating energy transfer from naphthalene to anthracene.

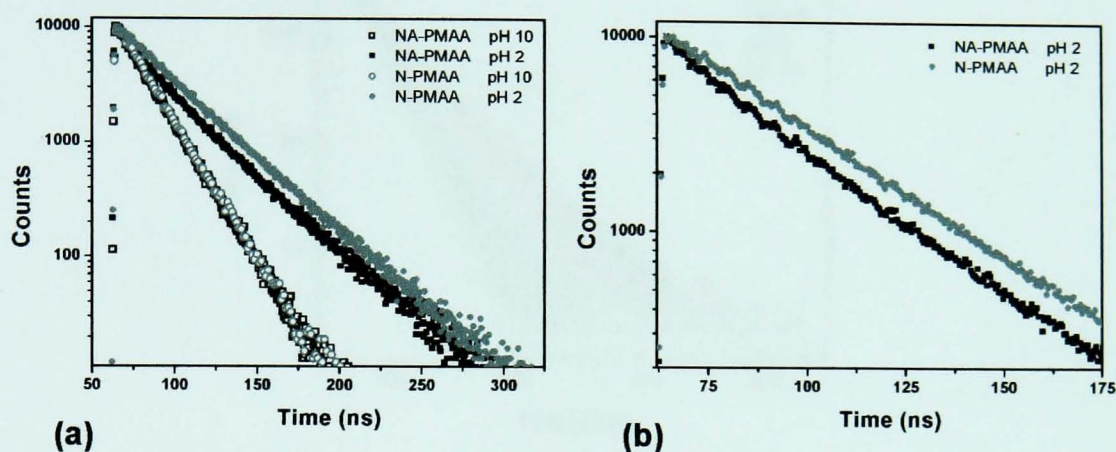


Fig. 5.5 (a) Naphthalene fluorescence decays for NA-PMMA and N-PMAA in acidic and basic conditions. Excitation and emission wavelengths are $\lambda_{ex}=290\text{nm}$ and $\lambda_{em}=310\text{-}550\text{ nm}$. (b) Deviation from linearity observed on NA-PMAA decay with respect of N-PMAA decay at pH 2.

We note that in acidic conditions in the presence of acceptor chromophores, the donor decays are rather more complex particularly at short times after its excitation. This complexity is understood as a consequence of a distribution of distances between different N-A pairs. The decay of donor in NA-PMAA at basic conditions does not appear to be so affected by this distribution. In such basic conditions average N-A distances are greater than the minimum R_0 necessary for 50 % of efficiency in ET, which means that there is no major perturbation in the naphthalene emission by the anthracene trap.

Assuming a distribution of distances would imply some N-A pairs closely spaced displaying shorter decay times, and other N-A pairs would be further apart displaying longer decay times. The range of N-A distances results in a range of decay times, which are statistically averaged in the measured decays. As a consequence multiexponential equations are needed to fit time resolved decays of the donor.

Naphthalene decays were collected over the whole pH range for N-PMAA and NA-PMAA as shown in Fig. 5.6. For NA-PMAA triple exponential functions of the form of eq.(4.1) were required to adequately describe the decay data when ET occurs (at low pH). At high pH the use of a double exponential (eq.(4.2)) was sufficient to fit the

decay data. N-PMAA decays were adequately fitted with double exponential over the entire pH range. In order to describe these results an average lifetime was calculated from eq.(4.3).

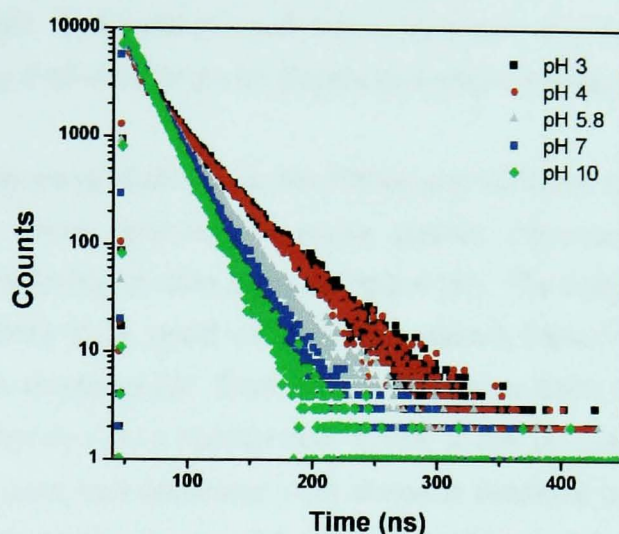


Fig.5.6 Naphthalene decays $\lambda_{ex}/\lambda_{em}=290/340\text{nm}$ collected at different pH for double labelled NA-PMAA sample.

By comparing NA-PMAA and N-PMAA average lifetimes (table 5.1) at low pHs we see that $\langle\tau\rangle$ are shorter for donor naphthalene in the presence of the anthracene trap than for donors without acceptor. At the maximum efficiency of energy transfer (pH 2) the naphthalene molecule in NA-PMAA remains excited 5ns less than in the N-PMAA sample at the same pH.

pH	$\langle\tau\rangle$ (ns) N-PMAA	$\langle\tau\rangle$ (ns) NA-PMAA
2.5	31.5	26.5
3.5	31.2	27
4.3	30.5	27
4.8	31.2	26
5	30	25.6
5.4	25.7	25
5.8	23	24
6.3	21.4	20
6.5	21	20
7.2	19.3	19
7.4	18.2	18.2
8	17	17.4
8.5	17	17
9.2	16	17
10	16.5	16.8

Table 5.1. Average lifetimes $\langle\tau\rangle$ comparison for N-PMAA and NA-PMAA samples in aqueous solution at various pHs. $\lambda_{ex}/\lambda_{em}=290/340\text{nm}$. Fig. 5.7 shows $\langle\tau\rangle$ for N-PMAA and NA-PMAA versus pH.

In the range $6 < \text{pH} < 10$ (above the neutralization point) there are no significant differences in average lifetimes of naphthalene in both samples. In such range of pHs, the more extended conformation of the chain due to coulombic repulsions does not allow significant quenching of donor excitation from acceptor which means no energy transfer. This unquenched donor emission explains the similar average lifetimes in the $6 < \text{pH} < 10$ range for double and single labelled PMAA.

Average naphthalene lifetimes for NA-PMAA and N-PMAA are plotted against pH in Fig.5.7. This curve showed the same pattern obtained from the change of fluorescence intensity or ratio I_{420}/I_{340} (Fig.5.4 (b)). The shape of the plot (as in the previous section) is a result of a conformational transition taking place in the polymer when changing pH. Such a transition goes from a relatively open coil at high pH (shorter $\langle \tau \rangle$) to a hydrophobic cluster at low pH (longer $\langle \tau \rangle$). From Fig.5.7 the inflection point that separates both states is obtained by fitting the data (using eq.(5.2)) and is located at a pH of 5.8 for NA-PMAA and 5.7 for N-PMAA.

The similarity between the neutralization values for double and single labelled polyelectrolytes indicates that the inclusion of the covalently bound acceptor does not affect significantly the behaviour of PMAA. These values are also in good agreement with the value of pH 5.7 yielded by Steady State measurements.

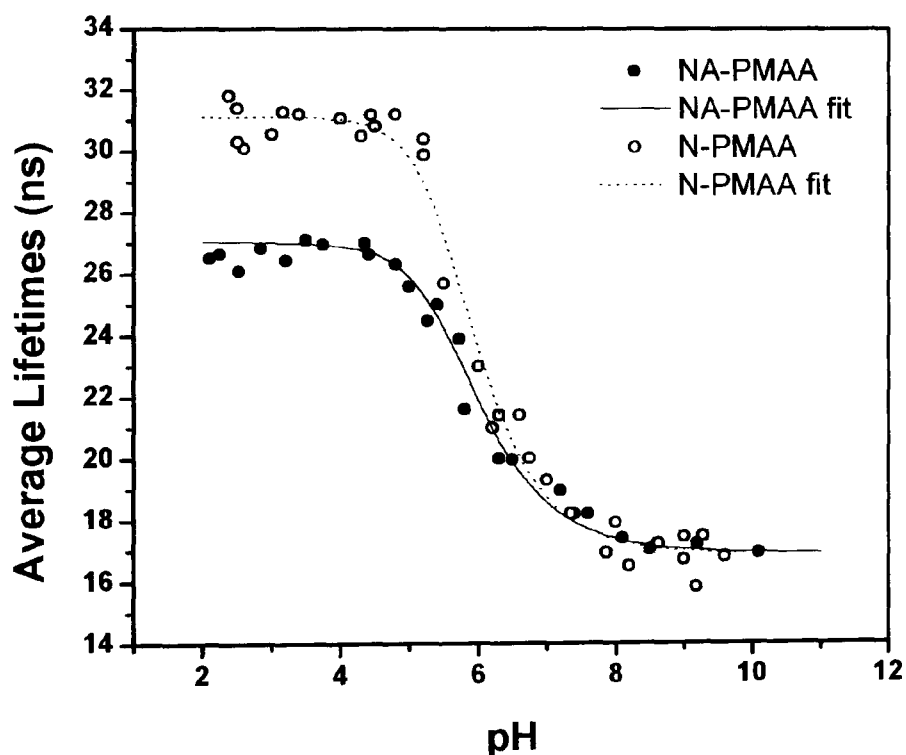


Fig. 5.7 Donor average lifetime $\langle \tau \rangle$ for NA-PMAA and N-PMAA in a range of different pH and fits at $\lambda_{ex}/\lambda_{em} = 290/370\text{nm}$. The data points are taken from Table 5.1

5.2.2.2 Donor-acceptor labelled PMAA

The different values of τ_i needed to fit the time dependence of donor decay in NA-PMAA reported different domains within the open or coiled conformation. Different domains are understood as microenvironments with different degrees of hydrophobicity and/or viscosity sensed by the chromophores. The explanation of different domains associated to different lifetimes has been discussed before for dansyl labelled PMAA systems,¹⁷ or for pyrene dispersed in PMAA.¹⁵

The fractional contribution of the different relaxation times used to fit the naphthalene fluorescence decays in NA-PMAA is shown in Fig.5.8. In the range $2 < \text{pH} < \text{transition point} \sim 5.8$ the values of τ_3 for NA-PMAA are $< 5\text{ns}$ and their fraction is close to 60%. $10\text{ns} < \tau_2 < 15\text{ns}$ and affects approximately 20% of the chromophores. τ_1 ($\sim 34\text{ns}$) remains approximately constant with a fraction of circa 20%.

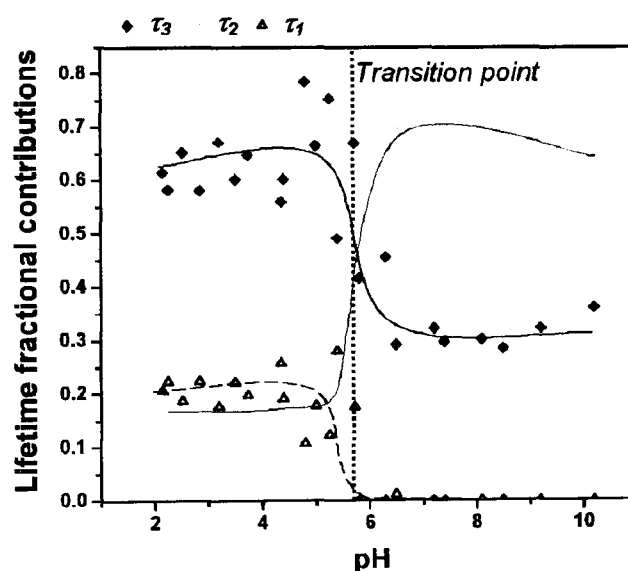


Fig. 5.8 Fractional contribution of lifetime parameters τ_i ($i=1,2$ and 3) used to fit the naphthalene decays in NA-PMAA at different pHs. The broken vertical line refers to the neutralization pH and the solid lines are guides to the eye.

Given the lifetime fluorescence data we could consider the model proposed by Ghiggino and Tan⁴⁷ to explain the evolution of lifetimes of chromophores located in different microenvironments. Using time resolved anisotropy measurements on PMAA labelled with terminal dymethylantracene, Ghiggino and Tan suggest that the polyelectrolyte adopts a 'pearl necklace' conformation in acidic conditions. Such a conformation would consist in rigid hydrophobic globular clusters of polymer linked

each other by more flexible polyelectrolyte segments. The different lifetimes then correspond to dyes trapped either in the clusters (longer τ_i) or in the more open segments (shorter τ_i). However, in our studies the labelled PMAA samples used were of a relatively low molecular weight and are unlikely to be capable of forming such structures.²⁸

5.2.2.3 Proposed Model: the 'Onion' model

In acidic conditions, the polyacid coils dramatically to avoid contact with solvent. We describe this hypercoiled conformation as an "onion like" structure with different levels of exposure to the solvent. In the nucleus with a contribution of 20% would be the most hydrophobic region with the methyl groups responsible for the closed structure. We suppose that there is negligible solvent present in this nucleus. Donor chromophores tightly trapped in this rigid pocket do not exhibit significant freedom of movement and as a result their decays are retarded to leave a relative large lifetime of $\tau_1 \approx 34\text{ns}$.

Surrounding the nucleus is a second region, again affecting 20% of the total chromophores. The chromophores located in this part displayed shorter relaxation times $10\text{ns} < \tau_2 < 15\text{ns}$ than the dyes trapped in the heart of the globules. These shortened lifetimes imply more freedom of movement and more chain flexibility. We assume some solvent molecules present in this second region

The outer layer would be the most hydrophilic part, being in close contact with solvent molecules and accounting for 60% of the total chromophores. Dyes in this third region would reach equilibrium faster than the previous ones with lifetimes of $\tau_3 < 5\text{ns}$. Another possibility is that naphthalene dyes are bonded to the end of the chain, in which case the decay would be faster than these of dyes bonded to backbone. This outer region may take into account such dyes. Our samples have been only allowed to 20% conversion at most during the synthesis in order to ensure a low degree of branching. Such a low degree of branching would imply a small number of chain ends. Therefore it seems improbable that 60% of chromophores with $\tau_3 < 5\text{ns}$ would be trapped at chain ends. This high percentage of chromophores with significant freedom of movement reinforces the suggestion that chromophores are trapped at the edge of an 'onion' like structure.

The lifetime results showed that this 'onion' conformation in acidic conditions remains unchanged in the range from pH 2 to the transition pH ~ 5.7 . It is probable therefore that the structure is impenetrable to changes in pH until the transition

(neutralization point) is reached. At pH ~ 5.8 the solvent molecules are able to penetrate the innermost regions with large density of COOH groups. The coulombic repulsions between these carboxylic groups are now sufficient to destroy the hydrophobic pocket and change the conformation of the polyelectrolyte.

In the pH range from the neutralization point to pH=10 it can be seen from Fig.5.8 that τ_1 disappears (as a triple exponential is not necessary to fit the decays) and that two exponentials suffice. τ_2 now appears in the range of $18\text{ns} < \tau_2 < 25\text{ns}$ with a contribution of 75% of the total chromophores. τ_3 is $< 10\text{ns}$ and contribute only in approximately 25 % of the total decay. The rigid heart of the globule disintegrates and the second region in the cluster that contributed 20 % to the decay in acidic conditions is swollen until it dominates with approximately 75% of the total decay forming the centre of the new structure. The outer region affects 20 % of the chromophores.

A schematic diagram of this structure is shown in Fig. 5.9. Spherical and tubular shapes were assumed at low and high pH respectively according to the results obtained from TEM on the samples under study.

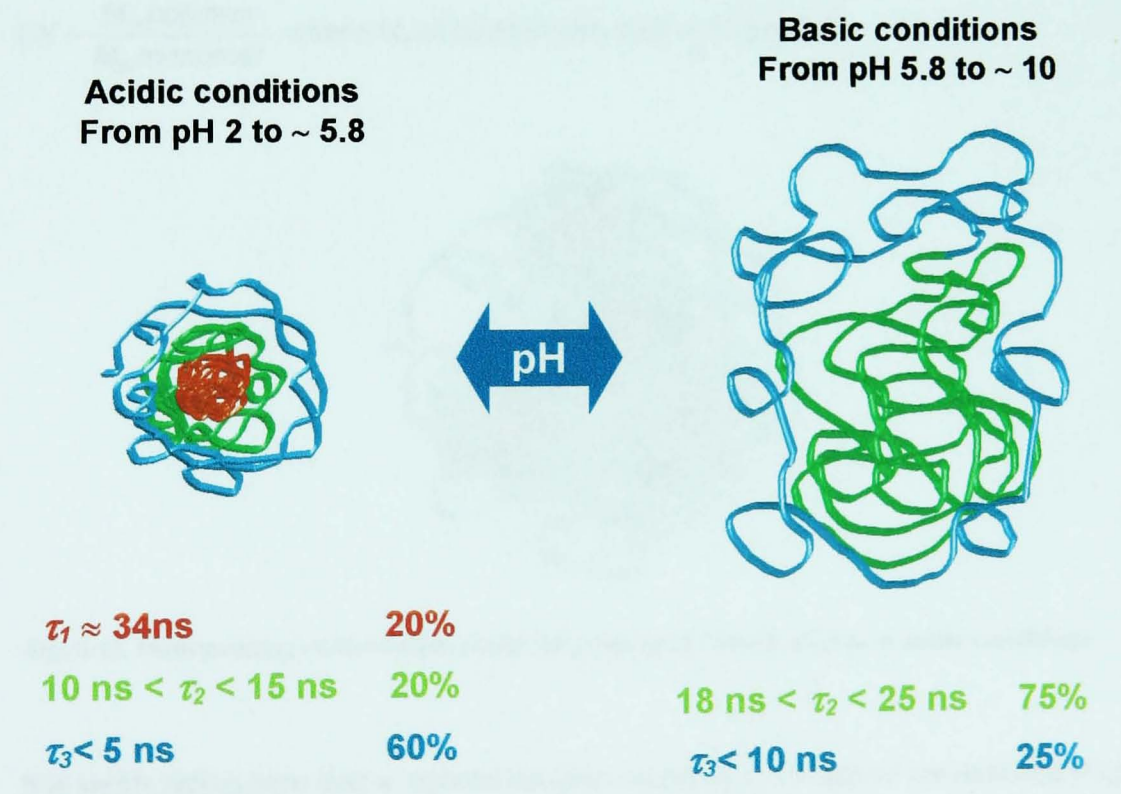


Fig. 5.9 Schematic diagram of the proposed 'onion' model to explain the conformation adopted by PMAA at acidic and basic conditions upon fractional contributions of lifetimes τ_i where $i=1,2,3$. In acidic conditions (left), the chain forms a layered structure with each layer corresponding to a different lifetime ($\tau_1 \sim 34\text{ns}$, $10\text{ns} < \tau_2 < 15\text{ns}$, and $\tau_3 < 5\text{ ns}$ respectively from the inside of the structure moving outwards). In basic conditions (right), the chain has a much more open structure with lifetimes of $18\text{ns} < \tau_2 < 25\text{ns}$ (inside the swollen coil) and $\tau_3 < 10\text{ ns}$ (at the outermost parts).

From Fig. 5.9, the blue region in acidic conditions may also be more extended to form a looser layer, possible even of a 'tadpole' form. Such form would be plausible if the electrostatic energies within the chain were enough to overcome the entropic cost of such a conformation. In terms of entropy an 'onion' conformation (Fig. 5.9) is more likely to occur than a 'tadpole' form.

Another possible model to explain the fact that at acidic conditions three decay times are required to fit the data would be a 'plum pudding' conformation (Fig.5.10). Such a conformation would have hydrophobic pockets with aggregates of COOH ($\tau_1 \approx 34\text{ns}$, 20%). A second layer would surround each pocket ($\tau_2 < 15\text{ns}$, 20%). Such structures would be placed in an open coil ($\tau_3 < 5\text{ns}$, 60%). However, a 'plum pudding' conformation suggests that when transition takes place, the structure would swell via a pearl necklace intermediate state. As mentioned above we do not believe our samples are capable of forming such structures due to their low molecular weight. As seen in section 4.1.2.1, the molecular weight of NA-PMAA is 80 kgmol^{-1} , which gives a degree of polymerisation of $N < 1000$ ($N = \frac{M_w \text{ polymer}}{M_w \text{ monomer}}$, where M_w of methacrylic acid is 86 gmol^{-1}).

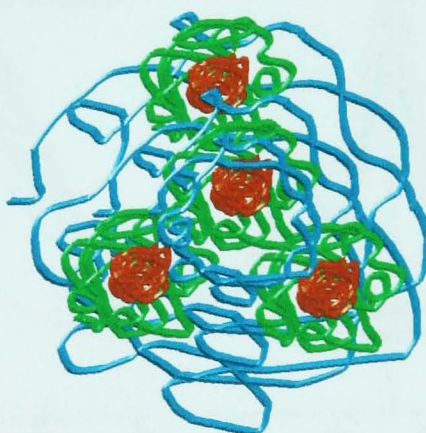


Fig. 5.10. Plum pudding conformation model adopted by the PMAA chains at acidic conditions

It is worth noting here that a layered structure such as the one that we describe (Fig. 5.9) is unlikely to be compatible with a cooperative swelling of the polymers. As the pH increases, the outermost parts of the chain would be expected to swell before the innermost regions, supporting, for example, previous conclusions of Raman spectroscopy experiments.²² Hence, the transition occurs as a progressive change.

5.2.2.4 Acceptor labelled PMAA.

The behaviour of donor and donor-acceptor labelled PMAA has been discussed in the previous section for samples in which the donor (naphthalene) is directly excited at $\lambda_{ex} = 290\text{nm}$. However, information about distance distributions can also be obtained also from the acceptor decay. Acceptor molecules generally absorb light at wavelengths used to excite the donors. As a consequence, the acceptor chromophores can be excited via two routes: direct excitation and energy transfer from the excited donor. Only the transfer of energy from the excited donor leads to information on distance distributions but this route is a minor contribution to the acceptor decay. The majority of such decays are due to direct excitation, which is why appropriate analysis of acceptor decays should also consider directly excited acceptors. Fig. 5.11 shows an excitation scan in a NA-PMAA sample, where the emission has been fixed at 420 nm (a characteristic emission wavelength of anthracene) at various pHs. The excitation range includes the excitation wavelengths of naphthalene and anthracene, 290nm and 370nm respectively. The contributions of both paths to excite the anthracene molecule can be observed at different pH.

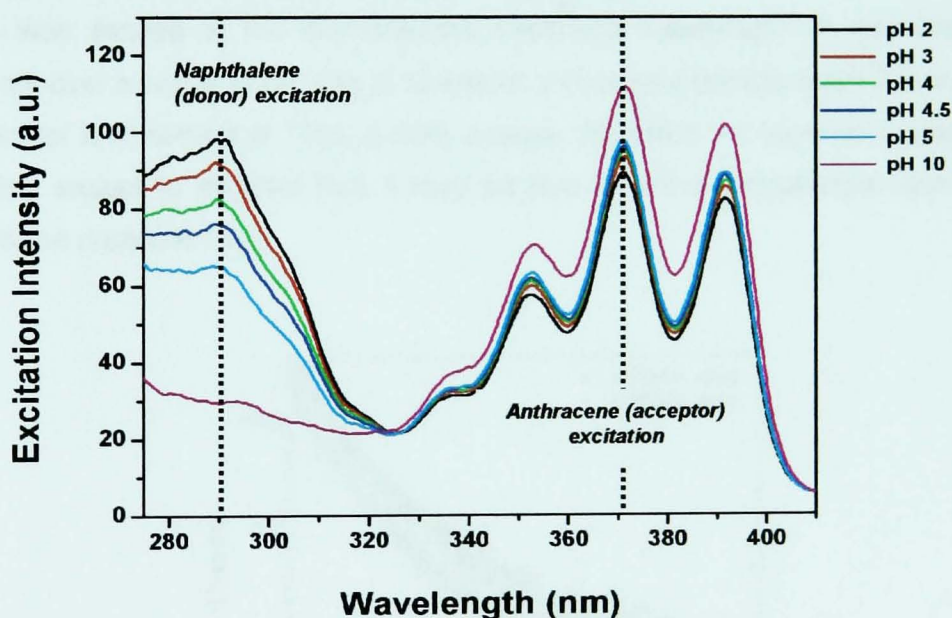


Fig. 5.11 Excitation scan in a range $\lambda_{em} = 270\text{-}410\text{nm}$ at fixed emission $\lambda_{em} = 420\text{nm}$ for a double labelled sample NA-PMAA

The ratio between anthracene excitation due to energy transfer from the excited donor and total excitation at different pH has been calculated from Fig. 5.11 and is shown in Fig. 5.12.

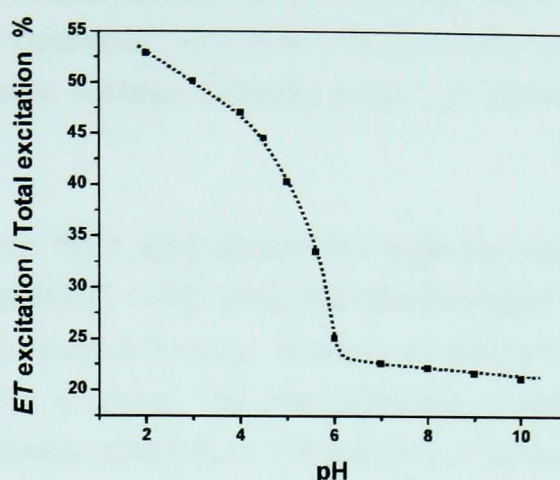


Fig. 5.12 Percentage of excitation in anthracene due to energy transfer from excited naphthalene at various pH. Emission was fixed at $\lambda_{em}=420\text{nm}$. Data fitted (dashed line) using eq.(5.2)

From Fig. 5.12 it can be seen that at low pH, the excited anthracene transfers circa 52% excitation to naphthalene. When the pH increases this percentage gets smaller implying that the major source of excitation of anthracene is its direct excitation. It is notable that the trend obtained from Fig. 5.12 mirrors the trends obtained in the previous section for naphthalene in Fig. 5.4 (b) and Fig. 5.7.

A-PMAA was excited at the characteristic excitation wavelength of anthracene $\lambda_{ex}=370\text{ nm}$ over a range of pH. Fig. 5.13 shows anthracene decays at pH 2 and pH 8. A shoulder is observed at 70ns in both decays, for which we have no plausible explanation except to suggest that it may be due to some instrumental artefact present in the measurement.

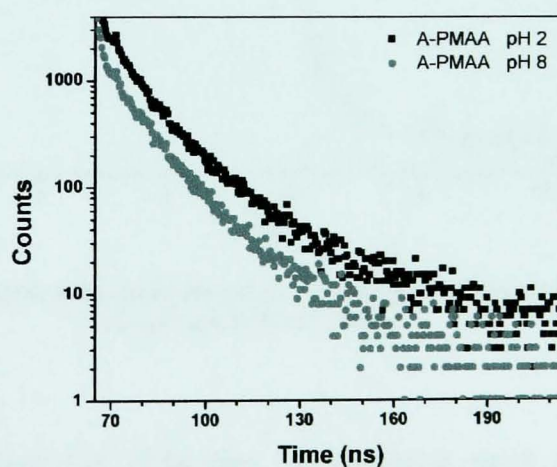


Fig. 5.13. Anthracene decays in A-PMAA measured at pH 2 and pH 10 at $\lambda_{ex}/\lambda_{em}=370\text{nm}/420\text{nm}$.

From Fig. 5.13 it can be observed that the anthracene decay in basic conditions is shorter than in acidic conditions. This trend was observed also in naphthalene decays but with a greater variation between acidic and basic conditions than is observed here.

Anthracene decays were fitted using double and triple exponential functions (eq. (4.2) and eq.(4.1) respectively). In this case, the complex decay in basic conditions was fitted by a triple exponential function. In acidic conditions the use of a double exponential function was sufficient. The short timescale of anthracene excitation make the decays particularly difficult to fit. The selection of different channels (each channel is 0.4565 ns wide) as the starting point of the fitting routine had large consequences in the lifetimes obtained. Although the individual amplitudes and the lifetimes obtained from the triple and double exponential fits do not have a well defined physical meaning and are subject to fitting artefacts, the average lifetimes derived from them is reliable and has an interpretable meaning. Nevertheless, the pH dependence of the anthracene average lifetimes $\langle \tau \rangle$ yielded the same trend as that obtained previously from naphthalene average lifetimes. Anthracene average lifetimes plotted against pH are shown in Fig. 5.14 and were fitted optimally using the same function described previously by eq (5.2).

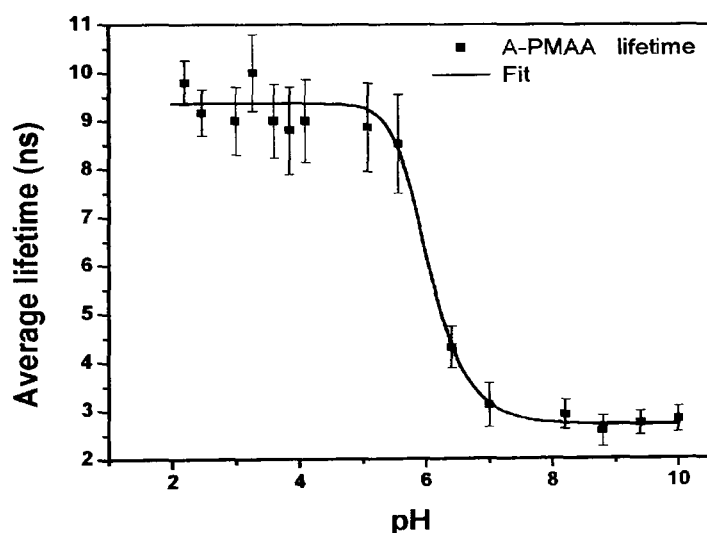


Fig. 5.14 Acceptor average lifetimes $\langle \tau \rangle$ for acceptor decays in A-PMAA at $\lambda_{ex}/\lambda_{em} = 370\text{nm} / 420\text{nm}$.

It can be observed from Fig. 5.14 that the inflection point of the fitted curve (corresponding to the pH at which the conformational transition takes place) is in good agreement with the value obtained previously upon excitation of naphthalene: pH ~5.8

5.2.3 Time Resolved Anisotropy measurements (TRAMS) in aqueous solution.

Anisotropy curves $R(t)$ for NA-PMAA were calculated using the method previously described in the experimental section. The pH-dependence of anisotropy decay for a NA-PMAA sample is shown in Fig. 5.15. For these fluorescence depolarization measurements the chromophore excited is the acceptor anthracene.

Fig. 5.15 shows longer anisotropy decays in acidic conditions due to the poor mobility of the dyes trapped in the coiled conformation. In basic conditions the decay is faster. A marked difference between the behaviour in acidic and basic conditions is observable. The transition mentioned in the previous section appears in these plots as a gap between the different behaviours occurring just after the transition pH was reached (pH \sim 5.8). The greater sensitivity of TRAMS compared to that of lifetime measurements allows us to observe this gap-effect which is not observed clearly for fluorescence decays over different pHs (Fig. 5.6)

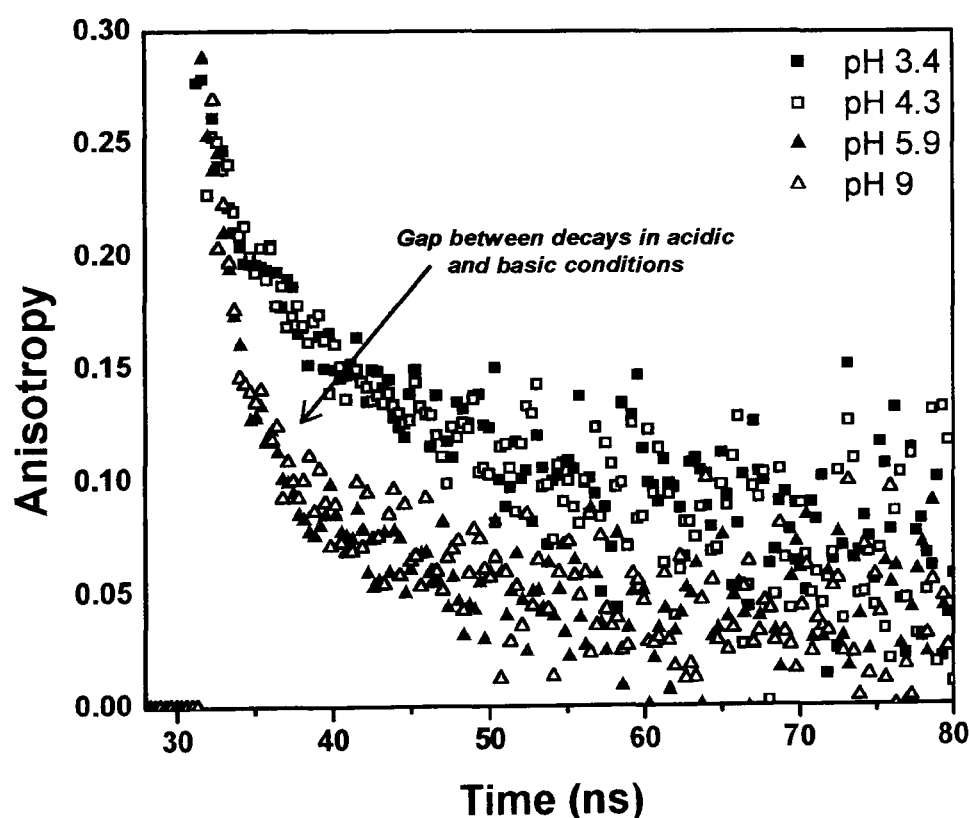


Fig. 5.15 Anisotropy decays for NA-PMAA at $\lambda_{ex}/\lambda_{em} = 370/450\text{nm}$ for different pHs.

Double (eq.(4.2)) and single exponential functions (eq.(4.5)) were used to fit the anisotropy decays over the whole range of pH. Due to the low fractional contribution of one of the components and the good fit reached with one rotational correlation time, a single exponential function was employed to fit the anisotropy decays. This approach was capable of broadly characterising the polymer dynamics (segmental mobility) within single polymer chains.

Correlation times τ_r corresponding to anthracene molecules and χ^2 values for wide range of pHs are shown in Table 5.2. A plot of these rotational correlation times as a function of pH is shown in Fig. 5.16

The curve shown in Fig. 5.16 was fitted using the same modified hyperbolic tangent function given in eq.(5.2) and the inflection point was thus calculated. The pH at which the transition takes place from these measurements was found to be at approximately pH 5.8, in good agreement with the previous results. The rotational correlation time-pH plot yielded a similar behaviour as that obtained from the donor average lifetime as a function of pH plotted in Fig. 5.7. However both curves in Fig. 5.7 and Fig. 5.16 showed slightly different behaviour in acidic and basic conditions.

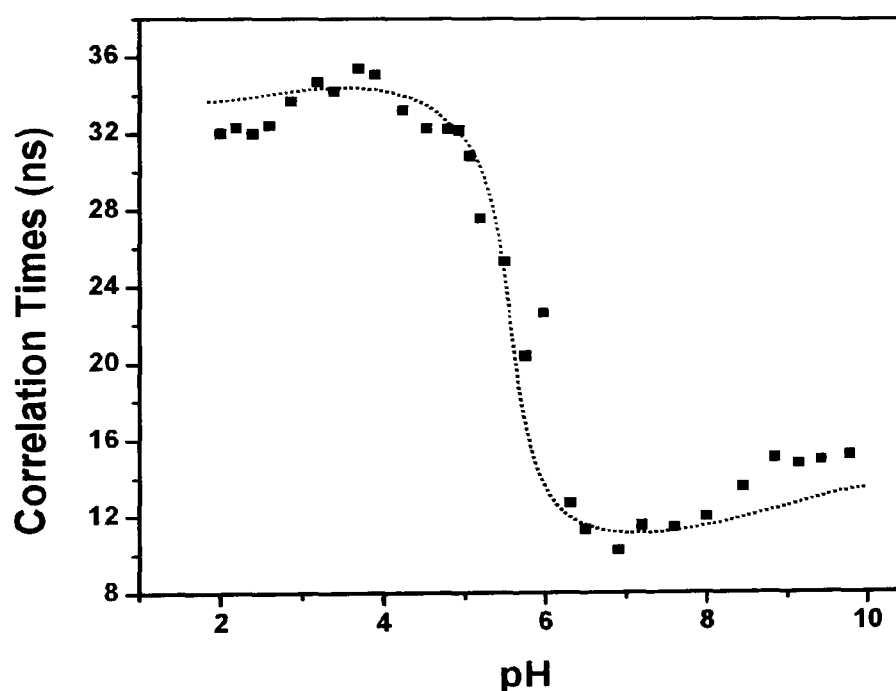


Fig. 5.16 Rotational correlation times vs pH for NA-PMAA at $\lambda_{ex}/\lambda_{em} = 370/450\text{nm}$. Data fitted (dotted line) using eq.(5.2).

pH	τ_c (ns) NA-PMAA	B pre-exponential factor	χ^2
2	31.98	0.1985	1.29
2.2	32.28	0.1943	0.96
2.4	31.97	0.1985	1.03
2.6	32.4	0.192	1
3.2	34.66	0.1873	1.16
3.4	34.17	0.1932	1.15
3.7	35.38	0.189	1.06
3.9	35.05	0.1982	0.99
4.2	33.18	0.1973	1.28
4.5	32.24	0.2011	1.14
4.8	32.25	0.1995	1.19
5	32.16	0.1859	1.05
5.2	27.54	0.1931	1.16
5.5	25.27	0.1897	1.18
5.7	30.8	0.1823	1.15
6	20.37	0.1794	1.4
6.3	12.64	0.1584	1.8
6.5	11.27	0.1687	1.6
7	10.2	0.1641	1.64
7.2	11.48	0.15	1.53
7.6	11.36	0.1636	1.55
8	11.92	0.1619	1.6
8.5	13.5	0.1551	1.54
8.8	15	0.1531	1.66
9	14.73	0.156	1.60
9.5	14.94	0.1569	1.5
9.8	15.18	0.1503	1.6

Table 2. Correlation times $\langle\tau_c\rangle$, pre-exponential factor and χ^2 for single exponential fit of anisotropy decay of NA-PMAA at various pHs at $\lambda_{ex}/\lambda_{em} = 370/450\text{nm}$

From Fig.5.16 at low pH τ_c is observed to have some dependence on the degree of acidity with a maximum value at pH ~ 4 . This effect would imply that the cluster adopted by the polyelectrolyte in acidic conditions would reach its smallest coiled conformation in the region of pH ~ 4 not long before the transition to a more open conformation takes place. The behaviour observed in τ_c in acidic media for NA-PMAA mirrors those observed for dansyl-PMAA¹⁷ and PMAA-1vinyl naphthalene³⁴ upon anisotropy measurements. There is a maximum in correlation time reflecting a minimum in the rate of segmental motion. This trend can be understood following Bednar et al¹⁷ who suggested that restrictions on the segments of PMAA due to attractive electrostatic interactions between carboxylate ions and carboxylic groups

before the transition to a swollen form could be responsible. At the region of $\text{pH} \sim 4$ the polyelectrolyte would be partially neutralized presenting both carboxylate anions and carboxylic groups at approximately similar quantities what would favour intramolecular hydrogen bonding between them.

The idea that electrostatic interactions restrict motion in the region of $\text{pH} \sim 4$ contradicts the explanation proposed in the fluorescence decay section of the present work. Fig. 5.7 shows an average lifetime of the excited donor naphthalene independent of pH in acidic media. From this independence of pH it was assumed no change in rigidity, hydrophobicity and size in each region of the onion like cluster in the zone $2 < \text{pH} < 5.8$ (transition point pH). The rate of segmental motion within the three different regions explained before would therefore remain constant in acidic media. The same pH independent segmental relaxation was derived from TRAMS measurements in N-PMAA.³⁴

At this point it is important to discuss the different characteristics of both: naphthalene and anthracene. The form of attachment of naphthalene to the polymer backbone, bound at two places to the chain, could affect the rate of relaxation of the polymer chain by locally stiffening the segments. Such an effect would make the probe not sensitive enough to the local liberation of macromolecular motion observable in full acidification³⁴ in Fig. 5.16. The anthracene molecule is bound to the backbone at a single point not constraining or giving rigidity to the polymer. Such dyes are able to rotate along two axes. Like the dansyl and vinyl-naphthalene labels, anthracene reflects rotation about its bond to the polymer and is independent of chain backbone anisotropy decays. The architecture of such molecules allows them greater sensitivity in detecting macromolecular segmental dynamics at different degrees of acidity due to their decoupled motions.

In basic conditions (Fig.5.16) a maximum in τ_r at $\text{pH} 10$ is observable. The coulombic repulsion between carboxylic anions is large at this pH and the aromatic benzene groups of anthracene sense such repulsion and so their movement becomes more impeded yielding locally higher τ_r . From the lifetime results of naphthalene in NA-PMAA such an effect is not observed maybe due to the lower sensitivity in lifetime measurements when compared to TRAMS.

5.2.4 Fluorescence Lifetime and TRAMS measurements in methanol.

The behaviour of PMAA in aqueous solution as a function of pH has been presented earlier. It was shown that at low pH the hydrophobic interactions between the polyacid and water make the chains collapse into compact globules of non-uniform structure. As a result, the change in conformation of PMAA when increasing the pH is not due to a homogeneous ionisation of polymer chains. Such a change does not occur as a cooperative process but instead as a stepwise (progressive) process involving initially only the outer regions of the coils. Fluorescence decays were fitted as multiexponentials as a result of those different sites sensed by the chromophores complicating the fluorescence behaviour. Consequently, fluorescence measurements have been performed with labelled PMAA in the simpler situation afforded by methanol solutions. In methanol the carboxylic groups of PMAA do not significantly dissociate, thus the weak polyacid behaves as neutral polymer (the PMAA charges are negligible). The results yielded from measurements in methanol served as a reference when compared to those obtained from PMAA in aqueous solutions.

Polymer solutions of donor, acceptor and donor-acceptor labelled PMAA were prepared in methanol (spectroscopic grade) 0.01 wt% and measured at room temperature.

Donor fluorescence decays were measured in a NA-PMAA sample in methanol and compared to the decays of the same sample in water at pH 2 and pH 10 and the results are shown in Fig. 5.17 (a). The decay in methanol was optimally fitted using a double exponential function (eq.(4.2)) yielding $\langle \tau \rangle = 16.8$ ns and $\chi^2 \approx 1$. Fig. 5.17 (b) shows the donor average lifetime of NA-PMAA in methanol with the average lifetimes in aqueous solution at various pH for the same sample.

The same route was followed for anthracene decays in the A-PMAA sample. The results obtained are shown in Fig. 5.18 (a) and (b). The decay in methanol was optimally fitted using a double exponential function (eq.(4.2)) yielding $\langle \tau \rangle = 4.5$ ns and $\chi^2 \approx 1$.

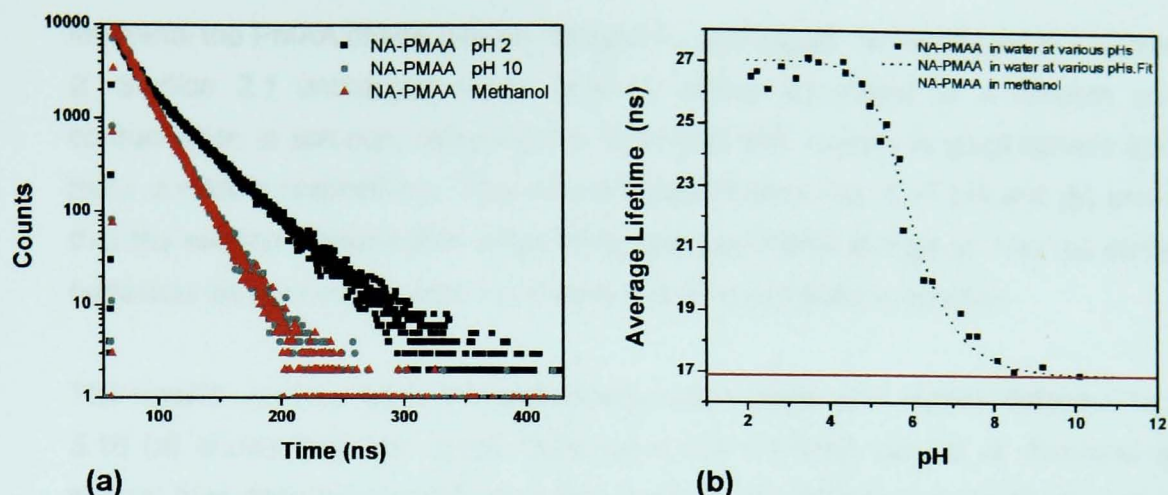


Fig. 5.17 (a) Naphthalene decays in the NA-PMAA sample in methanol and in aqueous solution at pH 2 and pH 10 with $\lambda_{ex} = 290\text{nm}$ and $\lambda_{em} = 310\text{-}550\text{nm}$. (b) The average lifetimes of naphthalene in the NA-PMAA sample in aqueous solution are plotted at various pHs. The average lifetime of naphthalene in the same sample in methanol ($\lambda_{ex} = 290\text{nm}$ and $\lambda_{em} = 310\text{-}550\text{nm}$) is plotted in red.

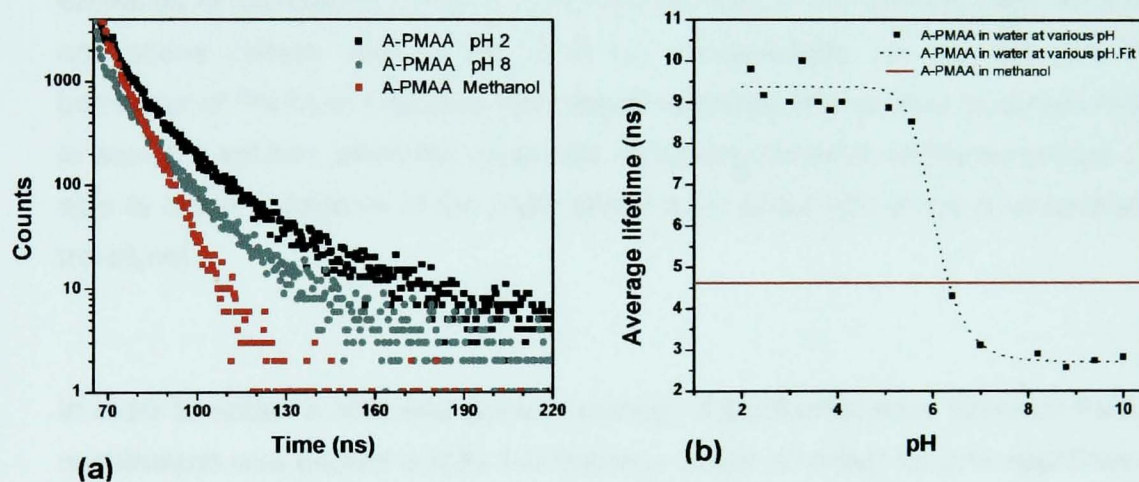


Fig. 5.18 (a) Anthracene decays in A-PMAA sample in methanol and in aqueous solution at pH 2 and pH 10 with $\lambda_{ex} = 370$ and $\lambda_{em} = 420\text{-}550\text{nm}$. (b) The average lifetimes of anthracene in PMAA-A sample in aqueous solution are plotted at various pHs. The average lifetime of anthracene in the same sample in methanol ($\lambda_{ex} = 370\text{nm}$ and $\lambda_{em} = 420\text{-}550\text{nm}$) is plotted in red.

From Fig. 5.17 (a) it can be observed that the fluorescence decay of naphthalene in methanol has a similar behaviour to its decay in an aqueous solution at pH 10. Furthermore, the plot of the naphthalene average lifetime in methanol (the red line in Fig. 5.17 (b)) overlaps clearly with the lifetimes in aqueous solution in the region of pH 10. It was assumed then that the fluorescence response of the chains in methanol matches the fluorescence responses obtained at high pH when the coulombic repulsions between ionised carboxylic acid stretch the polymer chains. In

methanol the PMAA chains can be considered uncharged. As introduced in *Chapter 2. Section 2.1* uncharged linear polymer chains are found in a random coil conformation in solution, following the SAW and RW models in good solvent and theta condition respectively. The results obtained from Fig. 5.17 (a) and (b) show that the swollen conformation adopted by charged PMAA at high pH has the same behaviour as the random coils adopted by uncharged PMAA in solution.

The results obtained when the anthracene was excited were slightly different. Fig. 5.18 (a) shows how the decay obtained in the A-PMAA sample in methanol is shorter than decays in aqueous solution at pH 8. The difference between decays in water and methanol was also found in the linearity of the decay in methanol when compared to the curved and multicomponent decays in aqueous solution. The plot of anthracene average lifetime in methanol (red line in Fig. 5.18 (b)) overlaps with the lifetimes in aqueous solution in the region of $\text{pH} \approx 6$ after the conformational transition takes place. The difference in this value of pH and that obtained from excitation of naphthalene in Fig. 5.17 (b) can be found in the different patterns in the anthracene decays seen in Fig. 5.18 (a). Nevertheless, we can say that the behaviour of PMAA in methanol (uncharged situation) is equivalent to its behaviour in aqueous solution when the coulombic repulsions between carboxylic groups are able to cause expansion of the chain above a pH of 5.8 (pH of the conformational transition)

In order to obtain a complete characterisation of the fluorescence decay of PMAA, naphthalene was excited and its fluorescence decay recorded for both naphthalene and naphthalene-anthracene labelled PMAA. The same procedure was performed for anthracene. Data are shown in Fig. 5.19 (a) and (b). Fig. 5.19 (a) shows that using methanol as the solvent, the behaviour of naphthalene is the same in naphthalene and naphthalene-anthracene labelled PMAA. This same result was obtained previously (see Fig. 5.5 (a)) when decays of N-PMAA and NA-PMAA were identical at pH 10. The fact that the behaviour of the donor is identical with and without the presence of the acceptor trap indicates that no energy transfer occurs between the pair. The absence of energy transfer between donor-acceptor in methanol indicates an open conformation of the chains as stated before. A similar behaviour between anthracene and anthracene-naphthalene labelled PMAA was observed in Fig. 5.19 (b) when exciting the anthracene chromophores.

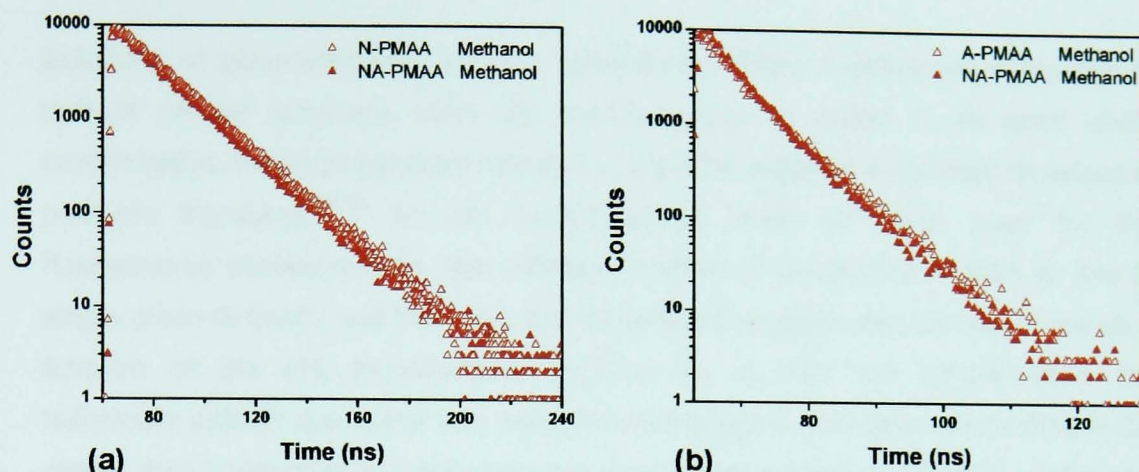


Fig. 5.19 (a) Naphthalene decays of N-PMAA and NA-PMAA samples in methanol with $\lambda_{ex} = 290\text{nm}$ and $\lambda_{em} = 310\text{-}550\text{nm}$. (b) Anthracene decays in A-PMAA and NA-PMAA samples in methanol with $\lambda_{ex} = 370$ and $\lambda_{em} = 420\text{-}550\text{nm}$.

TRAMS measurements were performed on a NA-PMAA sample in methanol in order to corroborate the results obtained for the lifetime measurements. Reasonably, the results obtained from TRAMS in methanol verify that PMAA chains in methanol and in basic conditions have the same behaviour. Fig. 5.20 (a) shows that NA-PMAA anisotropy decays faster in methanol than in aqueous solution in the basic region. This anthracene anisotropy decay in methanol was fitted using a double exponential function yielding $\langle \tau_c \rangle \approx 12\text{ns}$ and $\chi^2 \approx 1$. The equivalence of correlation times in methanol with respect to those in basic and acidic conditions has been schematised in Fig. 5.20 (b) as it has been done above.

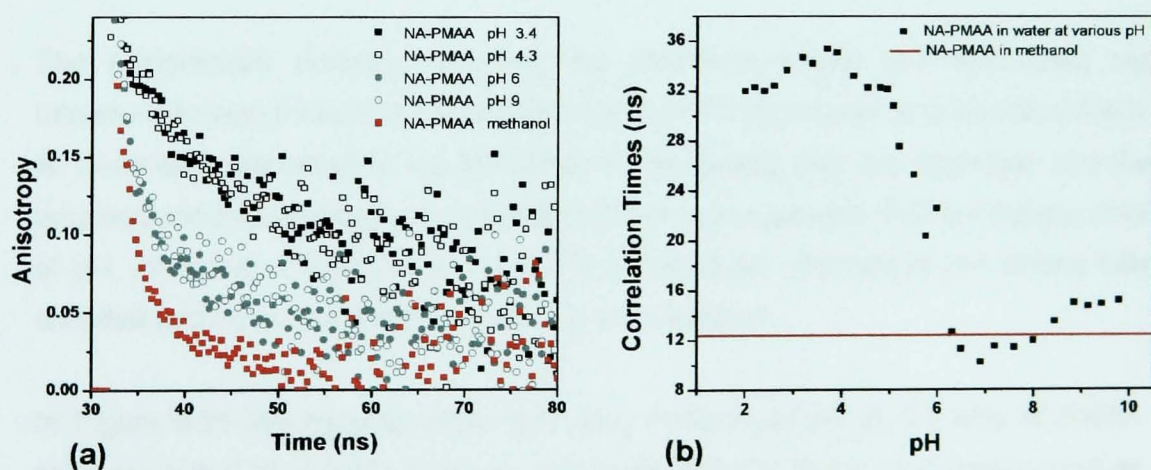


Fig. 5.20 a) Anthracene anisotropy decays in NA-PMAA sample in methanol and in aqueous solution at various pHs with $\lambda_{ex} = 370$ and $\lambda_{em} = 420\text{-}550\text{nm}$. 20b) Anthracene correlation times in NA-PMAA sample in aqueous solution at various pH. Plotted in red line is the average correlation time of anthracene in same sample in methanol with $\lambda_{ex} = 370\text{nm}$, $\lambda_{em} = 420\text{-}550\text{nm}$.

5.3 DYNAMIC LIGHT SCATTERING

Solutions of polyelectrolytes show a qualitatively different behaviour compared to that of neutral polymers. With the transition from a coiled to an open chain conformation, the hydrodynamic radius R_H (effective radius of a hydrated molecule in solution) increases.^{17,34} At low concentrations, such as those used for the fluorescence measurements, the diffusion coefficient calculated by DLS is due to single chain diffusion and therefore the hydrodynamic radius can be measured as a function of the pH. Nonetheless, experiments at this low concentration are technically difficult due to the very weak scattering signal. At higher concentration the chains start "clustering" and forming large aggregates leading to diffusion coefficients that do not reflect single chain conformations. Such aggregations can be minimized by shielding the polyions by adding salt. However such shielding can also inhibit conformational transitions (by screening the charges) such as those described in the present chapter.

Indeed, concentrations between 1 and 100 mg/ml at low ionic strengths exhibit two so-called "diffusive modes" in the relaxation time distribution.⁴⁸ The first, "fast mode", is attributed to coupled polyion (single chain) and counterion diffusion processes.

The second, "slow mode", reflects the formation of multi chain domains or temporal aggregates and its origin is believed to arise from long-range electrostatic interactions rather than hydrophobic aggregation. When the ionic strength of the system increases, the scattered intensity from the polyelectrolyte (fast mode) also increases^{49,50} while the signal of the slow mode becomes weaker and finally disappears. Whether this fact is due to the burying of the slow mode or because the aggregates vanish at all, has not been clarified.

The compromise between shielding the interchain forces and minimizing the intrachain forces is found at concentration of 0.1 wt% of polymer and 0.01 M of NaCl. At lower salt concentration the interchain forces prevail over the intrachain and the polymers tend to aggregate into clusters whose hydrodynamic radii are independent of pH. At higher concentrations of salt, the intrachain interactions are almost fully shielded and no coiled-uncoiled transition was detected.

In Figure 5.21 the hydrodynamic radii as a function of pH in 0.1 wt% of PMAA solutions with 0.01 M NaCl is shown. The hydrodynamic radius cannot be treated as the exact size of the polymer because it is related to the diffusive properties of the polymer in its hydrated/solvated state, and so is expected to be larger than a size determined from real-space measurements. This is because it includes the effect of the solvent that is part of the hydrodynamic sphere detected by light scattering.

The transition from the coiled to the open chain conformation is seen at pH 5.8 in good agreement with the value obtained from fluorescence measurements. We also note that in swelling, the chain increases in size from $R_H = 7.7$ nm at low pHs to 15 nm at high pHs

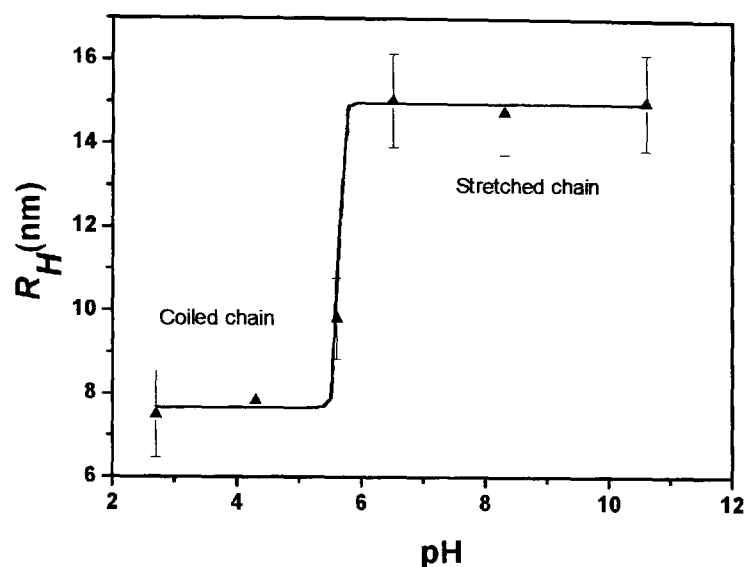


Fig 5.21 Hydrodynamic radii as a function of pH for PMAA as measured by dynamic light scattering at 0.1 wt% of PMAA and 0.1 M NaCl. The size of the polymer nearly doubles for solutions with pH greater than 5.8 (the neutralization point measured here).

5.4 TRANSMISSION ELECTRON MICROSCOPY

Two samples at the two extremes of pH, respectively 2 and 10 have been analysed by TEM. Polymer solutions have been negatively stained with uranyl acetate. This staining agent is used because it fixes organic structures at the molecular level extremely rapidly⁵¹ (~10 ms), arresting structural changes in macromolecules due to drying effects, and they interact with the electron beam producing phase contrast. Negative staining electron microscopy has been largely used for studying and understanding structural properties of sub-cellular compartment, proteins, and nucleic acids.⁵²

As already pointed out in the DLS discussion, one of the major issues with polyelectrolytes is to avoid the formation of aggregates. Such aggregates have also been observed by TEM in the present work (due mainly to water loss in the fixing process). It should also be noted that the uranyl acetate staining agent requires times of the order of ms to fix the polymers, which is much larger than all of the polymer relaxation times. However, the presence of the staining agent highlights

dense domains and therefore information on the single chain conformation can be extracted.

The two micrographs in Fig. 5.22 show two different architectures, which have been observed by TEM on the two samples. At low pH, the aggregates seem to be the result of the assembling of several chains coiled to form globules with average size of 4-5 nm (calculated over 5-6 specimens).

At high pH, where aggregation does not occur, the chains seem to have more tubular structures and their size has more than doubled (average size 12-14 nm). These results support the conclusion obtained by fluorescence techniques where compact coiled structures are present at low pH but after the transition point the polymer chains adopt extended conformations.

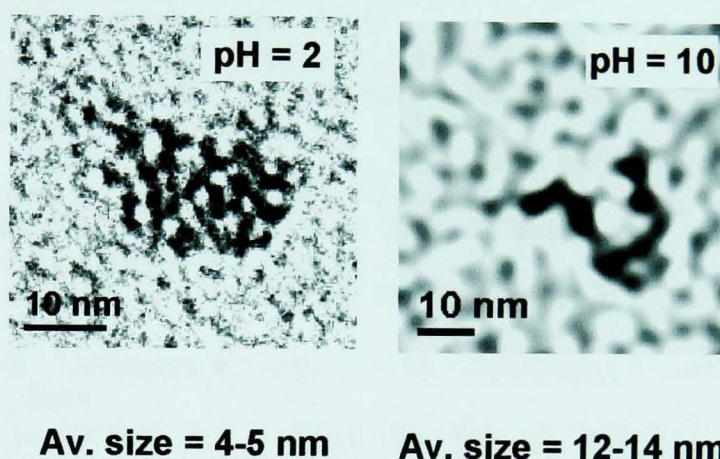


Fig. 5.22 TEM micrographs for NA-PMAA samples at pH 2 (a) and 10 (b). The image at pH 2 shows an aggregate of what seem to be individual coils, and in (b) a single chain is observed.

We note that the dynamic light scattering measurements reveal larger chain sizes than those for TEM, as expected. The difference is most dramatic at low pH, where the light scattering reveals domains that are nearly 80% larger than those as measured by TEM, whereas at high pH there is only a ~10% difference in size. If this is not due to artifacts in the TEM measurement, it might suggest that the outermost layer in the "onion" model described above is very loosely connected to the inner regions of the chain. These regions will not stain effectively for the TEM measurements, but they may well be solvated for the measurement of R_H .

Assuming that the globules formed at low pH are spherical and that the volume of a globule is given by $a^3 N$ (where $a=0.3\text{nm}$ for MAA and $N<1000$ for our sample), we could use the simple relation $(a^3 N) = (4\pi/3)(R/2)^3$ obtaining average globules sizes of $R<4\text{nm}$. Such value is closer to the values obtained from TEM measurements. A

quantitative calculation of volume and area of each region in the onion-like conformation at acidic conditions (Fig. 5.9) could be made.

REFERENCES :

- (1) Tripathy, S.; Kuma, J.; Nalwa, H. S., Eds. *Handbook of Polyelectrolytes and Their Applications*; American Scientific Publishers, 2003; Vol. Vols1-3.
- (2) Takahashi, M.; Yoshikawa, K.; Vasilevskaya, V. V.; Khokhlov, A. R. *J. Phys. Chem. B* **1997**, *101*, 9396-9401.
- (3) Wensel, T. G.; Meares, C. F.; Vlachy, V.; Matthew, J. B. *Proc. Natl. Acad. Sci.* **1986**, *83*, 3267.
- (4) Katchalsky, A.; Spitnik, P. *J. Polym. Sci* **1947**, *2*, 433.
- (5) Mandel, M. *Eur. Polym. J.* **1970**, *6*, 807.
- (6) Mandel, M.; Leyte, J. C.; Stadhonder, M. G. *J. Phys. Chem.* **1967**, *71*, 603.
- (7) Barone, G.; Crescenzi, V.; Quadrifoglio, F. *Ric. Sci* **1965**, *35*, 1069.
- (8) Katchalsky, A. *J. Polymer. Sci.* **1951**, *7*, 393.
- (9) Noda, I.; Tsuge, T.; Nagasawa, M. *J. Phys. Chem.* **1970**, *74*, 710.
- (10) Anufrieva, E. V.; Birshtein, T. M.; Nekrasova, T. N.; Ptitsyn, C. B.; Sheveleva, T. V. *J. Polym. Sci. Part C* **1968**, *16*, 3514.
- (11) Eisenberg, H. *J. Polym. Sci* **1958**, *30*, 47.
- (12) Barone, G.; Crescenzi, V.; Pispisa, B.; Quadrifoglio, F. *J. Macromol. Chem* **1966**, *1*, 761.
- (13) Barone, G.; Crescenzi, V.; Liquori, A. M.; Quadrifoglio, F. *J. Phys. Chem.* **1967**, *71*, 2341.
- (14) Chen, T. S.; Thomas, J. K. *J. Polym. Sci* **1979**, *17*, 1103-1116.
- (15) Olea, A. F.; Thomas, J. K. *Macromolecules* **1989**, *22*, 1165-1169.
- (16) Delaire, J. A.; Rodgers, M. A. J.; Webber, S. E. *J. Phys. Chem.* **1984**, *88*, 6219.
- (17) Bednar, B.; Trnena, J.; Svoboda, P.; Vajda, S.; Fidler, V.; k, P. *Macromolecules* **1991**, *24*, 2054-2059.
- (18) Soutar, I.; Swanson, L. *Eur. Polym. J.* **1993**, *29*, 371.
- (19) Crescenzi, V.; Quadrifoglio, F.; Delben, F. *J. Polym. Sci, Part A2* **1972**, *10*, 357.
- (20) Delben, F.; Crescenzi, V.; Quadrifoglio, F. *Eur. Polym. J.* **1972**, *8*, 933.
- (21) Daoust, H.; Thanh, H. L.; Ferland, P.; St-Cyn, D. *Can. J. Chem.* **1985**, *63*, 1568.
- (22) Koenig, J. L.; Angoud, A. C.; Semen, J.; Lando, J. B. *J. Am. Chem. Soc.* **1969**, *91*, 7250.
- (23) Moan, M. *Journal Appl. Cryst.* **1978**, *11*, 519.
- (24) Moan, M.; Wolf, C.; Cotton, J. P.; Ober, R. *J. Polym. Sci.* **1977**, *61*, 1.
- (25) Moan, M.; Wolf, C.; Ober, R. *Polymer* **1975**, *16*, 781.
- (26) Plestill, J.; Hlavata, D.; Labsky, J.; Ostanevitch, Y. M.; Bezzabotonov, V. Y. *Polymer* **1987**, *28*, 213.
- (27) Plestill, J.; Ostanevitch, Y. M.; Bezzabotonov, V. Y.; Hlavata, D.; Labsky, J. *Polymer* **1986**, *27*, 213.
- (28) Heitz, C.; Rawiso, M.; Francoise, J. *Polymer* **1999**, *40*, 1637-1650.
- (29) Schwartz, G. *J. Mol. Biol.* **1965**, *11*, 64.
- (30) Kalyanasundaram, K.; Thomas, J. K. *J. Am. Chem. Soc.* **1977**, *99*, 2039-2044.
- (31) Zana, R.; Lianos, P.; Lang, J. *J. Phys. Chem* **1985**, *89*, 41-44.
- (32) Chu, D.-Y.; Thomas, J. K. *Macromolecules* **1984**, *17*, 2142-2147.

- (33) Clements, J. H.; Webber, S. E. *J. Phys. Chem* **1999**, *103*, 9366-9377.
- (34) Soutar, I.; Swanson, L. *Macromolecules* **1994**, *27*, 4304-4311.
- (35) Forster, T. *Discuss. Faraday Soc.* **1959**, *27*.
- (36) Lakowicz, J. R. *Principles of Fluorescence Spectroscopy*, 2nd Edition ed.; Kluwer Academic/Plenum Publishers: New York, 1999.
- (37) Forster, T. *Modern Quantum Chemistry*, Academic Press: New York, 1965.
- (38) Webber, S. E. *Chem. Rev* **1990**, *90*, 1469-1482.
- (39) Guillet, J. E.; Rendall, W. A. *Macromolecules* **1986**, *19*, 224-230.
- (40) Liu, G.; Guillet, J. E.; Al-Takrity, E. T. B.; Jenkins, A. D.; Walton, D. R. M. *Macromolecules* **1990**, *23*, 1393-1401.
- (41) Soutar, I.; Swanson, L.; Imhof, R. E.; Rumbles, G. *Macromolecules* **1992**, *25*, 4399-4405.
- (42) Olea, A. F.; Thomas, J. K. *Macromolecules* **1989**, *22*, 1165-1169.
- (43) Olea, A. F.; Rosenbluth, H.; Thomas, J. K. *Macromolecules* **1999**, *32*, 8077-8083.
- (44) Yekta, A.; Winnik, M. A.; Farinha, J. P. S.; Martinho, J. M. *J. Phys. Chem. A* **1997**, *101*, 1787-1792.
- (45) Wu, P.; Brand, L. *Biochemistry* **1994**, *33*, 10457-10462.
- (46) Liu, G.; Guillet, J. E.; Al-Takrity, E. T. B.; Jenkins, A. D.; Walton, D. R. M. *Macromolecules* **1991**, *24*, 68-74.
- (47) Ghiggino, K. P.; Tan, K. L. *Polymer Photophysics*; Chapman and Hall: London, 1985.
- (48) Mori, H.; Seng, D. C.; Lechner, H.; Zhang, M.; Muller, A. H. E. *Macromolecules* **2002**, *35*, 9270-9281.
- (49) Kazakov, S. V.; Galaev, I. Y.; Mattiasson, B. *International Journal of Thermophysics* **2002**, *23*, 161-173.
- (50) Fundin, J.; Brown, W.; Vethamuthu, M. S. *Macromolecules* **1996**, *29*, 1195-1203.
- (51) Zhao, F.-Q.; Craig, R. J. *Struct. Biol.* **2003**, *141*, 43-52.
- (52) Alberts, B.; Johnson, A.; Lewis, J.; Raff, M.; Roberts, K.; Walter, P. *Molecular Biology of the Cell*, Fourth ed.: New York, 2002.

Chapter 6

Swelling behaviour of polybase and polyacid brushes

We present in this chapter Neutron Reflectometry experiments performed in both poly((diethylamino)ethyl methacrylate) (PDEAMA) and poly(methacrylic) acid (PMAA) brushes (synthesised as described in *Chapter 4. Section 4.2.1*) in aqueous media as a function of pH. For every brush the volume fraction–depth profile at each measured pH is presented together with the data fits. In the polybase section a subsection containing preliminary data analysis is presented.

6.1 POLYBASE BRUSH: POLY[(DIETHYLAMINO) ETHYL METHACRYLATE] (PDEAMA)

PDEAMA brushes were clamped in the sample cell described in *Chapter 4. Section 4.2.2 (Fig.4.12)* and measured at various pH (with a mixture of D₂O and NaOH or HCl as appropriate). We restrict ourselves here to considering the brush conformation as the pH decreases.

The initiator surface density of the two polybase brushes employed was determined by x-ray reflectometry to be 1.1 nm² and 0.5 nm² per molecule. The brushes dry thicknesses were 13 nm and 27 nm respectively, as measured by neutron reflectometry. We use these values as necessary parameters for our data analysis. The brush dry thickness is understood as the thickness of the brush in absence of

solvent (i.e. in air). The dry thicknesses were measured also by X-ray and ellipsometry yielding values within ~10% of the neutron results.

6.1.1 Preliminary data analysis using a hyperbolic tangent function

The reflectivity data were preliminarily fitted to model profiles using a Monte Carlo fitting algorithm as well as a steepest descent fitting routine.¹ Monte Carlo methods are defined as a class of computational algorithms simulating the behavior of various physical and mathematical systems. They are distinguished from other simulation methods by being stochastic, that is nondeterministic in some manner usually by using random numbers (or more often pseudo-random-numbers) as opposed to deterministic algorithms.²

We chose a simple model accounting for single layers of silicon oxide and initiator (both with thickness and roughness) to fit the reflectivity data; the brush profile ϕ was fitted to a hyperbolic tangent function $\phi = \phi_0 \left(1 + \tanh \frac{(\Delta - y)}{\delta} \right)$ where ϕ_0 is the volume fraction of brush at the initiator layer, Δ and δ are constants, and y is the distance from the initiator layer. With the aim of limiting the number of parameters, we used the scattering length densities set from reflectometry experiments performed on the dry brush in air. This enables us to acquire information about the thickness and scattering length density of the initiator layer, which we could use in the case of the brushes in solution. The dry brush thickness yielded also the thickness of the brush layer in the dry state, which fixes the amount of PDEAMA that we could fit to in the swollen case (i.e. the integrated area under the hyperbolic tangent volume fraction profile must be constant and equal to the brush thickness). Fig. 6.1 shows a schematic diagram of the different layers or regions comprising the brush in solution.

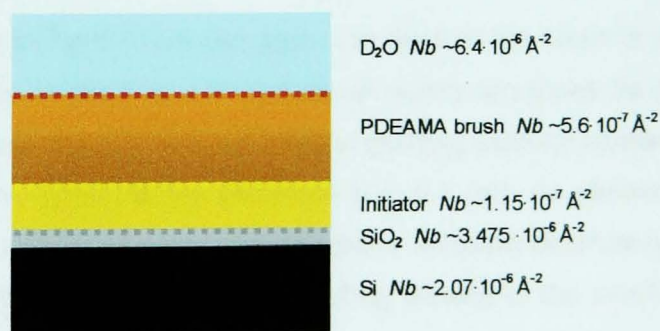


Fig. 6.1 Schematic diagram showing the different layers (with their corresponding roughness represented by dotted lines) comprising the PDEAMA brush in solution. It is shown also the scattering length densities (Nb) of each different region. This diagram is not to scale.

Typical data and fits for one of the PDEAMA brush are shown in Fig. 6.2. There are some deviations between the data and the fit curves; this is due to the fact that the fits were very constrained. The values of normalized χ^2 were between 5.7 and 11.0 suggesting that the model used to analyze the reflectivity data is too simplistic and provide poor quality fits.³

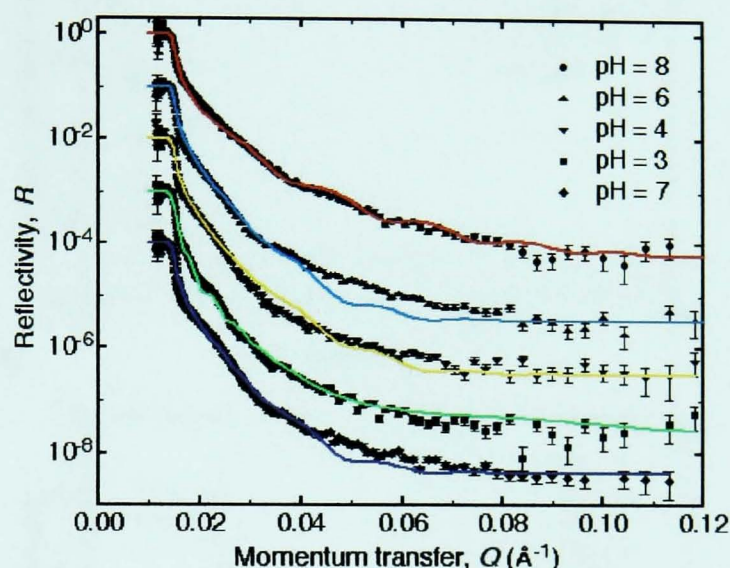


Figure 6.2. Neutron reflectivity data and fits for a PDEAMA brush, of dry thickness 27nm, in D₂O as a function of pH. For clarity of viewing the data are shifted down vertically from each other by a factor of 10. The fits are to a hyperbolic tangent volume fraction profile

$\left(\phi = \phi_0 \left(1 + \tanh \frac{(\Delta - y)}{\delta} \right) \right)$, where ϕ_0 is the volume fraction of brush at the initiator layer, Δ and δ are constants, and y is the distance from the initiator layer). The values of χ^2 for the best fits are 5.9, 10.2, 5.7, 7.5, 11.0, 6.7 (in order of decreasing pH).

Volume fraction-depth profiles for the two PDEAMA brushes are shown in Fig 6.3. As a first outcome, it can be seen from the profiles that the brushes are collapsed for values of pH > 4, but to different degrees (i.e. the width of the hyperbolic tangent profile δ , increases with decreasing pH). For pH < 5, the brush is stretched.

From the volume fraction profiles (Fig.6.3) we can also observe that the 13nm brush (smaller grafting density) swells at pH 3 to a thickness of nearly ten times its dry thickness (Fig. 6.3(a)). In contrast, the 27nm brush (higher grafting density) swells at pH 3, to a thickness of only two times its dry thickness (Fig.6.3 (b)). As shown in Chapter 3. Section 3.2.4.2, the swelling degree of weak polyelectrolyte brushes (i.e. the brush height) depends on the molecular weight, grafting density of the brushes and pH. The difference in the degree of swelling of both brushes suggests then an effect of grafting density (we do not expect the molecular weight of these brushes to vary dramatically and the pH at which swelling is observed is ~3 for both brushes).

In this way, a dense brush (high σ) of long chains (high N) may swell less than a not so dense brush (low σ) of shorter chains (low N) (according to eq.(3.39) at the same pH, $h \sim N\sigma^{-1/3}$).

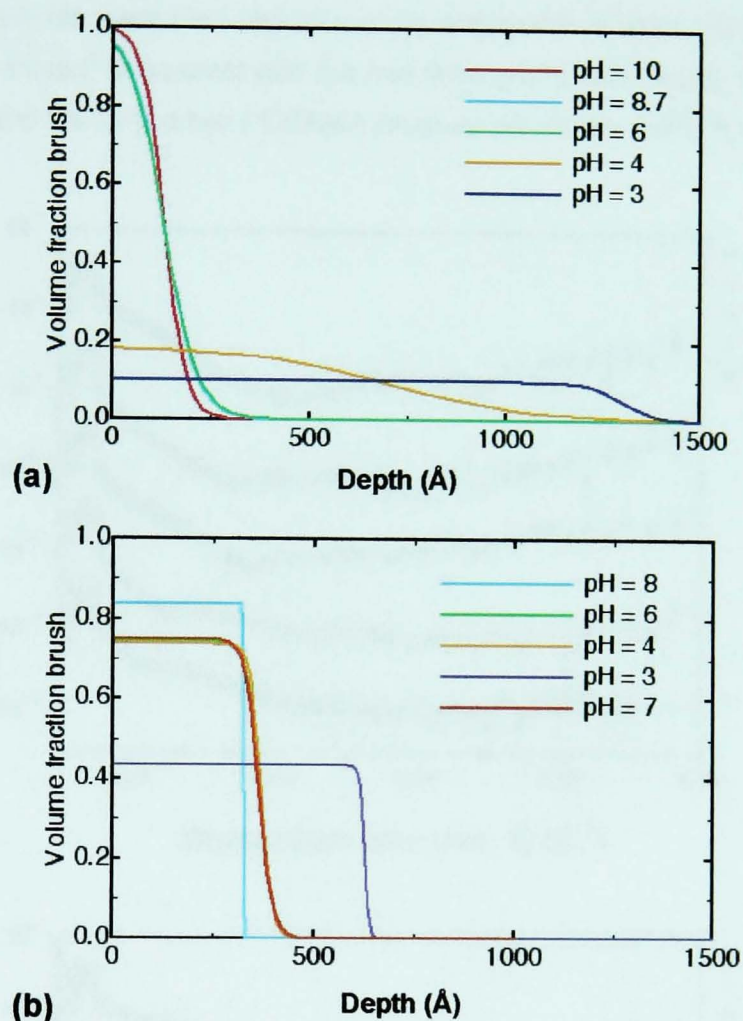


Fig. 6.3 Volume fraction-depth profiles for the two PDEAMA brushes as a function of pH. The dry thicknesses are 13 nm (smaller σ) (a) and 27nm (higher σ) (b). The profiles in (b) corresponds to the data and fits shown in Fig. 6.2

6.1.2 Data analysis using the slab-fit programme.

The same reflectivity data obtained from the two PDEAMA brushes (13 nm and 27 nm of dry thickness) were analysed using the slab-fit programme described in *Chapter 4. Section 4.2.2.2*. The silicon oxide and initiator layer were not present in the volume fraction profiles extracted from the best fits. This is due perhaps because they often are imprecise and can be subsumed into the brush-substrate roughness (see appendix 1 for the plots of the scattering length density Nb versus depth for the brushes in solution). Such a roughness was affected by irregularities

caused by an incomplete coverage of the silicon with the self-assembled monolayer (the brush was observed using scanning force microscopy (SFM) to cover ~80% of the surface, with patches of holes at other parts of the surface). Nevertheless, the slab-fit programme provided high quality fits and values of normalized $\chi^2 \approx 1$. The features of such fits were also reproduced by a downhill simplex fitting routine to a trilayer profile model⁴ in contrast with the free-form profiles yielded by slab-fit. Typical data and fits for the two PDEAMA brushes are shown in Fig.6.4.

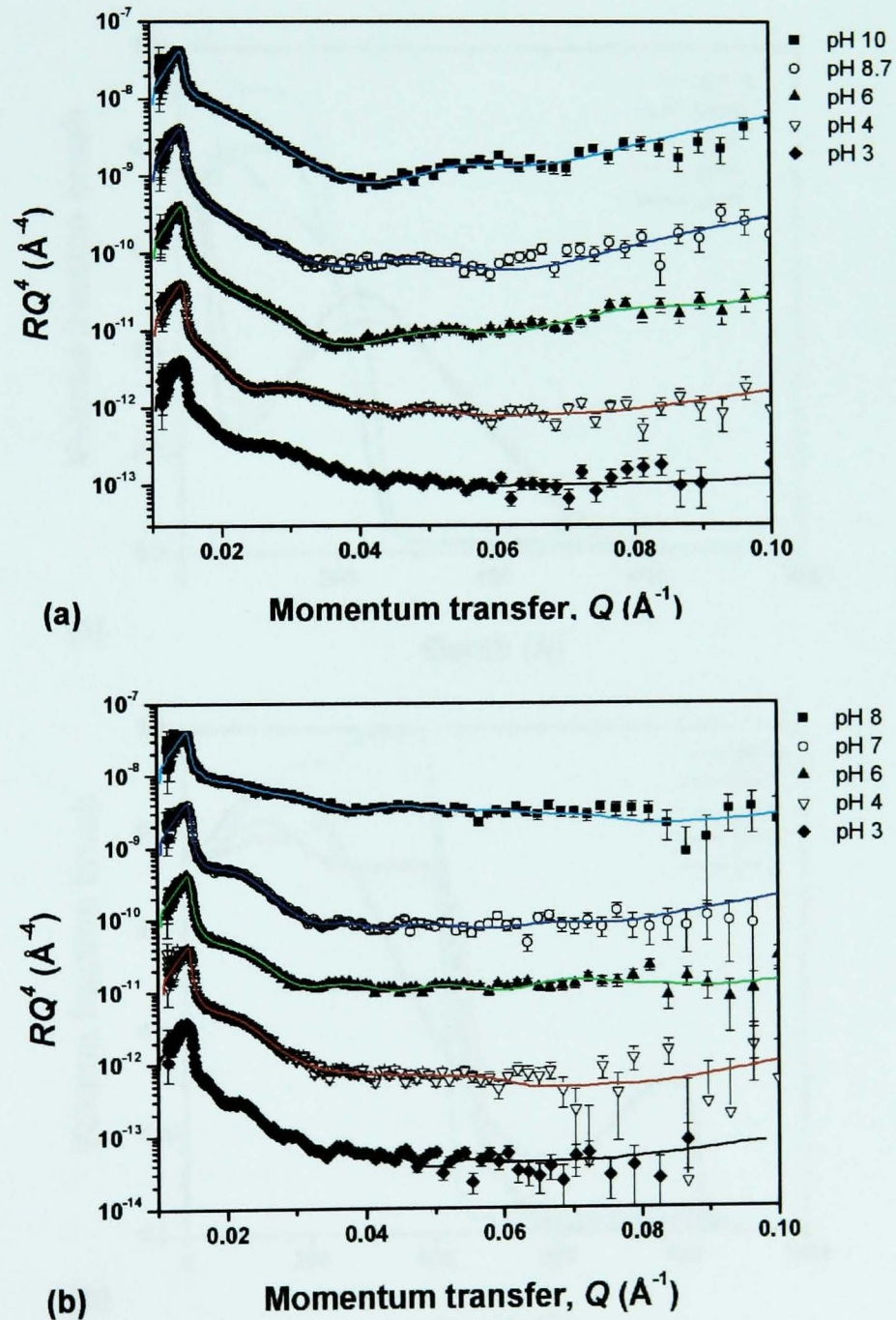


Fig. 6.4 Neutron reflectometry data and fits for PDEAMA brushes of 13nm (a) and 27nm (b) as a function of pH. The data are shown in the Porod form (eq. (4.24)) RQ^4 , where Q is the neutron momentum transfer on reflection and R is the reflectivity. Such form enhances the quality of the fits relative to a $R(Q)$ plot (Fig. (6.2)). For clarity of viewing the data are shifted down vertically from each other by a factor of 10. Fringes are observed at pH 3 due to a well defined thickness in the sample or parts of it. The values of χ^2 were ≈ 1 .

The corresponding volume profiles obtained from the fits shown in Fig.6.4 are shown in Fig. 6.5. The brush volume fraction to which all the profiles (i.e. all the pH) tend at 0Å depth is $\phi_{brush}=0.74$. This volume fraction is equivalent to the scattering length density of the silicon given by $Nb(z=0) = (Nb_{D_2O})\phi_{D_2O} + (Nb_{brush})\phi_{brush}$ where $Nb(z=0)=Nb_{silicon}$ and $\phi_{D_2O} = 1 - \phi_{brush}$. The broadness of these profiles (Fig.6.5) close to the substrate shows the effect of the interfacial roughness, which has contributions from oxide and initiator layers.

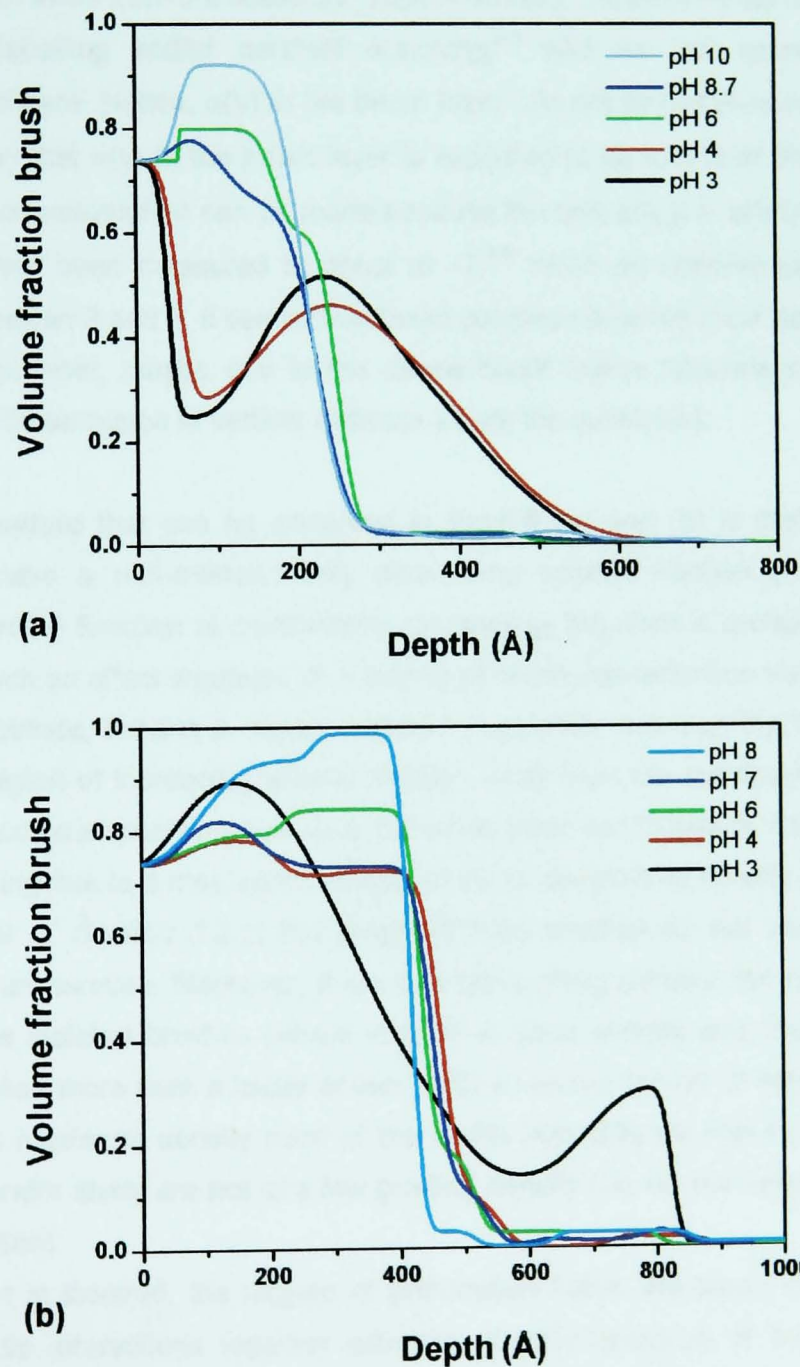


Fig. 6.5 Volume fraction-depth profiles for the two PDEAMA brushes as a function of pH as obtained from the NR data and fits shown in Fig. 6.4. The dry thicknesses are 13 nm (a) and 27 nm (b). The mass conservation routine is flexible to within $\pm 10\%$.

It is clear from the profiles shown in Fig. 6.5 that at low pH the brush is swollen. In the 13nm brush (Fig.6.5 (a)) the swelling occurs at pH=4 in good agreement with the profiles shown in Fig.6.3 (a). The 27nm brush swells only at pH 3 again in good agreement with the behaviour observed in this brush from the preliminary fits (Fig. 6.3 (b)).

It is important to understand that the pH we measured (within ± 0.5) is the pH of the external solution (reservoir). As discussed in *Chapter 3. Section 3.2.4.2*, the pH inside the brush region is controlled by the local degree of dissociation $\alpha(y)$, where y is the depth away from the substrate. Experimentally, measurements of $\alpha(y)$ involve complex labelling and/or contrast matching,^{5,6} and for this reason it is not considered here. Hence, $\alpha(y)$ in the brush layer has not been measured. However, we can say that $\alpha(y)$ in the brush layer is expected to be less than that in the bulk α^b . Such an assumption can be made because the bulk pK_b (i.e. pK_b of PDEAMA in solution) has been measured to occur at ~ 7 ,^{7,8} while we observe swelling at pH values between 3 and 4. It seems that these polybase brushes must be weaker than the bulk polymer, maybe due to the dense brush layers (discrete parallel layers within the brush region at vertical distance y from the substrate).

Another feature that can be observed in Fig.6.5 (a) and (b) is that the swollen brushes have a non-monotonically decreasing volume fraction profile (i.e. the volume profile function is consistently decreasing but then it increases again in value). Such an effect suggests an increase of brush concentration towards the end of the substrate, leaving a region depleted in polymer between the substrate and another region of increasing volume fraction away from the substrate. We refer to this unusual brush conformation as a 'depletion zone' conformation. One might think this as being due to a mushroom conformation at low grafting density (as described in *Chapter 3. Section 3.2.1*) but polyelectrolyte brushes do not show 'depletion zones' when swollen. Moreover, if we had low grafting density, the brushes would behave as isolated brushes (single chains) in good solvent and thus they would have swollen more than a factor of two. With a volume fraction of between 0.3 and 0.5 at the maximum density point of the profile (Fig. 6.5) we can be sure that the brushes under study are not at a low grafting density (i.e. do not have a mushroom conformation).

As the pH is lowered, the degree of protonation inside the brush increases. The electrostatic interactions together with the osmotic pressure of the counterions cause the swelling of the brush. Generally, in charged brushes the swelling begins in the outer part of the brush i.e. in the region closer to the external solution and away from the substrate. This is due to the fact that the brush is less dense away

from than close to the substrate (typical of a monotonically decreasing volume fraction-depth profile). Hence, the degree of ionization progressively decreases closer to the surface.⁹ Our profiles shown in Fig.6.5 seem to indicate the contrary with the swelling taking place at the substrate and with a collapsed region (entangled region) near the free chain ends. Such a collapsed region is indicated in the data for pH 3 in Fig. 6.4 (b), where the periodicity of fringes suggest a well defined thick layer; using eq. (4.29) such thickness is $d \approx 2\pi/\Delta Q \approx 75\text{nm}$.

Some Scanning Force Microscope (SFM) measurements were performed on the 13 nm PDEAMA brush at low and high pH, they are shown in Fig. 6.6. The tip used was an unfunctionalized silicon nitride tip. In this figure the line profiles show an increase in swelling by a ratio of between 50 and 100% in agreement with the volume fraction–depth profile obtained from the NR data fit (Fig. 6.5 (a)). However, the thickness obtained from SFM differs from that yielded by the neutron data, which suggest that the SFM tip may have penetrated the brush. Despite that, the SFM measurements confirm the swelling of the PDEAMA brush upon pH.

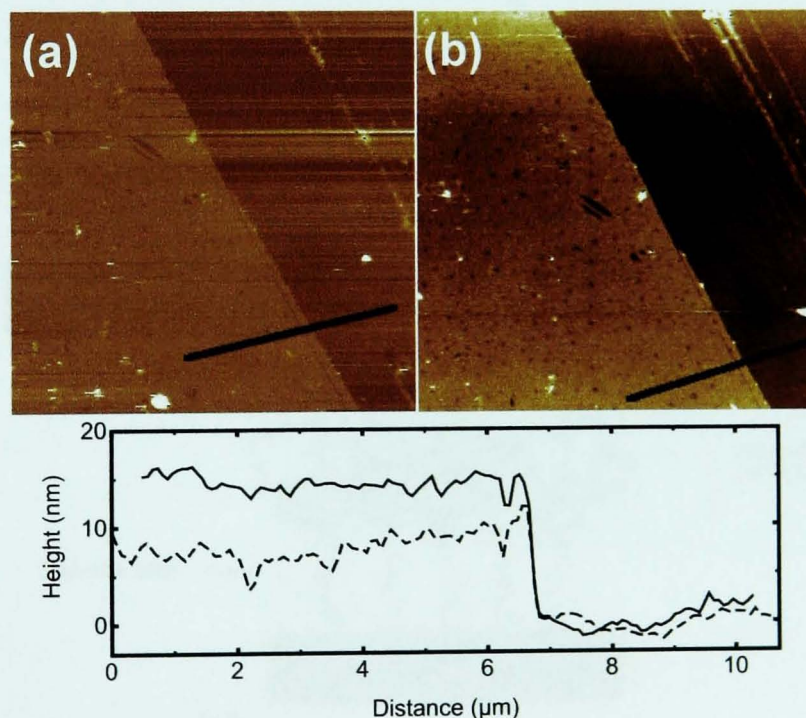


Fig. 6.6 *In situ* images of the 13nm brush for (a) pH =10 and (b) pH =3. Here the imaged region is slightly smaller than the 13nm of the reflectivity measurements. The scratch in the brush is used to measure the height of the brush relative to the substrate. The black line in each plot represents the location of the line scan in the figure below. From such line scans, we can see that the brush at pH 3 has swollen to nearly twice its size in pH=10. (Image taken by C.C. Dang).

6.1.2.1 Possible explanation of the 'depletion zone'

A possible explanation we find to the 'depletion zone' structure obtained from Fig. 6.5 (a) and (b) is that the brushes (within the timescale we measured them) are not in thermodynamic equilibrium with the bulk solution but instead in a long-lived metastable equilibrium due to entanglements.

As discussed in *Chapter 3. Section 3.2.2.2 b)* the 'grafting from' method provides brushes with high grafting densities, making the brush to become entangled as it grows from the surface. When the brush swells at low pH, these entanglements will not unravel, as one would expect them to do. Instead they gradually turn into tighter structures till there is no further three-dimensional movement in the brush. Assuming that initially the brush starts swelling at the substrate, the entanglements will be pushed vertically in the direction of the external solution and away from the substrate. The point where the brush is greatly entangled is the point away from the substrate where the brush fraction is at its larger value i.e. second peak of the black and red curves in Fig 6.5 (a) and second peak in the black curve in Fig. 6.5 (b). In order to maintain the electroneutrality of the system once the metastable equilibrium is reached, this entangled region cannot be charged. A schematic diagram of the proposed explanation is shown in Fig. 6.7

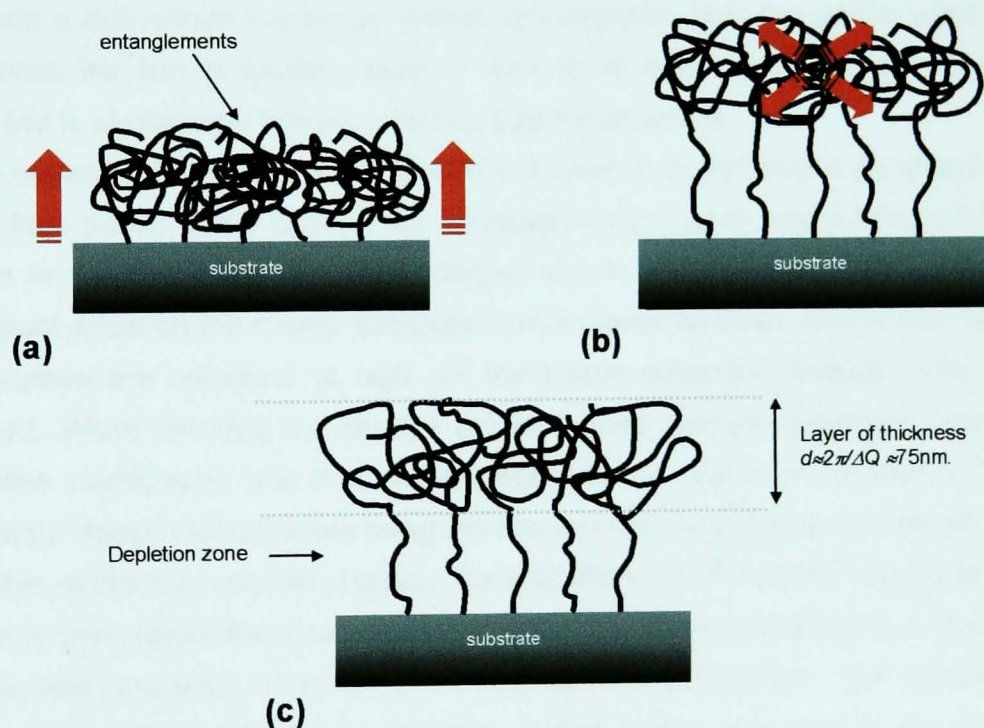


Fig. 6.7. Schematic diagram showing the expeculative explanation of the 'depletion zone' structure obtained from the data analysis (using slab-fit) of the swollen PDEAMA brushes. (a) Represents the initial stage of swelling occurring at the substrate, where the entanglements are pushed away from the substrate. (b) The entanglements away from the substrate continue swelling becoming tighter till the constraints imposed by the system geometry stop their movement. (c) Shows the final long-lived metastable state reached by the system, where a well defined layer is formed and corresponds to the peaks observed in the volume fraction-depth profiles (Fig. 6.5) in the region away from the surface.

No reports of neutron reflectometry on PDEAMA brushes created by ATRP have been found in the literature. Neutron reflectometry measurements performed in a block copolymer poly (2-(dimethylamino) ethyl methacrylate-*block*-methyl (methacrylate) (PDEAMA-*b*-MAA) 'grafted to' a silicon surface were reported by An et al.¹⁰ By using the 'grafted to approach' the resulting brush generally leads to low grafting density¹¹ and thus the DEAMA-*b*-MAA experiments should not be expected to reproduce our results. In fact such copolymer brush presents a monotonic decline in the brush volume fraction-depth profiles.¹⁰

An interesting consideration to our model would be that swelling-deswelling cycles could lead to disentanglements. Such cycles should be based on very long timescales to make the relaxation of disentanglements take place. We attempted to look at the hysteresis in the data at low and high pH values, but possibly due to the timescale employed, we did not get reliable results.

A different explanation for the profiles obtained in Fig. 6.5 in acidic conditions relates to the substrate affecting the counterion distribution within the brush. Previous reflectivity studies of the counterion density in films (not brushes) of a weak polyacid (poly[5-(2-trifluoromethyl-1,1,1-trifluoro-2-hydroxypropyl)-2-norbornene], PNBHFA)⁶ revealed a nonuniform counterion profile with depletion near the silicon substrate and when the film is swollen. Such a nonuniform distribution of counterions is attributed to electrostatic behaviour induced by the substrate.

In the present case of polybase brushes the counterion depletion that we observe is away from the substrate causing the entangled brush region that is schematically shown in Fig. 6.7. The negatively charged silicon substrate could then have a significant effect on the charge distribution within these brushes. In this way, when the brushes are collapsed at high pH the silicon substrate remains negatively charged. When lowering the pH the grafted chains become positively charged (negative counterions) and thus are extended due to coulombic repulsions. The negatively charged silicon drives away the counterions and at the same time attracts a fraction of the fixed positive charges. The final state (pH 4 and 3 for the 27nm and 13 nm brushes respectively) is a neutral surface, due to the condensation of positive charge, and counterion depletion at the polymer/solution interface. The counterion cloud screens the fixed charges and thus inhibits further stretching of the chains crating a layer of well-defined thickness (~75nm). A schematic diagram of the proposed explanation is shown in Fig. 6.8

Deeper theoretical considerations should take into account the different dielectric constants of the various layers present in our system. Such differences in dielectric constants are not considered here.

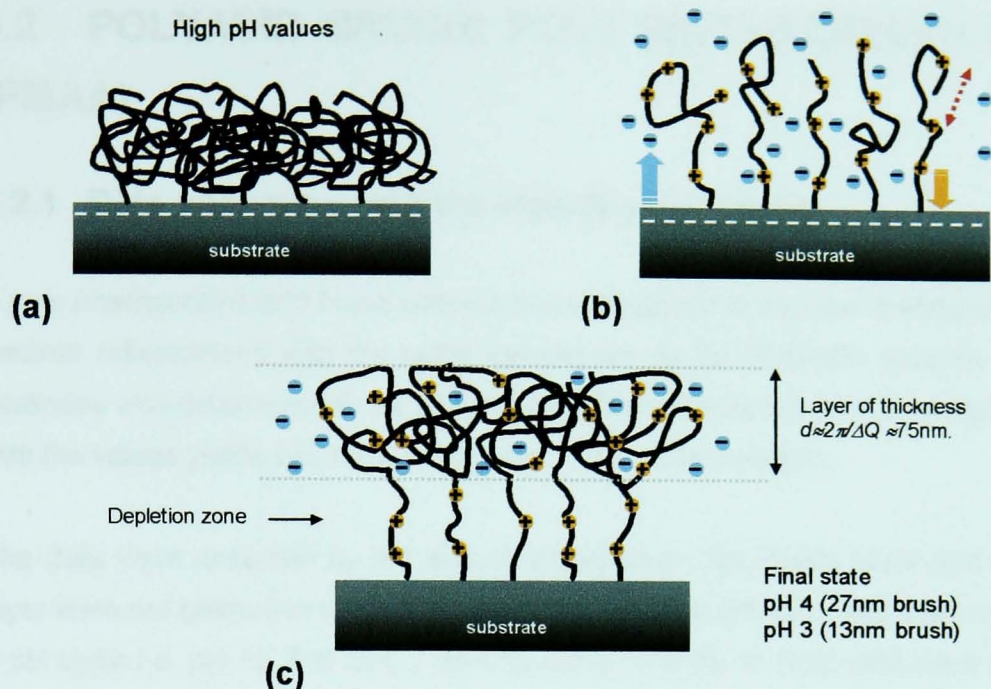


Fig. 6.8. Schematic diagram showing the explanation of the 'depletion zone' structure obtained from the data analysis (using slab-fit) of the swollen PDEAMA brushes. This second explanation is based on substrate effects. (a) At high pH the brush is collapsed and the substrate is negatively charged (white dashed line). (b) At lower pH values the chains are positively charged $+$ (negatively charged counterions $-$). The substrate drives away counterions into the outer region of the brush (blue arrow). The grafted chains are stretched due to coulombic repulsions between their positively charged groups (red arrow). The fixed positive ions close to the surface are attracted by it (orange arrow). (c) Shows the final state reached by the system (pH 4 and 3 for the 27nm and 13 nm brushes respectively). The substrate is rendered neutral. A well-defined layer (75nm thickness) is formed and corresponds to the peaks observed in the volume fraction-depth profiles (Fig. 6.5) in the region away from the surface.

A third explanation might perhaps be related to the non-monotonic volume fraction-depth profiles observed in the computer simulations of von Goeler and Muthukumar, who observed an increase in concentration near the extremity of the brush.¹² Essentially, the dense brush is swollen by electrostatic repulsion acting all around it. At the extremity of the brush, the driving force for swelling only comes from within the brush because, at the edge, half of the repelling components are missing thus the system will have a lower self-repulsion energy. Lower self-repulsion away from the surface means less stretching force and therefore a denser brush at the ends. If such an explanation is responsible for the observed density profiles, the effect is much stronger here than in the simulations. It would certainly be necessary to include counterions explicitly in any future simulations, which has not been the case in the work referred to here.

Brushes synthesised by ATRP are likely to be osmotic brushes where the counterions are located within the brush and cause it to swell by their gain in entropy on swelling (osmotic swelling).¹³ However, the volume fraction profiles that we obtain from the PDEAMA brushes are not expected from any of the present theories of polyelectrolyte brushes.

6.2 POLYACID BRUSH: POLY (METHACRYLIC) ACID (PMAA)

6.2.1 Data analysis using the slab-fit programme.

A poly (methacrylic) acid brush was measured in aqueous solution at various pH via neutron reflectometry with the same sample cell as for PDEAMA brushes. Its dry thickness was determined to be 20 nm by neutron reflectometry, in good agreement with the values yielded by ellipsometry and X-ray measurements.

The data were analyzed by the slab-fit programme (the silicon oxide and initiator layer were not present in these fits). We considered the PMAA brush data regarding a pH cycle i.e. pH 10, 5.8, 3.4, 7 and 10 run 2. The fits to such data were of good quality and the values of normalized χ^2 were $\chi^2 \leq 2$.

Typical data and fits for the PMAA brush at various pH are shown in Fig. 6.9. Fig. 6.10 shows the corresponding volume fraction-depth profiles obtained from the fits presented in Fig. 6.9

From Fig. 6.10 we see again that all the profiles at 0Å depth depart from a brush volume fraction of $\phi_{brush}=0.74$ equivalent to the scattering length density of the silicon.

At the first run of pH =10 the brush is swollen; when lowering the pH (upon addition of HCl) it remains swollen even at pH 5.8. At that value of pH is where the PMAA in bulk solution has its neutralization point, as we have shown in *Chapter 5*. However, the profile at pH 5.8 appears to be swollen to the same degree as that at pH 10 but with a shape of a 'depletion zone' conformation.

When the pH is decreased to pH 3.4 the brush is collapsed by approximately 50% with respect to the swollen state. In such a collapsed state (pH 3.4) the maximum brush volume fraction is at 0Å depth: $\phi_{brush}=0.74$. At larger depths away from the surface the brush volume fraction-depth profile falls continuously suggesting a significant fraction of water in the collapsed state of the PMAA brush. For instance at 100Å depth the brush volume fraction is $\phi_{brush}(y=100 \text{ \AA})\sim 0.6$, implying 40% of water content (Fig. 6.10, pH=3.4 profile).

As the solution is driven back to basic conditions the swelling becomes observable at pH 7. At such a value of pH the degree of swelling presents no significant difference to that observed for pH 10 run 2 (~800Å). The volume fraction-depth

profiles (Fig. 6.10) illustrate the swelling behavior of the polyacid brush in a pH cycle where hysteresis seems to be present.

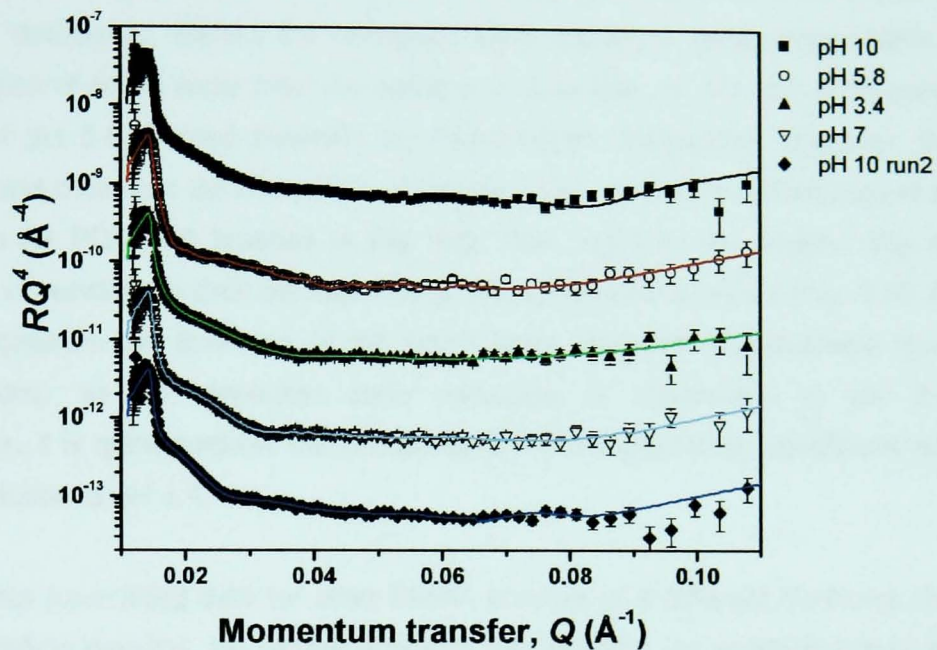


Fig. 6.9 Neutron reflectometry data and fits for a ~20nm PMAA brush as a function of pH. The data are shown in the Porod form $RQ^4(Q)$ where Q is the neutron momentum transfer. For clarity of viewing the data are shifted vertically from each other by a factor of ten. The values of normalized χ^2 were 1.1, 2, 1.4, 1.8 and 1.9 for pH values of 10, 5.8, 3.4, 7 and 10 run 2.

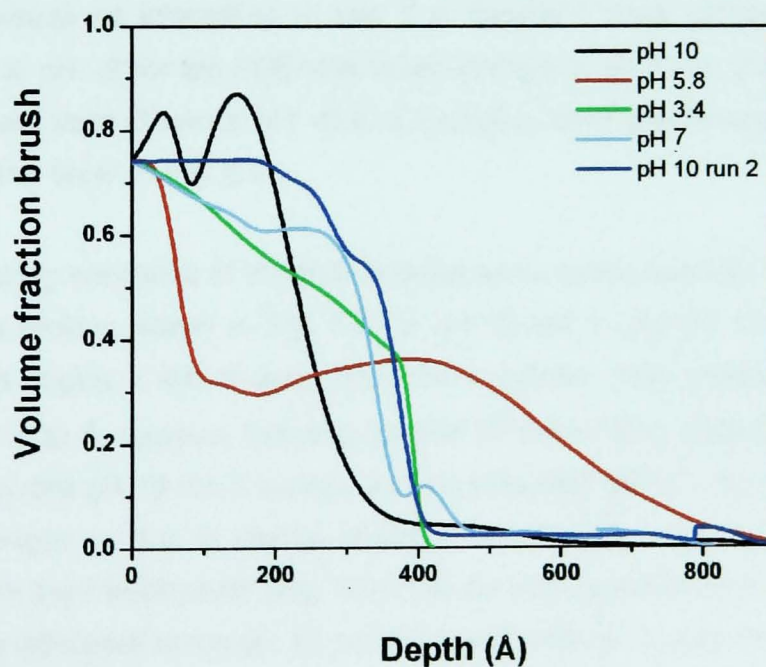


Fig. 6.10 Volume fraction-depth profile for the PMAA brush (~20nm dry thickness) as a function of pH as obtained from the NR data and fits shown in Fig.6.8. The mass conservation routine is flexible within 10%.

With regards to the shape of brush profile exhibited at pH 5.8 (Fig. 6.9) we can say that NR data were thoroughly fitted and the 'depletion zone' profile corresponded to the best fit. We make the conjecture that at pH 5.8 the PMAA brush is in overall swollen but the polyelectrolyte layer starts shrinking more and more as the ionic strength is decreased. Before the collapsed state occurs, a conformation with a defined region of brush away from the surface is observed, i.e. the 'depletion zone' structure at pH 5.8, formed basically by hydrophobic interactions. However, the maximum and minimum density points of the depletion are not as differentiated as those seen for PDEAMA brushes in Fig. 6.5. That might be the reason why no fringes are observable in their corresponding reflectivity data at pH 5.8 (Fig. 6.8). As the pH decreases the shrinking of the brush layer becomes progressively more homogeneous, so no 'depletion zone' structure is observable at pH 3.4. Furthermore, it is quite possible that the brush is in thermodynamic equilibrium with the bulk solution at pH 3.4.

As we do not have fitted data for other PMAA brushes of a different thickness (i.e. different grafting density), we cannot evaluate appropriately the swelling and brush profile features of the PMAA brush obtained here (as well as the pK_a value). Nevertheless, we venture ourselves to establish a similarity between the results yielded by the polybase brushes and this of the polyacid brush. It might occur that the 'depletion zone' structure takes place at the pK of the brush, which we observed to be at pH between 3 and 4 for the PDEAMA brush and at $pH \leq 5.8$ for the PMAA brush. It would be interesting to see if a 'depletion zone' profile would still be displayed at $pH \sim 2$ for the PDEAMA brush in Fig.6.5. Similarly, if at $pH \sim 4$ (before the collapsed state shown at $pH = 3.4$) a 'depletion zone' profile would be displayed for the PMAA brush in Fig. 6.9.

In the swelling behaviour of the PMAA brush some hysteresis was found in the pH cycle. The profiles shown in Fig. 6.9 for pH 10 run 1 and pH 10 run 2 are very different at depths $\leq 400 \text{ \AA}$ away from the substrate. Both profiles expand up to depths of $\sim 800 \text{ \AA}$, however this may be due to some fitting artifacts. Nevertheless we can say that pH 10 run 2 yielded a more collapsed conformation than pH 10 run 1, which might be due to charge shielding effects. The sharp swelling transition observed in the PMAA brush (Fig. 6.9) may be very sensitive to the exact value of pH; so the difference in the pH 10 profiles (run 1 and run 2) may actually be due to them falling on either side of the transition. Hysteresis is thus likely to be due to a difference in ionic concentration between the first and second pH cycle.

Other PMAA brushes of different grafting densities exposed to pH cycles should be able to reproduce such a result.

REFERENCES

- (1) Ryan, A. J.; Crook, C. J.; Howse, J. R.; Topham, P.; Geoghegan, M.; Martin, S. J.; Parnell, A. J.; Ruiz-Perez, L.; Jones, R. A. L. *J. Macromol. Sci. B:Phys* **2005**, *44*, 1103-1121.
- (2) Robert, C. P.; Casella, G. *Monte Carlo statistical methods*; Springer-Verlag: New York, 2004.
- (3) Ryan, A. J.; Crook, C. J.; Howse, J. R.; Topham, P.; Jones, R. A. L.; Geoghegan, M.; Parnell, A. J.; Ruiz-Perez, L.; Martin, S. J.; Cadby, A.; Webster, J. R. P.; Gleeson, A. J.; Bras, W. *Faraday Discuss.* **2005**, *128*, 55-74.
- (4) Jones, R. A. L.; Norton, L. J.; Shull, K. R.; Kramer, E. J.; Felcher, G. P.; Karim, A.; Fetters, L. J. *Macromolecules* **1992**, *25*, 2359-2368.
- (5) Tran, Y.; Auroy, P.; Lee, L. T. *Macromolecules* **1999**, *32*, 8952-8964.
- (6) Prabhu, V. M.; Vogt, B. D.; Wu, W.; Douglas, J. F.; Lin, E. K.; Satija, S. K.; Goldfarb, D. L.; Ito, H. *Langmuir* **2005**, *21*, 6647-6651.
- (7) Amalvy, J. I.; Wanless, E. J.; Li, Y.; Michailidou, V.; Armes, S. P.; Duccini, Y. *Langmuir* **2004**, *20*, 8992-8999.
- (8) Butun, V.; Armes, S. P.; Billingham, N. C. *Polymer* **2001**, *42*, 5993-6008.
- (9) Israels, R.; Leermakers, F. A. M.; Fleer, G. J. *Macromolecules* **1994**, *27*, 3087-3093.
- (10) An, S. W.; Thirtle, P. N.; Thomas, R. K.; Baines, F. L.; Billingham, N. C.; Armes, S. P.; Penfold, J. *Macromolecules* **1999**, *32*, 2731-2738.
- (11) Kopf, A.; Baschnagel, J.; Wittmer, J.; Binder, K. *Macromolecules* **1996**, *29*, 1433-1441.
- (12) Goeler, F. v.; Muthukumar, M. *Macromolecules* **1995**, *28*, 6608-6617.
- (13) Pincus, P. *Macromolecules* **1991**, *24*, 2912-2919.

Chapter 7

Poly (methacrylic) acid network /brush interactions as a function of pH

7.1 INTRODUCTION

The aim of the preliminary measurements presented in this chapter is to show how the interface between a polyelectrolyte network and a grafted polyelectrolyte layer (brush) in an aqueous environment varies upon changes in the pH.

A comprehensive understanding of the swelling behaviour of poly(methacrylic) acid in bulk solution has been achieved (*Chapter 5*). In addition, we have studied the swelling behavior of polyelectrolyte (polybase and polyacid) brushes (*Chapter 6*). With such accomplishments, the ultimate goal of the project presented here is to create reversible adhesion of the polyelectrolyte network to the inorganic substrate (polyelectrolyte brush). Such a goal will be considered a success once the adhesion of the charged network onto the polyelectrolyte grafted layer, when the solvent deteriorates, is characterized in a well-controlled and reproducible way. Fig. 7.1 shows a schematic diagram of how adhesion could be achieved in a system formed by a PMAA network in contact with a PMAA brush upon changes in pH

Studies regarding switchable adhesion at polymer/polymer and polymer/solid interfaces are widely found in the literature as they are of great importance for numerous applications, from microelectronics to the aircraft industry.¹ The current situation concerning solid-elastomer adhesion has been well summarized by

Brown.^{2,3} For instance, the Johnson Kendall and Roberts (JKR) technique⁴ has been used to examine the effects of different surface treatments of poly(dimethylsiloxane) (PDMS) on adhesion^{5,6} as well as to examine the effect of tethered chains on adhesion.^{2,3,7} Such a technique measures well defined contact areas at low rates of deformation. Contact angle measurements have also proven to be a powerful means of examining the wetting behaviour of switchable polymer films.⁸⁻¹⁰ JKR and contact angle are well-understood methods widely used in different types of systems with the purpose of probing adhesion. However, 'traditional' adhesion tests such as these are limited for measuring the contact area between gel and brush when immersed in solution.

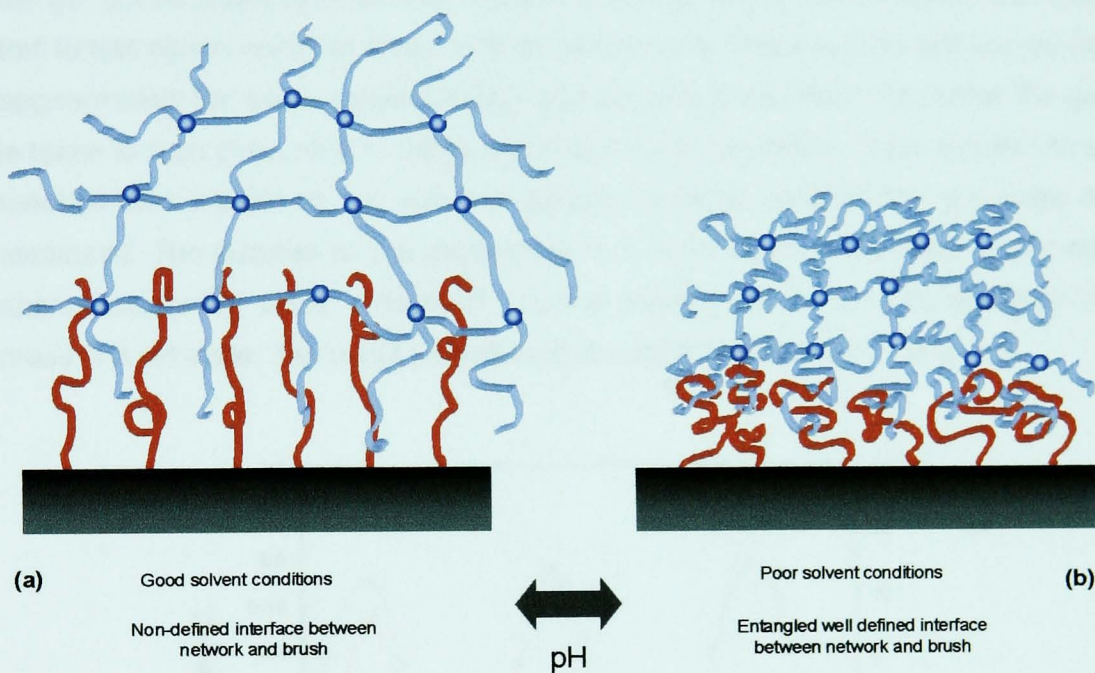


Fig. 7.1 Schematic diagram showing the conformational behaviour of a system formed by a poly (methacrylic) acid network (blue) in contact with a poly (methacrylic) acid brush (red) in an aqueous environment as a function of pH. In (a) we show how, in good solvent conditions, both network and brush will expand maximising their contact with the solvent. An interface between them is not well defined. (b) Shows how in poor solvent conditions the brush and network will collapse together forming an entangled interface. Such system should be reversible. The solid blue circles show the crosslink points.

We introduce and test here a new technique as a good means to measure interactions between polymer networks and brushes when immersed in aqueous solution. An important aspect offered by this technique is that measurements are performed *in situ*. The preliminary results presented constitute an initial stage from where the ultimate goal of adhesion can be achieved.

The chapter introduces first the preliminary results yielded by the system PMAA gel and blank silicon. Such an arrangement serves as a reference for the system formed by PMAA gel and grafted PMAA layer (brush) onto blank silicon. A section regarding future directions for these measurements follows the preliminary results.

7.2 PRELIMINARY CONTACT AREA MEASUREMENTS

As described in *Chapter 4. Section 3.3.1* the gel employed for the measurements has an average crosslink density of one crosslinker every 60 units of PMAA. Since the gel will be exposed to several extreme changes of pH, we performed a simple test to test conservation of mass. In this test the gel is driven to high and low pH (at approximately the same values for high and low pH) three times. Each time the gel is taken to high (low) pH it is left to equilibrate (by pH stability). Once equilibrium is reached and the pH of the external solution remains constant the gel mass is measured. The purpose of this experiment is to verify that the gel takes in and out approximately the same amount of external solvent i.e. there is conservation of mass in a pH cycle. The result yielded by this experiment is shown in Fig. 7.2.

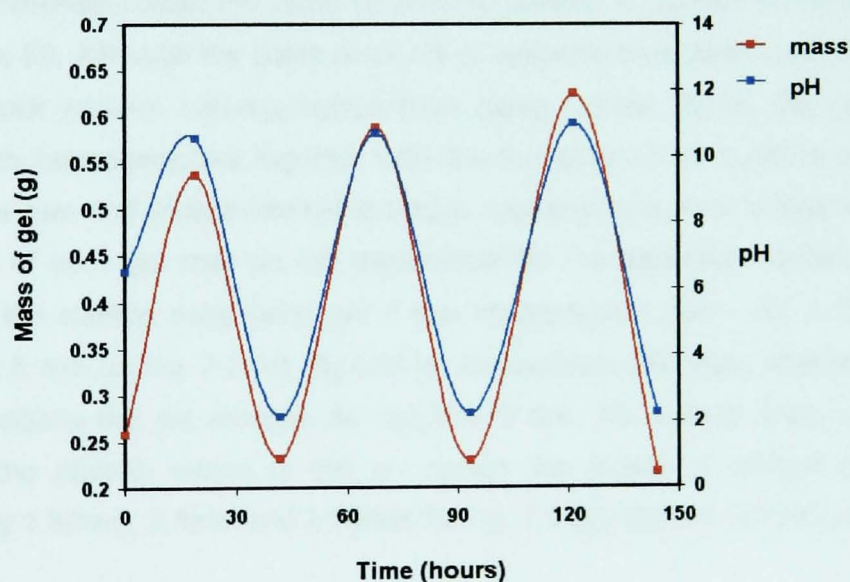


Fig. 7.2 Mass variation of a poly(methacrylic) acid gel ($\rho_c^{gel} \sim 60$, dry thickness 0.15g) in a pH cycle. The high and low pH values are $10.5 < \text{pH} < 11$ and $\text{pH} \sim 2.2$ respectively. Mass were measured when equilibrium was reached between the gel and the external solution.

From Fig. 7.2 we can see that the absorption and expulsion of water by the gel follows rapidly the change in pH. Before starting the pH cycle, the gel is left to swell in water (pH 7) in order to remove the free chains that have not been properly

crosslinked in the gelation process. Neutral pH corresponds then to the first point in Fig.7.2

The gel masses at pH values of 10.5, 10.7 and 11 were of 0.53g, 0.58g and 0.62g respectively. With a dry thickness of 0.15 g the gel increases its volume by a factor of 3.5, 3.8 and 4 at pH 10.5, 10.7 and 11 respectively. Such a large change in mass for such small increments of pH in basic conditions indicates that the gel responds strongly to small variations in the degree of ionization of the reservoir. At low pH values of pH \sim 2.2 the mass was \sim 0.22 g. Because the same amount of solution is taken from the reservoir in each run (at high pHs) we can confirm that the system is reproducible. When driven to acidic conditions the amount of solvent that is expelled into the outer solution is also measured to be approximately the same. There is no loss of polymer in the gels when exposed to cyclic changes in pH.

7.2.1 Poly (methacrylic) acid network and silicon

Contact area measurements of a PMAA hemispherical gel (lens) and a clean silicon wafer (set-up described in *Chapter 4. Section 4.3.3*), upon changes in pH are shown in Fig. 7.3 (a), (b) and (c). Each plot shown in Fig. 7.3 corresponds to a different PMAA gel synthesised under the same conditions (*Chapter 4. Section 4.3.1*) to yield a gel of $\rho_c^{gel} \approx 60$. Although the same amounts of reagents have been used in each gel, this cannot prevent heterogeneities from being formed during the gelation process. Such heterogeneities together with the formation of air bubbles provide gels with their own and unique internal structure. Consequently, this 'uniqueness' in the structure of each gel may be the responsible for the dissimilar contact areas observed at the starting point (after pH 7 has equilibrated to pH \sim 4): 1.19 mm, 1.7mm and 1.5 mm for Fig. 7.3 (a), (b) and (c) respectively. Likewise, after swelling in basic conditions the gel reaches its equilibrium (i.e. the contact area remains constant in the plateau region of the pH curve); the length of contact area is approximately 1.37mm, 2.1mm and 3.25mm for Fig. 7.3 (a), (b) and (c) respectively.

In the present measurements we will focus on the timescale employed for the gels to reach swelling equilibria rather than on the precise values of contact area themselves. Since the purpose of these tests is to show interactions occurring between gel and brush (Fig. 7.1) attention will be centred in the case of going from low pH (pH \sim 2) to high pH (pH \geq 10.5).

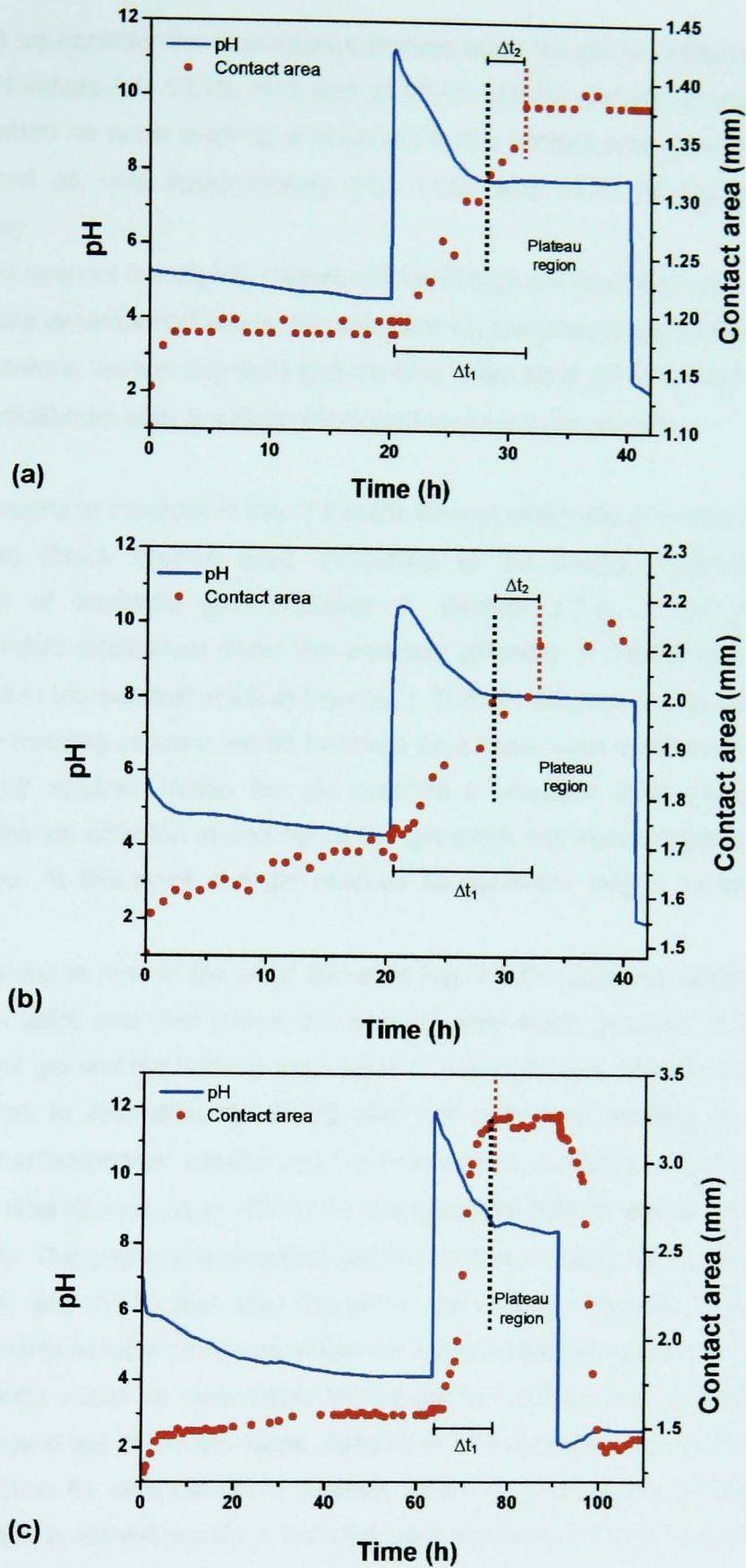


Fig. 7.3 Contact area measurements upon changes in pH for a poly(methacrylic) acid gel in contact with blank silicon. The plots (a), (b) and (c) are for different PMAA gels prepared under identical conditions ($\rho_c^{gel} \sim 60$). Each experiment starts with the gel at pH 7 and left to equilibrate. After a change in pH equilibrium is reached when the measured pH remains constant ($\Delta\mu_i = \Delta\mu_i^*$). The equilibrium point in the pH curve is presented as a black dashed line, which is followed by a plateau region. A red dashed line marks the point at which the contact area stops increasing. Δt_1 is the time taken for the contact area to become constant when the pH is increased. Δt_2 is the time gap between the equilibrium pH and that where the growing of contact area stops.

In Fig. 7.3 we consider the time interval starting when the pH is suddenly increased to high pH values (pH 11.25, 10.5 and 11.85 for (a), (b) and (c) respectively) and finishing when no more swelling is observed in the contact area (dashed red line). This interval Δt_1 was approximately 11h, 11.5h and 11.7h for (a), (b) and (c) respectively.

Taking into account the slightly diverse values of high pH reached in (a), (b) and (c) and possible experimental errors, the values of Δt_1 are in good agreement with each other. Therefore, we can conclude that the time taken for a gel in contact with silicon to reach equilibrium after a sudden increment in pH is $11\text{h} < \Delta t_1 < 12\text{h}$.

Another feature to consider in Fig. 7.3 is the time at which the pH in the reservoir is equilibrated (black dashed line). According to the theory regarding swelling equilibrium of ionisable gels (*Chapter 3. Section 3.3.3*), a gel reaches its thermodynamic equilibrium when the chemical potential of mobile ions in the gel equals that in the external solution ($\Delta\mu_i = \Delta\mu_i^*$). The ion diffusion in and out of the gel during the swelling process would translate as a continuous variation in the pH of the external solution. When the pH reaches a constant value (followed by a plateau), the ion diffusion in and out of the gel stops and hence equilibrium should be reached. At this point, the gel reaches its maximum degree of swelling (eq. (3.52)).

It is interesting to note in the plots shown in Fig. 7.3 the delay Δt_2 between the pH equilibrium point and that where the contact area stops growing. If interactions between the gel and the surface were small or not significant, one would expect the contact area to stop growing shortly after the maximum swelling of the gel is reached (thermodynamic equilibrium). For that reason Δt_2 ideally should be zero or a very small time interval. Δt_2 is $\sim 0\text{h}$ for (c) and approximately 2h and 3h for (a) and (b) respectively. The possible explanation we find for these values of Δt_2 (2h and 3h for Fig. 7.3 (a) and (b)) is that after the pH in the external reservoir is equilibrated rearrangements of local structures within the network are still occurring. In this way, charge effects would be responsible for the gel to continue unfolding after the ion diffusion in and out of the gel stops. Tanaka et al first studied the dynamics of the relaxation time for gels placed in solvents based in Darcy's law of flow.^{11,12} The Darcy's law is a derived equation that describes the flow of a fluid through a porous medium (gel). However, a precise mathematical formulation for a gel swelling dynamics (i.e. what limits the rate of swelling of a gel in a macroscopic system) has not been done until recently by Yamaue et al.^{13,14}

We consider the time taken for the contact area to stop decreasing when the system is driven back to acidic conditions as Δt_3 . From Fig. 7.3(c) we see that $\Delta t_3 \sim 11$ h.

7.2.2 Poly (methacrylic) acid network and brush.

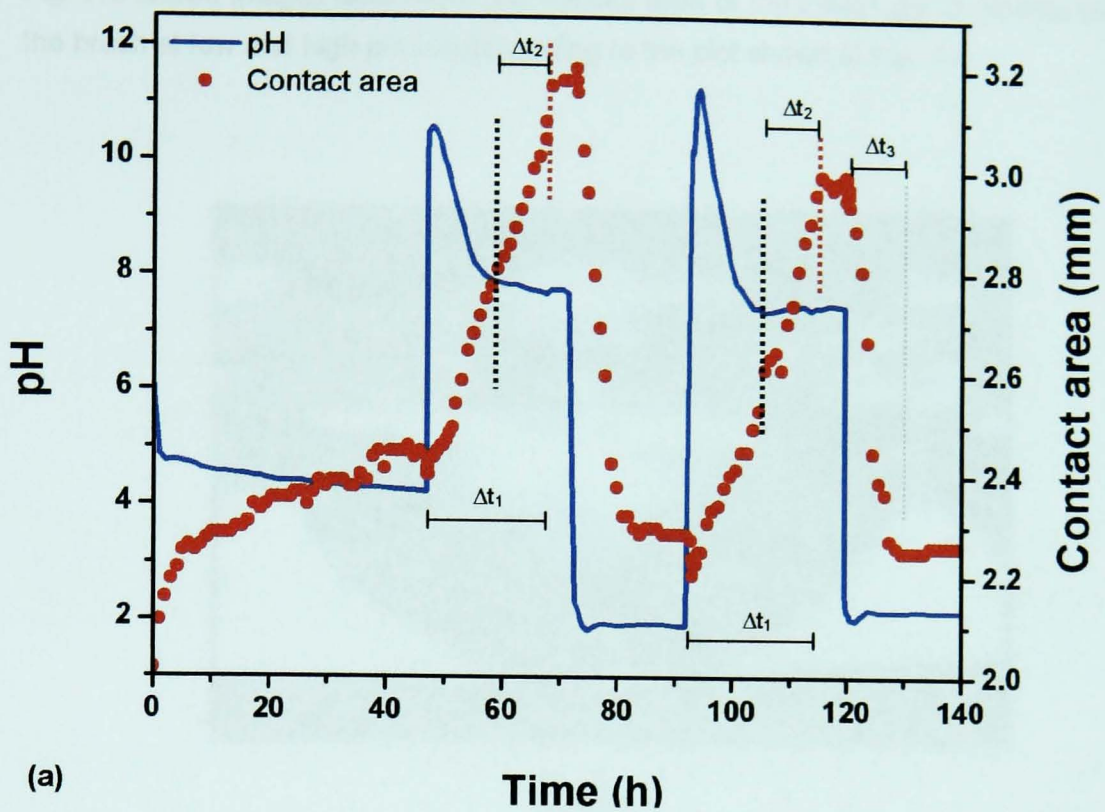
Contact area measurements of a hemispherical PMAA gel (synthesised at identical conditions to those exposed in the previous section) in contact with a PMAA brush were performed in a pH cycle and shown in Fig.7.4. The PMAA brush had a dry thickness of circa 14nm.

The experimental set-up, initial pH of the experiment and *modus operandi* were the same as those employed for contact area measurements of the gel in contact with blank silicon. The gels employed were able to withstand two pH cycles, however when driven to high pH for the third time internal cracks were observed. Hence the mass uptake was of three times.

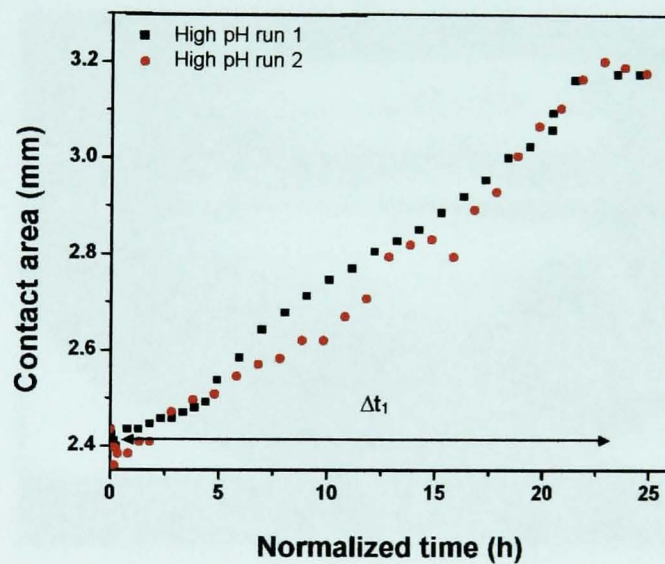
From Fig. 7.4 (a) the time interval Δt_1 is approximately 21.4 h and 22.8 h for high pH run 1 (pH=10.5) and run 2 (pH~11) respectively. The similar time taken for the gel to fully expand for the first and second time in the pH cycle is visibly shown in Fig. 7.4 (b). Such a finding suggests that the behaviour of a gel left to equilibrate in water (final pH ~4) and suddenly driven to basic conditions is equivalent, with respect to the equilibration time, to that from a gel at pH ~2 taken to the same basic conditions. In other words, it seems that when a polyacid gel and brush are left to equilibrate in water at pH~7 they interpenetrate each other.

It is also worth noting the time taken for the contact area to stop decreasing when the system is driven back to acidic conditions. When the gel contact area is at its maximum length (high pH, gel fully swollen), the time taken to reach its minimum length (low pH, gel contracted) Δt_3 is approximately 11.3h and 10.4h for pH 2 run 1 and run 2 respectively. These results confirm that the gel behaves in a cyclic manner when expelling solvent in a pH cycle.

We obtained $\Delta t_2 \sim 8.5$ h and 10h for high pH run 1 and run 2 respectively. We turn to an explanation for the observed values of Δt_i ($i=1,2,3$) in the next subsection.



(a)



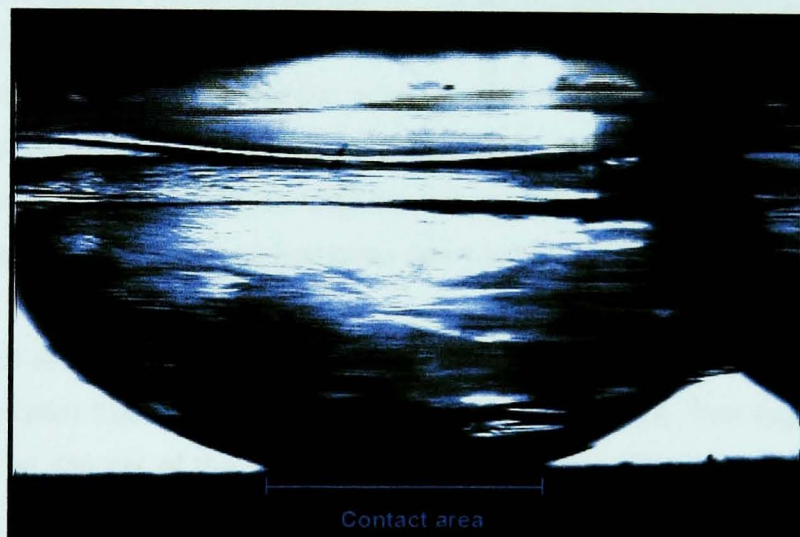
(b)

Fig. 7.4 Contact area measurements upon changes in pH for a poly (methacrylic) acid gel ($\rho_c^{gel} \sim 60$) in contact with a poly(methacrylic) acid brush (dry thickness 14nm). (a) The pH cycle starts with the gel in water and left to equilibrate. Then, the pH is taken to values of pH 10.5, 2, 11.2 and 2. Following a change in pH, equilibrium is reached when the measured pH remains constant. After the pH has been increased the equilibrium point is presented as a black dashed line, which is followed by a plateau region. A red dashed line marks the point at which the contact area stops increasing. Δt_1 is the time taken for the contact area to become constant when the pH is increased. Δt_2 is the time gap between the equilibrium pH and that where the growing of contact area stops. Δt_3 is the time taken for the contact area to shrink and become constant when the pH is suddenly decreased. (b) Shows in detail the contact area behaviour when high pH is reached for the first and second time in plot (a). In order to show with more clarity the symmetry of the system, the time scale of high pH runs and contact area of the 'high pH run 2' have been normalized. With this approach both plots depart from the same origin.

Fig. 7.5 shows images taken from the contact area of the PMAA gel in contact with the brush at low and high pH corresponding to the plot shown in Fig. 7.4.



pH =2



pH ~11

Fig. 7.5 Photographs taken from a PMAA gel ($\rho_c^{gel} \sim 60$) in contact with a PMAA brush (dry thickness 14nm) at pH 2 and ~11. From both photographs it can be seen how the contact area between the gel and the brush is visibly increased at pH~11. Both pictures have been taken with the system in equilibrium. The time interval between the first and second picture is of $\Delta t_1 \sim 22.8h$

7.2.2.1 Comparison with measurements performed on blank silicon

In order to have a clearer image of the different Δt_i ($i=1,2,3$) obtained for the gel in contact with blank silicon and brush such values are presented in Table 7.1.

	$\Delta t_1(\text{h})$	$\Delta t_2(\text{h})$	$\Delta t_3(\text{h})$
PMAA gel /blank silicon	$11 < \Delta t_1 < 12$	$0 \leq \Delta t_2 \leq 3$	11
PMAA gel /brush	$21 < \Delta t_1 < 23$	$8 < \Delta t_2 \leq 10$	$10.4 \leq \Delta t_3 < 11.4$

Table 7.1. Table showing the values of Δt_1 , Δt_2 and Δt_3 obtained from contact area measurements on the systems: PMAA gel in contact with blank silicon and PMAA gel in contact with PMAA brush upon changes in pH. Δt_1 , Δt_2 and Δt_3 for PMAA gel /blank silicon are obtained from Fig. 7.3. Δt_1 , Δt_2 and Δt_3 for PMAA gel/brush are obtained from Fig. 7.4

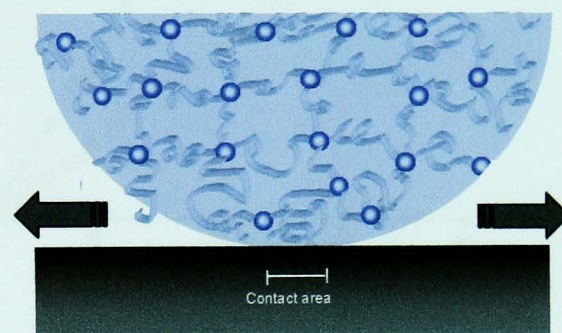
From Table 7.1 we see that Δt_1 is nearly identical to Δt_3 for a PMAA gel /blank silicon system. This means that when the pH is increased, the contact area of the gel in contact with the surface reaches equilibrium within the same timescale than in the situation where the pH is lowered. In other words, the time taken for the gel to fully swell is equivalent to that taken for the gel to contract. This is the typical behaviour of an isolated gel. Hence, the interactions between gel and blank silicon can be considered negligible. In the same way the values obtained for Δt_2 are small (the possible explanation of why $\Delta t_2 \neq 0$ has been given in *section 7.2.1*).

In the case of the PMAA gel in contact with the brush, we can see that Δt_1 is approximately twice than that obtained for PMAA gel and silicon. This suggests that when increasing the pH of the solution to an average pH ~ 11 , the presence of a polyacid layer attached to the silicon retards Δt_1 by a factor of two when compared to blank silicon. A schematic diagram demonstrating such an effect is shown in Fig.7.6.

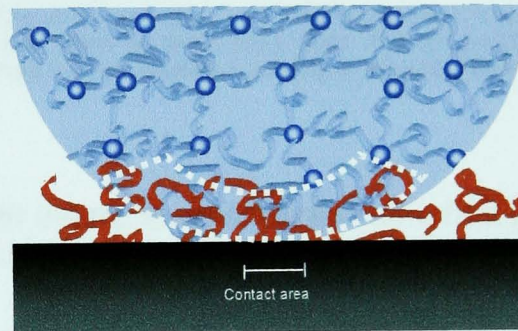
The values obtained for Δt_2 , $8\text{h} < \Delta t_2 \leq 10\text{h}$ in the system PMAA gel/brush must also be considered. Δt_2 has been defined as the time gap between the equilibrium pH (ion diffusion in and out of the gel is stopped $\Rightarrow \Delta\mu_i = \Delta\mu_i^*$) and that where the growing of contact area stops. In the presence of a brush the contact area is not yet in equilibrium when $\Delta\mu_i = \Delta\mu_i^*$. Instead, when the reservoir is equilibrated in pH, the gel continues spreading over the brush for an average of ~ 9 hours. This suggests a time scale greater than that of an isolated gel or a gel in contact with a non-responsive surface ($0 \leq \Delta t_2 \leq 3$ for PMAA gel/blank silicon). The expansion of the

contact area over the brush surface is not just ruled by the kinetics of an isolated gel but also by the kinetics of swelling of the responsive brush.

These early results show interactions occurring at the interface between gel and brush. A possible reason for the weak interactions may be due to an electrostatic repulsion still remaining between the two components of the system (both brush and gels are made of polyacid chains). This would mean that the gel effectively slides over the brush, almost as if it were lubricated. However our experiments, which suggest a slight increase in adhesion, demonstrate that this cannot be the complete explanation for the observed behavior. Further experiments are being performed.



(a)



(b)

Fig. 7.6 Schematic diagram showing a hemispherical collapsed PMAA gel in contact with (a) blank silicon and (b) PMAA collapsed brush, swelling at high pH conditions. In (a), the non-responsive surface does not impede the contact area to grow, bearing $\Delta t_1 \sim 11h$. In (b), the interface (represented as a region limited by white dashed line) formed between the gel and grafted chains coiled together offers resistance to the expansion of the contact area, and as a result $\Delta t_1 \sim 22h$.

The growing processes of the contact area of the system gel/blank silicon when the pH is suddenly increased, obtained from Fig. 7.3 (a), (b) and (c), have been normalized with respect to their time scale and averaged. Similarly, for the system gel/brush, an average has been calculated from the plots presented in Fig. 7.4 (b)

(growing process of the contact area at high pH run 1 and 2). Both average curves summarize the results obtained to date and are shown in Fig. 7.7

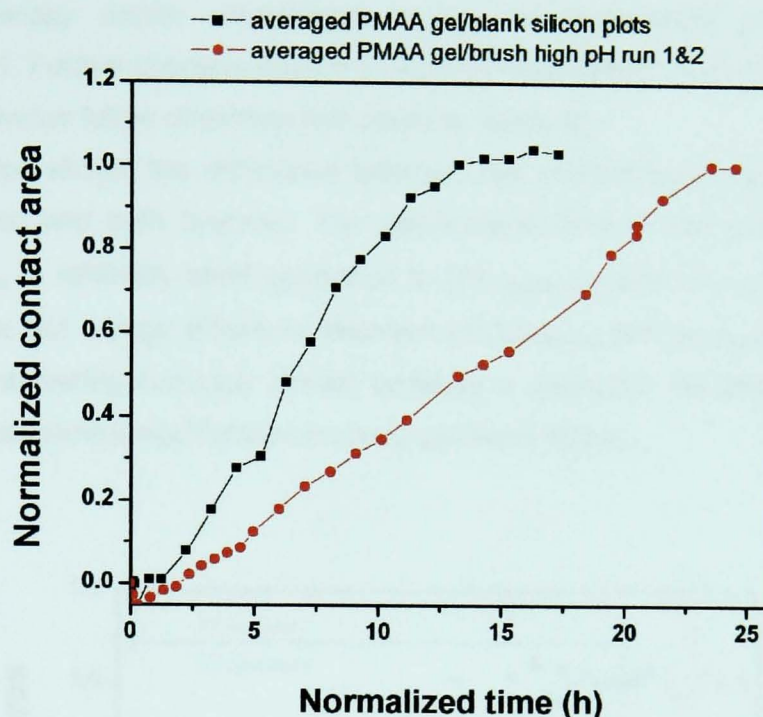


Fig. 7.7 Averaged contact area measurements of a PMAA gel in contact with a blank silicon (black) and a PMAA brush (red) when the system goes from acidic to basic conditions (time interval Δt_1). The averaged PMAA gel/blank silicon curve is taken from the plots presented in Fig. 7.3 (a), (b) and (c). The averaged curve for PMAA gel/brush is taken from Fig. 7.4. The time has been normalized in order to have both plots departing from same origin. The length of the contact area has been normalized yielding a dimensionless value.

7.2.2.2 Comparison with measurements performed with a gel of different crosslink density on a different brush

Further contact area measurements have been performed using a different gel and brush. A new PMAA gel (gel 2) has been synthesised to yield approximately one crosslink point every 85 units of PMAA, less crosslinked than the previous gel (gel 1). Crosslink density is related to gel hydrodynamics. The new brush is a PMAA brush (brush 2) of dry thickness $\sim 17\text{nm}$ (thicker than the previous brush (brush 1)). Measurements of the contact area of the new PMAA gel and brush in a pH cycle have been carried as in the previous section. Again, we focus on the case where the system in acidic conditions is suddenly driven to basic conditions employing a time Δt_1 to reach equilibrium. Fig. 7.8 shows the contact area measurements of PMAA gel 1/blank silicon, PMAA gel 1/brush 1 and PMAA gel 2/brush 2 in the case where their initial low pH is increased to pH values of approximately pH ~ 11 .

From Fig. 7.8 it can be seen that the value of Δt_1 obtained from the system PMAA gel 2/brush 2 is approximately 20 hours. $(\Delta t_1)_{\text{gel2/brush2}}$ is similar to $(\Delta t_1)_{\text{gel1/brush1}}$ with approximately 2 hours of difference. Such a difference might be due to the different grafting density and/or crosslinking density of brush2/gel2 with respect to brush1/gel1. Further characterisation is required to determine such matters; the next section provides future directions that could be followed.

Fig. 7.8 also shows the difference between the contact area measurements on blank silicon and both brushes. The equilibration time of the system gel/silicon $(\Delta t_1)_{\text{gel1/silicon}}$ is relatively short compared to $(\Delta t_1)_{\text{gel2/brush2}}$ and $(\Delta t_1)_{\text{gel1/brush1}}$. The fact that there is not a large difference between $(\Delta t_1)_{\text{gel1/silicon}}$ and $(\Delta t_1)_{\text{gel/brush}}$ (1 and 2) is not very interesting because almost certainly a gel/brush combination could be made to yield similar equilibration times to gel/blank silicon.

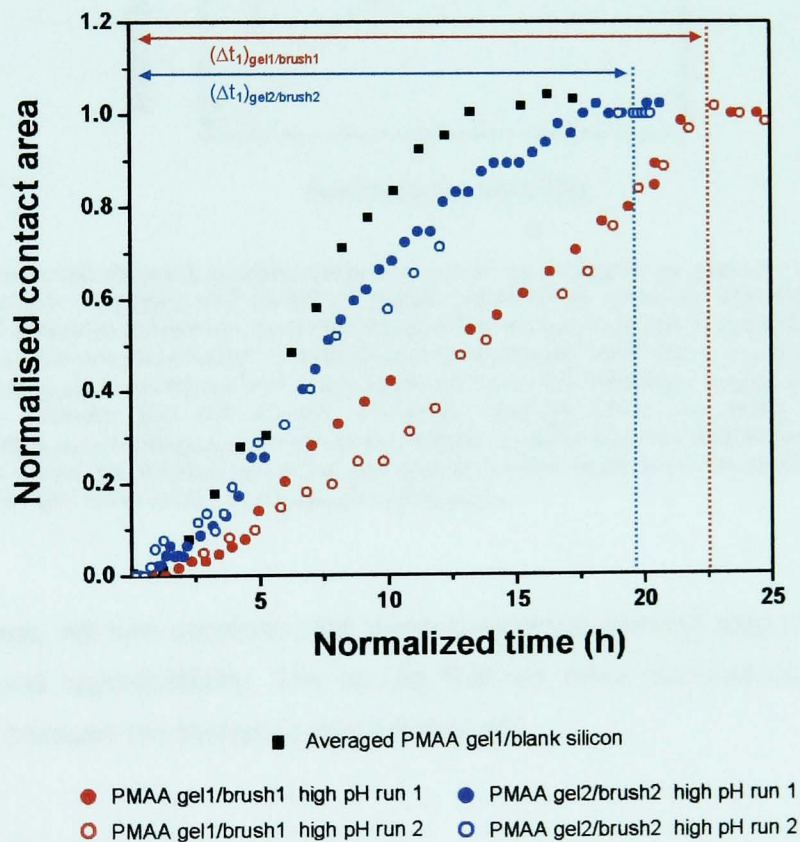


Fig. 7.8 Measurements of the contact area in the systems PMAA gel1 /blank silicon, PMAA gel1 /brush1 ($\rho_c^{gel} \sim 60$ and dry thickness of brush1 $\sim 14\text{nm}$) and PMAA gel 2/brush 2 ($\rho_c^{gel} \sim 85$ and dry thickness of brush 2 $\sim 17\text{nm}$) when the pH is increased. In PMAA gel 1/blank silicon, the average curve obtained from Fig. 7.7 is included. This curve serves as a reference for those obtained from gel and brush. In PMAA gel1/brush1 and PMAA gel 2/brush 2 the two runs at high pH have been plotted. The red and blue arrows represent the time interval Δt_1 yielded by PMAA gel 1/brush 1 and PMAA gel 2/brush 2 systems respectively.

One could speculate that the interactions (possible adhesion effect) between gel 2/brush 2 are weaker than those for gel 1/brush 1 since $(\Delta t_1)_{gel2/brush2} < (\Delta t_1)_{gel1/brush1}$. In this way, a shifting of the gel/brush contact area curves in the direction of (in the opposite direction of) the gel/blank silicon curve would render low (high) degrees of adhesion. It would be interesting to test different gel/brush systems to achieve minimum and maximum degrees of adhesion, reached when $(\Delta t_1)_{gel/brush} \approx (\Delta t_1)_{gel/silicon}$ and $(\Delta t_1)_{gel/brush} \gg (\Delta t_1)_{gel/silicon}$ respectively. (Fig.7.9)

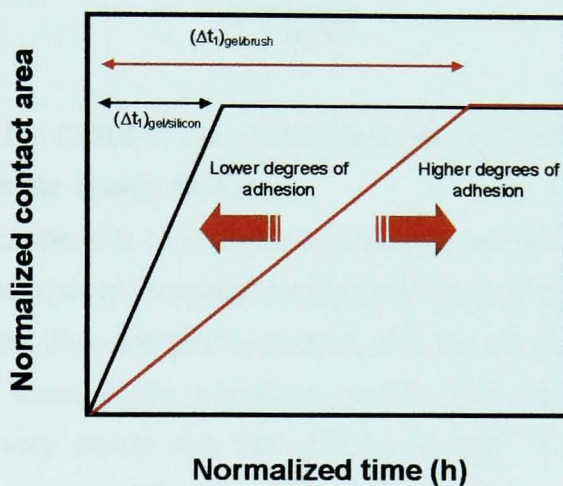


Fig. 7.9 Schematic diagram showing plots of normalized contact area against normalized time for a gel/brush (red plot) and gel/blank silicon (black plot) systems. The lower or greater degrees of adhesion between a gel and a brush would be given by the magnitude of $(\Delta t_1)_{gel/brush}$. A shifting of the red plot towards the black plot (towards left hand side), would render smaller values of $(\Delta t_1)_{gel/brush}$ and thus lower degrees of adhesion. The minimum degree of adhesion (no interaction between gel and brush) would be reached when the black and red plot overlap $\Rightarrow (\Delta t_1)_{gel/brush} \approx (\Delta t_1)_{gel/silicon}$. In the same manner, greater degrees of adhesion between gel and brush would be reached when the red plot is further apart from the black plot (moving towards the right hand side) $\Rightarrow (\Delta t_1)_{gel/brush} \gg (\Delta t_1)_{gel/silicon}$

Nonetheless, we can conclude that these preliminary contact area measurements offer a good reproducibility. The results that we have obtained so far are also important because the system is controlled *in situ*.

7.3 FUTURE DIRECTIONS

In this section, we provide a few routes that could be followed with the aim of achieving an improved characterisation of the interactions between polyacid gel and brush upon variations in pH.

In order to have a better understanding of the role that the gel (lens) play in the system gel/brush, they could be mechanically characterized via rheology measurements. Such measurements provide the elastic modulus of the network i.e. the shear modulus G (*Chapter 3. Section 3.3.3.1*) via analysis of the applied stress and resulting strain. Thus, gels in a range of pH could be measured. Knowing $G=G(pH)$, the fundamental JKR equation⁴ can be applied in order to calculate the interfacial adhesion energy γ as

$$\gamma = \frac{r^3 G}{6\pi R^2}, \quad (7.1)$$

where r and R are the radius of the contact area and gel respectively, which can be measured, and G is the elastic modulus.

A major practical problem is to understand how the adhesive energy γ varies with the surface concentration of “connector molecules” (grated chains), as very often, at high grafting density, the strength decreases. For simple grafted PDMS layers de Gennes predicted theoretically a grafting density limit after which the adhesion energy increases very slowly with the grafting density.¹⁵ Experimental studies of adhesion enhancement in PDMS elastomer in contact with PDMS layers as a function of surface grafting density have been performed.¹⁶ It would be interesting to accomplish the same thing in a PMAA gel/brush system. As exposed in the previous section, straightforward measurements of contact area of PMAA gel/brush systems using brushes of different σ at same ρ_c^{gel} could easily be performed. Once the optimum σ is found, other parameter that can be varied in order to achieve a stronger interface would be ρ_c^{gel} .

Contact angle measurements could be performed on the PMAA brushes. By adding drops of HCl or NaOH on the substrate surface the degree of hydrophobicity could be quantified. We have used blank silicon as the reference for the measurements performed on brushes. Other substrates could also be tested; for example, a silanated substrate should provide a more hydrophobic surface, which should be an interesting comparison.

As for PDEAMA and PMAA brushes (*Chapter 6*), neutron reflectometry measurements should provide details on the shape of the interface between gel and brush as a function of pH. In addition, it will provide *in situ* measurements of the kinetics and degree of interpenetration. Contrast matching must be provided in a PMAA gel/brush system. The simple case would involve a deuterated PMAA brush that can be achieved using deuterated monomer MAA during the synthesis process

(Chapter 4. Section 4.2.1.1). By placing the deuterated PMAA brush in contact with the PMAA network, the interpenetration between brush and network could be observed. Information such as the equilibration time Δt_1 of a PMAA gel/brush when the pH is changed is an essential parameter for such measurements. Indeed, such an experiment has been performed but unfortunately the Δt_1 timescale was not known at that stage. Knowing that the timescale taken for a PMAA gel/brush system to equilibrate is $\Delta t_1 \geq 20$ hours offers the possibility of acquire NR data at different stages of the swelling process as at the final swelling equilibrium.

We have performed measurements showing that there is a difference between the behaviour of PMAA gel/blank silicon and PMAA gel/brush systems, which may be due to adhesion. However, in practical terms this adhesion seems unlikely to be enough. In performing these experiments one would like to notice a bonding between substrate and gels, which we did not. It may well be that the neutralized PMAA is not hydrophobic enough to fully collapse. Although, for the reasons discussed in the present chapter, we believe we have observed an attractive interaction between the gel and the brush we might find better results using a different system. Candidate systems might include PDEAMA brushes and gels, or maybe even a mixed gel/brush system in which one component is a polyacid and the other a polybase. In this latter case an enhancement in the interactions between the polyacid and polybase components of the system should be observed. In any case, adhesion tests could be performed following the same method exposed in the present chapter.

REFERENCES

- (1) Creton, C.; Fabre, P.; Dillard, D. A.; Pocius, A. V. *Adhesion Science and Engineering. 'The mechanics of adhesion'*, Elsevier: Amsterdam, 2002; Vol. 535.
- (2) Brown, H. R. *Macromolecules* **1993**, *26*, 1666.
- (3) Brown, H. R. *Annu. Rev. Mater* **1991**, *21*, 463.
- (4) Johnson, K. L.; Kendall, K.; Roberts, A. D. *Proc. R. Soc. London A* **1971**, *324*, 301.
- (5) Deruelle, M.; Leger, L.; Tirrell, M. *Macromolecules* **1995**, *28*, 7419-7428.
- (6) Chaudhury, M. K.; Whitesides, G. M. *Langmuir* **1991**, *7*, 1013-1025.
- (7) Creton, C.; Brown, H. R.; Shull, K. *Macromolecules* **1994**, *27*, 3174-3183.
- (8) Minko, S.; Muller, M.; Motornov, M.; Nitschke, M.; Grundke, K.; Stamm, M. *J. Am. Chem. Soc.* **2003**, *125*, 3896-3900.
- (9) Sidorenko, A.; Minko, S.; Schenk-Meuser, K.; Duschner, H.; Stamm, M. *Langmuir* **1999**, *15*, 8349-8355.

- (10) Mansky, P.; Liu, Y.; Huang, E.; Russell, T. P.; Hawker, C. *Science* 1997, 275, 1458.
- (11) Tanaka, T. *Sci. Am* 1981, 244, 110-123.
- (12) Tanaka, T.; Fillmore, D. J. *J. Chem. Phys* 1979, 70, 1214-1218.
- (13) Yamaue, T.; Doi, M. *Phys. Rev. E* 2004, 69, 041402.
- (14) Yamaue, T.; Doi, M. *J. Chem. Phys* 2005, 122, 084703.
- (15) F. Brochard-Wyart; P. G. de Gennes; Leger, L.; Marciano, Y.; Raphael, E. *J. Phys. Chem* 1994, 98, 9405-9410.
- (16) T. Vilmin; Tardivat, C.; L. Leger; Brown, H.; Raphael, E. *Europhys. Lett.* 2004, 68, 543-549.

Chapter 8

Conclusions

8.1 SINGLE POLY (METHACRYLIC) ACID CHAINS IN SOLUTION.

A detailed study of the pH-induced conformational transition of poly(methacrylic) acid in aqueous solution using three fluorescence techniques (non-radiative energy transfer, fluorescence lifetime, and time-resolved anisotropy measurements), dynamic light scattering, and transmission electron microscopy has been performed. The first four techniques reveal the collapse transition to occur at a pH of between 5.7 and 5.8, in agreement with numerous earlier measurements.

Fluorescence lifetime measurements reveal three lifetimes for the hypercoiled PMAA, which we interpret as (three) different regions of solvent concentration within the polymer chain. Such a result suggests that the polymer expansion is progressive rather than cooperative. A progressive expansion means that different parts of the polymer chain swell differently; as the pH increases, the outermost parts of the chain would be expected to swell before the innermost regions. TEM and dynamic light scattering measured the size of the polymer chains, with the former yielding an absolute size, and the latter a hydrodynamic radius. For our particular samples, the chain is observed to expand in size by approximately a factor of two as it passes from acidic to basic solution.

The behaviour of PMAA in methanol (PMAA in methanol has negligible charge) is equivalent to its behaviour in aqueous solution at $\text{pH} > 5.8$ (pH of the conformational transition) when the coulombic repulsions between carboxylic groups are able to cause expansion of the chain.

8.2 POLY[(DIETHYLAMINO) ETHYL METHACRYLATE] (PDEAMA) AND POLY(METHACRYLIC)ACID (PMAA) BRUSHES

We have performed neutron reflectometry experiments to demonstrate the pH-induced conformational transition of PDEAEMA and PMAA brushes. For the PDEAMA brushes the experiments were performed on two samples of different thickness. A swelling transition occurs at a pH of ~ 4 . The structure at values of pH $> \sim 4$ is of a collapsed polymer, but at lower values of pH (swollen brush), there is a configuration in which there is a region depleted in the polymer between the substrate and another peak in polymer density away from the substrate, which is not predicted by present theories. We suggest that such a structure might be due to the synthetic route to these brushes creating entanglements, which are not released during the swelling, leading to a situation of a metastable equilibrium. This is in contrast to data for brushes synthesized using a "grafting to" technique, which are generally of a lower molecular weight and/or grafting density, and so will not exhibit the structure that we observed for our brushes because they cannot get so entangled. Another possible explanation proposed suggests the substrate might affect the counterion distribution in the films.

Experiments were performed on one PMAA brush. The polyacid brush was exposed to a pH cycle and measured. The structure at values of pH ≥ 5.8 is of an expanded brush. At pH=3.4 the structure is of a collapsed brush. When driven back to basic conditions the swelling becomes observable at pH 7 and pH 10 run 2. However at pH 10 run 2 the volume fraction-depth profile is quite dissimilar to that observed at pH 10 run 1. Thus, in the swelling behaviour of the PMAA brush hysteresis was found in a pH cycle. In order to evaluate properly this result, other PMAA brushes of different thickness (i.e. different grafting densities) should be measured.

8.3 POLY (METHACRYLIC) ACID NETWORK/BRUSH.

We introduce and test here a new technique as a good means to measure interactions between polymer networks and brushes when immersed in aqueous solution. The important feature offered by this technique is that measurements are performed *in situ*.

We have performed measurements showing that there is a difference between the behaviour of PMAA gel/blank silicon and PMAA gel/brush systems, which may be due to adhesion. In PMAA gel/blank silicon when the pH is increased, the contact area of the gel in contact with the surface reaches equilibrium within a similar timescale as to when the pH is lowered. In other words, the time taken for the gel to

fully swell is equivalent to that taken for the gel to contract. This is the typical behaviour of an isolated gel indicating that the interaction between the gel and the silicon surface is independent of whether the gel was swelling or contracting.

When the silicon is coated with a PMAA brush Δt_1 is approximately twice than that obtained for PMAA gel and silicon. This suggests that when increasing the pH of the solution to pH ~11, the presence of a polyacid layer attached to the silicon retards the time taken to reach equilibrium when compared to blank silicon. The expansion of the contact area over the brush surface is not just ruled by the swelling of the gel but also by the swelling of the responsive brush. These early results show interactions occurring at the interface between gel and brush. Varying the grafting density and/or crosslink density of the polyelectrolyte brush and gel respectively is a useful means to control the interaction between the brush and the gel.

Appendices

Appendix 1

Polybase brushes: scattering length density as a function of depth.

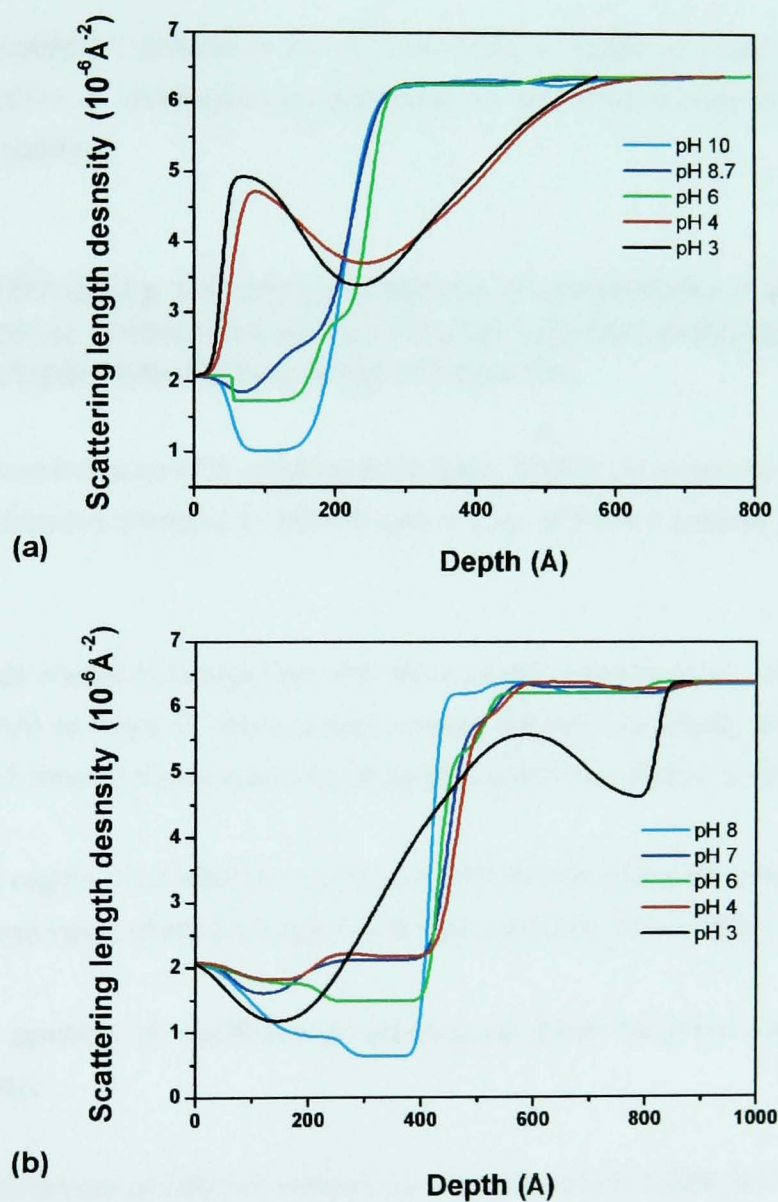


Fig. A1.1 Scattering length density-depth profiles for the two PDEAMA brushes as a function of pH as obtained from the NR data and fits shown in *Chapter 6, Section 6.1.2, Fig. 6.4*. The dry thicknesses are 13 nm (a) and 27 nm (b).

Appendix 2

Calculation of chromophore concentration in poly(methacrylic) acid

In this appendix I provide a list of instructions to follow in order to calculate the concentration of chromophores (naphthalene and anthracene) in labelled PMAA from UV spectra.

A2.1 Obtaining absorbance values of naphthalene and anthracene chromophores in double labelled poly(methacrylic) acid sample (NA-PMAA) from UV spectra.

1: Run baseline scan with spectroscopic grade MeOH (or whatever solvent is being used to dissolve sample) in both cuvettes (the reference cuvette and the sample cuvette).

2: Replace MeOH in forward cuvette with sample (approximately 10mg dry polymer (NA-PMAA) in 10ml of spectroscopic grade solvent accurately weighed) and run spectrum 3 times (usually scanning at wavelengths from 200nm to 500nm).

3: Adjust region of interest by zooming in with mouse. Read off average anthracene absorbance value direct from spectra at approximately 370 nm (A_1).

4: Note position of naphthalene absorbance peak maximum at approximately 290nm (A_2).

5: Load spectrum of polymer containing only anthracene labels from memory. Read off anthracene absorbance value direct from spectra at approximately 370 nm (\bar{A}_1), in this case without the presence of naphthalene.

6: Adjust axes by zooming in on region of interest and copy this file. Paste into window containing the spectra of the unknown sample (NA-PMAA).

7: Note the ratio of anthracene absorbances at $\sim 370\text{nm}$ (i.e. unknown NA-PMAA_(370nm)/ known A-PMAA_(365nm)) = $A_1 / \bar{A}_1 = X$. Fig. A3. 1 shows A_1 , A_2 and \bar{A}_1 in UV spectra containing an unknown NA-PMAA and known A-PMAA sample respectively.

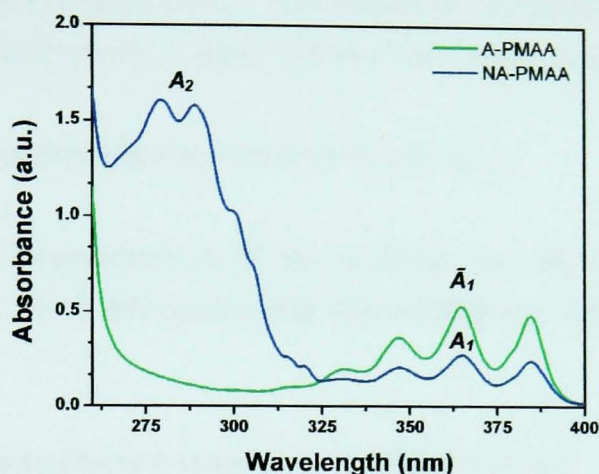


Fig. A2.1 UV absorption spectra of NA-PMAA and A-PMAA sample in methanol 0.01 wt% scanning from 200 to 400 nm. The absorbance of anthracene in an unknown NA-PMAA and known A-PMAA samples are A_1 and \bar{A}_1 respectively (at $\sim 370\text{nm}$). The absorbance of the naphthalene from the NA-PMAA sample previous to correction is A_2 (at $\sim 290\text{nm}$). Spectra taken from Chapter 4. Section 4.1.2.2. Fig. 4.2.

8: Start 'spectra arithmetic' program and take X times the A-PMAA sample spectrum away from the unknown spectrum (unknown in top selection window, A-PMAA sample in lower window). The anthracene peak in unknown PMAA spectrum at $\sim 370\text{nm}$ should resolve to zero.

9: Read off naphthalene response at wavelength value from above (point number.4). The new value is the corrected value for the absorbance $A_{2\text{-corrected}}$, generally $A_{2\text{-corrected}} < A_2$.

10: Calculate values of naphthalene and anthracene labels (mol%) as follows below.

A2.2 Concentration of naphthalene and anthracene chromophores in double labelled poly(methacrylic) acid sample (NA-PMAA) from UV spectra.

1: Once that the absorbance is known for naphthalene and anthracene, we use the following equation

$$A = \varepsilon cl, \quad \text{therefore} \quad c = \frac{A}{\varepsilon l}, \quad (\text{A2.1})$$

where c is the concentration of naphthalene or anthracene expressed in mol/l, l is the cuvette length (1 cm) and ε is the extinction coefficient (calculated from calibration for each chromophore). The extinction coefficient of anthracene and naphthalene are $9028 \text{ mol}^{-1}\text{cm}^{-1}$ and $7154 \text{ mol}^{-1}\text{cm}^{-1}$ respectively.

2: Calculate the concentration in mol/l from eq.(A3.1) : c_1

3: Calculate the concentration in g/l : C_1 by doing $c_1 \times M_w = C_1$, where M_w is the molecular weight (M_w of anthracene and naphthalene are 276.21 and 152.2 g/mol respectively).

4: Repeat for a second label if required: c_2 (mol/l) and C_2 (g/l).

5: See the total concentration of polymer which was put into solution initially in g/l : C_3 .

6: Calculate the concentration of primary (i.e. non-fluoro) monomer (C_4) in g/l as follows $C_4 = C_3 - (C_1 + C_2)$.

7: Convert C_4 to mol/l by dividing by M_w of primary monomer methacrylic acid (M_w of methacrylic acid is 86.02 g/mol): c_4

8: Calculate *Mol%* labels by:

$$(\text{Mol}\%)_1 = \left(\frac{c_1}{c_1 + c_2 + c_4} \right) \times 100 \quad \text{and} \quad (\text{Mol}\%)_2 = \left(\frac{c_2}{c_1 + c_2 + c_4} \right) \times 100, \quad (\text{A2.2})$$

In all cases ignore c_2, C_2 and $(\text{Mol}\%)_2$ if a second label is no present in the system.

Appendix 3

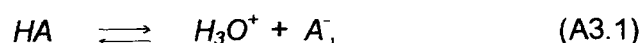
Basic concepts related to acids and bases

A3.1 Acids and bases

An acid (often represented by the generic formula HA) is defined by the Brønsted-Lowry theory as any substance that can donate a proton to another substance. The acid is said to be dissociated after the proton is donated. A base (often represented by B) according to the same theory is any substance that can accept a proton from another substance.

These definitions make no mention of the solvent (and apply even if no solvent is present); however, by far the most important medium is aqueous solution, and we confine our attention to that.

In water the following equilibrium occurs between an acid (HA) and water, which acts as a base:



Where A^- is the conjugate base of the acid and H_3O^+ is the hydronium ion, a representation of the state of the proton in aqueous solution. In aqueous solution, the water is protonated to form hydronium ion, H_3O^+ . This is often abbreviated as H^+ even though the symbol is not chemically correct. The terms "hydrogen ion" and "proton" are used interchangeably; both refer to H^+ .

The acidity constant or acid dissociation constant K_a is the equilibrium constant for the reaction of HA with water and is expressed as

$$K_a = \frac{[A^-][H_3O^+]}{[HA]}, \quad (\text{A3.2})$$

where the bracketed terms represent the equilibrium concentrations of the various species. The more complete the dissociation of HA (i.e. the reaction equilibrium lies far to the right; the acid is almost completely dissociated to H_3O^+ and A^-), the greater will be the value of K_a . An acid is considered to be strong if K_a is unity or greater. For example, the K_a value for hydrochloric acid (HCl) is 10^7 .

Weak acids have small K_a values (i.e. at equilibrium significant amounts of HA and A^- exist together in solution; modest levels of H_3O^+ are present; the acid is only partially dissociated). For example, the K_a value for acetic acid is 1.8×10^{-5} . Most organic acids are weak acids (i.e. carboxylic acid).

It is common to express values of K_a in terms of its negative logarithm pK_a :

$$pK_a = -\log K_a. \quad (A3.3)$$

A high value of pK_a (positive values) signifies a very small value of K_a (because $K_a = 10^{-pK_a}$) and hence a very weak acid. Strong acids have pK_a of zero or less.

As for it has been done for acids in eq.(A3.1), for a base B in water, the characteristic proton transfer equilibrium is given by



where HB^+ is the conjugate acid of the base B . We can express this equilibrium reaction in terms of the basicity constant K_b as

$$K_b = \frac{[HB^+][OH^-]}{[B]}, \quad (A3.5)$$

where, as above, the bracketed terms represent the equilibrium concentrations of the various species. Although K_b can be used to assess the strength of a base, it is also common to express proton transfer equilibria involving a base in terms of its conjugate acid as



By multiplying the expressions obtained for K_b and K_a in eq.(A3.5) and (A3.6) respectively, we obtain

$$K_a K_b = [H_3O^+] \cdot [OH^-], \quad (\text{A3.7})$$

where $[H_3O^+] \cdot [OH^-]$ is called ionization constant, dissociation constant, or self-ionization constant of water and is symbolized by K_w . This means that, in a very small proportions) water is dissociated as



in which one H_2O is acting as the acid and the other is the base.

In pure water at 25 °C, $K_w = [H_3O^+] \cdot [OH^-] = 10^{-7} \times 10^{-7} = 1.00 \times 10^{-14}$ ($pK_w = -\log K_w$) and $pK_w = -\log (1.0 \times 10^{-14}) = 14$. The product of the hydrogen ion and hydroxide ion concentrations in any aqueous solution will always be 1.00×10^{-14} at 25 °C. The consequences of this imply that if the concentration of H^+ is large, that of OH^- will be small, and *vice versa*. This means that H^+ ions are present in all aqueous solutions, not just acidic ones. When $[H^+] > [OH^-]$, $[H^+] < [OH^-]$ and $[H^+] = [OH^-]$ we have acidic, basic and neutral solutions respectively.

A3.2 pH calculations

The possible values of $[H^+]$ and $[OH^-]$ in an aqueous solution can vary many orders of magnitude, ranging from about $10^{1.3}$ to $10^{-15.3}$. It is convenient to represent them on a more compressed logarithmic scale. We use the pH scale to denote hydrogen ion concentrations as

$$pH = -\log[H^+] \quad \text{from where} \quad [H^+] = 10^{-pH}. \quad (\text{A3.9})$$

We can also define pOH as

$$pOH = -\log[OH^-]. \quad (\text{A3.10})$$

By adding pH (eq.(A3.9) to pOH (eq.(A3.10)) we obtain that

$$pH + pOH = pK_w (=14.0 \text{ in pure water at } 25 \text{ }^\circ\text{C}) \quad (\text{A3.11})$$

In a neutral solution at 25 °C, because the concentrations of H_3O^+ and OH^- are equal, the pH will be 7.0. A higher pH corresponds to a basic solution, a lower pH to an acidic solution.